Understanding Emissions from the Thermal Treatment of Intermediate Level Radioactive Waste

Alex Stone

A Thesis Submitted to the

Materials & Engineering Research Institute Sheffield Hallam University

in partial fulfilment of its requirements for

The Degree of Doctor of Philosophy

January 2024

Candidate's Declaration

I hereby declare that the thesis entitled "Understanding Emissions from the Thermal Treatment of Intermediate Level Radioactive Waste" is a result of my original work and investigation. I have not been enrolled for another award of the University or any other organisation whilst undertaking this research degree. Material contained within the thesis has not been used in the submission of any other academic awards. All work has been conducted in accordance with the SHU Principles of Integrity in Research and Research Ethics Policy.

Name: Alex Stone

Date: 10th January 2024

Award: PhD

Word Count: 52661

College: College of Business, Technology and Engineering

Director of Studies: Professor Paul A. Bingham

Acknowledgements

Firstly, I would like to thank the entire team at Sheffield Hallam University for helping me through my PhD. My director of studies Prof. Paul Bingham has given me much needed guidance over the years and I can't thank him enough for his time, teaching, advising and reviewing my work. I am indebted to the SHU staff members who have supported my studies with experimental analyses and Dr. Anthony Bell, Dr. Alex Scrimshire, Dr. Francis Clegg. The entirety of Paul's team have always been welcoming and helpful whenever you need a hand so I would also like to acknowledge their help over the duration.

Funding for the project was provided by the Nuclear Decommissioning Authority, National Nuclear Laboratory and Transcend consortium. With supportive funding from the National Nuclear User Facility. Thank you to the supervisory and support team, Donna McKendrick, Ed Butcher and Mike Harrison at the National Nuclear Laboratory for invaluable advice and checking over the PhD period.

I would also like to show my gratitude to the National Oceanography Centre in Southampton and the National Nuclear User Facility for allowing me to access equipment that enhanced this project and allowed me to learn so much more. Particularly Richard, Frances and Dave who supported and supervised me with my active research at NOCS.

My amazing Mum and Dad have always been there for me at every step and have made me the person I am today and as such be able to complete this. Of course, I would like to thank my amazing wife, Philippa, who has stayed with me throughout all of this for some reason. My PhD has been ongoing through house moves across the country, wedding planning, starting new jobs and without the support from her I would not have been able to cope with it all.

Abstract

Practical applications of vitrification and usage of glass matrices has highlighted the importance of understanding these materials to a higher standard. This includes prioritising closing gaps in the past research to make the process safer and more effective for the future. One of the clear areas is the loss of radioactive/volatile components of waste upon heat treatment or vitrification. It is widely known that caesium, iodine and chlorine are all lost to some degree through volatilisation mechanisms at elevated temperatures and therefore understanding the extent of these processes is key to maintaining a total inventory of radioactive material on nuclear licenced sites. During this study we have found that iodine loaded into glass compositions: Mixture Windscale (MW), calcium-zinc (CaZn) and a silica-free version of CaZn, is the most volatile (100% loss at 1200 °C) of the three elements investigated, however, all lost mass upon heat treatment. The volatilisation can be reduced for iodine and caesium by introducing common wastes to the system. Clinoptilolite and Corroded Magnox Sludge (CMS) were studied and the loss of atomic caesium was found to show a 15-21 wt% improvement in retention in both MW and CaZn glass when loaded with up to 30 wt% clinoptilolite, the effect being less pronounced for CMS. Iodine retention also improved, a maximum of 16 - 33 wt% iodine was found in base glasses upon 40 wt% clinoptilolite, CMS again having less of an effect on the retention at the same waste loading (4.5 wt%), theorised to be due to the binding of caesium or iodine to the waste before melting. Atmospheric changes were investigated changing from air to nitrogen which had a positive effect on retention of caesium (+ 8 wt%) and significantly so for iodine (+74 wt%). This is a demonstration of the importance of oxygen in these systems, the two sources of oxygen are from the glass frit/waste and from the atmosphere with the atmospheric oxygen being readily available and able to react before the glass frit melts increasing the proportion of gaseous iodine and to some extent caesium.

Glossary of Terms

- AGR – Advanced Gas Cooled Reactor
- AMU – Atomic Mass Unit
- BO – Bridging Oxygens
- CAS – Calcium Aluminosilicate
- CaZn – Calcium / Zinc (UK base Glass)
- CCIM – Cold Crucible Induction Melter
- CPM – Counts per Minute
- FTIR – Fourier Transform Infrared Spectroscopy
- GDF – Geological Disposal Facility
- HLW – High Level Waste
- ICV – In-Container Vitrification
- ICP-MS – Inductively Coupled Plasma-Mass Spectrometry
- ILW – Intermediate Level Waste
- LLW – Low Level Waste
- IR – Infrared
- MW – Mixture Windscale (UK Base Glass)
- NBO – Non-Bridging Oxygen
- PCM – Plutonium Contaminated Material
- PVC – Polyvinyl Chloride
- RWM – Radioactive Waste Management
- SEM – Scanning Electron Microscope
- SIXEP – Site Ion Exchange Effluent Plant
- SLS – Soda Lime Silica
- T_g – Glass Transition Temperature

- VLLW – Very Low Level Waste
- WL – Waste Loading
- XANES – X-ray Absorption Near Edge Structure
- XPS – X-ray Photoelectron Spectroscopy
- XRD – X-ray Diffraction
- XRF – X-ray Fluorescence

List of Figures

Chapter 5

Figure 5.52 The effect of temperature on glass composition of MW with addition of 1 % chlorine (added as NaCl) from 800 – 1200 °C (t=0)

Figure 5.53 XRD pattern of CaZn frit melted at 800 – 1200 °C with the addition of 1 % Cl added as NaCl. ▲= NaCl Halite (Phase ID: 01-071-4661)

Figure 5.54 Change in glass content (analysed by XRF) of CaZn incorporated with 1 wt% chlorine remelted between 800 – 1200 °C (t=2h)

Figure 5.55 XRD data of CaZn glass containing 1% Cl (t=2h) remelted at 800 – 1200 °C ▲= SiO_2 Quartz (Phase ID: 01-070-3755), ■ = $Li_2B_4O_7$ (Phase ID: 01-086-5516)

Figure 5.56 Effect of heat treatment temperature (800 – 1200 °C) on density of MW glass systems, t=0 remelted with NaCl and 1 wt% chlorine already in the glass network. Error bars represent +/- 0.001 g for each measurement which is smaller than the points.

Figure 5.57 Images of crucible corrosion from chlorine containing samples. a) Crucible completely corroded by glass/NaCl. b) Leaking of the crucible and fusing to the working tube. c) Fusing of a sample to the working tube of the pyrolysis instrument, nickel liner used to protect tube

Figure 5.58 The effect of temperature on dopant glass content of MW and CaZn with addition of 1 % of the additive (Cs, I or Cl) from 800 – 1200 °C (t=0). Grey = MW, Red = CaZn, ● = Caesium, ▶ = Chlorine, ■ = Iodine

Figure 5.59 The effect of temperature on dopant glass content of MW and CaZn containing 1 % of the additive (Cs, I or Cl) from 800 – 1200 °C (t=2h). Grey = MW, Red = CaZn, ● = Caesium, ▶ = Chlorine, ■ = Iodine

Chapter 6

Figure 6.1 Images of the crucibles after pouring CaZn glasses loaded with clinoptilolite with a particle size of 500 – 2500 µm (a) and <500 µm (b). From left to right 10, 20, 30, 40, 50 wt% waste loading.

Figure 6.2 Images of glasses/products from waste loaded 0% SiO_2 CaZn glass samples from 10, 20, 30, 40, 50 wt% (left to right). a) Clinoptilolite waste loaded (glare from backlight caused some problems with images). b) CMS waste loading

Figure 6.3 XRD patterns of clinoptilolite loaded from 10 – 50 wt% (bottom to top) into 0% SiO_2 CaZn glass

Figure 6.4 XRD patterns of CMS loaded from 10 – 50 wt% (bottom to top) into 0% SiO_2 CaZn glass ▲= $Mg_{0.35}Zn_{0.65}Al_2O_4$ Gahnite (Phase ID: 04-017-1029), ■ = $LiMgBO_3$ (Phase ID: 04-009-5597)

Figure 6.5 XRF concentration data points of CaZn glass/product with the addition of 10 – 50 wt% clinoptilolite all with the addition of 1 wt% Cs added as Cs_2CO_3.

Figure 6.6 Caesium concentration data points of CaZn glass/product with the addition of 10 – 50 wt% clinoptilolite all with the addition of 1 wt% Cs added as Cs_2CO_3.

Figure 6.7 XRD traces of clinoptilolite waste loaded CaZn glass with the addition of 1 wt% Cs as Cs_2CO_3 from 0 – 50 wt%.

Figure 6.8 Active ^{137}Cs retention in CaZn glass with the loading of clinoptilolite between 10 – 50 wt% analysed by gamma spectroscopy.

Figure 6.9 Images of clinoptilolite loaded samples in CaZn glass after heat treatment at 950 °C with the addition of 10 bq of ^{137}Cs. Left to right 10, 20, 30, 40, 50 wt%.

Figure 6.10 XRF concentration data points of CaZn glass/product with the addition of 10 – 50 wt% CMS all with the addition of 1 wt% Cs added as Cs_2CO_3.

Figure 6.11 Caesium concentration data points of CaZn glass/product with the addition of 10 – 50 wt% CMS all with the addition of 1 wt% Cs added as Cs_2CO_3.

Figure 6.12 XRD traces of CMS waste loaded CaZn glass with the addition of 1 wt% Cs as Cs_2CO_3 from 0 – 50 wt%. ▲= Forsterite Mg_2SiO_4 (Phase ID: 01-085-1346), ● = Kotbite $Mg_3(BO_3)_2$ (Phase ID: 01-073-1541), ■ = Periclase MgO (Phase ID: 04-007-3405).

Figure 6.13 Active ^{137}Cs retention in CaZn glass with the loading of CMS between 10 – 50 wt% analysed by gamma spectroscopy.

Figure 6.14 Images of CMS loaded samples in CaZn glass after heat treatment at 950 °C with the addition of 10 Bq of ^{137}Cs. Left to right 10, 20, 30, 40, 50 wt%.

Figure 6.15 Active ^{137}Cs retention in CaZn glass with the loading of clinoptilolite between 10 – 50 wt% analysed by gamma spectroscopy.

Figure 6.16 Images of clinoptilolite loaded samples in 0% SiO_2 CaZn glass after heat treatment at 950 °C with the addition of 10 Bq of ^{137}Cs. Left to right 10, 20, 30, 40, 50 wt%.

Figure 6.17 Active ^{137}Cs retention in CaZn glass with the loading of CMS between 10 – 50 wt% analysed by gamma spectroscopy.

Figure 6.18 Images of clinoptilolite loaded samples in 0% SiO2 CaZn glass after heat treatment at 950 °C with the addition of 10 Bq of ^{137}Cs. Left to right 10, 20, 30, 40, 50 wt%.

Figure 6.19 TGA data for 5 wt% iodine doped MW glasses with and without the addition of 10 wt% clinoptilolite over the temperature range 0 – 1200 °C

Figure 6.20 DTA data for 5 wt% iodine doped MW glasses with and without the addition of 10 wt% clinoptilolite over the temperature range 0 – 1200 °C

Figure 6.21 MS data traces of 5 wt% iodine doped MW glasses with and without the addition of 10 wt% clinoptilolite over the temperature range 0 – 1200 °C. AMU 254.

Figure 6.22 TGA data for 5 wt% iodine doped MW glasses with and without the addition of 10 wt% clinoptilolite over the temperature range 0 – 1200 °C

Figure 6.23 DTA data for 5 wt% iodine doped MW glasses with and without the addition of 10 wt% CMS over the temperature range 0 – 1200 °C

Figure 6.24 MS data traces of 5 wt% iodine doped MW glasses with and without the addition of 10 wt% CMS over the temperature range 0 – 1200 °C. AMU 254.

Figure 6.25 TGA data for 5 wt% iodine doped CaZn glasses with and without the addition of 10 wt% clinoptilolite over the temperature range 0 – 1200 °C

Figure 6.26 DTA data for 5 wt% iodine doped CaZn glasses with and without the addition of 10 wt% clinoptilolite over the temperature range 0 – 1200 °C

Figure 6.27 MS data traces of 5 wt% iodine doped CaZn glasses with and without the addition of 10 wt% clinoptilolite over the temperature range 0 – 1200 °C. AMU 254.

Figure 6.28 Active ^{129}I retention in CaZn glass with the loading of clinoptilolite between 10 – 50 wt% analysed by LSC.

Figure 6.29 Images of clinoptilolite loaded samples in CaZn glass after heat treatment at 950 °C with the addition of 10 bq of ^{137}Cs. Left to right 10, 20, 30, 40, 50 wt%.

Figure 6.30 TGA data for 5 wt% iodine doped CaZn glasses with and without the addition of 10 wt% clinoptilolite over the temperature range 0 – 1200 °C

Figure 6.31 DTA data for 5 wt% iodine doped CaZn glasses with and without the addition of 10 wt% CMS over the temperature range 0 – 1200 °C

Figure 6.32 MS data traces of 5 wt% iodine doped CaZn glasses with and without the addition of 10 wt% CMS over the temperature range 0 – 1200 °C. AMU 254.

Figure 6.33 MS data traces of 5 wt% iodine doped CaZn glasses with and without the addition of 10 wt% CMS over the temperature range 0 – 1200 °C. AMU 18.

Figure 6.34 Active ^{129}I retention in CaZn glass with the loading of CMS between 10 – 50 wt% analysed by LSC

Figure 6.35 Images of CMS loaded samples in CaZn glass after heat treatment at 950 °C with the addition of 10 bq of ^{137}Cs. Left to right 10, 20, 30, 40, 50 wt%

Figure 6.36 Active ^{129}I retention in CaZn glass with the loading of clinoptilolite between 10 – 50 wt% analysed by LSC. Some of the error bars are smaller than the points. Red line represents a linear fit trendline.

Figure 6.37 Images of Clinoptilolite loaded samples in 0% SiO_2 CaZn glass after heat treatment at 950 °C with the addition of 10 bq of ^{137}Cs. Left to right 10, 20, 30, 40, 50 wt%

Figure 6.38 Active ^{129}I retention in 0% SiO_2 CaZn glass with the loading of CMS between 10 – 50 wt% analysed by LSC. Red line represents a linear fit trendline.

Figure 6.39 Images of CMS loaded samples in 0% SiO_2 CaZn glass after heat treatment at 950 °C with the addition of 10 bq of ^{137}Cs. Left to right 10, 20, 30, 40, 50 wt%. Some samples broke on removal from the furnace work tube.

List of Tables

Table 8.1 Comparison of iodine containing MW and CaZn glasses under air and nitrogen atmosphere.

Chapter 9

Table 9.1 Total mass loss from 0 – 1200 °C at 5 °C/min in MW and CaZn base glass for all elements and the midpoint temperature of the mass change event associated with the dopant.

Table 9.2 Temperature at which peak ion current is found for m/z ion 254 from MS iodine data over different glass systems and iodine (as NaI) doping concentrations.

Table 9.3 Waste loading at which crystallisation occurred by XRD

Table 9.4 Caesium and iodine retention as measured by pyrolysis method (^{137}Cs is product, ^{129}I in captured gas)

Table 9.5 Comparison of the iodine peak temperature detected by MS for AMU 254 for MW and CaZn glass with and without carbon additives Xanthan gum and graphite loaded to 1 wt%.

Table of Contents

Chapter 1 Introduction

The UK is in custody of 137,559 m^3 (170,100 tonnes)[1] of radioactive waste, both from operations and decommissioning. This was produced either from ongoing civil power operations or legacy radioactive waste which arose primarily from power generation, and the subsequent reprocessing of spent nuclear fuel leading to a stockpile of plutonium (for civil fuel and nuclear weapons) and Intermediate Level Waste (ILW) from fuel cladding and effluent treatment operations starting in 1950[2]. Since 1990, operational ILW has been treated and converted into cemented products, for long term storage and ultimate disposal in a Geological Disposal Facility (GDF), when it becomes available. Most historical legacy wastes are stored at Sellafield in storage silos or ponds and therefore we first need an understanding of the site.

Sellafield is a former nuclear power generation, fuel reprocessing and research facility on the west coast of the Cumbria, covers 650 acres of land and contains the world's largest store of civil plutonium[3]. The site was used to create some of the country's first reactors such as the Windscale and Calder Hall reactors[4], store the majority of the radioactive waste in the UK, and reprocesses fuel from the UK and overseas reactors[2]. Some of the notable processes that are either still running today, or have recently entered the process of decommissioning, are[1,5–7]:

- Thermal Oxide Reprocessing Plant (THORP) (closed 2018, now in decommissioning phase)
- Magnox Reprocessing Plant (closed 2022)
- Site Ion Exchange Effluent Plant (SIXEP)
- Enhanced Actinide Removal Plant (EARP)
- Fuel Handling Plant (FHP)
- Segregated Effluent Treatment Plant (SETP)
- Waste Vitrification Plant (WVP)

- Sellafield Mixed Oxide (MOX) Fuel Plant (SMP)

Nowadays Sellafield is used as an interim storage and treatment facility and is the largest radioactive clean-up site in the UK. Large volume storage locations include[6,8,9]:

- Magnox storage pond (waste retrieval and decommissioning phase)
- THORP ponds (decommissioning phase)
- Magnox swarf storage silo (MSSS) (waste retrieval and decommissioning phase)
- Pile Fuel Storage Pond (PFSP) (waste retrieval and decommissioning phase)

The majority of radioactive waste in the UK will arise in the future from decommissioning of radioactively compromised structures such as nuclear power stations. For example, 4,287,000 m^3 of radioactive waste will arise from future decommissioning projects at Sellafield and Magnox reactor sites and 133,000 m^3 is already in storage at Sellafield in containers or ponds[10]. Some waste streams have been separated already at the source and as a result can be more easily treated because of their homogeneous nature. An example of this is sand and clinoptilolite which originates from the 'Site Ion Exchange Process' (SIXEP) used for treating contaminated effluent from Sellafield[7].

The ponds and silos currently used at Sellafield are not a long-term solution[10]. For example, metallic wastes such as Magnox fuel cladding will have undergone corrosion during underwater storage, leading to a waste stream which is a combination of the original metal and sludges[11]. There is therefore motivation to retrieve waste from the historical storage facilities and transfer them to more modern facilities, prior to the implementation of treatment and disposal. These facilities are responsible for long term storage and an issue which arises is the presence of radionuclide pollutants which are common for all the wastes in question. The leaching of these from storage could pollute groundwater, soil and seawater causing damage to the environment. Radionuclides are unstable radioactive isotopes that emit gamma, beta or alpha radiation, all of which have the potential to be hazardous to humans and the environment[12]. These are separated into different groups relevant for nuclear waste management for example: fission products and minor actinides (long lived and short lived)[13]. One

crucial factor is longevity (half-life) of the radionuclide as this determines when the radioactivity of the component will decay to acceptable levels. Most minor actinides (e.g. ^{237}Np, ^{241}Am, ^{243}Am $^{244-246}$Cm) commonly found in nuclear waste are very long-lived with half-lives between 432 and 214,000 years[13] with the exception of ^{244}Cm which has a shorter half-life of 18.1 years. Fission products have a much broader variety of half-lives. ^{135}Cs, ^{137}Cs, ^{90}Sr, ^{99}Tc, ^{129}I which are more common,[14–16] have half-lives in extremes (2.30×10^6 , 30.17, 28.60, 2.13×10^5, 1.57×10^7 years, respectively[16–18]). These products are of interest to the waste management community as they have high mobility in environmental systems (discussed more in section 1.2). Environmental mobility is of particular interest to researchers in the field as some radioactive waste may not have a high activity but if environmental exposure occurs from the wasteform there may be a larger potential for contaminating the biological landscape. Caesium, iodine and chlorine are typical for this due to their chemical properties[14] and since they are present so commonly in radioactive waste these certainly should be prioritised when considering management[19–21].

The primary source of waste containing ^{135}Cs, ^{137}Cs, ^{90}Sr, ^{99}Tc, ^{129}I, Cl is the fission reactions that occur for generation of nuclear power. This results in fission products from spent fuel and effluent. This could potentially mean that building structures such as concrete, steel, wood and soil could be contaminated with radioactive elements and therefore need to be treated the same/similarly as the pure radioactive waste when decommissioning occurs. The current method for handling decommissioning when a power plant reaches the end of its operational life span (normally 30-60 years) is that it is taken out of active power generation service and enters a defueling stage where the fuel is removed to a cooling pond and, once sufficiently cool, transported to Sellafield, for treatment/storage[22,23]. The final stage of decommissioning is the removal/demolition of redundant facilities and their decommissioning. The contamination of the land and demolition waste amounts to a large volume of radioactive rubble that must be dealt with. This waste is usually surface contaminated and is likely to be disposed of via decontamination or cementation techniques.

Approximately 99% of the UK's radioactive waste (by volume) is categorised as intermediate or low level; most of this arising from legacy wastes and decommissioning of sites[22]. Low level waste (LLW) is categorised in the UK as containing radioactive materials not exceeding 4 GBq of alpha activity or 12 GBq of beta/gamma activity per tonne whereas intermediate level waste has to be above those values to be classified. The wastes that are classified as high level waste (HLW) are heat generating and also exceed the LLW thresholds[10]. This means that the LLWs and ILWs cover a very wide range of materials such as graphite, sludges and resins as well as contaminated construction materials like cement, sand and mild steel.

Some LLW and ILW in UK is currently being considered for treatment by vitrification (figure 1.1) which is the transformation of a material into a glass by applying heat (discussed more in section 2.3.3). This technique incorporates hazardous radionuclides in the glass structure and provides a matrix for the waste that has higher stability and is less likely to leach compared to cementitious wasteforms, therefore ensuring the prolonged safe storage in geological repositories. This durability coupled with its thermal and radiation stability has made vitrification the standard process for the immobilisation of HLW worldwide. Moreover, in the context of ILW and LLW, it provides a method for large volume reductions. It then follows that glass technology plays an important role in understanding the waste form during this treatment[24].

During vitrification, powdered 'base' glass (or 'frit') is added to the melter to create a pool of liquid glass. One of the 'base' glass compositions used to vitrify HLW in the UK is 'Mixture Windscale' (MW)[25] which uses an alkali boro-silicate glass network to contain hazardous components of the waste. Silica (SiO_2) by itself could perform this task; however, the temperatures required for this would be difficult and costly so instead fluxes (such as B_2O_3, Li_2O, and Na_2O) are added that

Figure 1.1 Inside a GeoMelt 'In-Container' vitrification tank[26] (Veolia, 2020)

disrupt the silica network, lowering the viscosity, and reducing the required operating melting temperature. Additionally, elements in the reagents or waste also enter the atomic structure of the glass, which in turn further affects its properties. However, the waste streams considered in this project are very variable and therefore has the potential for a variety of different glass, ceramic and metal phases upon vitrification[27].

The ILW of most interest to Sellafield for vitrification can be categorised into groups:

- Plutonium Contaminated Material (PCM) Waste
- Sand/Clinoptilolite
- Magnox Sludge

PCM waste arises from many different processes including, plant operations, decommissioning and research, for this reason many different types of PCM waste exist, however, they are all contained in a very similar way. Most of the operational waste is 'double bagged' in plastic PVC bags and then packaged in a 200L steel drum which is lined with an outer and inner layer of PVC[6]. For decommissioning waste the contaminated materials are sealed in a steel inner liner before surrounding with three layers of PVC and then stored in a 200L steel drum similar to the other PCM wasteforms. It is of note that some of the drums have become damaged and therefore have been protected in 'Nova Drum' overpacks which add another layer of protection to the storage. This packaging contains the original drum in fibreglass and that is then sealed in a drum slightly bigger than 200L, crimped and radio frequency (RF) welded so that the container can only be opened with manual

grinding or drilling. There are 243,600 drums of PCM in storage[6] and this number is set to rise with the ongoing decommissioning of many of the sites around the UK.

Under UK legislation some LLW, and all ILW/HLW is planned to be stored in a GDF with identification of the location being undertaken by Nuclear Waste Services (formally Radioactive Waste Management)[28]. A GDF uses multiple barriers, the last of which being the natural geology of an area, to shield the packages underground to a significant degree such that they no longer emit harmful quantities of radioactivity, and to retard the rate of release of radionuclides, in line with the disposal safety case. The site will not just rely on rock formations to protect the waste but also sophisticated engineering which will provide barriers to entry into the ecosystem through air or ground water. In addition to these the wasteform itself is a barrier as well as the container the waste is in.

1.1 Nuclear Fuel Cycle

To understand the treatment, emissions and technologies available we first look at the radioactive waste generated in the UK and where that is (or was) generated. After the discovery of uranium and plutonium's fission properties in 1938[29] they have been a commodity for use in power and

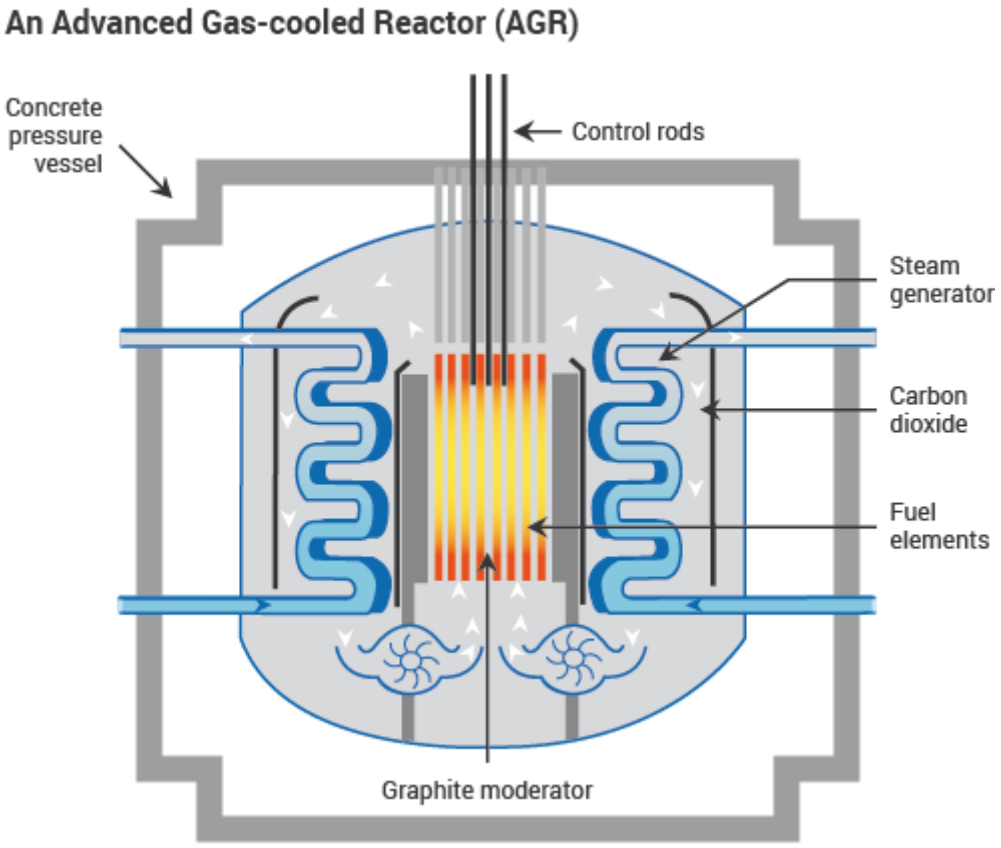

Figure 1.2. Diagram of an Advanced Gas-cooled Reactor (AGR)[30]

military applications. For power generation, uranium is in the form of enriched UO_2 pellets (increased ^{235}U concentration compared to natural $^{235}U/^{238}U$) encased in fuel cladding made of graphite, zirconium alloy or stainless steel[31] depending on the reactor. Another fuel form is a mixed oxide fuel (known as MOx) made from recycling reprocessed spent fuel which contains a mix of uranium (~90 %) and plutonium oxides (~10 %)[29]. In reactors (figure 1.2) heat produced from the radioactive decay of ^{235}U is used to produce water vapour which rises, turns a turbine and generates power. When ^{235}U has decayed to the point where the heat generation is too low the spent fuel rod will be removed and (in the UK) stored in ponds[28] ready for decommissioning as HLW. Most resultant elements of this decay

are defined as fission products, minor actinides or plutonium. From mine to storage the path (figure. 1.3) all radioactive material takes has the potential to contaminate and therefore it is vital to understand how the process works in its entirety.

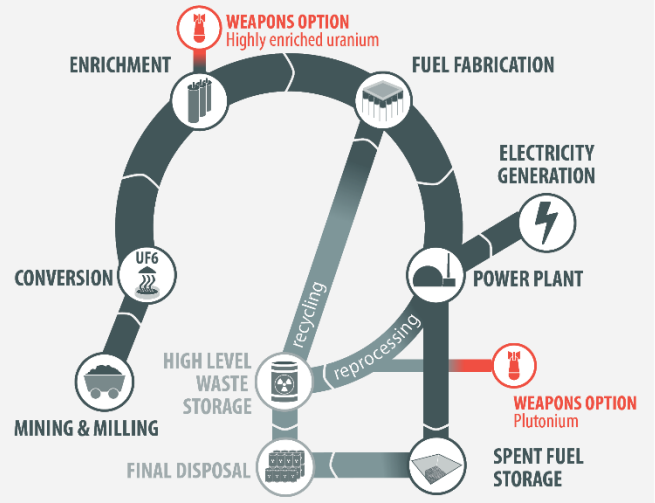

Figure 1.3. A representation of the UK nuclear fuel cycle[32]

The UK has no economically viable source of uranium ore and therefore there is no radioactive waste produced as a result of mining or milling operations[33]. Springfields, a nuclear fuel production facility, in Lancashire supplies of the majority of the enriched uranium fuel in the UK satisfying the large demand for UO_2 fuel. Before enrichment can happen, however, an intermediate must be formulated, UF_6 as it only contains one naturally occurring isotope and the only differences in mass will be from uranium. Naturally uranium presents[31] in ore as UO_2 and UO_3 and for conversion to UF_6 many steps occur from powder form UO_x. Firstly, the powder is treated with nitric acid and sulphuric acid to improve surface area for improved chemical reactivity. This is then reduced with hydrogen in a high temperature rotating kiln to produce dry UO_2 which is then fed into a fluorination kiln in the presence of gaseous HF to produce UF_4. UF_4 needs to then be converted to UF_6 with gaseous fluorine in a complex chain of reactors and filters that eventually result in condensation of liquid UF_6 which is sent in liquid form for enrichment. Many steps of this process produces waste, for example from scrubbers and filters which need to be sent off for disposal.

The fuel cycle is linked to the UK nuclear weapons programme as the enrichment process can be used for production of fission bombs. ^{235}U and ^{239}Pu were both used for fission nuclear bomb weaponry, all

based around the theory of nuclear chain reactions. The nuclei would be bombarded with neutrons which would add to the mass of the nucleus causing instability and splitting the atom into other heavy and light elements with a massive release of energy[29].

1.2 Volatile Radioactive Species

Of particular interest in this study are the volatile components of the radioactive waste inventory in the UK. These can occur through various means, however, most are present due to decay reactions from the fission of ^{235}U and less commonly from neutron capture or intentional addition in reactors[34]. Cs, I and Cl have already been identified as particular elements of concern and the sources and properties of these products will now be considered.

1.2.1 Caesium

Caesium is present in radioactive waste almost exclusively from ^{235}U fission reactions in reactors or weapons from the subsequent decay of ^{129}I, ^{137}Xe and ^{135}Xe in decay chain reactions[17]. There are some smaller contributions from decommissioned medical and industrial markers which contain ^{137}Cs as either a calibrator or a beta/gamma source. It is a problematic radionuclide in wastes because of its volatility, high energy radiation, half-life and environmental mobility[35] (see table 1.1). It has a half-life of 30.4 years and during this period is a high beta/gamma emitter which makes it more hazardous than many other radionuclides[36].

Radioactive Element	Half Life	Decay Mode	Mobility*
^{137}Cs	30.4 years	High beta/gamma	High
^{129}I	15.7 million years	High beta	High
^{135}Xe	9.14 hours	Beta	High (Gaseous)
^{137}Xe	3.8 minutes	Beta	High (Gaseous)
^{235}U	703 million years	Neutron/alpha	Low
^{99}Tc	211,000 years	High Beta	Low

Table 1.1 Key characteristics of some radioactive elements. *Mobility is measured by many different techniques such as depth sampling in soil and solubility in water and therefore is defined as low – high.

In the current waste inventory in the UK ^{137}Cs contributes 23,000,000 TBq of activity equating to 28.75% of the total activity in HLW and 500,000 TBq equating to 20% of the total ILW inventory[1].

Caesium has other isotopes (AMU – 134, 135) that do not contribute as much to the concentration or activity however, the isotopic distribution by activity is: 0.35% ^{134}Cs, 0.001% ^{135}Cs and 99.65% ^{137}Cs. Because of this ^{137}Cs is the most monitored and regulated isotope of caesium. The primary issues with caesium are the high energy radiation it emits and the potential for mobility in the biosphere by either air, land or water. Caesium is mobile in all these systems with ^{137}Cs being mobile in soil[37], groundwater[12,35] and also form gaseous species upon heating[38]. Because of this there a large risk to environment and public health especially from thermal processes or treatment that might exacerbate caesium volatilisation. In this study caesium is investigated in its carbonate form (Cs_2CO_3) and is added to glass frits and batches to determine the effects on properties and volatility. Other caesium compounds were considered (CsCl, Cs_2O ,CsI), however, Cs_2CO_3 closely represents the state which caesium will occur in nuclear waste environments and will not interfere with other analytes.

1.2.2 Iodine

Iodine makes up around 0.69 wt% of the mass of uranium fission from reactor fuel rod decay[34] with an isotopic distribution of 23.5 wt% stable ^{127}I and 76.5 wt% beta emitter ^{129}I after storage for 2 years. 2.1 wt% ^{131}I does occur at removal of the fuel rod, however, with a half-life of 8 days this is a short-lived radionuclide and does not present in most stored waste in any meaningful concentrations. As a very mobile element through soil and water radioactive iodine could contaminate the ecosystem if released and therefore has been monitored for a long time by UK regulatory agencies[39,40]. In this study iodine is investigated as NaI and is added to glass frits and batches to determine the effects on properties and volatility. Other iodine compounds were considered (KI, solid I_2, iodates), however, NaI closely represents the state which iodine will occur in nuclear waste environments.

1.2.3 Chlorine

In the UK, chlorine presents in radioactive waste in the form of PVC[10] and chlorine contamination from intentional chlorination of the cooling water[41]. PVC is a hydrocarbon polymer containing chlorine (figure. 1.4) that was used for a significant amount of waste storage and operation solutions in the

1950's and onwards when many nuclear power and defence projects were commissioned. It was originally used because of its strength and rigidity, however, it was later found that upon exposure to radiation the material changed in shape, colour and mechanical strength[42]. The other issue with this material is that it generates chlorinated gases upon degradation by either thermal or radiological processes[21].

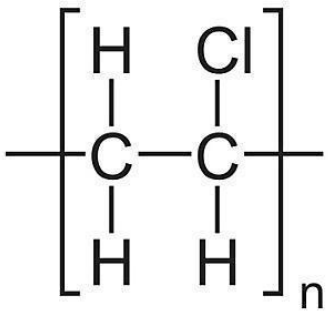

Figure 1.4. Structural Formula of PVC

Upon degradation (be it thermal or radiological) PVC could emit radioactive and inactive chlorine containing gases which need to be controlled and quantified. Another source is from chlorinated cooling water, intentionally added at 0.5 – 1.5 mg/L to reduce the effects of biofouling in reactor circuits[41]. This source could contaminate other reactor components that go into decommissioning and therefore present in waste thermal treatment processes. Chlorine is known to form a range of organic compounds in cooling water and can be deposited on graphite mediators and tubing in the circuit. In this study chlorine is investigated as NaCl and is added to glass frits and batches to determine the effects on properties and volatility. Other chlorine compounds were considered (LiCl, $CaCl_2$, PVC), however, for simplicity NaCl was used and closely represents the state which chlorine will occur in nuclear waste environments and will not interfere with other analytes/glasses. Any impact from these dopants will be discussed in chapter 5.

1.3 Waste Streams

Earlier we discussed the radioactive waste streams that have high volume in the UK. The wastes of particular interest in this study are sand / clinoptilolite and Magnox sludge as they are high volume wastes that are more homogeneous and better for application of thermal treatment. Waste streams are a key part of our work in chapter 6 where we see the effect of waste type and quantity on volatile agents.

1.3.1 Magnox Sludge

This waste originates from magnesium containing fuel cladding from Magnox reprocessing procedures. Plutonium and uranium were extracted using the PUREX (plutonium uranium reduction extraction) process[43] which dissolves the fuel in strong nitric acid and removes the valuable uranium and plutonium by complexing with tributyl phosphate. After the acidification step any solids are removed from the process and what remains of the Magnox fuel is a liquid liquor (or raffinate) which is left to be treated. The primary source of Magnox sludge is in the medium - long term storage in ponds (before reprocessing) of Magnox fuel since 1950[44], the magnesium alloy cladding of which corrodes into a highly active sludge[45], named corroded Magnox sludge (CMS). The storage pond in question is primarily used for the storage of these fuels and therefore the settled sludge waste produced is homogenous in nature especially compared to other ILWs. Compositionally sludge from this pond is predominantly $Mg(OH)_2$ particulates with small amounts of magnesium metal from any uncorroded cladding that may have disconnected during corrosion[8] and water. Other than the base components there is also contamination from fuel decay (U, Pu, Cs, I, Sr), tritiated water (^3H) and water treatment agents[46]. The particle size varies in Magnox sludge, however, the majority is below 1000 µm. The most common particle size fraction is between 1 – 5 µm with 26 wt% of the sludge falling into this range. 70 % of the weight is contributed to from particles larger than this and 10 wt% is from particle sizes between 190 – 1000 µm.

1.3.2 Sand / Clinoptilolite

Sand and clinoptilolite mixture is a by-product of the SIXEP process, an effluent treatment plant designed to remove aqueous radionuclides by ion exchanging them in a large column packed with this material. The aqueous waste streams (one of which is the aqueous raffinate remaining after reprocessing[47]) pass through the filter beds and larger ions such as strontium and caesium exchange for (generally sodium or potassium) ions in the structure of clinoptilolite[7,48]. The beds are then replaced after a certain number of runs and the contaminated material stored in silos until future treatment. Clinoptilolite is used for its reliable ion exchange properties in many different fields including pool cleaning and dietary supplements[49].

For the nuclear industry it was found that one particular source of clinoptilolite exchanged ^{137}Cs and ^{90}Sr much more readily than those from other mines around the world. This was Mud-Hills clinoptilolite which is a mineral mined in the Mojave desert, California, United States of America and performs more efficiently than 14 other commercially available clinoptilolites from around the world[48]. One of the factors was 'breakthrough' of strontium and caesium however there is no publicly available data/figures on mud hills clinoptilolite these are normally quoted in papers as 'better' than other clinoptilolite materials. As a stable inorganic mineral it satisfies the requirements for ion exchange materials in the nuclear industry[47]:

- Resistant to ionising radiation
- High thermal stability
- High chemical stability
- Selectivity of ion intake

Given this, the operators of Sellafield site decided to exclusively use Mud-Hills clinoptilolite as their ion exchange material in the SIXEP process. In columns at SIXEP this process normally removes 98.7 % of the ^{90}Sr and 99.7 % of the ^{137}Cs from aqueous feedstocks.

The structure of clinoptilolite can be defined as zeolitic with three different crystalline aluminosilicate materials[50] with the general formula $M_{3\text{-}6}(Si_{30}Al_6)O_{72}$.$20H_2O$ where M is either Ca, K or Na, X-ray diffraction patterns for which are shown in figure 1.5. Tetrahedra of SiO_4 and AlO_4 make up the unit cell with large cavities with an overall negative charge[47] which enables positive ions to insert themselves. The ratio of aluminium and silicon often varies in zirconia material but with clinoptilolite these stay consistent even between Ca, K and Na variations. Due to interactions with groundwater the mineral can contain more calcium, potassium and magnesium ions at the exchange of sodium, Ca^{2+} and Mg^{2+} have the potential to compete with ^{137}Cs and ^{90}Sr when ion exchanging and therefore are undesirable.

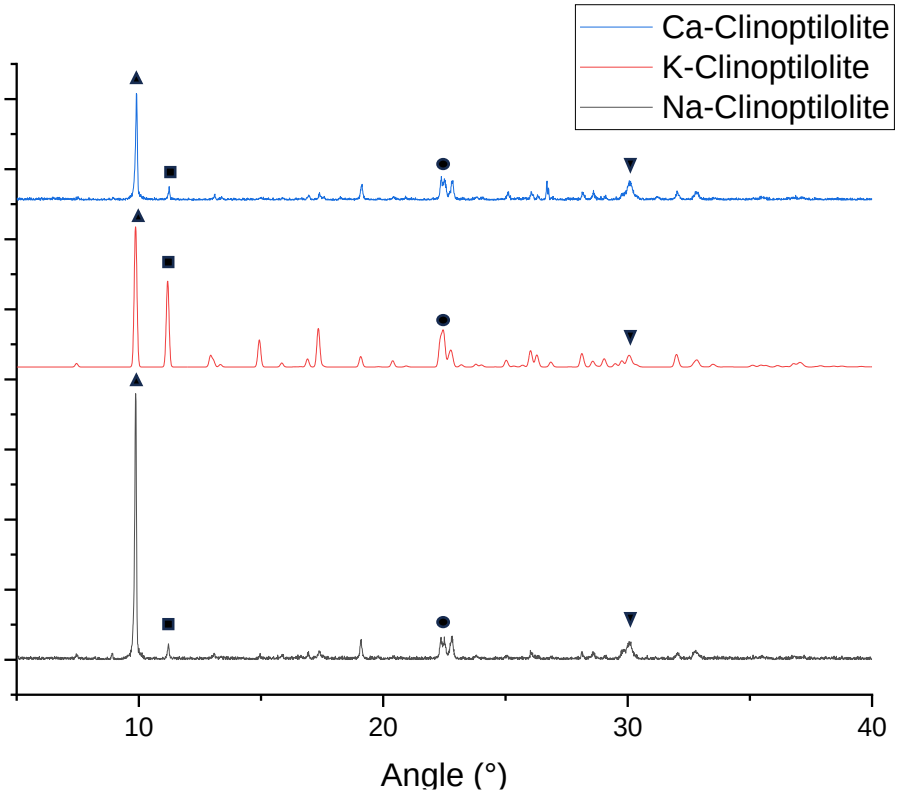

Figure 1.5. X-ray diffraction patterns of three clinoptilolite minerals Ca –, K – and Na – Clinoptilolite[51] Symbols indicate common Bragg peaks, ▲= 9.8 °, ■ = 11.2 °, ● = 22.4 °, ▼ = 30.5 °

As a waste stream in storage its properties are marginally different to the initial material. Besides having ion exchanged radionuclides in their structure, the particle size is also different. As a raw material its size is between 0.5 – 3 mm, whereas after treatment at a maximum the largest single particle size fraction is 35.9 % between 0 – 1.2 µm, however, 64.1 % of the weight is above this size

between 1.2 – 23.7 µm. The range of sizes is very large in certain fractions, as in another settled sand / clinoptilolite mixture 81.5 % of the mass is above 500 µm.

1.3.3 Other Potential Arising Wastes

Graphite has been used as a moderator in fission reactors for a long time, historically used in Magnox reactors[52] graphite contains the fuel and slows down the speed of the nuclear chain reaction[53]. Graphite is now used as a mediator in advanced gas cooled reactors (AGRs) to control the nuclear chain reaction, however, not in older liquid cooled systems. The UK has the largest store of contaminated graphite in the world by mass and it is classed as ILW by the NDA. This comes from the de-canning of the used fuel rods from power generation around the country as the outer irradiated graphite shell is cracked and peeled off the internal fuel rod[54]. More will arise from decommissioning as reactor cores also contain a significant quantity of graphite[52]. RWM in the UK will condition the waste before long term storage by either:

- Cementation and transport to higher level geological disposal facility
- Decontamination and subsequent disposal of less radioactive graphite at near surface sites
- Other future arising pre-treatment technologies for safe storage

One problem with pumping sludge and slurry wastes such as Magnox and sand / clinoptilolite is the particles agglomerating and sticking to the sides of the piping in which they are being transported. A potential deflocculating agent for reducing this effect is xanthan gum[55] a naturally occurring organic compound used as a thickener in food[56] and a deflocculator in industry[57]. Whilst not a large contributor to the waste inventory the addition of this as a deflocculator could have other impacts on waste treatment further down the chain. Graphite and xanthan gum will also be considered in chapter 6 alongside sand/clinoptilolite and CMS for exploring volatility effects on caesium, iodine and chlorine.

1.4 Thermal Treatment Technologies

Many thermal techniques exist for the treatment of waste in industry some of which have been or will be applied to radioactive and toxic waste. Because we wish to perform experiments using similar conditions to that found in industry it is important to understand these going forward. As one of the leading thermal techniques, vitrification is recognised by the International Atomic Energy Agency (IAEA) as a way of treating waste to reduce environmental impact[58]. As the name suggests, it involves the heating of waste (usually with glass forming reagents) to temperatures normally exceeding 1100°C and then, once liquified and then cooled and vitrified the product is usually deposited into a separate container for long-term storage. One of the main reasons for processing the waste in this way is to reduce leaching and the concentration of organics which has been a problem with many current storage methods and historically has been the source of contamination in local areas[59]. Vitrification can provide protection from this and other issues occurring because of the properties of the final glassy wasteform[60]:

- Immobilisation of a wide range of elements
- Volume reduction
- Radiation tolerance
- High chemical durability

The technique also benefits from a large existing knowledge base in the commercial glass sector for melter technology and glass making. Glass has the potential to remain in its state for millions of years, for example, geological samples of obsidian[61] have been estimated to have stayed structurally unchanged for millions of years. For most thermal treatments more than one stage is required to provide a suitable final wasteform and to reduce foaming. For HLW in the UK calcination is a pre-treatment step before vitrification, dissolved in a highly active liquor (HAL) and is then baked in a rotating kiln to produce a powder[25]. This is then gravity fed into an induction melter at around 1050 °C with glass frit and subsequently poured in steel containers for storage[62]. In this study we will maintain

a melting temperature similar to that found in HLW treatment (1050 – 1150 °C) and not exceed this to ensure we remain consistent with industrial procedure. This section will now give an overview of melting technologies that are available and used within the nuclear industry.

1.4.1 Cold Crucible Induction Melting

The first thermal treatment technology we will discuss is cold crucible induction melting (CCIM) which was developed in Germany in 1931[63] for melting of alloyed metals. The approach was modified later on for the conditioning of nuclear waste in France at the La Hague facility[64]. CCIM has been used for the conditioning of HLW by many countries including France, Russia and the USA[63]. The process of melting is done by induction coils (figure 1.6) that run around the crucible producing an electromagnetic field in the centre containing the waste, the crucible

itself is (usually water) cooled. With this setup the melter can provide significant corrosion protection to the crucible walls as the material in contact with the walls will be largely unmelted due to the cooling[11]. This is especially useful for some radioactive wastes as the products can be incredibly corrosive to crucibles and can reduce the lifespan of the melter. They can be scaled up to large industrial sized units which can be used for high throughput, continuous HLW treatment which has been implemented in France and the USA whilst also being used for ILW in Russia[64]. Generally, the CCIM systems have been more commonly used for homogeneous liquid wastes such as sludges to be

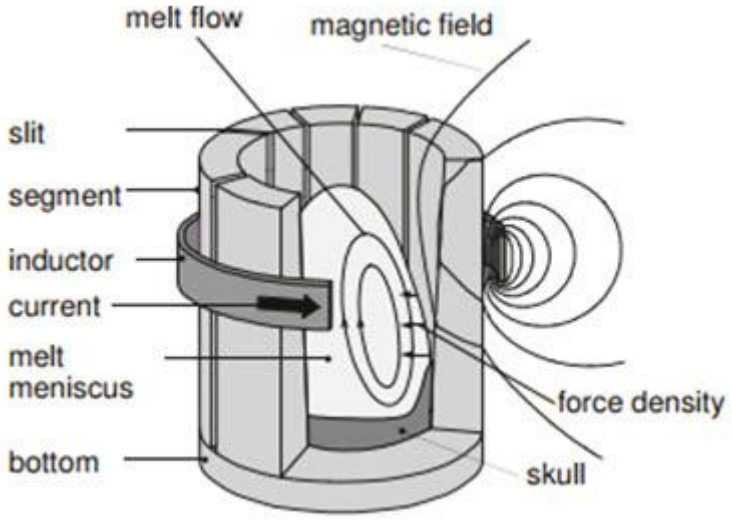

added to the glass forming agents. CCIMs function with a cold cap which, similarly to the walls, is a lower temperature part of the melt that usually contains unmelted batch and waste materials. The cold cap can have negative and positive impacts on the volatility of particulate pollutants but it is thought that it can act as a capture/filter for volatile compounds.

Figure 1.6. Diagram of CCIM operation[65]

The disadvantage of this thermal treatment technique is that it may have issues in dealing with large solid waste melting and the operating temperature is normally much higher than other technologies which can increase volatilisation of components[66].

1.4.2 Joule Heated Ceramic Melting

The next thermal treatment technology under consideration is the Joule heated ceramic melter (JHCM) which is the most widely used worldwide because of its reputation as a proven technology. JHCMs use electrodes to heat the glass/waste by passing high current through the conducting parts of the waste which is then increased as the waste becomes liquid. The liquid melt is fed in through the roof (figure 1.7) and is in contact with refractory walls when heated which does give it a disadvantage over CCIM as refractory corrosion is an ever present and expensive problem[64]. As reliable as the system is, the pouring of glass from the output has always presented challenges. One workaround for this and other issues is a process called in-container vitrification, an example of which has been developed by Veolia[26], this is the Geomelt system (figure. 1.1). In-container vitrification (ICV) works in a similar way where electrodes are used to heat the waste and frit to temperatures exceeding 1000°C, however, the melting vessel is also the containment for the wasteform. The benefit of this is that the viscosity of the glass for pouring is no longer a factor which means high viscosity glasses such as soda lime silicates can be used where they could not be for continuous processes. Different glass compositions being available could lead to increases in waste loading, however, included in this package is the electrodes themselves therefore volume and cost are both increased. As the container is considered part of the waste, the process of ICV is a batch process which means that the volume of

waste processed at any given time is significantly reduced when compared to continuous processes such as CCIM.

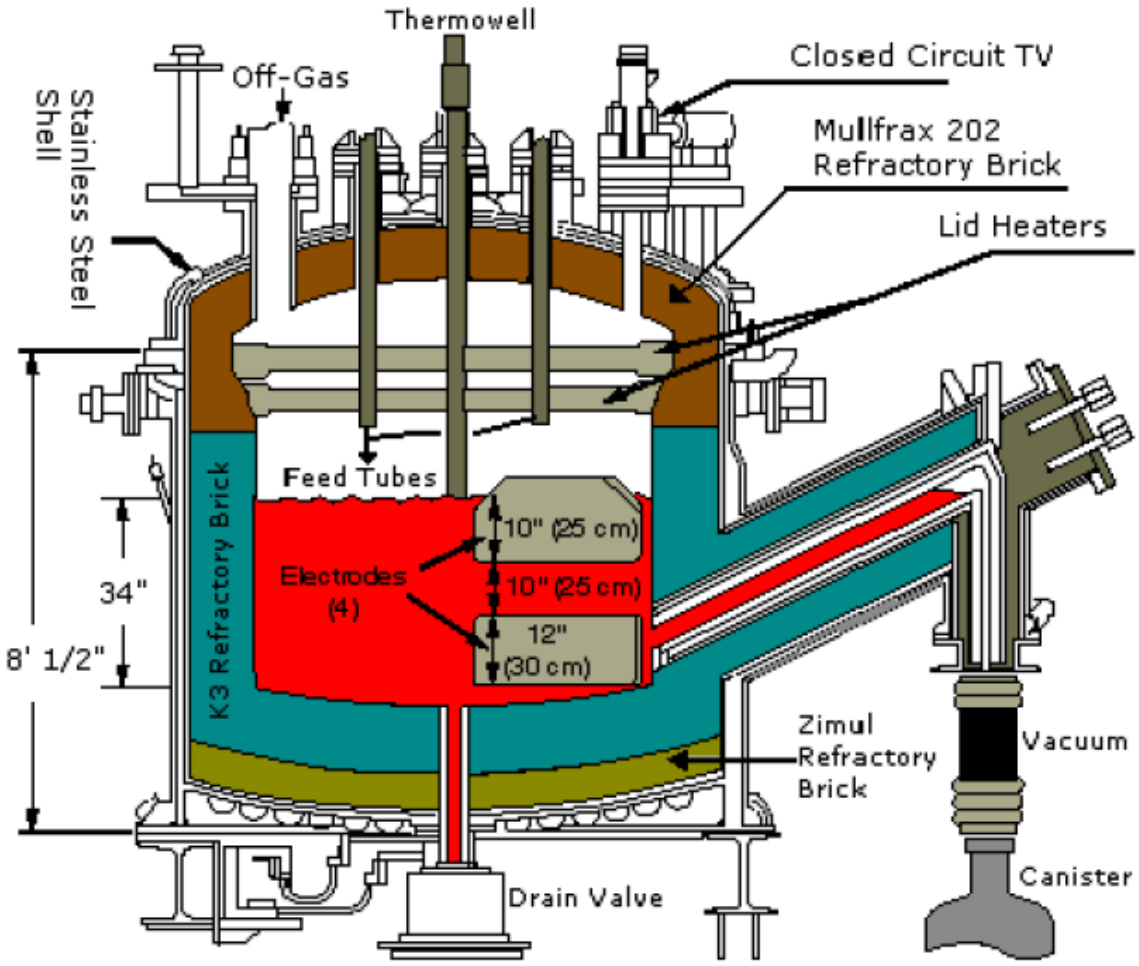

Figure 1.7. Joule Heated Ceramic melter[64]

1.4.3 Plasma Melting Technology

Plasma heat treatment is similar to other continuous processes, but, the energy is imparted to the waste/glass by plasma arc electrodes above the chamber. This technique has been used to treat municipal waste for some years[64] and now it is being applied to radioactive ILW and LLW in Switzerland at the Zwilag facility[24]. Originally applied to metallurgy, plasma heating has the potential to be more effective towards heterogeneous batches with materials such as cements, metals and ceramics which is very common among UK PCM. In fact, the Zwilag facility is designed to be fed by steel barrel (figure 1.8) not dissimilar to the PCM barrels in UK storage. The main negative with this thermal treatment

technology is the high temperatures the waste is subjected to which results in total destruction of organics and high volatilisation. Nearly all plasma plants need to operate with a sophisticated off-gas conditioning system to deal with this.

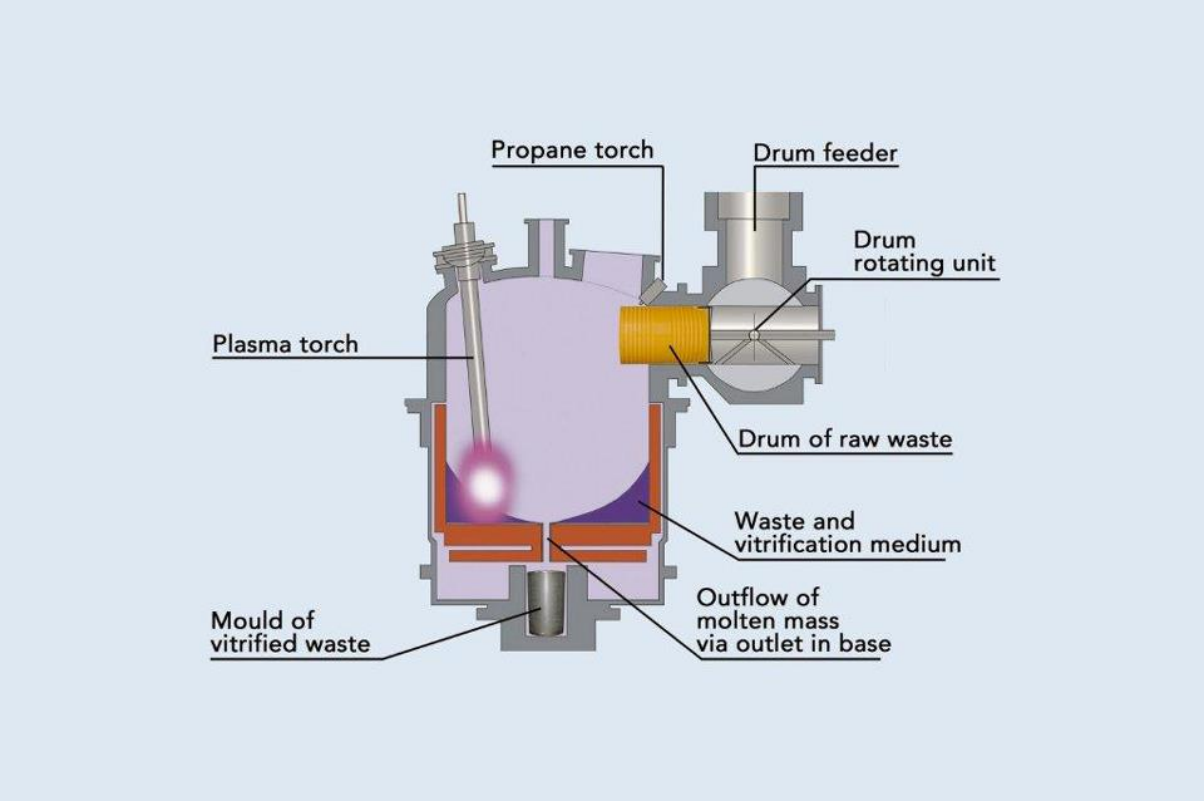

Figure 1.8. ZWILAG Plasma Treatment Facility[67]

1.4.4 Hot Isostatic Pressing

The final processing technique under discussion is hot isostatic pressing (HIP) which has been in development since the 1950s for the treatment of radioactive contamination (figure 1.9). The process involves heating and compressing at high pressure to form either a ceramic or glass-ceramic similar to geological composites found in nature[68]. Initially HIP was used to produce nuclear fuel packages for reactors and after this it was developed in the UK at Sellafield and the ANSTO Lucas Heights facility in Australia for the processing of plutonium[64]. The nature of this technique means it can be used for many different heterogeneous wastes, however, compared to vitrification the volume reduction is smaller which ultimately means the waste packets at the end are larger in volume. In addition, HIP is

a batch process and can only be used on a small kg scale currently but has very little emissions in terms of off gas due to being in sealed containers[66].

Figure 1.9. Hot Isostatic Pressing canister before and after processing[69]

A few other techniques are of note such as other furnaces that have proven to be effective. Rotary kiln, cyclone and electric arc all fall into these categories, however, they are not commonly used unless in specific circumstances for example contaminated soil processing. These all have issues with the amount of volatilisation occurring in these melts usually due to high temperatures.

These techniques all have potential to be a ILW treatment technology and could present some significant differences to the end wasteform. CCIM, HIP and JHCM if used to treat waste are likely to have melting temperatures between 1050 – 1150 °C, whereas plasma would exceed these temperatures significantly to around 1400 – 1500 °C. However, given the current HLW method of CCIM we suggest that the use of melting temperatures in this study should be between 1050 – 1150 °C. The temperatures used in this study reflect the melting temperatures available for different thermal treatment technologies, therefore we will look at upper limit glasses for plasma (1400 – 1500 °C) and lower limit glasses for CCIM/HIP/JHCM (1000 – 1150 °C).

Chapter 2 Glasses in the Nuclear Industry

Waste from the nuclear industry is remediated by the use of high temperature melting of the material and this could be applied to ILW with research. The development of thermal treatment for nuclear waste many waste remediation bodies worldwide have opted for glassy end products by adding fritted glass or batch raw materials to the radioactively contaminated waste and melting both together to incorporate them into each other. This is to ensure the wasteforms' durability over potentially millions of years on a 'geological timeframe' where the final product remains as close, physically and chemically, to the initial product as possible[66]. This includes but is not limited to physical properties such as mechanical strength, radiation tolerance, shock resistance, thermal resistance (to freezing or high temperature events), viscosity and volume. The total package has to withstand the acute shock of transport and also the prolonged effects of potentially thousands to millions of years storage. Figure 2.1 demonstrates the barriers that are put in place to protect the biosphere from contact with the radioactive waste over this timeframe[70]. A principal barrier is the encapsulation of the radionuclide in the treated wasteform, whether that be a cemented, ceramic, glass or glass-ceramic matrix. A successful wasteform will reduce the release of radioactive material in the event any of the other barriers fail and remain unchanged in case of any change in temperature from decay, changes in radioactive release or mechanical strain. It must also not leach upon contact with any solvent as this could remove radioactive material and deposit it elsewhere without the safety and stability that the wasteform provides. The next two barriers are engineered barriers that are put in place to reduce the chances of release to environment in the event of the wasteform failing in any way. In direct contact with the waste is the waste package that contains the wasteform and ensures that it remains dry, ventilated and encapsulated.

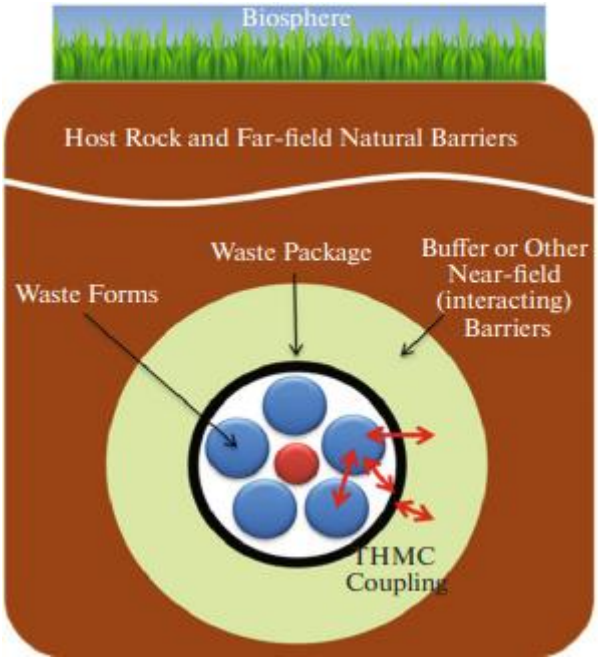

Figure 2.1. Representation of the barriers between radioactive waste and the biosphere[66]

For example, in the UK this could include stainless steel containers, concrete boxes, cast iron, copper, titanium, nickel alloy, and carbon steel canisters[71], in Sweden and Finland copper canisters are used for their corrosion resistance. The next is a group of THMC (thermal, hydraulic, mechanical and chemical) barriers. These are larger in scale and are designed to contain and protect all of the packages in storage by adding a buffer between the geology of the landscape and the waste package. This could include, air gaps, backfills and seals[72]. Clay backfills have been used at high level Swiss disposal sites by NAGRA (Nationale Genossenschaft für die Lagerung radioaktiver Abfälle) and are proposed as a future barrier for Canadian, Finnish, Japanese Spanish and Swedish GDFs[73]. Most backfills use a mixture of sand and bentonite because of its thermal, hydrological and mechanical properties in order to keep the material dry whilst not swelling significantly.. There is also a high radiation dose required to amorphise the backfill which keeps the material properties consistent. A natural barrier is the final layer of protection using the geology of the formations around the GDF to protect and dry the wasteform. The features of these rock formations could include[28]:

- High Strength metamorphic or aged sedimentary, using natural strength and non-permeability

- Sedimentary rock such as clay, using natural non-permeability
- Rock salt formations, using their natural drying properties

To satisfy the high demands of the wasteform requirements, glass and glass/ceramic hosts were postulated by many radioactive waste treatment organisations around the world. Currently the UK uses a borosilicate glass composition to vitrify its HLW and as of 2013 the UK had 844 m^3 of vitrified HLW product[28] in interim storage. The borosilicate glass network provides a flexible structure which waste actinides and other elements can insert themselves in, ionically between non-bridging oxygen atoms or covalently bonded to silica atoms figure 2.2. These are dissolved in the glass forming materials or frit upon heating and dispersed throughout the randomly ordered structure.

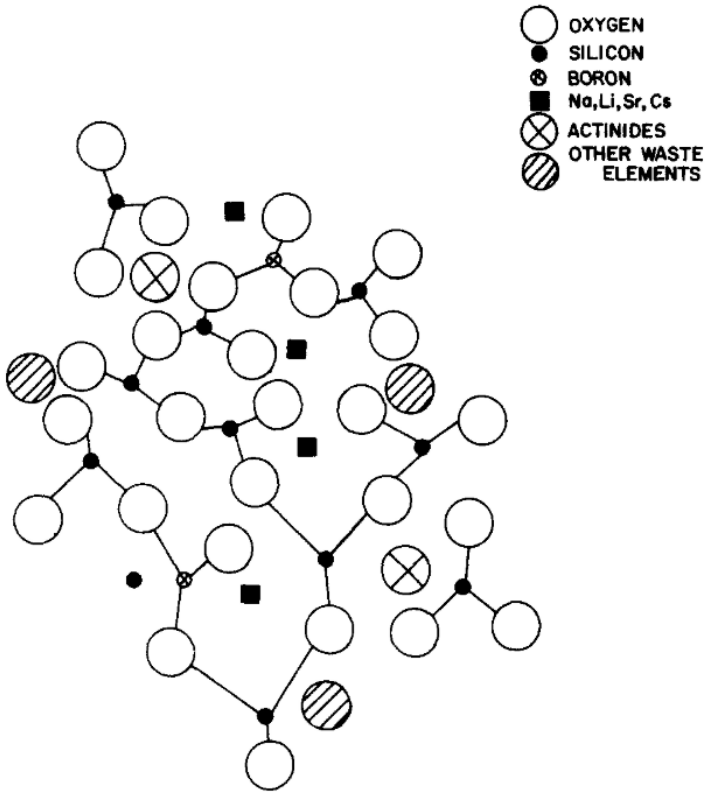

Figure 2.2. Illustration of waste incorporation into a borosilicate glass network[74]

Jantzen *et al.* outlines the current countries using glass based hosts (table 2.2) and the glasses that are used[66]. Most use silicate and borosilicate glasses because of their lower melting temperatures, durability and waste loading, however, Russian waste treatment of HLW uses an alumino-phosphate glass because of its lower operating temperature and its potential[77] to capture aluminium and volatile

waste components such as ^{129}I, $^{35.5}Cl$ or ^{137}Cs. Most other organisations have avoided phosphate glasses (table 2.1), however, because of the durability and high corrosivity of the melt on the crucible or refractory[75]. Phosphate glasses have equivalent or poorer chemical durability and resistance to moisture compared to borosilicates, the reasons for this are the lower covalent bond enthalpy of P-O bonds (335 kJ/mol) compared to Si-O Bonds (452 kJ/mol) and the percentage of NBOs also being larger in pure phosphate glasses (~60 %). This is mediated by the addition of aluminium.

	Durability and Stability[66]	**Solubility of Pu, U, Am (wt%)**	**Processing Temperature**[76–78] **(°C)**	**Countries in Use**[79]
Borosilicate	Good	0.55 – 40	1000-1500	BEL, CAN, CHE, CHN, FRA, GER, JPN, KOR, UK, US
Aluminosilicate	Excellent	30	1350	CAN
Soda Lime Silicate	Good	19 – 52.7	1250	None
Phosphate	Good - Poor	2 – 10	1100	RUS

Table 2.1 Glass types used for nuclear waste immobilisation[66]

Compositions for waste encapsulation glasses currently in use are listed below in table 2.2, most being variations on borosilicate glasses. In the 'other' row notable oxides are Li_2O which is a major component in the UK CaZn glass as well as the French HLW glass. K_2O makes up around 8 wt% of the Korean waste glass and TiO_2 appears in many compositions in small quantities. Silica content varies

	Composition (wt%)								
	BEL HLW	GER HLW	US LAW, HLW	UK HLW (CaZn)	FRA HLW (Hauge)	JPN HLW	CHN HLW	KOR LILW (DG2)	RUS LILW, HLW
SiO_2	52.7	50.4	49.8	47.6	47.2	46.6	44.9	41.5	-
B_2O_3	13.2	14.8	8.0	23.4	14.9	14.2	12.3	12.5	-
Na_2O	5.9	10.3	8.7	8.6	10.6	10.0	11.6	8.0	21.2
Al_2O_3	2.7	2.6	4.0	4.2	4.4	5.0	5.0	7.3	19.0
CaO	4.6	4.5	1.0	6.0	4.1	3.0	6.7	10.5	-
MgO	2.2	1.8	1.4	-	-	-	4.4	1.9	-
P_2O_5	-	-	-	-	-	0.29	-	0.8	52.0
Other*	18.7	15.6	27.1	10.2	18.8	20.9	15.1	17.7	7.8

Table 2.2 Outline of glass compositions used globally[62,66,80] *Other components of the glass composition not common between countries (e.g. Li_2O, K_2O)

between 41.5 - 52.7 wt% and the B_2O_3 content between 8 – 23.4 wt% except for the boron-free phosphate glass. One of the main differences between the borosilicate glass types is in the oxide additives used such as lithium, potassium and titanium. Some compositions also commonly add magnesium to produce stable secondary phases for the immobilisation of some problematic elements[81]. The other is in borate content between US and UK based glasses which are different because of the different types of waste that the glasses are required to incorporate in each country.

Many of the radioactive waste glasses used in the nuclear industry are borosilicates influenced by the French R7T7[81] and reference glass SON68[82]. MW/CaZn was developed independently for HLW immobilisation in the UK and the DWPF/LAWA44/HAN28F glasses developed in the USA[83]. The UK developed its simpler 4 component glass optimised with lithium oxide when Hall et al[84] and Dalton et al[85] discovered a reduced leach rate when substituting sodium for lithium oxide. Over 14 days the leach rate with no lithium was 7.3 x 10^{-7} g/cm^2 whereas for lithium containing glasses this reduced to 4.4 x 10^{-9} g/cm^2. During these studies other additives were also attempted, TiO_2, Fe_2O_3, CaO, ZnO, Nd_2O_3 and Al_2O_3, and these were found to not improve the leaching rate which was one of the main decision factors when they were being developed, the only exception was Al_2O_3 where the leach rate was significantly reduced but at a trade-off of an increased viscosity and crystallising the glass. For these reasons initially aluminium was not a component (table 2.2) of the original UK reference glasses which were, in time order, M5, M22 and the later MW[86] which were developed over 20 years.

The more complex 7 component CaZn glass is a modified MW glass intended to create more durable calcium molybdate crystalline secondary phase as MW has issues with the formation of water soluble 'yellow phase' once the solubility limit of Mo is exceeded[87]. Table 2.3 shows the evolution of these glasses to include new components. CaZn composition was altered to include Al_2O_3, CaO and ZnO substituting out SiO_2 and Na_2O and increasing B_2O_3 content to combat viscosity increase inherent with the Al_2O_3 increase.

	Composition (wt%)							
	FRA Waste Glasses		UK Waste Glasses					Comparison
	R7T7	SON68	M5	M22	MW	CaZn	MW ½ Li	International Simple Glass
SiO_2	45.28	45.85	55.48	68.51	61.75	47.6	63.42	56.2
B_2O_3	13.97	14.14	29.28	14.94	21.88	23.4	22.50	17.3
Na_2O	10.1	10.22	10.29	11.17	11.05	8.6	11.35	12.2
Al_2O_3	4.94	5.00	-	-	-	4.2	-	6.0
CaO	4.02	4.07	-	-	-	6.0	-	5.0
ZrO_2	2.72	2.75	-	-	-	-	-	3.3
Li_2O	1.97	1.99	4.95	5.38	5.33	4.2	2.74	-
ZnO	2.5	2.53	-	-	-	6.0	-	-

Table 2.3 Development of UK base glasses for encapsulation of radioactive waste[62,81,86]. International simple glass (ISG) is a benchmarking research glass intended to provide a comparison.

Phase separation (for example the molybdate formation in CaZn)[88] is common in radioactive waste glass research, however, is generally undesirable in the end product. Separations from the glasses could be more soluble in water, less durable or start fault lines in the glass that leads to an overall reduced lifespan of the wasteform[87]. There have been many papers modifying glass compositions to reduce phase separation from certain 'problematic' elements such as molybdenum[89], sulphur[90], platinoids (Ru, Rh, Pd)[62], iron, nickel, chromium and cerium. However, in some cases the waste loading of certain elements can be increased without compromising on durability. This is due to the loading capacity of the glass being overcome and the precipitated stable crystals dispersing throughout the glass homogeneously more akin to a glass/ceramic. Another composition of note is the international simple glass (ISG) which is a benchmarking research glass simplified from French SON68 intended to provide a comparison glass so that multiple countries could collaborate and share data[91], it is included in table 2.3 as a comparison to an international standard.

2.1 Structure of Glasses

Glass is defined as "an amorphous solid with no long range order that exhibits glass transition behavior"[92]. Glass transition occurs as a material is heated and reaches a viscoelastic state where the atomic structure becomes disordered which is represented also by enthalpy change. The material becomes softened and can be deformed more easily, this is separate to melting temperature where

the material transitions from solid to liquid. If a material is cooled slowly crystallisation will occur after passing under the glass transition temperature. However, if this material is rapidly cooled there is potential for glass to be formed from a supercooled liquid. This essentially freezes the structure of the liquid retaining the disordered and amorphous structure that is characteristic of glass[60]. This temperature that is known as the glass transition temperature (T_g) and can be used to approximate when the supercooled liquid solidifies.

For a substance to be a glass certain structural criteria need to be met. In work by Zachariasen[92] he established that silicate glasses formed SiO_4 tetrahedra which were bonded at each corner via Si-O-Si bridges (figure 2.3). From these results he created empirical rules for glass forming structures:

- The material must contain a high number of cations atoms which are surrounded by oxygen triangles or tetrahedra
- The only connections that can occur is bonding at the corners of these triangles and tetrahedra
- Some oxygen atoms must be bonded to two of these triangles or tetrahedra

Under these rules a glass is likely to form, however, there must still be other conditions fulfilled as a requirement for production of a successful glass. These mostly can be encompassed as overcoming the enthalpic and entropic barriers that stop a glass from forming.

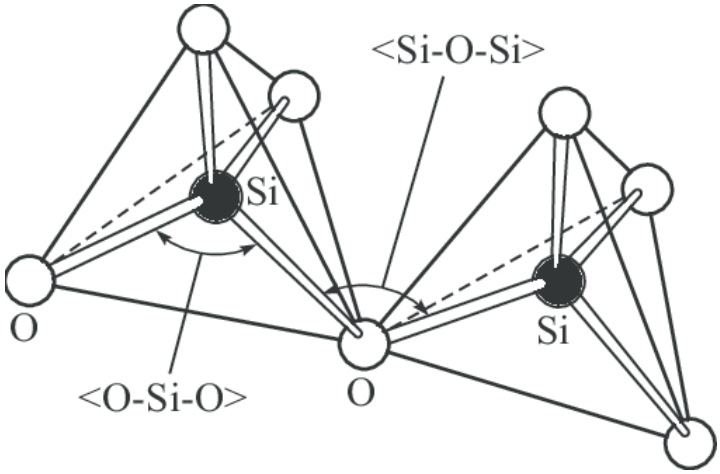

Figure 2.3. Diagram of silica tetrahedra linked to another tetrahedra[93]

Glass structure is sometimes defined by the number of oxygen atoms bonded to each atom (usually the glass former eg. Si, B) and the number of bridging or non-bridging oxygen atoms. Bridging oxygens are named as such because they are covalently bonded to two glass forming atoms connecting the structure together[94]. There are also non-bridging oxygens (NBOs) which are oxygen atoms not connected to another glass forming atom terminating in a negatively charged ion. Certain glass components can alter or interrupt this structure by inserting between the oxygen and glass forming atoms resulting in an increase in NBOs.

One such component is flux (for example Na_2O, CaO) which ionically bonds to the negative oxygen vacancy creating a break in the structure[95]. Particularly in silicate glasses the concentration of non-bridging oxygen atoms in the structure can reveal properties of the glass as a whole and provide a model for the bulk material. This can be notated by Q-speciation which is the concentration of a certain tetrahedron unit depending on how many bonds the tetrahedra have to oxygen atoms in the glass structure. A defect free glass with no modifiers will likely consist fully of Q_4 units meaning in a silicate glass a silicon atom has four adjacent bonded bridging oxygen atoms. In vitreous silica (SiO_4) that tetrahedron will be bonded directly to another tetrahedron by an oxygen atom (figure 2.3) and will have a Si – O bond angle[96] around 147 °.

The variation in positioning of these tetrahedra is what differentiates amorphous silica from crystalline forms of silica such as quartz or cristobalite. This seemingly small change can have a large effect on physical properties of the material even transparency and strength. Figure 2.4 highlights the structural differences (2 dimensionally) between the two materials, the tetrahedra are still the same individually, however, how they link together is different, the ordered atomic structure in 2.4 (b) represents a crystalline form of silica whereas vitreous silica has a disordered structure in 2.4 (c).

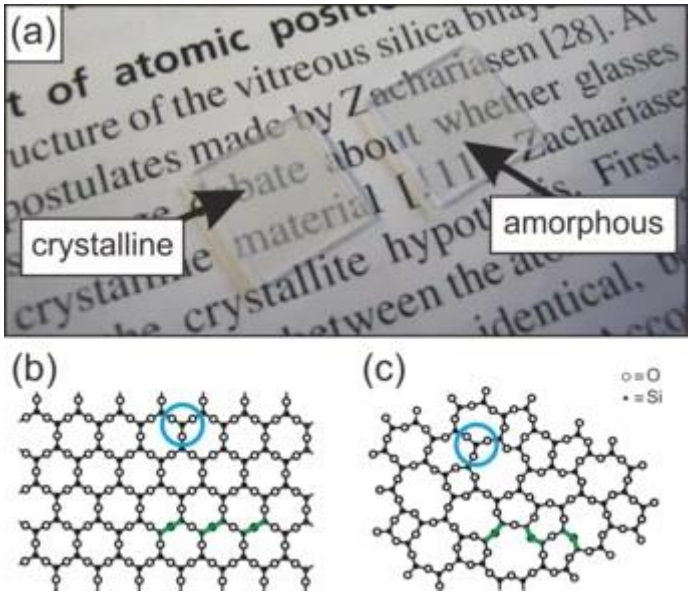

Figure 2.4. Comparison between crystalline and amorphous atomic structures of silica a) Image of quartz (left) and amorphous silica (right). b) Atomic structure of crystalline silica. c) demonstration of the atomic structure of amorphous silica[97]. Structure is represented in 2d and therefore the 4th coordinated site is not visible.

As alkali ions are added into the structure a decrease in Q_4 unit concentration and an increase in Q_3-Q_1 occurs as units of the bridging oxygen bonds in the network are disrupted with alkali ions. These are called glass or network modifiers and will be discussed in more detail in section 2.3.

In silicate glasses the covalent glass forming bonds are between silicon and oxygen atoms to form tetrahedra that can be defined by Q_n speciation. Borate glasses however, can contain different coordination numbers readily and therefore cannot be described directly in the same way (see figure 2.5). Borate units in glasses are still bond by corners of their structure by oxygen atoms, however, one of the differences in structure comes from the possibility of three coordinated BO_3 and four coordinated BO_4 groups arising. In pure vitreous B_2O_3 boron and oxygen exist as a network of predominantly six membered rings consisting of three BO_3 groups[98] and joined together by B – O bonds at each boron atom coupled with van der Waals interactions between rings. The interactions are weak as B – O bonds (536 kJ/mol, T_m= 171 °C) are less strong than Si – O (452 kJ/mol, T_m=1700 °C) resulting in a lower melting temperature compared to pure silicate glasses and a much lower strength[99] with another trade-off that most borate glasses are much more water soluble[100].

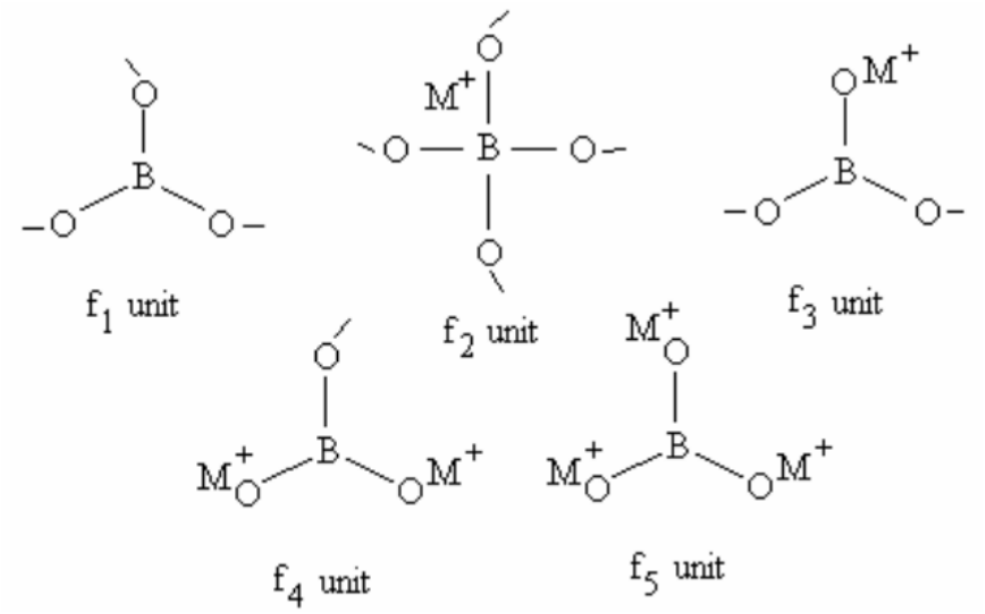

Figure 2.5. Borate subunits that can exist in boron containing glass systems, M^+ represents a positive alkali ion[101]

Alkali borate glasses can have groups within the structure which are defined as units f1 - f5, shown in figure 2.5. Some of these require alkali ions to exist which can apply to both amorphous and crystalline borates. We have seen previously that glassy B_2O_3 consists only of BO_3 units and therefore must only satisfy the f_1 unit conditions. However, upon the addition of an alkali metal we can see two different coordination numbers can occur for each individual group structures spanning units f_1 to f_5. This is corroborated by experimental studies[98] which show an increase in four coordinated tetrahedral borate groups upon increasing alkali concentration. For lithium oxide this reaches a maximum of 45% of glass proportionally being four coordinated at 38 mol% Li_2O which drops more upon increasing concentration (figure 2.6).

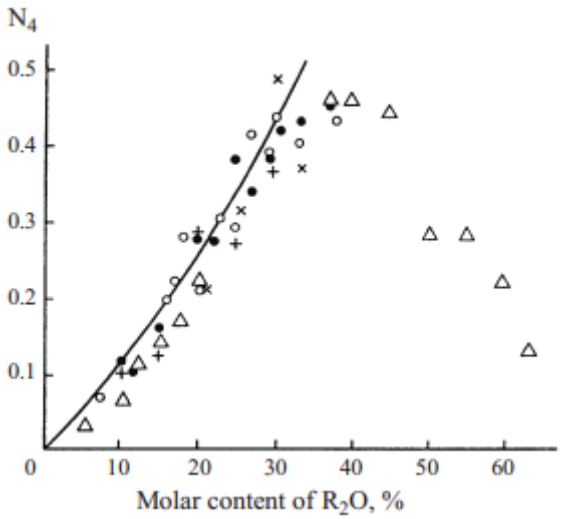

Figure 2.6. Proportion of four coordinated boron (N_4) dependant on alkali (R_2O) concentration[102], • = Na_2O, ○ = K_2O, △ = Li_2O, + = Pb_2O, x = Cs_2O

2.2 Modifiers and Formers

As we have discussed batch reagents used in glass melting can have many different properties and effects on the melt environment such as viscosity, softening temperature and on the final products colour, durability, etc. They can be designated as any number of the following[92]:

- Glass Formers
- Flux
- Glass Modifiers
- Colourants
- Fining agents

These properties may change for each reagent depending on the glass they are in, but the categories still describe the effect of those materials. Table 2.4 shows common batch materials used in the commercial and nuclear glass industry all of which are added to either form glasses, increase durability or reduce processing temperature.

Batch Material	Oxide	Effect on Glass
SiO_2 (Sand)	SiO_2	Glass Forming
H_3BO_3 (Boric Acid)	B_2O_3	Glass Forming
$NH_4H_2PO_4$	P_2O_5	Glass Forming
Li_2CO_3	Li_2O	Network Modifier
Na_2CO_3 (Soda Ash)	Na_2O	Network Modifier/Flux
K_2CO_3 (Potash)	K_2O	Network Modifier/Flux
PbO	PbO	Network Modifier/Flux
ZnO	ZnO	Intermediary
$CaCO_3$ (Limestone)	CaO	Network Modifier
$MgCO_3$/$Mg(OH)_2$	MgO	Network Modifier, Chemical Durability, Hardness
$Al(OH)_3$	Al_2O_3	Intermediary, Hardness
Fe_2O_3	Fe_2O_3	Strength, Purity of Colour (low concentration), Colourant (high concentration)
Cs_2CO_3	Cs_2O	Flux, Charge Compensation

Table 2.4 Example batch materials and their effect on glass chemistry[89,92,103–109]

Colourants and fining agents are primarily used in the commercial glass industry to improve the appearance, clarity or colour of a glass and therefore have less importance in nuclear waste vitrification. Network modifiers are commonly alkali oxides such as Li_2O or Na_2O based on their ability to interrupt the network[110] to decrease viscosity, improve workability and reduce melting temperatures in silicate systems. This occurs by ions interrupting the linked network of (for example) Si – O, B – O, Al – O bonds to create oxygen atoms than are ionically bonded rather than covalently bonded[111,112] to another glass forming atom. This can be applied to all the alkali metals in group 1 of the periodic table[99]. The strength of these bonds are much lower[92] which has the effect of lowering melting temperature of the glass system. Without these commercial and nuclear glasses would cost significantly more to produce, volatilise more of the raw materials/waste and emit more carbon through use of energy/fuel. PbO is an interesting example of a well-used glass component that acts a modifier without being in group 1 or 2 of the periodic table[113]. Originally used for commercial glasses lead has been used in more modern applications such as radiation shielding glass, optics and sealants[114]. Rarely discussed in the nuclear industry due to its toxicity[115] PbO has some interesting characteristics that have been studied, resistance to devitrification and lowered melting temperatures

and increased chemical durability[113], however, it is unlikely these will ever overcome the toxicity safety case for using this material.

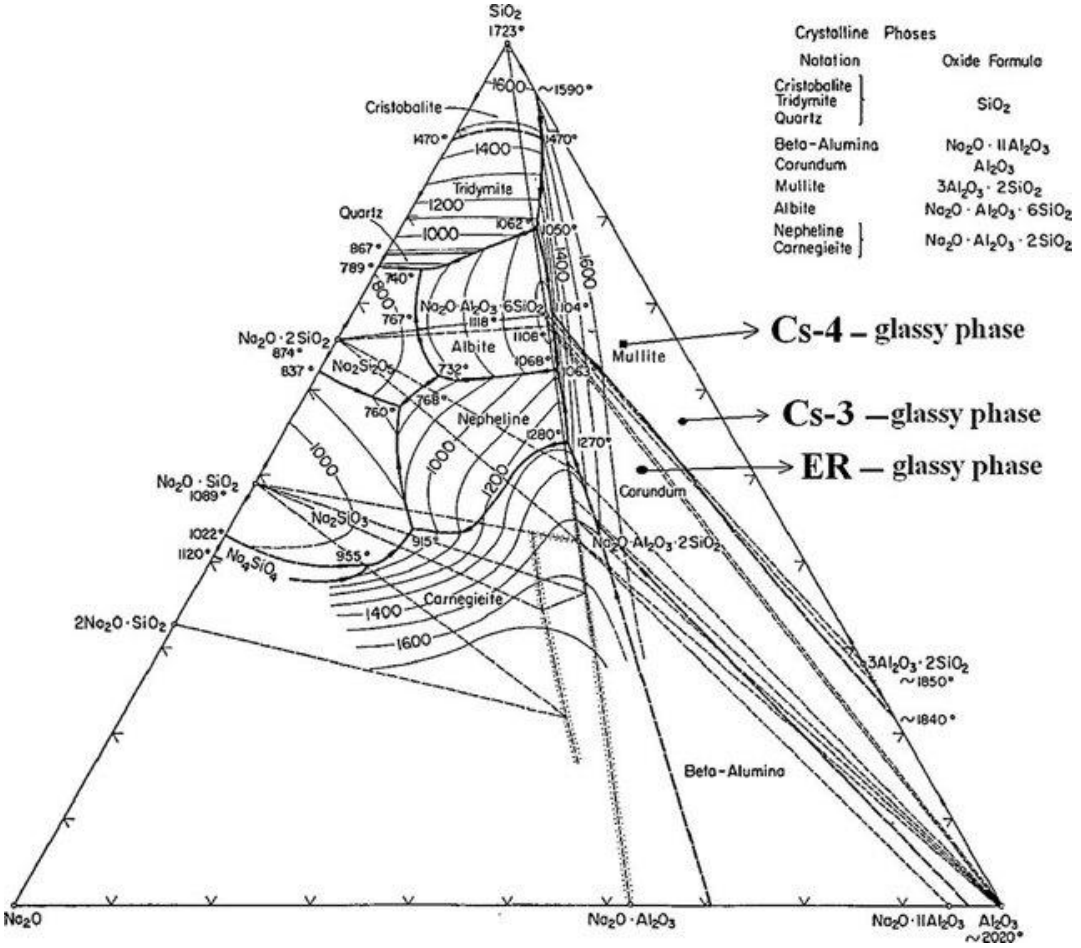

Figure 2.7. Phase diagram of the Al_2O_3.Na_2O.SiO_2 systems[116]

Al_2O_3 and ZnO (components of the CaZn formulation) are intermediary compounds[103,107] in the glass structure which in this case means they can fulfil the role of a network former or modifier depending on the composition. The glass modifier aspect is evident in simple two component aluminosilicate matrices[117] as in the phase diagram liquidus (figure 2.7) temperature decreases as aluminium content increases (reaching a minimum T_{liq} at 577 °C at 87.8 mol% Al / 12.2 mol% Si), viscosity reduces[118] as aluminium content increases, however, increasing T_g [103]. The coordination of aluminium in the structure can change to facilitate this. The NMR of silicate glasses show a higher proportion of NBOs when containing alumina[118], disrupting the Si-O network similar to alkali modifiers. However, the formation of alumina units and Al – O – Si and Al – O – Al bonding also suggests that aluminium can glass form[118].

In aluminoborate glasses aluminium has mainly a forming role in the system with a coordination number of between 4 and 6. Upon the addition of Li^+ and Mg^{2+} modifiers aluminium coordination number decreases in a similar manner to silicon containing glasses. Coordination can vary from 4-6 in glasses reducing in coordination with a higher proportion of silica/borate[119]. In the waste glasses in table 2.3 aluminium concentration is low and therefore there is a higher proportion of 4 coordinated aluminium ions. Given this, it can be shown that modifiers impact the role that aluminium has in silicate and borate glasses more glass forming aluminium units exist with increasing charge stabilising elements[120] such at Li^+ and Mg^{2+}.

Zinc acts in a different way, however, the charge stabilisation facts can be applied to ZnO where Zn – O – Si bonds can form and also zinc ions can interact with the network interstitially[103], increasing the proportion of NBOs. The glasses formed from zinc bearing additives require a glass former to remain amorphous whereas aluminium oxides do not. As the role of zinc is slightly different to Al_2O_3 although as T_g increases (to a lesser degree) in silicate melts there is more likelihood to form glass/ceramic phases such as Zn_2SiO_4, $NaAlSiO_4$ and $KAlSi_2O_6$.

2.3.1 Effect of Water

Most glass batches will contain chemically bound water in them either physisorbed water from moisture in the air or chemically bound into the crystal structure. With the case of vitrified sludges water is a component of the waste[27], particularly for Magnox sludge waste and sand/clinoptilolite mixtures as they contain 8.37 – 15.05 wt% water by mass and this could have an effect on the properties of the glass and even volatility[121], this therefore cannot be discounted. This can have a large effect on the structure of the glass by introducing hydroxyl groups such as Si-OH into the network, this can reduce the concentration of non-bridging oxygens which has implications for the properties of the glass. The usual effect on commercial glasses is calculating for weighing error in batches, however, in natural glasses there is a large increase in hydroxyl groups[92]. Water vapour from the batch or

atmosphere reacts with glass forming oxides to terminate the group in a hydroxyl by a version of the following reaction:

$$Si - O - Si \; + \; H_2O \rightarrow Si - OH + Si - OH$$

Addition of halides and reduction in melting temperature can have an effect on the quantity of -OH bonds forming in the glass structure which can affect the properties of the glass, drying of gas above the melt can also reduce this.

2.3 Incorporation of Key Elements into Glass Structures

2.3.1 Caesium in Glass

Caesium is a group I element and exists as Cs_2O in amorphous glasses, its oxide effects the glass melt conditions similarly to sodium and other alkali metals. The element is not used in many commercial glasses other than very specific optical and ion exchange applications[122] therefore its primary occurrence is in nuclear waste glasses when adding waste that contains decaying minor actinides. In the structure Cs^+ ions depolymerise the glass network by creating non bridging oxygen atom sites and charge compensating BO_4 and AlO_4 subunits in that vacancy[13]. These can then be classified as a network modifier cation when applied to the borosilicate glass network. Increasing caesium content in silicate glasses has been shown by O'Shaughnessy et al[123] to increase $Q_{1\text{-}3}$ speciation and decrease the concentration of Q_4 species, this effect increases with temperature. Parkinson et al[19] also saw a large increase in Q_3 species upon raising Cs concentration in MW and similar type radioactive waste borosilicate glasses confirming this. This can be seen by NMR where Q_2/Q_3 units are much more common in borosilicate glasses containing 35 mol% Cs_2O compared to 15 mol% when substituting for boron.

Other physical properties in borosilicate glasses are also effected; as Cs_2O concentration increases Parkinson et al described an increase in density and molar volume in borosilicate glasses related to

the relatively large size of Cs atoms in the glass structure reducing void sizes throughout the structure[19]. In addition, T_g is lower for glasses containing caesium which is an effect of modifying the glass structure similar to sodium fluxes where bonds are weakened in the silicate structure[124] to reduce melting temperature. In pure B_2O_3 borate glass the addition of caesium also creates a more disconnected network with more NBOs and the proportion of 4 fold boron sites decreasing with increasing caesium content[122] with the potential for crystalising caesium petaborate ($Cs_2O.5B_2O_3$) or triborate ($Cs_2O.3B_2O_3$) in pure boric oxide. Januchta et al[125] developed a caesium based aluminoborate glass with the formula $25Cs_2O – 20Al_2O_3 – 55B_2O_3$. Caesium and aluminium were added improve the glass properties by decreasing the brittleness of soda lime silicate/aluminosilicate/borate compositions. In this glass boron and aluminium are acting as glass forming agents with caesium modifying the network similar to its role in silicate glasses. Brittleness was greatly decreased compared to reference soda lime silicate and aluminosilicate glasses on the addition of caesium to aluminoborate glass and resistance to cracking was improved. The reason for this is that the highly polarisable nature of the caesium atom and modifier properties allow for a less rigid structure and less internal stresses that are key to stopping crack propagation. In these glass systems density is comparably very high (2.89 g/cm^3) due to the caesium void filling in a manner akin to the silicate glasses in Parkinson et al's work[19]. These effects come with a significant trade off in hardness where the caesium aluminoborate glass has a Vickers hardness and Young's modulus three times lower than standard soda lime silicate or aluminosilicates[125]. This is due to two major factors, large caesium ions creating disruption of the O-O / B-O bonds and the lower strength of borate glasses compared to silicate glasses[126].

Looking at caesium compared to other stable alkali group 1 metals (Li, Na, K, Rb, Cs) in aluminoborate glasses we see large differences in properties as a significantly larger ion is inserted into the structure[127]. Compared to other ions caesium has a much larger effect of the transition temperature of a glass[99]. Figure 2.8 shows that 25 mol% Cs_2O and Rb_2O doped aluminoborate glasses have a

transition temperature around 415 °C and this increases linearly up the field strength of group 1 oxides to a maximum T_g of 475 °C substituting Li_2O.

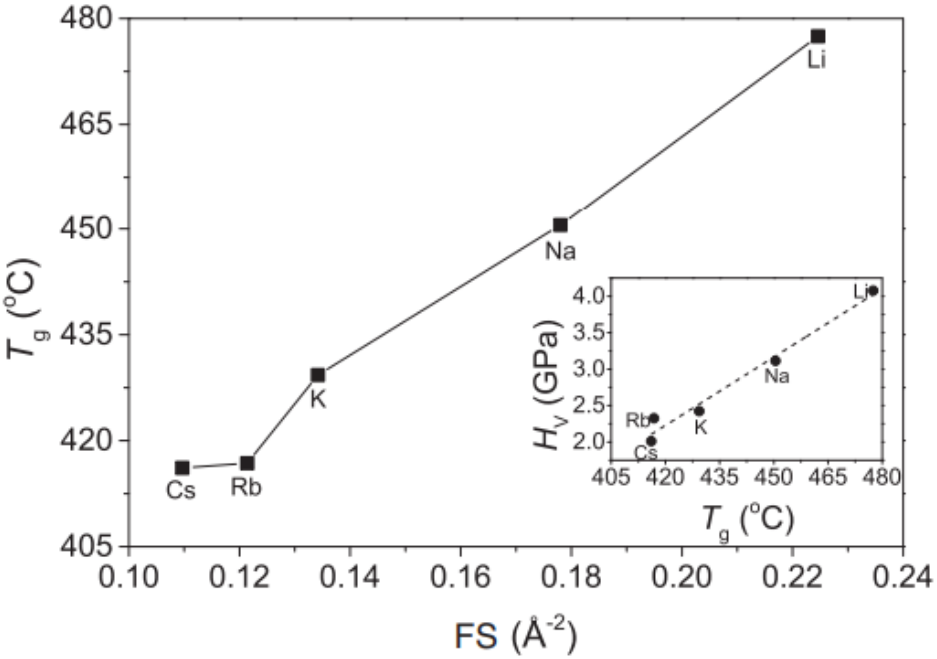

Figure 2.8. Effect of field strength from group 1 cations on glass transition temperature and Vickers hardness (H_v) in aluminoborate glass ($20Na_2O–25Al_2O_3–55B_2O_3$)[99] .

In addition, Vickers hardness (H_v) increases along with T_g and field strength, Cs_2O being the lowest in hardness and T_g[99]. Given these studies we can see a link between caesium content and the softness of the glass it is incorporated in, along with a lowering of T_g to a higher degree than all other alkali metals that are known to produce these effects. Similarly, rubidium has the same effect on the T_g of the glass but a different hardness indicating an exception to the linear trend between T_g and hardness.

Caesium is considered quite volatile and mobile for an element in group 1 (discussed more in section 2.4.1), therefore when incorporating into a glass, melting temperature and leaching rate are normally among the most important factors. As a result of these factors, most glasses studied are processed at around 950 – 1150 °C to minimise volatilisation[128]. There are some high temperature glasses that succeed in retaining more than expected[128], an aluminosilicate used by Bart et al[13] containing 3 - 10 wt % Cs melted at between 1400 – 1600 °C showed a loss of up to 5 wt% of the caesium added, significantly lower than other reported losses (up to 10 wt%).

The role of caesium in phosphate glasses has been heavily studied. Whilst not common in the nuclear industry there have been some waste glasses[129] that use phosphates in the Russian decommissioning sector[66]. This glass is made up of phosphorus – oxygen (P – O) bonds and has the ability to form a low temperature glass purely by itself with the possibility to incorporate many waste components including alkali metals such as caesium. Mostly phosphate glasses seem to follow similar trends to silicates and borates on the addition of caesium, density increase and T_g decrease[130]. As can be seen in Figure 2.9 which shows the relationship between T_g and caesium concentration in caesium-phosphate glasses. Compared to other alkali metals in phosphate glasses caesium reduces transition temperature more than Li_2O and Na_2O.

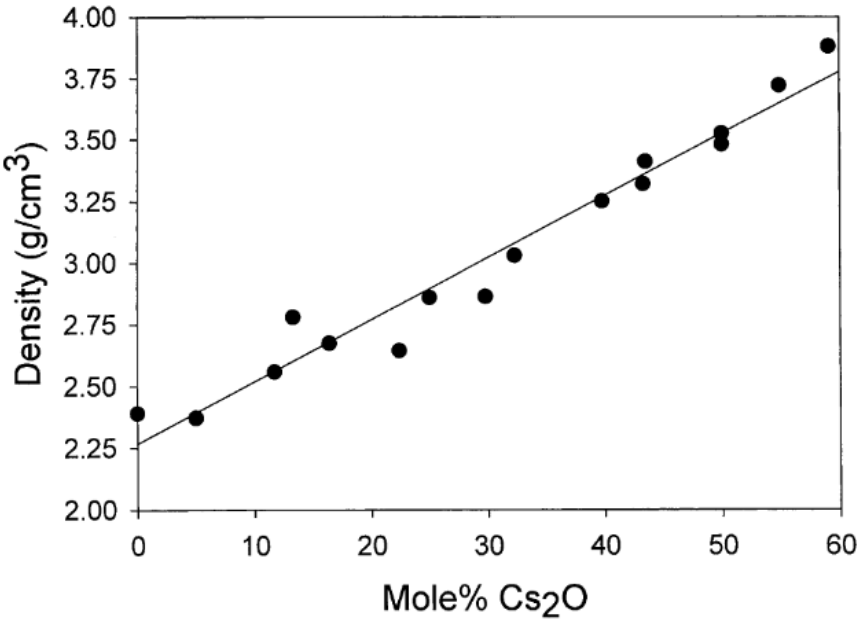

Figure 2.9. Effect of Cs_2O content on the density of $xCs_2O.(1-x)P_2O_5$ phosphate glasses[130]

The effect of titanium on caesium containing borosilicate glasses was investigated by Bannerjee et al[128]. Substituting boron for titanium up to 10 wt% *Bannerjee* showed that caesium was less likely to enter the gas phase and was instead retained in the glass by up to 60 wt% more than titanium free glasses. The structure of these glasses dictates the ability of caesium to be retained, titanium is an intermediary that can fill either network forming/modifying roles depending on the composition and can decrease lattice energy. There is evidence in this study to suggest caesium preferentially interacts

with Ti^{4+} units over Si tetrahedra which could give rise to the increases we see in retention. Another effect of TiO_2 units is a reduced leach rate of caesium theorised to be due to this interaction with titania instead of silica sites.

In addition to amorphous hosts it is notable that caesium boasts a wide range of potential ceramic matrices and as discussed previously can be prepared as a stable glass-ceramic. Common glass ceramic phases that caesium presents as are hollandites[13,131,132], Cs-Leucites[133] and apatites[129] which as are all considered chemically stable for radioactive wasteforms either as a standalone ceramic or dispersed through a glass-ceramic matrix.

2.3.2 Iodine in Glass

In commercial glasses iodine does not normally have a use therefore most occurrences are due to impurities or in the waste treatment sector. In glasses requiring temperatures above ~800 °C iodine has poor solubility[134] due to most of the reagents' thermal decomposition or boiling point temperatures (table 2.5) being lower than the softening point of most glasses used in the nuclear industry or below the melting point of most batch reagents.

Reagent	Decomposition Temperature$^{(dec)}$/Boiling Point$^{(boil)}$ (°C)
NaI	600$^{(dec)}$
AgI	600 $^{(dec)}$
CuI	298 $^{(dec)}$
HI	-35 $^{(boil)}$
I_2O_5	275 $^{(dec)}$
I_2	185 $^{(boil)}$
$NaIO_3$	695$^{(dec)}$
$Ca(IO_3)_2$	540 $^{(dec)}$

Table 2.5. Common iodine species and their respective decomposition/boiling temperatures[134–136]

Iodine is generally present in three redox states I^-, I_2, IO_3^- each having an oxidation state of -1, 0 and +5 respectively. In most radioactive waste streams the iodine[137] is present as salts such as AgI, PdI_2 and NaI with an oxidation state of -1, during heating, redox reactions[134] occur oxidising the iodine to 0 and +5. If the iodine remains non-oxidised it will remain in the melt as negatively charged I^- with a hydrogen ion, sodium or other alkali counter ion, alternatively it will vaporise as its respective salt for

example $Na^{+}_{(l)} + I^{-}_{(l)} \rightarrow NaI_{(g)}$. In the aqueous state I^{-} is interchangeable with iodate species based on the oxidative nature of the atmosphere and/or solution at room and elevated temperatures (figure 2.10). We can use this model as an equivalent for glass melting where the interfacial mass transfer rate constant (k_{mt}) relates to retention in the glass melt and the interactions within the solution can produce all three species previously mentioned.

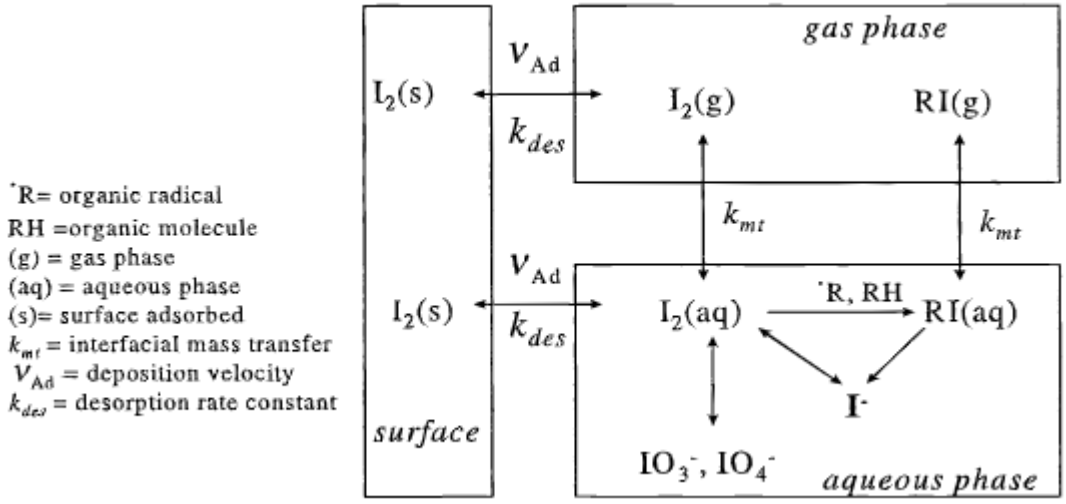

Figure 2.10. Reaction pathways for iodine in the aqueous, gaseous and surface adsorbed phase[138]

The pathways shown in figure 2.10 include the possibility of I (-1) oxiding to I (0) and this is one of the most common volatility event occurrences in high temperature reactions as I_2 gas forms from this decomposition reaction at a lower temperature than salt evaporation. In high iodine melts (>10 %w/w) purple iodine gas can be seen emitting from the liquid surface[137]. The other common state, iodate (IO_3^-) species, has iodine in a 5+ oxidation state and is present at a much lower concentration in radioactive waste, forming iodate salts such as $NaIO_3$ and $Co(IO_4)_2$. The aqueous solubility of iodate species is generally higher than the other iodine containing species[39] with lower melting and boiling points comparatively (see Table 2.6). Solid I_2 has the lowest melting and boiling point with gaseous iodine shown to sublime to a minor degree at room temperature[39].

	Properties		
Species	Iodine Solubility g/L**	Melting Point (°C)	Boiling/Decom. Point (°C)
I^-	$9.7x10^{-15}$ - $2.4x10^{-3}$	250 – 588*	354 – 1505*
IO_3^-	$5.9x10^{-10}$ – 1.6	>200	200 – 540 (decom.)
I_2	-	114	185

Table 2.6. Comparison of iodine species' physical properties[39] *excluding HI. **Solubility in water.

In borosilicate glasses solubility is generally between 1 – 2 wt% meaning that up to 99 wt% of iodine is lost in the gaseous phase either lost at the melt surface or entrained as I_2 bubbles[136]. Studies show that iodine mostly occurs in borosilicate glasses as I^- surrounded by alkali ions such as Na^+ charge compensating the negative charge. X-ray Absorption Near Edge Spectroscopy (XANES) data from Riley et al[136] showed that spectra was consistent with major (non-crystalline) $Na^+ I^-$ clusters alongside minor I_2 entrained gas bubbles decreasing with iodine loading. Above the solubility limit of the glass iodine salts have been shown to precipitate, $Na_8(AlSiO_4)_6I_2$ has been shown to crystallise upon cooling if the iodine solubility limit of the glass is exceeded[137]. This occurred by the formation of a low viscosity phase on the melt surface that solidified after cooling and is theorised to be because the sites in the glass structure for iodine have been filled. In simulant radioactive waste glasses iodine can form alkali salts such as $NaI.2H_2O$ and KI in concentrated conditions. By X-ray Photoelectron Spectroscopy (XPS) Jolivet *et al*[139] found that iodine was predominantly speciated as -1 valency NaI in nuclear waste glasses ISG and a glass developed in the US named NH. There was some evidence in this study to suggest the minor formation of $NaIO_3$ (under 3.5 mol%) in the glass with iodine in a 5+ valency, however, the low concentrations suggest this is not the most common form in most glass structures. It is important to understand these mechanisms as they impact how we continue with experiments to improve the loading of iodine.

Jolivet et al also investigated the impact of iodine on glass transition temperature over a range of concentrations finding that an increase in iodine incorporation related to a lower glass transition temperature in both borosilicate systems. At 1 mol% iodine in the glass structures T_g was shown to reduce by up to 40 °C in ISG glass.

2.3.3 Chlorine in Glass

Chlorine has been present in glass compositions for almost 3000 years[140] and has been found in Mesopotamian, Roman and modern day glasses. Most of the early glasses were thought to contain this unintentionally because of impurities present in the raw materials, however, modern day commercial glasses intentionally use chlorine as a fining agent to remove sulphate contaminants and improve clarity[141]. In radioactive waste chlorine is an unintended contaminant which could be in any state (solid, liquid or gas), in various different chemical forms and in different oxidation states ranging from to -1 to +7. As discussed in section 1.2.3, this generally presents from chlorinated cooling water or PVC plastics in radiological environments. In commercial glasses concentrations from 0.5 – 3 wt% are common[142], in nuclear waste glasses chlorine retention typically rarely exceeds 0.5 wt% even despite the large concentration of chlorine in some ILW[143]. This suggests a decomposition reaction occurring before glass softening and therefore the chemical state chlorine is within the batch is of importance to dissolution and retention. The solubility of chlorine in molten glass is low with significant volatilisation in most compositions[142] increasing with dwell time at maximum temperature. Jin et al[144] found that in American borosilicate radioactive waste glasses chlorine dissolved to a limit of 2.06 wt% decreasing with chromium content. The undissolved chlorine is volatilised as Cl_2 and HCl or presents as a NaCl salt crystallisation layer on the melt surface.

Speciation of chlorine has been found to substitutive for oxygen in silicate at a 2:1 ratio (2 chlorine atoms fill one oxygen vacancy)[145,146], this was also consolidated by Bureau et al[147]. Thomas et al[148] studied the effects, such as solubility and the effect of quantity of iron in the glass structure, on chlorine in the melting of the mineral basalt (major components silicon, aluminium, calcium, iron)[149]. Chlorine added as HCl has a maximum of 1.06 wt% waste loading in molten basalt under high pressure (100 MPa). Beerman et al[146] increased this to 1.50 wt% with the same basalt material and chlorine reagent, iron was found to have little effect even up to higher concentrations of 15.69 wt%. It was found that the presence of other halogens (X) decreased the solubility of chorine similar to data in Hrma et al (2010)[150] suggesting X^- ions filling similar vacancies in the glass structure. The only positive

effect on solubility chlorine has is on sulphur where an increase in retention has been noted to sulphate impurities in radioactive wastes and commercial glasses[148,151].

McKeown et al[143] studied radioactive waste and the speciation chlorine has in sodium, aluminium borosilicate glasses (analysed by X-ray absorption). They use a composition similar to Ca/Zn with silica (42.22 wt %), borate (9.70 wt%), alumina (5.81 wt%), calcium (2.63 wt%) and lithium (2.50 wt%) all present in the glass, only omitting ZnO. Compared with other chlorine containing raw materials they found that Cl^- (-1) was the most common oxidation state in the same silicate glass with varying calcium content. They also noted that calcium additions to the glass frit had marked effect on the bonding within the resultant chlorine containing glass. The likelihood here is that chlorine preferentially bonds to calcium in the glass structure rather than other cations such as silicon. This could have important implications for increasing chlorine retention in glasses by increasing calcium content. Major bonds for these systems were found to be Cl-Cl, Cl- Ca and Cl-O by EXAFS leading to a theoretical model of chlorine bonding in these systems (figure 2.11).

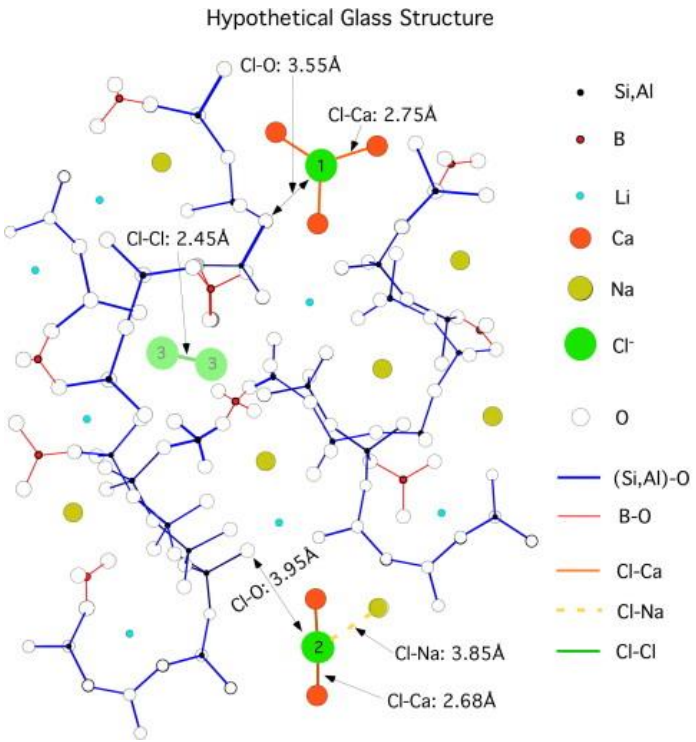

Figure 2.11. Theoretical model of chlorine incorporation into calcium containing borosilicate glass systems from McKeown et al[143]. Hand designed and not computer model based.

In figure 2.11 the chlorine sites labelled 1 (3 x Cl-Ca) and 2 (2 x Cl-Ca, 1 x Cl-Na) are most frequent to occur and site 3 (Cl-Cl) much less in comparison. This shows charge compensation from calcium and sodium ions stabilising chloride ions and enabling a higher proportion of solubility. This does slightly conflict with the simpler view Thomas et al[148] took because in McKeown's model two chlorine atoms do not necessarily substitute for one oxygen atom, however, this still occurs in an oxygen vacancy.

2.4 Mechanisms of Volatilisation from Key Elements

In section 2.3 we discussed how elements which are known to be volatile can be incorporated into a glass structure. In this section we highlight the ways losses can occur in high temperature reaction pathways. All glass melts will be subject to some loss of mass through volatilisation of raw materials during the heating process. In the field of nuclear waste this can also include the constituents of the waste and release to atmosphere.

From glass melts volatilisation occurs at the liquid gas phase barrier between the heated liquid glass and the gaseous environment in the melter. Three steps effect the interaction at the barrier[152]:

- Transport by diffusion or convection to the surface of the liquid
- State change at the surface either by reaction or decomposition
- The concentration of the gas at the surface of the liquid melt

Diffusion is the transport of material from a low to high concentration down the concentration gradient therefore we can determine that concentration at the surface of the melt will have an effect on the volatility. If we assume concentration is independent of diffusion however, and just consider movement to the surface we can use Fick's second law (equation 1)[153] to kinetically understand diffusion through a unit area in one direction.

$$Equation\ 1: F = -D\ \frac{dC}{dx}$$

Where F is the transfer rate through solution, C is the concentration of the solute, x is the distance to the area of low concentration, in glass melt volatilisation this could be considered as the distance between the solute and the surface. Term D is the diffusion coefficient and can very largely depending on concentration and solution/solute interactions. From this we can see that diffusion effects are proportional to concentration and inversely proportional to the distance from the low concentration area (be that in the solution/melt or to the surface of the fluid). Cable et al[154] describes a concentration gradient, illustrated in figure 2.12, where species X dissolved in a solution is lost at the surface causing an area of low concentration. Other high concentration areas of X are then more likely to diffuse to the surface where they state change to a gas by chemical reaction, decomposition or evaporation, repeating the process.

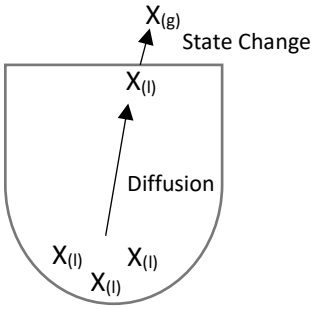

Figure 2.12. Effects of diffusion on volatile solutes

Thermodynamically this can also be described by looking at the activation energies of each process combined in the equation below as the term Q and the temperature of the glass melt[78].

$$\text{Equation 2: } D = D_o e^{\frac{-Q}{RT}}$$

Where D is diffusion, D_o is a factor which describes the concentration of the solute independent of temperature, Q is related to the enthalpy of migration (ΔH_m), R is the gas constant and T is the temperature. Schaffer[78] describes the effects of this relationship in silicate glasses and shows that as temperature increases diffusion and mass transport is higher due to the energy in the melt increasing which in turn increases depolymerisation in the system. Pure silica glass has significantly less diffusion comparably to silicate glasses with modifiers such as CaO, K_2O or Na_2O. Borosilicate glasses also had significantly more diffusion though the melt than most other silicate glasses (figure 2.13).

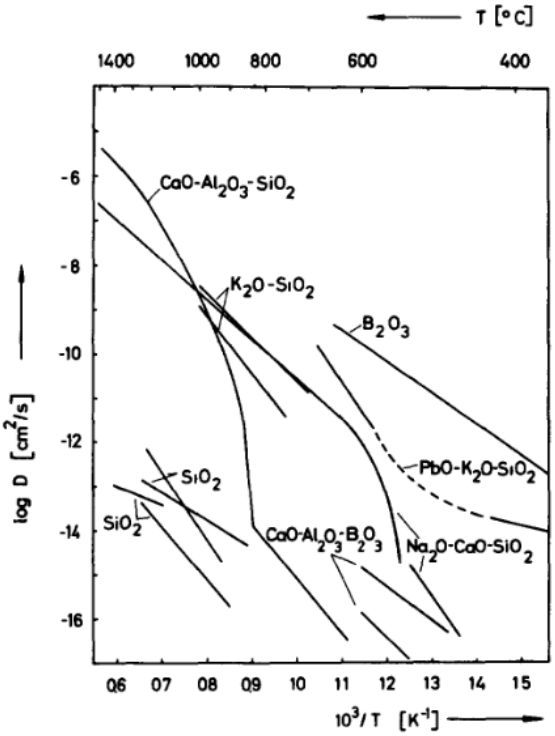

Figure 2.13. Oxygen diffusivity through various silicate glasses as a function of temperature[78]

Another transport mechanism is mass transfer[155] which is an effect from the bulk movement of solution independent on concentration of either the solution or solute. This is a more complex effect that takes into account electromigration, convection, stress and chemical potential to find to total flow of mass. One result of mass transport is that the experimentally measurable value of viscosity has a large effect on the movement of atoms through solution. Using the example of silicon atom (A) and oxygen atom (B) moving through the liquid silicate glass using the ball bearing model[156] Cooper et al showed that oxygen migrating around the circumference of a silicon atom was relative to temperature (T), viscosity (η) and atomic radii (r) of the rate dependent atom (in this case silicon) (see equation 3). The same model can be applied to modifier atom and NBOs depending on which is the rate dependent atom for viscosity. By this model we can presume for most borosilicate glass melts viscosity, temperature and concentration have the largest effect on diffusion to the surface of the melt and by extension the volatility from molten glass.

$$Equation\ 3\text{:}\ \frac{D_B \eta}{kT} = \frac{1}{4\pi r}$$

Knowing the major factors which cause volatility from liquid glass we can then use this data to change procedure or conditions that would cause excessive mass loss. For example, we have discussed the effect of temperature, if we can lower the temperature a glass is melted at (above its melting temperature and without hitting a region of phase separation/crystallisation) we can produce the same or similar glass with potentially less loss of the components added in the batch, frit or waste. Another factor is time as all diffusion and mass transport is rate dependent, therefore a longer time at temperature would volatilise more molten glass and dissolved species.

Next, we will individually look at the volatilisation chemistry of caesium, iodine and chlorine as elements that have particular interest in the field of nuclear waste (see section 1.2).

2.4.1 Caesium

Loss of caesium has been reported in radioactive waste glasses above 650 °C[157], considerably lower than the temperatures considered for thermal treatment (1050 – 1400 °C). Any significant or cumulative loss could present issues with release to environment, filter blocking and accountability. Comparatively caesium is more volatile than other similar metals in nuclear waste such as ruthenium and strontium, although, similar to technetium or rhenium[158](see table 1.1). Volatility of caesium from glass melts is predominantly a diffusion-based process with temperature and concentration having the largest effect on the total mass loss[159]. Banerjee et al studied the loss of caesium from premade borosilicate glasses and in all compositions caesium loss was shown to be exponential to temperature. This was a result of the increased diffusion upon exposure to higher temperatures at a similar or same rate to the mass loss of the melt. They also noticed a relationship between activation energy of diffusion in specific borosilicate compositions with varying additives (Ca, Zn, B, Ba). As activation energy of diffusion decreases due to the variations in the glasses caesium loss also is seen to be lower which suggests D_0 having a larger impact on diffusion and loss in these systems. This is because ionic linkages are more prevalent in these glass systems which in the case of caesium incorporation in silicate glasses, stabilises the Cs^+ ions.

Species that caesium forms upon decomposition, boiling or evaporation are varied and many papers have reported a wide range of compounds, especially in borosilicate systems. Table 2.7 shows the types of caesium species that have been reported from the addition of either caesium chloride, oxide or carbonate to the glass melt.

Gaseous Species	Reference
Cs	Asano et al[160] Bonnell et al[158]
Cs_2O	Asano et al[160]
CsOH	Bonnell et al[158]
$CsBO_2$	Asano et al[160] Asano et al[161]
$Cs_2(BO2)_2$	Asano et al[161]
$CaNa(BO_2)_2$	Asano et al[161]
$CsTcO_4$*	Kim et al[15]

Table 2.7. Gaseous caesium species reported by various studies (*in the presence of Tc)

Of particular interest to this study is the relationship caesium has with boron upon volatilisation. Multiple studies have recorded caesium boron species in off gas measurements from borosilicate glasses and boron has a stabilising effect on ^{137}Cs in glass[162]. In addition, other gases have been detected that contain other metals from radioactive waste[15], for example $CsTcO_4$. Mass loss of caesium from these species has been found to range from 0.18 – 0.24 mg/cm^3 in borosilicate glasses (loaded at 2.5 mol%) after 24 hrs of heating at 900 °C increasing to 0.70 – 2.31 mg/cm^3 at 1000 °C [159]. Other studies have shown a 11 wt% loss of total Cs at 1400 °C after 24 hrs in titanosilicates (loaded at 2.1 wt%)[163]. This shows a clear relationship between temperature and volatility of caesium from glass, higher temperatures volatilising more caesium.

Some investigation into the effects of alternative glass reagents has been completed by Banerjee et al for Ca, Zn, B and Ba and by Spalding et al[37] for Cs in soil vitrification. Banerjee et al discovered that zinc is very advantageous in reducing caesium volatility. They describe this being due to the size of the ZnO_4^{-2} anion being larger than BO_4^- subunits and therefore forming stronger ionic bonds with Cs^+ ions than the boron, calcium, and barium subunits. ZnO in glass making is usually defined as an intermediary reagent[92,103] which can act as a network modifier and also has network forming properties in certain glass systems. Given this, there is likely a component of zinc in borosilicate glasses

that has formed ZnO_4^{-2} units which stabilise alkali ions similarly to SiO_2. Conversely calcium and barium ions acted more akin to network modifiers only and created a higher concentration of non-bridging oxygen atoms which ultimately increases diffusion and mass loss of caesium when melted. Spalding et al[37] describes a relationship between chlorine and an increased mass loss of caesium in soil samples. In raw soil samples caesium was reported to begin to lose mass in the sample at 1000 °C (measured by radioactivity of ^{137}Cs) reaching its maxima at 1250 °C where 8 mol% ^{137}Cs was lost. When Spalding added NaCl the caesium lost from heating at 1200 °C was greatly increased up to 80 % at a maximum 8 mol% Chlorine. This effect was not as pronounced using PVC plastic as the chlorine source rather than NaCl where 8 mol% Cl only represented a 34 % loss of caesium, however, the change upon chlorine addition is still dramatic. This is important for the nuclear industry as not all chlorine sources may react the same upon vitrification, the chemical and physical state the pollutant/radionuclide is in has a large effect on its retention into a glass or ceramic wasteform. This soil vitrification may be different to glass systems as very little liquid phase interactions between the most matrix and analyte are occurring, however, this gives a picture of the effects that these additives may have on a final glass product.

2.4.2 Iodine

As one of the most volatile elements[164] studied in our work, iodine is of great interest to the nuclear sector in addition to its mobility in environmental systems, long half-life and high decay beta energy. In thermal treatment iodine suffers the same issues as caesium in that the temperature these systems get to is considerably larger than the decomposition temperatures for most iodine compounds. In table 5 in section 2.3.2 we discussed the decomposition temperatures for common iodine species in glass melts and these range from 185 – 695 °C. This means that iodine in most forms will likely decompose earlier than most other components and maybe even below the softening point of the glass used in the case of borosilicates. This speaks to one of the more important factors in evaporation of iodine from glass melts, batch preparation rather than melter conditions and glass composition, however, all play a part in iodine loss/retention.

The general volatility of halogens happens in the order of F < Cl < Br < I where iodine is significantly more volatile compared to the other stable halogens[20]. This has been shown by *Hrma* in radioactive waste trials in United States simulant waste where LAW with glass forming reagents showed that iodine at a concentration of 0.25 wt% retained ~20% in Duramelter 100 trials[165]. This was calculated by XRF of the glass at the end of the trial, however, an attempt at off-gas analysis was also made finding a deficit of iodine in the capture solutions. This is likely a result of condensation and deposition of I_2 and iodine salts in the ducting/tubing pre-capture vessel. This tells us something of the nature of iodine where it is likely to stick to furnace walls, tubing, ducting and catch on filters easily in a large scale vitrification tank especially when the temperature drops. In a glass melt environment *Bell et al* looks at iodine loss from glass dissolution in lithium iodide containing borate glass frit[152]. Iodine shows a largely linear relationship with the square root of time at elevated temperature. They also theorise that the mechanics of volatilisation are mostly diffusion based, however, do show signs of a more complex system that involves both diffusion and mass transport as the rate determining factors. This more complex mechanism happens at the start of melting which indicates the importance of temperature and melting time on volatility of this component.

Xian et al used bismuth zinc borate glasses to immobilise iodine in air and found up to 80 % mass loss in all samples, showing high levels of volatilisation[166]. These glasses, however, do have a higher affinity for iodine in the structure of the material and due to this show less mass loss than borosilicate glasses (~90 %), either due to the chemical interactions with bismuth or due to the lower melting temperatures required for those glasses. Another interesting comment is the effect that nitrogen has on these systems where changing the atmosphere showed to significantly reduce the mass loss of iodine from these melts. This is thought to be due to oxygen interacting with iodine in decomposition reactions earlier in the melting process and stimulating the production of I_2 gas even before the melting point of the glass in some cases although more studies into this process must be done to better understand it. These properties require us to treat the melting of sodium iodide into glass for example as two separate stages of melting/reaction:

1. Molten salt phase where only the iodine, counter-ion and the atmosphere interact with one another.
2. Dissolution, diffusion and mass transport into the glass matrix

The result of this is that many different factors effect iodine loss and the control of iodine in radioactive waste melters is a challenge that will involve control of:

- Melting temperature
- Melting time
- Glass composition
- Iodine oxidation state (-1, 0, +5)
- Iodine counter-ion (if applicable)
- Convection
- Atmosphere at the surface of the melt

The molten salt phase adds a complexity where reactions can happen with other salts that may be present in the waste/batch. This can happen when over the solubility limit of the glass where a molten salt layer forms on top of the melt or before the glass frit/batch becomes liquid[167]. Iodine and caesium have been shown to volatilise readily from Li, Na and K molten salts[168], during this phase unstable CsI forms and has higher vapour pressure than all the other salts in solution. In other systems iodine is generally lost from aqueous solutions as iodine gas (I_2) as the species are thermally oxidised by reaction with oxygen and dissolved protons[169] (equation 4) with a small fraction of hydrogen iodide present at lower temperatures.

$$Equation\ 4.\ 2I^- + 2H^+ + \frac{1}{2}O_2 \rightarrow I_2 + H_2O$$

There is also scope for organic iodide compounds reacting to form gaseous and aqueous RI compounds in solutions and glass melts from aqueous dissolved I_2 (figure 10). This is particularly important for radioactive waste melts in ILW because they may contain high amounts of contaminated organic

matter from wood and plastic. Wren et al[138] also mentions the higher likelihood of iodine reacting with organic compounds if they have any atoms that become radicalised which is more common in active waste streams[170]. These organic radicals have the chance of forming in glass melts from reaction shown in equation 5 and releasing as RI species into off gas streams. There is the possibility of highly radioactive organic waste glass having a different rate of iodine loss compared to inactive glasses due to this accelerated radiolysis and formation of RI compounds.

$$Equation\ 5.\quad I_2 + R^{\cdot} \rightarrow RI + I^{\cdot}$$

Radiolysis processes are usually accelerated by presence of water by formation of OH radicals which is a large component of most ILW forms[1], however, in glass processing the effects of this may be minimal as the high temperatures dry the waste rapidly. Wren et al describes that energetically favoured reactions are I_2 generation dominated with minor hydrolysis reaction of HOI reported by Lin[171] and presence of iodo-phenol (C_6H_4IOH), iodine containing ketones and methyl iodide (CH_3I).

2.4.3 Chlorine

Chlorine follows similar physical volatilisation paths to iodine with molten salt interactions occurring before and during melting in tandem with dissolved chlorine following more traditional diffusion-based routes[20,142,148]. NaCl melts at 801 °C compared to NaI melting at 660 °C both of which is normally lower than (or around) the softening point of glass frit. At least some volatilisation will occur before dissolving in the glass, chlorine less so than iodide[20]. This is one of reasons mass loss from chlorine containing melts can be dramatic, commercial glasses are often forced to add more chlorine than intended in final compositions to allow for volatilisation[111].

Time the glass melt is at high temperature has a significant effect on the volatility of chlorine with 3 hours at 1300 °C almost halving the mass of chlorine in molten silicate glass[142]. In the same study 1.95 wt% Cl reduced to 1.08 wt% over the 3 hour period with the majority of the mass loss occurring with the first 20 minutes displaying the unstable nature of chlorine at high temperatures. After 4 days at this temperature 0.6 wt% remained in the glass, a non-linear relationship is likely for chlorine

evaporation mechanics in this case because the difference in volatility over the 3 hour to 4 day period is significantly less than the 0 – 3 hour period. Hrma et al[20] looked at the retention of chlorine under a number of conditions in low activity glasses and found similar solubility limits at 1300 °C with the majority of the chlorine being lost in the first 10 minutes of dwelling. One of the conditions they summarised was temperature between 1300 – 1400 °C finding a volatility of 1.6 – 2 g per gram of glass, initially a linear function however, at lower temperatures the gradient of this change is considerably different suggesting a different method of gaseous phase transition. Melter technologies were compared as well as physical state of the 'waste' showing a significant change in chlorine (and iodine) loss based on the preparation and methods. Electrode based melting methods reliably perform better than plasma and gas fired cyclone melters, however, the variation with that group is also quite large. Molybdenum electrodes perform better, however, there are multiple variables within the data that results in this comparison between Mo, Inconel and carbon electrodes to be only indicative of the effect of electrode material on chlorine volatility[172]. Somewhat more reliable data from Shade et al[172] shows that the state of chlorine containing material (or feed) being added to the fritted glass is of importance to retention, pellets retained twice as much chlorine when compared to slurry. This may be because the pellets allow the glass to soften more before becoming molten whereas slurry has a higher surface area to volume ratio and is likely to melt (and phase change) at a higher rate than pellets. This applies to the halogens chlorine, iodine and fluorine.

As we have explored, mass of chlorine added into glass batches are normally lower after melting. The extent of this was explored by Matlack et al[173] in their melter trials for LAW in the USA. They showed a linear relationship between chlorine addition and volatilisation in a LAW borosilicate although above 0.6 wt% chlorine addition the graph becomes unreliable.

The species that chlorine forms upon decomposition, reaction or evaporation from the glass melt environment are usually predictable with a few variations on some occasions. The most common gaseous high temperature species[174,175] are HCl and Cl_2 with infrared spectroscopy (FTIR) being used

in nuclear waste vitrification tanks finding predominantly these two species[20]. Particulate species are more common for chlorine when compared to iodine, however, for one reason because its higher melting temperature means that in high temperature processes chlorine can condense in cooler parts of the system. Atmospherically chlorine exists as a pollutant predominantly as HCl and organic particulate chlorides[174,176] eg. Polychlorinated biphenyls, furans as some of their more stable states. Other notable minor contributions are from HOCl, $ClNO_2$, $Cl^{\cdot}$ radicals and Cl_2. Polyvinyl chloride (a major component of ILW) in fact is known to decompose readily into HCl at temperatures as low as 200-380 °C along with many other volatile organic compounds[177,178]. This happens first because the C-Cl bonds are weaker than the C-C bonds meaning they are the first element to thermally degrade. The minor amounts of HOCl that can form from high temperature reactions are very reactive and normally do not survive long enough in the gas stream to consider, however, they have been present in some volcanic silicate melts in low concentrations[115].

Chlorine like many of the halides will readily form radicals which can form organic gaseous molecules as we explored in the iodine volatility section 2.4.2. Radicals more readily form with chlorine atoms than other halides, HCl is able to react rapidly with OH and $HOO^{\cdot}$ radicals. Above 226 °C 1% or more of the total chlorine content is made up of radicals, however, this only occurs for a short period due to the reactive nature of $Cl^{\cdot}$ species and recombining is less likely due to being kinetically limited[138,176]. When reacting these can commonly form metal halides and chloro-organic compound in the presence of organic gas phase components (mainly aromatic) such as benzene, PCBs and dioxins[176,179].

2.5 Real-Time Gas Sampling Technology Survey

One focus of research in this study was gas detection of off gases from the glass/waste melts therefore it is important to understand the gas analysis systems and their viability in this study. Many different techniques can be used for analysis, however, it will be easier and more cost effective to use a system that can target many different components at once. There are a number of systems that allow this so to narrow these down cost, components measurable, versatility and other viability factors will be factored in. In table 2.8 we can see the simplest and most practicable system is the capture of gases via impingement that uses an absorption solution and therefore for lab scale analysis this method will be carried forward as capture from pyrolysis tubes (section 3.3.6). Whilst the method is well applied to lab scale analysis for larger operations with more funding, continuous instrumental analysis has a faster response time and does not need to be monitored by personnel as frequently.

2.5.1 Raman Spectroscopy

Raman spectroscopy is a technique that has been used for years for determining bonding and structure of solids and liquids. Only recently have there been developments in using it for gas analysis. It uses inelastic scattering of light based on Stokes and anti-Stokes scattering which interacts with the analyte.

The scope of this technique is still being developed; however, literature suggests a broad group of analytes. Schluter et al[180] discussed the use of Raman gas analysis to monitor anaesthetic levels simultaneously and with a fast response rate. While more complicated than the simple component gases such as O_2 and N_2O, the spectra are still distinct even for a complex molecule such as isoflurane. This comes about by the reactivity of C-H bonds for this process which could apply to some of the components in the waste gas such as dioxins, furans, VOCs and decomposition products of PVC.

Technique	Benefits	Limitations	Cost	Components Measurable
On-line Raman	-Wide analytical range -Simultaneous analysis of multiple components -Distinctive single interference peaks -Portable -Fast response time	-Not all uses are known yet -Gas needs to be kept above dew point -Unknown limits of detection for most analytes	ff	VOCs, NO_x, CO, CO_2, NH_3, HCl, N_2, O_2, Radionuclides, Potential for any Raman active gas molecule.
On-line FTIR*	-Well established -Mobile -Fast response time -MCERTs certified -Limits of detection up to 2000ppm	-No measurement of diatomic analytes (eg. O_2, N_2) -H_2O interference -Gas needs to be kept above dew point	fff	Any non-diatomic gas molecule including but not limited to Radionuclides, VOCs, NO_x, CO, CO_2, NH_3, HCl, SO_2
Impingement to ICP-MS**	-Simple set-up -Fast response time -Can use other techniques for analysis of solutions	-No real time data -Impingement solution needs to change for each analyte -Only gives elemental analysis	£	Elemental analysis of most components
Flame Ionisation Detector	-Fast response time	-Limited analytes -Fuel gas need	fff	VOCs, C_xH_{2x+2}
Electrochemical Cell	-Versatile -Very portable	-Separate cell needed for each analyte -Cell eventually needs to be replaced -Gas needs to be cooled	ff	NO_x, O_2, CO, CO_2, SO_2
Gas Chromatography	-Wide range of analytes	-Difficulties making in-situ system -Method development needs to change depending on analyte	ff	Most volatiles
Mass Spectrometry	-Wide range of analytes	-Difficulties making in-situ system -Delicate technique	fff	Most low AMU volatiles

Table 2.8. Overview of gas detection techniques[180–182], *Fourier Transform Infrared Spectroscopy, **Inductively Coupled Mass Spectrometry

Caesium borate, a known pollutant from caesium containing wastes, has similar chemistry to that of organic C-H group containing molecules and therefore may present a similar distinctive spectrum. In the same paper they also showed the spectra of diatomic molecules such as nitrogen and oxygen which is not possible for many spectroscopic techniques such as FTIR (discussed in the next chapter). These show as clear distinctive bands which makes for easy deconvolution of the analyte peak and a potential for simultaneous measurement of components like oxygen, CO_2 and NOx. The standard deviation given for Schluter's measurements were between 0.03 and 0.12 for CO_2, N_2, N_2O and O_2 when compared to gas chromatograph data which shows a promisingly low level of error for Raman gas measurement of these components.

2.5.2 Fourier Transform Infrared Spectroscopy (FTIR)

FTIR has been used for many years in the stack emissions testing world to measure various pollutants from solid organic compounds to gaseous combustion products. The scope of FTIR is quite wide given its large range and great resolution especially for analytes containing certain bonds which are very IR active. FTIR depends on the stretching and bending of bonds in a molecule at certain frequencies of infrared radiation. For example carbon monoxide (C-O) has a very specific stretching and bending frequency which is distinctive on the spectrum and therefore can be easily assigned and quantified, some have even used the technique for detection of gaseous metals such as copper and gold[183].The most common use in emissions testing is for simultaneous measurement of combustion gases, hydrogen chloride and VOCs. The peaks are very distinctive and have good separation with only minor interferences from other gas species which makes for simple analysis. Emission FTIR was the method of choice for Heland & Schäfer[181] when determining combustion gas concentrations from aircraft exhausts getting reliable results for CO, H_2O, NO, N_2O and CO_2. They were able to find a distinction between the combustion gas spectra and simultaneously measure most pollutants. They also highlighted some problems with interference with other common gaseous compounds (see table 2.9),

a common interferer being moisture (H_2O), therefore to use this system a cooler condenser may have to be used beforehand unless measuring water content of gas.

Analyte	Interferences	Main Absorption Band (cm^{-1})
CO_2	None	2380-2400
CO	None	2160-2180
NOx	H_2O, CO, CO_2	1620-2200
CH_4	H_2O	3055-3075
SO_2	H_2O, CO_2	1350-1370

Table 2.9. FTIR Interferences

2.5.3 Multi Gas Analysers

These are a set of gas analysers that use a multitude of systems to detect multiple gases at the same time. They normally use electrochemical cells and other fast reliable techniques such as zirconia and paramagnetic cells. There are a few multi gas analysers available on the market such as the Horiba series which utilises a variety of techniques to analyse CO, NOx, CO_2, O_2 and SO_2 simultaneously by splitting the sample gas and passing it over the cells measuring voltage change or spectroscopic information (Horiba, 2015). The Horiba systems use non-dispersive infrared spectroscopy (NDIR) to analyse SO_2, CO, CO_2 specifically through three separate detectors. Interference is a massive problem between these three analytes especially with NDIR so firstly a filter is needed to be developed so that only frequencies of interest were recorded by the detector.

Chapter 3 Experimental Methodology and Techniques

In this chapter, we will discuss the theory surrounding the various methods used to acquire/process data and throughout the results and discussion in chapters 5-8. We will then move on to highlight the exact procedure we have used for each experimental set including masses used and reagent or raw materials. This will include weighing procedures, instruments, processing equipment and software used. Details of the usage of any computer software used are not included, however, the name and version of the software will be added for reference.

3.1 Glass Batch Preparation

Solid powder batches were prepared by weighing raw materials (dried at 110 °C for a minimum of 24 hours) on a balance to an accuracy of 0.001g into a sample bag and mixed thoroughly in all dimensions to ensure an even distribution of material throughout the sample. Some raw materials required special handling, caesium carbonate and sodium iodide are very hygroscopic materials and therefore need to be kept under dry conditions in order to ensure accurate weighing and repeatability. Boric acid is a reproductive toxin and a major component in most of the batches including borosilicate and borate glass formulations. These hazardous reagents were used in a powder handling cabinet to minimize exposure and control risk. All raw materials used were high purity >99%. Finished batches would then either be stored in sealed samples bags or transferred directly into a crucible to be placed in a furnace (sections 3.2) or pyrolyser (section 3.3). These mixed batches were also to be analysed by TG-MS (section 3.5.5).

3.2 Use of Furnaces

Muffle furnaces used for melting in experiments for this study were conducted in Elite Thermal system furnaces (models: BRF13/25, BRF16/5 and BRF16/10) and Nabertherm B180 muffle furnace. The Nabertherm B180 and BRF13/25 was primarily used for annealing or low temperature heat treating of glass, ceramic or end product materials at temperatures between 21 – 800 °C, BRF13/25 and BRF16/5 model furnaces were used for melting of batch materials or remelting of glass frit at higher temperatures between 800 – 1450 °C. Samples produced this way could then be analysed by the techniques described in section 3.4.

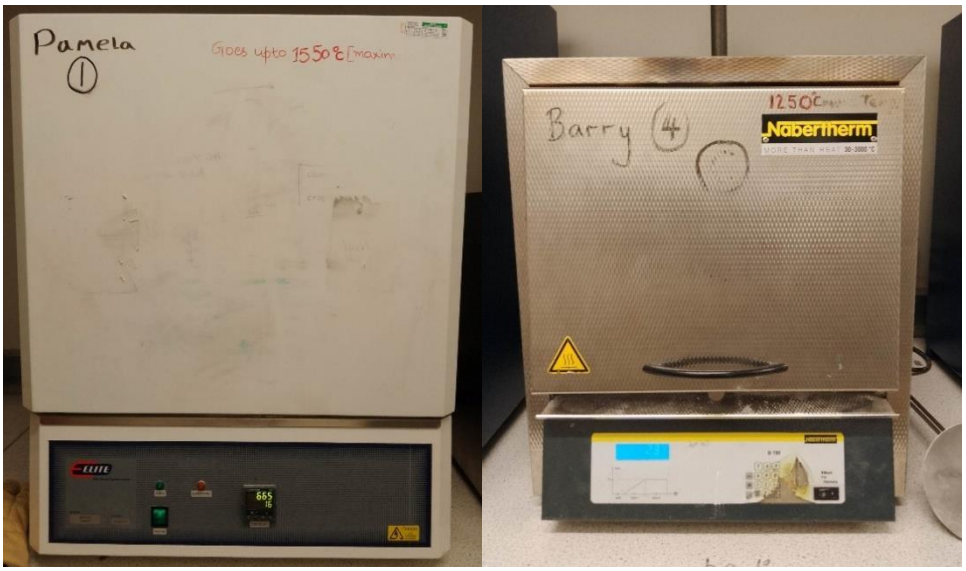

Figure 3.1. Images of melting/annealing muffle furnaces used, high temperature furnace Elite BRF16/10 (Left), lower temperature furnace Nabertherm B180 pictured (Right)

3.3 Analysis Techniques

3.3.1 Density

3.3.1.1 Theory

Measurements in this study were completed using the Archimedes method of density calculation. This is a simple method of determining density by weighing the sample of unknown density accurately in air and suspended in a liquid of known density (figure 3.2). This is based on the principles of buoyancy

with the magnitude of this force being equivalent to the density of the unknown solid sample. Equation 3.1 shows a simplified relationship between mass and density based on the buoyancy of the liquid remaining constant at a fixed temperature[184,185].

$$Equation\ 3.1\ \ \rho = \frac{m_L}{m_L - m_0}(\rho_0 - \rho_L) + \rho_L$$

ρ is the density of the solid, ρ_0 is the known density of the liquid, ρ_L is the density of air, m_L is the mass of the solid in air and m_0 is the mass of the solid in liquid. It is worth noting that the density of water and air changes depending on temperature so in this method these are measured throughout the test to ensure the density is kept constant[184,186].

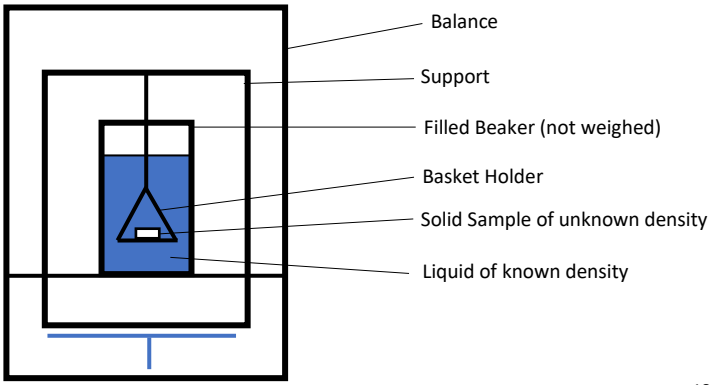

Figure 3.2 Diagram of density measurements by buoyancy method[184]

The limitations of this method are that temperature affects the density of the submergent liquid which can introduce error into the calculation if the variation happens during the measurement. Another limitation is the internal structure of the sample must be cavity free to obtain an accurate measurement. This is particularly troublesome for glass samples as bubbles in the solid phase can be frozen into the structure during cooling. A 1 mm diameter bubble of air can cause a buoyancy effect equivalent to 0.5 mg of mass[184] which can increase the error in the density measurement especially when the sample size is small.

Figure 3.2. Image of density measurement balance, Kern ALJ densimeter

3.3.1.2 Methodology

To determine density of a sample firstly the material was inspected to discover if there was a significant amount of bubbles or if the sample was water soluble. These would not be suitable samples for this method of density determination and therefore were skipped or analysed with a note that readings may not be accurate, however, all other inactive samples were measured for density by this method. The balance (Kern ALJ densimeter, 0.0001g resolution) (figure 3.3) was then turned on and left to internally calibrate after which it was tared to 0 g. A beaker was filled with ~ 300ml of deionised water and then placed on the stainless steel rest (not weighed). The weighing basket was then placed in the beaker and rested on the weighing arm, the balance was then again zeroed. The temperature of the water in the beaker was taken and using density of water tables the actual density of water at that temperature was input into the instrument for later calculations. The sample was then placed on the top weighing pan in air and recorded. After, the sample was taken off and placed in the water on the weighing basket suspended in water, this was recorded. The instrument then output a density value based on the density of water, mass in air and mass in water which was also recorded. The

sample was repeated twice more then taken out dried and stored. The temperature of the water was measured every sample to determine if a change in temperature had occurred and if this was the case the density of water value would be changed in the instrument. Additionally, the water was changed every 5 samples to eliminate any contamination of the water from samples being submerged or the environment.

3.3.2 Inductively Coupled Plasma Mass Spectrometry (ICP-MS)

3.3.2.1 Theory

ICP-MS is a technique originally produced in 1983 for analysis of multiple trace elements in liquid matrices[187]. The data output from this is an elemental breakdown of the composition of the solution and can provide useful information for low concentration samples (ppm ppb and even ppt)[187,188], digested glass/soil/sediment samples[188,189], biological samples[188], forensic science[189] and environmental analysis[190]. The design of the instrument couples a method of ionising the sample into a charged gas stream with detection of the ions by mass spectrometry (mass/charge ratio). Figure 3.4 illustrates the basic inner workings of the instrument with the ioniser/atomiser at the front (left on the diagram) of the flowchart diagram and mass spectrometer/signal processing at the back end (right on the diagram).

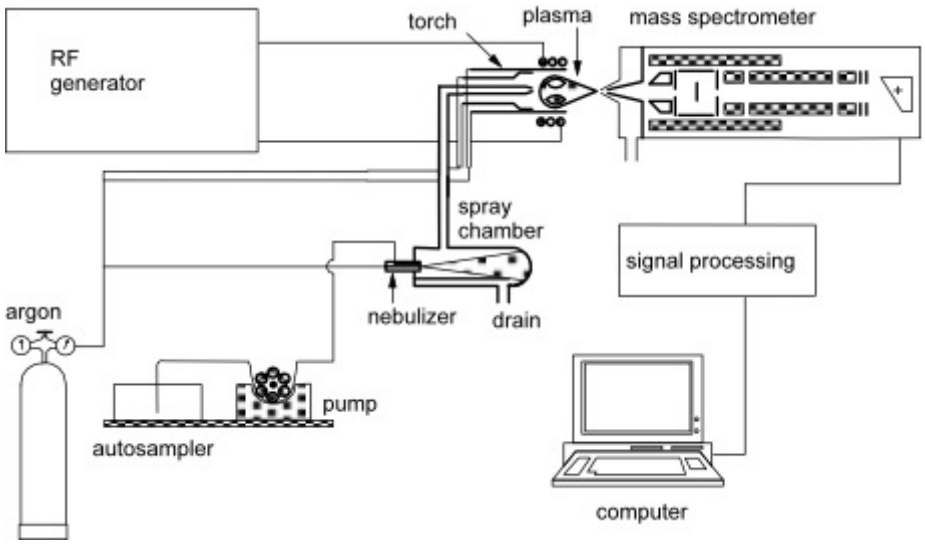

Figure 3.4 Schematic diagram of an ICP-MS unit[191]

Firstly, the sample is extracted from a vial by peristaltic pump at a constant flow rate which is fed into a nebuliser producing a fine spray of the sample into the spray chamber. The nebulizer uses pressurised argon gas input at the nozzle site to create a mist of ultrafine liquid droplets. The fine aerosol of sample is then sent into the torch and any excess is extracted from a drain at the base of the spray chamber. The purpose of the plasma torch is to ionise the analyte to created charged positively particles atomised to a degree that the detector can analyse them. The plasma is created by high energy electrons in an argon atmosphere under a high intensity radio frequency which creates a plasma arc around at 10,000 K. The gas stream from the plasma torch is then injected into the mass spectrometer made up of a mass separation (usually triple quadrupole) and then a detector to analyse each mass fragment. Various mass separation units exist in mass spectroscopy (quadrupole, magnetic and time of flight) the most common in ICP-MS being triple quadrupole which uses radio frequencies to create channels for specific ions. The role of this section is to separate the ions in the gas stream by mass/charge ratio for the detector.

3.3.2.2 Methodology

Samples needed to be in a liquid state for analysis by our method, this was used for the elemental analysis of off-gas solutions from the system created at Sheffield Hallam University and the capture solutions from pyrolysis of Southampton (see section 3.3.6). These capture solutions were diluted x25 by volume, sample was mixed, a 4 ml aliquot was taken with a 1-10ml micropipette, added to a 100 ml volumetric flask and filled the mark with type 1 deionised water. The diluted sample was then taken and decanted into a 10 ml ICP-MS vial compatible with the sample changer and labelled. The vials were then place in the sample changer ready for analysis.

Figure 3.5. Image of Agilent Technologies 8800 Triple Quad ICP-MS and sample changer

The instrument (figure 3.5) was then internally calibrated by use of a SmartTune™ solution which contains a range of elements to cover light and heavy. The system then adjusted for torch alignment, system modes and quadrupole ion deflector detection from known standards made of from a solution of concentrated reference material. The range of the calibration solutions were adapted to cover the suspected range of concentrations in the diluted samples (for example for an expected concentration of 6 ppm in a sample a range of calibrations standards would be 0, 2, 4, 6, 8 and 10 ppm).

3.3.3 X-ray Diffraction (XRD)

3.3.3.1 Theory

X-ray diffraction (XRD) is a technique used to find crystalline phases in materials by detecting the scattered X-rays from a sample at certain angles depending on the surface of the material. This method can be qualitative or quantitative depending on the methods used, however, more commonly XRD is used for qualitative phase determination.

$$Equation\ 3.2 \qquad n\lambda = 2d\ sin\theta$$

Equation 3.2 shows Braggs Law[192] which describes the relationship between the crystal surface and the angle at which X-rays are diffracted from the material where n is the order of diffraction, λ is the wavelength of the X-ray from the source, d is the crystal spacing and θ is the angle at which the incident X-ray is relative to the sample surface. A crystalline structure of the material is what defines

the angle at which X-rays scatter and this ultimately creates a 'fingerprint' of the material based on specific 2θ angles and intensities at each angle. These are dependant on the d-spacing of the crystal, miller indices and other crystal parameters specific to a crystalline material.

Quantitative XRD can be completed by finding the relative intensity of each peak compared to a standard reference material, this is called Rietveld refinement. It finds a mass percentage of each crystalline phase over the surface analysed. A known amount of the reference material (usually silicon powder) is added to the sample and mixed well before sealing into the holder, this produces a single well pronounced peak that other analyte peaks can be compared to.

Sample state for this technique can be solid or liquid[193] the most common (and predominant in this study) being solid powder XRD. Other common forms of solid sample preparation include pressed pellets where the sample is mechanically pressed under high force in the presence of a binder (e.g. Cellulose) to create a fused pellet. This does create an interference peak from cellulose, however, this can normally be subtracted easily, manually or processed through software. A solid sample can also be measured without powering as a monolith. Liquid samples are possible with specialised holders and instruments, however, these are rarely used due to the difficulties in sample preparation and measuring.

3.3.3.2 Methodology

The material to be analysed by XRD was first powdered to approximately 500 µm to load into the instrument. Powdered sample was then loaded into a stainless steel sample holder of 20 mm aperture for larger volume samples and 10 mm aperture for samples with more limited volume. In the rare occasion that the sample was too small in volume to fill any of these sample holders the powder was dispersed over a silicon wafer using acetone and dried. Once the sample was prepared the holder was loaded onto a sample carousel and placed inside the instrument (Panalytical X-Pert^3 PRO). Collection was completed between 10 – 90 ° 2θ with a step size of 0.016 °

Figure 3.6. Image of XRD unit used for powdered samples, Panalytical X-Pert^3 PRO

Any non-powdered monolith samples were instead loaded onto the sample stage of the Panalytical Empyrean 3rd gen as bulk material, powder samples were the preferred method, however, for samples that required being one solid piece for other analyses the other method was used.

The instrument (figures 3.6 and 3.7) was set to 40 keV and 40 mA of power from copper K_α X-ray source with a scan length of 2 hours. After analysis the data was outputted to a computer and processed using HiScore plus software. Processing included background subtraction to highlight major peaks, peak finding and search/match against a database of known spectra. The best match(es) to the spectra that satisfies all the major peaks will be assigned and designated as the crystal structure of that sample, amorphous samples without peaks that did not satisfy any of these criteria were saved without background correction or peak assignment.

Figure 3.7. Image of XRD unit used for bulk samples, Panalytical Empyrean 3rd gen

3.3.4 X-ray Fluorescence (XRF)

3.3.4.1 Theory

XRF uses high energy X-rays to rapidly determine elemental composition of a solid glass, powder or even liquid samples. This occurs by the irradiation of a sample with sufficient energy to overcome the particular elements binding energy which moves an electron from the inner orbital of the atom[194]. This leaves an electron deficient orbital which is unstable therefore an electron from an outer orbital moves to fill that vacancy (figure 3.8). As this event occurs a fluorescent X-ray emits from the atom at a specific (lower) energy relating to the difference in energy between the two orbitals the electron has moved from[195]. This characteristic energy defines the element by the type of transition and the energy of that transition. The type of transitions are named as L – K (K_α), M – K (K_β) and M – L (L_α) where K is the innermost p orbital, L is the second most stable 3p orbital and the M shell above that.

‘α’ transitions occur over one shell (eg. L – K) whereas ‘β’ occurs over two (eg. M – K). Small atoms will only have a K_{α} spectral line as they do not have enough orbitals to allow M (or higher) shell transitions.

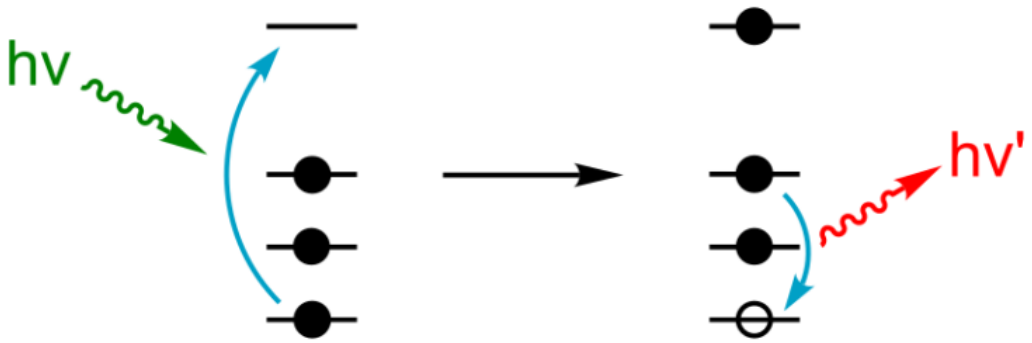

Figure 3.8. Diagram of the radiation induced electron interactions that XRF theory is based around[196]

Whilst this technique is non-destructive in terms of composition and crystallisation there is a colour change that occurs due to defects caused by radiation damage from the high energy X-rays. Whilst this does not effect the composition or any other factors measured in this study it may have a noticeable effect on density[197] and therefore all density measurements should be undertaken before XRF analysis.

3.3.4.2 Methodology

For XRF specific sample preparation procedures are needed to process the samples and acquire meaningful data. Standard sample preparation for samples containing only ‘heavy’ elements (above neon in atomic mass) were prepared as fused beads with the sample material effectively dissolved in a lithium tetraborate frit 99.5 wt% with 0.5% NaI at 1050 °C. Before the melting process the sample was powered and 1g was thoroughly mixed with 10 g lithium tetraborate flux. This was then placed in a 10 ml platinum crucible and held into the clamp arms of a Claisse® LeNeo® Fluxer fused bead maker (figure 3.9). The sample was then run on an automatic programme heating to 1050 °C at a heating rate of 15 °C / min dwelling for 30 mins and then poured onto a platinum mould. This was then cooled for 10 mins to anneal the fused bead and after this removed and sealed in a labelled bag. Fused bead method was used for the base glass analysis whereas other samples were poured manually and polished. This separate method will be given in relevant chapters.

Figure 3.9. Image of XRF fused bead maker, Claisse® LeNeo® Fluxer

For any samples containing lighter elements than previously mentioned the sample was kept whole and grinded to a flat surface on a Buehler Metaserv® 250 grinder-polisher (figure 3.10) stepwise with 400 – 1000 silicon carbide grit paper.

Figure 3.10. Image of rotary grinder, Buehler Metaserv® 250 grinder-polisher

Samples that cracked significantly or were too small to fit in the sample holder for XRF were not used and repeated. The benefit of not using fluxed fused beads is an increased signal from the sample due to it not being diluted and an ability to measure boron/iodine without having an artificially inflated boron/iodide signals in the XRF spectra interfering with the result. The sample was then placed a stainless steel sample holder with a 30, 20 or 10 mm aperture depending on the size of sample (fused samples fitting in a 30 mm aperture holder). These were placed in the sample changer of the instrument, a Rigaku ZSX PrimusIV (figure 3.11) using water cooling and a vacuum atmosphere to 1 Pa.

Figure 3.11. Image of XRF instrument, Rigaku ZSX PrimusIV

Each holder with sample enclosed was then subjected to 30 kV and 80 mA of power from a rhodium K_{α} 4 kW X-ray source for 25 minutes scanning the spectra from B Ka lines upwards in atomic mass varying from 30 mm to 10 mm spot size depending on the respective aperture used. After exposure samples were removed and labelled, if completed on the same sample XRF was always completed last due to the radiation damage potentially causing differences in future analyses. Contamination from the alumina crucibles used during the melting procedure can cause a higher alumina content that the true value which can produce some error in the results. Processing of the data can result in other components increasing or reducing because of this.

3.3.5 Thermogravimetric Mass Spectrometry (TG-MS)

3.3.5.1 Theory

This technique precisely measures the mass loss of an analyte over temperature/time and analyses the gas extracted by mass spectrometry. The standard instrumentation for the thermogravimetric portion uses two alumina weighing arms connected to a very sensitive precision balance which finds the total mass of each of the two arm ends[198]. One of the arms is a reference which should not vary with temperature as much as possible, candidates for this are powdered refractory type materials such as alumina, silica or an empty crucible as very few thermal events occur between the analysis temperature range of the instrument. The purpose of the reference is to have a comparative weight to the sample to calibrate the two pans when being tared and to correct for buoyancy due to the change in density as temperature changes. This is particularly important for differential thermal analysis (DTA) which measures the difference in heat flow between the two 'pans' highlighting endo/exothermic events that occur within the material. For example, these include glass transition[199], evaporation[178], crystallisation[200] thermal decomposition[201] and melting[199] (figure 3.12). As heat is applied evenly to the two crucibles any mass changes are measured and compared against each other for example if the sample is moist the mass loss of water will be noticed by the difference in one of the singular arms from the reference[202]. Over the sample and reference pans is a purging gas flow which can be either reactive (oxygen) or inert (nitrogen) depending on what is required.

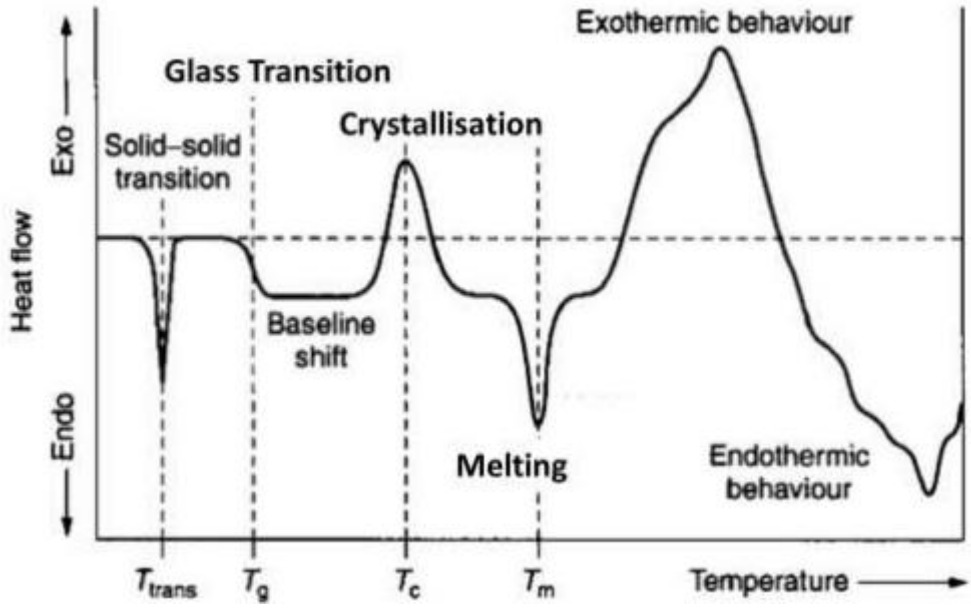

Figure 3.12. Diagram of common thermal events in differential thermal analysis traces

The mass spectrometry portion of the instrument takes the gas flow from the heated chamber and analyses it by separation of the molecules/fragments by mass. This can produce data that relates certain temperatures to gas evolution and gives information about the specific species present in that gas. Most TG-MS systems use triple quadrupole mass analysers as the most readily available MS unit, however, other magnetic or time of flight analysers can also be retrofitted for a higher resolution. A high resolution, however, is not normally required as many data points are being taken for each temperature reading. The gas flow must be kept at above 180 °C to avoid condensing gas particles in the tubing and lines which could alter the results of the run and potentially contaminate other future runs by producing mass peaks where they do not occur or subtracting them where they should. This is a large problem for coupled instruments, mass spectrometry and FTIR being the most common. Certain gaseous analytes may also condense at temperatures exceeding 180 °C and therefore may contaminate connecting tubing where the furnace is volatilising substances up to 1500 °C. This should be brought into account when mass loss is seen in the thermogravimetric spectra but no peaks seen in the mass spectra as the likelihood is that this is condensing somewhere in the system.

3.3.5.2 Methodology

The instrument used for this study was a TA instruments Discovery SDT 650 thermogravimetric analyser with an mks Cirrus^{TM} 3 mass spectrometer and auto-sample changer (figure 3.13). Gas transfer heated lines were kept at 300 °C for the entire run and reference material was 20 mg alumina powder in a 600 µl alumina crucible supplied by Almath crucibles ltd.

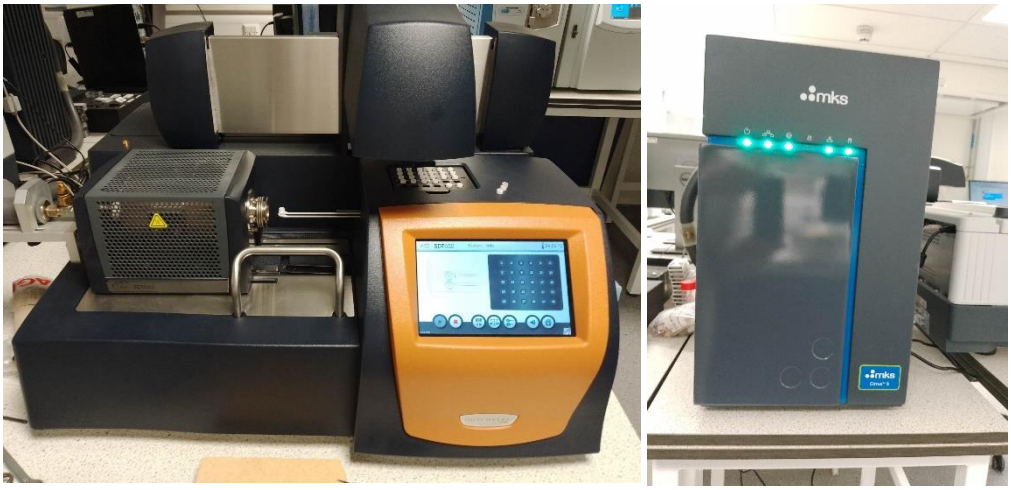

Figure 3.13. Images of thermogravimetric analyser, TA instruments Discovery SDT 650 (Left) Mass spectrometer analyser, mks Cirrus^{TM} 3 (Right)

Firstly, the empty crucibles and standard were tared automatically by the instrument and the reference material calibrated. Then approximately 20 mg of the sample was weighed into a small 60 µl alumina crucible and placed into the sample changer tray. The programme was then set to automatically place the reference and sample crucibles on the weighing arms one at a time and then close the furnace tube surrounding the sample and reference. The instrument was then set to set the flow of the gas to either nitrogen or air depending on the experiment being run and then equilibrated for 10 mins to achieve a constant temperature. After this step the furnace ramped at 10 °C / min to the max set point of the run (900-1250 °C) and held at maximum temperature for the required time for the run (maximum 2 hours). The furnace is then left to cool below 50 °C at which point the sample is removed and the next is loaded (or the run ends if it is the last in the series). Any remaining material is discarded with the crucible.

3.3.6 Pyrolysis

Crucibles were needed to fit the pyrolyser work tubes that could withstand high heating/cooling rates and contain 1-5 g borate glasses with 1 ml of an aqueous radioactive spiking solution. Alumina crucibles cannot withstand high heating rates and therefore quartz was chosen as the crucible material. These were bespoke fabricated by MultiLab in an open half cylinder boat form (dimensions L 125 mm x W 20 mm x H 10 mm).

Solutions needed to be prepared before the experiments were carried out. These were:

- 0.5 mol% Tetramethylammonium Hydroxide (TMAH)
- 10 bq/ml CsCl stock solution 100 µl / g
- 20 bq/ml NaI stock solution 60 µl / g

These were prepared by diluting down the stock solutions (99.5 % TMAH, 2.3 kbq/ml CsCl, 1.4 kbq/ml NaI) to their respective target concentrations.

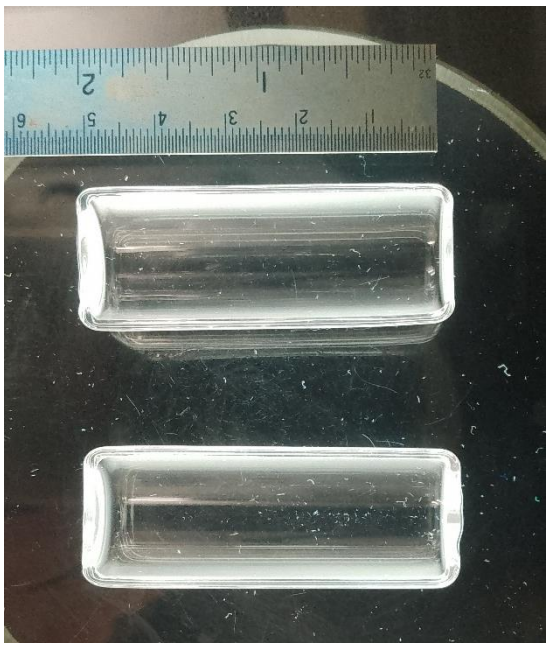

Figure 3.14. Image of quartz boat dimensions for pyrolysis

The quartz boat was weighed, recorded and 2 g of sample also weighed into the boat. The boat and samples were then sealed in a storage box and taken to the pyrolysis instrument for doping and

putting into the working tube. 50-100 ml borosilicate bubbler bottles were then pre-weighed and filled with 20 ml of absorption solution (0.5% TMAH for iodine and 0.1M HNO_3 for caesium) with the final total mass also being recorded. At the same time the furnace was also set to pre-heat the centre zone to 800 °C. The sample in quartz boat was then spiked with 1 ml of the dopant solution to add: 20 Bq of activity and 0.01g of I- for iodine, 10 Bq of activity and 0.02 g Cs^+ for caesium, 0.02g Cl^- for chlorine. The doped samples and crucibles are then placed in the sample section of the furnace and end caps placed to seal the working tubes for controlled gas flow. The flow gas was set to air and flow rate kept constant during the test. The sample section of the furnace was then set to run to heat at 15 °C/min to 110 °C holding for 1 hour to dry and then 950 °C to heat at 15 °C/min maximum temperature and then held at temperature for 1 hr. After the programme was finished the bubbler glassware was disconnected, weighed post-test and decanted into 30 ml plastic bottles. The furnace was left to cool to room temperature and the glass samples in crucible removed the next morning. The crucibles were then analysed by gamma spectroscopy counting for 1 hour for caesium/iodine and in a large batch by SEM-EDX for iodine/chlorine. Bubbler solutions after liquid scintillation counting (LSC) were analysed by gamma spectroscopy for caesium/iodine and ICP-MS for iodine/chlorine.

Figure 3.15. Image of pyrolyser instrument used in this study, Raddec Pyrolyser 6

3.3.6.1 Gamma Spectroscopy

3.3.6.1.1 Theory

This technique quantifies gamma rays from a sample, measuring and quantifying the energies of the gamma emission. Detectors are normally passive scintillator materials that respond to gamma ray excitation for example, semiconductor units using germanium[203]. The material produces a voltage relative to the energy of the gamma emission by causing a flow of electrons from the excitation which is amplified to a detectable signal[204]. The casing is normally made of lead for shielding purposes and constantly cooled with liquid nitrogen to improve the efficiency of the detector.

3.3.6.1.1 Methodology

This method was used for ^{137}Cs activity determination of the resultant glass. Firstly the gamma spectroscopy instrument needed to be calibrated for the geometry of the sample, in this case the shape of glass in a crucible upright in the chamber. This was done by drying 1 ml of the stock ^{137}Cs to the quartz crucible pictured in figure 3.13 at 100 °C for 1 hour. This was then used as a standard reference of the maximum ^{137}Cs activity possible if no loss occurred and gave the geometry of the following samples. Solid samples from pyrolysis that required gamma radiation counting were placed in the instruments central well and sealed in. The sample was then counted for gamma activity for 1 hour.

Figure 3.16. Images of gamma spectroscopy instrumentation

3.3.6.2 Liquid Scintillation Counting (LSC)

3.3.6.2.1 Theory

LSC is a technique which measures β radioactivity in a liquid sample by using a fluorescent compound which is excited by radiation to produce light energy[205]. The fluorescent compound has been modified over the years from crystalline organic materials such as napthelene and anthracene in solution to the modern form we use today polyphenol oxidases or PPO (today optimised and branded as GoldStar cocktail)[206]. The compound (or collection of compounds) selectively absorbs the β radiation becomes excited and flashes visible light as the electron decays from its excited state. The light emission is relative to the radiation the compound is exposed to and using this the β activity of the sample can be found.

This technique is especially useful for low energy beta emitting elements due to the difficulty in measuring these by other methods. Tritium (H_3) especially was very challenging to analyse due to its low energy radiative emissions[205]. Previously solid scintillators were used which took hours to analyse β radiation and had difficulty with low energy emitters. LSC is able to analyse samples within minutes and its used routinely for tritium analysis.

3.3.6.2.2 Methodology

Samples for LSC analysis were taken from the solutions resulting from pyrolysis capture of iodine from samples which were initially doped with iodine (and blanks). 5 ml of bubbler solution were taken and mixed with 15ml of GoldStar™ liquid scintillation cocktail (Meridian Biotechnologies) in a clear 30ml scintillation vial. This was then placed in a Perkin Elmer Quantulus 1220 liquid scintillation counter (figure 3.16) and counted for 1 hour with 2 hours of initial darkness exposure adjustment.

Figure 3.17. Image of liquid scintillation counter instrument, Perkin Elmer Quantulus 1220

Chapter 4 Glass Composition Development

4.1 Introduction

The work in this chapter focusses on four groups of glasses, however, these were developed and modified for various experimental procedures to optimise the properties that were required (e.g. composition, melting temperature).

In this chapter we will discuss the different compositions and properties of all the glasses used in this study from the high temperature systems melting at 1400 °C, 1150 °C to lower temperatures at 950 °C.

Using the information from the four original base glass candidates one was taken forward to develop new glass systems in section 4.7 which are designed to be able to function as nuclear waste matrixes at 950 °C. One of the main factors for volatilisation is temperature of the melt environment which, to create a fully amorphous glass, is limited by how the glass crystallises if we are creating a final product that is a suitable wasteform. Therefore, to minimise volatilisation behaviour by reducing melting temperature (whilst maintaining an amorphous end product) we need to modify the glasses we already use. If we used the original borosilicate compositions at the lower temperatures the glasses would likely be below the softening points and therefore the additive/radionuclide would be much harder to incorporate into the structure and has a higher chance of forming a non-stable crystalline end product. CaZn was determined to be the most suitable glass for waste incorporating at 950 °C because of its lower melting temperature, its ability to incorporate waste and its current use in the nuclear industry.

To achieve the target melting temperature and to allow the glass to accept silica containing wastes such as clinoptilolite we modified CaZn by reducing the concentration of silica in the frit and increasing the concentration of all other components on a pro rata basis.

4.2 Methodology

Firstly, initial glass development was on the two common radioactive waste base glasses used in the UK (MW and CaZn), and two commercial base glasses a calcium aluminosilicate glass (CAS) and soda lime silica (SLS) glass (compositions shown in table 4.1 in the next section). Glasses were formulated by weighing and mixing dried batch materials and then placing in an alumina crucible for melting. Temperatures of 1450 °C, 1400 °C and 1150 °C and a dwell time of 2 hours were required to process the batch materials in an electric melting furnace (see table 4.1). SLS was melted at 1450 °C, CAS at 1400 °C and both MW and Ca/Zn at 1150 °C.

Glass modification studies are undertaken by removing SiO_2 from MW and CaZn glass as described in the previous section. To firstly understand the melting properties of each product the compositions (see tables 4.3 & 4.4) were melted at different silica concentrations (0 – 50%) in 20 g batches. The quality of the glass was then assessed by XRD and ease of pour to determine and crystalline phases that could solubilise waste components in future experiments. The glass set (MW or CaZn) which remained the most amorphous over this range was selected to continue and then the 0% SiO_2 variation was selected to allow the highest waste loading. Frit of these glasses were made in 250 g batches and melted at 950 °C and then milled to below 500 µm to form a homogeneous glass powder for future experiments.

4.3 Base Glasses

4.3.1 Glass Compositions

Compositions of the base glasses used in this study are shown in table 4.1.

	Composition (wt%)							
	MW		CaZn		SLS		CAS	
	Target	Analysed	Target	Analysed	Target	Analysed	Target	Analysed
SiO_2	61.75	58.57	47.60	44.52	72.60	71.23	56.80	55.58
B_2O_3*	21.88	25.41	23.40	27.32	-		-	-
Na_2O	11.05	10.69	8.60	8.20	13.10	13.50	-	-
Al_2O_3	-	-	4.20	4.65	0.70	2.19	17.80	18.85
CaO	-	-	6.00	5.80	8.80	8.36	25.40	25.57
Li_2O*	5.33	5.33	4.20	4.20	-	-	-	-
ZnO	-	-	6.00	5.31	-	-	-	-
MgO	-	-	-	-	4.30	4.01	-	-
K_2O	-	-	-	-	0.50	0.71	-	-
Total	100.01	100.00	100.00	100.00	100.00	100.00	100.00	100.00
Melt Temperature (°C)	1150		1150		1450		1400	

Table 4.1. Primary base glass compositions. Analysed by XRF. *Lithium and boron content estimated.

MW and CaZn glasses we have discussed in section 2.1 are borosilicate glasses and well documented in the UK nuclear waste decommissioning field. Calcium aluminosilicates (CAS) glasses are different glass systems with the majority of the modifier content being CaO, a higher melting temperature than most borosilicates and have been used for E-glass formulations in glass fibre manufacturing for decades[76]. In addition, at 1400 – 1450 °C both SLS and CAS had very high viscosity causing the sample to have difficulty pouring from the crucible.

4.4 Characterisation of MW and Ca/Zn Batch Materials

Both batches of glass showed similar trends in TG-MS traces with mass losses and major peaks occurring at similar temperatures, with the exception of a few peaks (figure 4.1) that are individual to certain batch material reactions that occur in MW and CaZn batches. CaZn also loses more mass in total (24.57 wt%) than MW (21.92 wt%), this is mostly due to the batch materials containing more carbonates and losing mass as carbon dioxide rather than loss of the glass forming/modifying/structural components. Calcium and lithium are both added as carbonates ($CaCO_3$

and Li_2CO_3) in the CaZn batch and as a result of thermal decompositions that release carbon dioxide. Both glass batches had a significant mass loss at 130 °C (11.92 % for MW and 12.72 % for CaZn) with an endothermic shoulder peak in the DTA at 168 °C representing two distinct water evaporation reactions. In addition, both had very similar DTA patterns between 500 – 1200 °C although mass losses were more severe and slightly delayed in CaZn compared to MW with similar thermal events. The significant differences in DTA data between the two glass systems come from one peak at 286 °C in the CaZn trace and 484 °C in the MW trace.

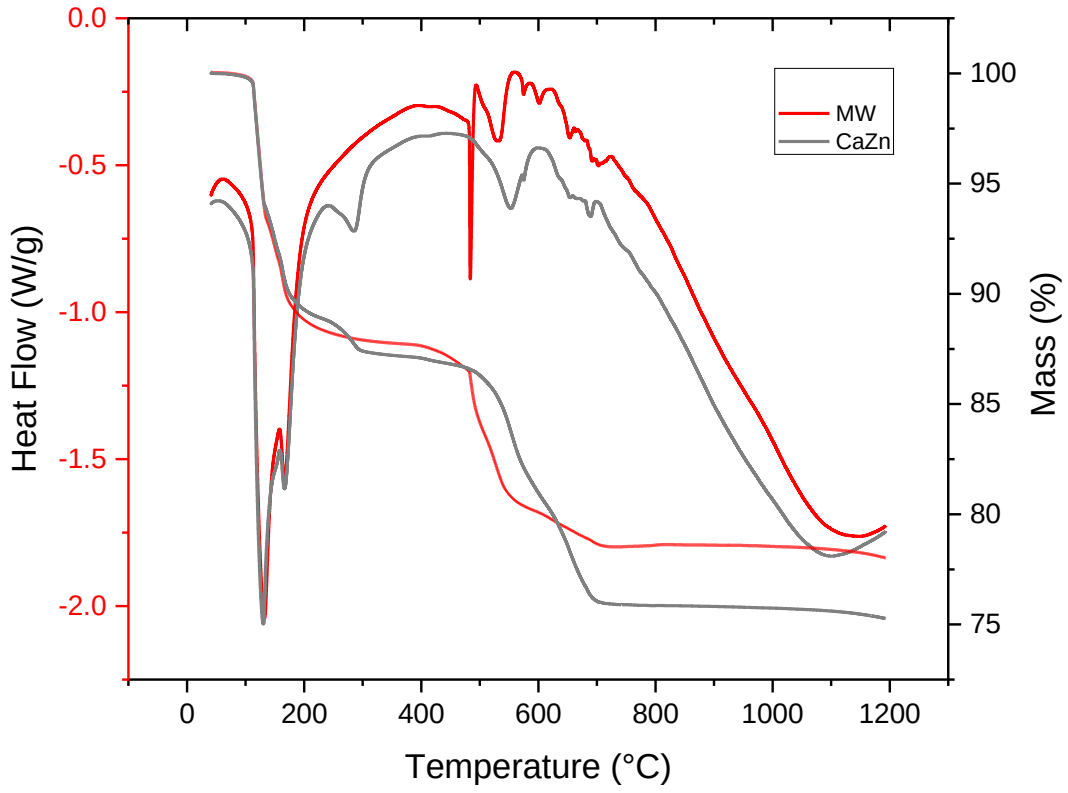

Figure 4.1. TG-MS trace of MW and CaZn base glass starting from batch materials

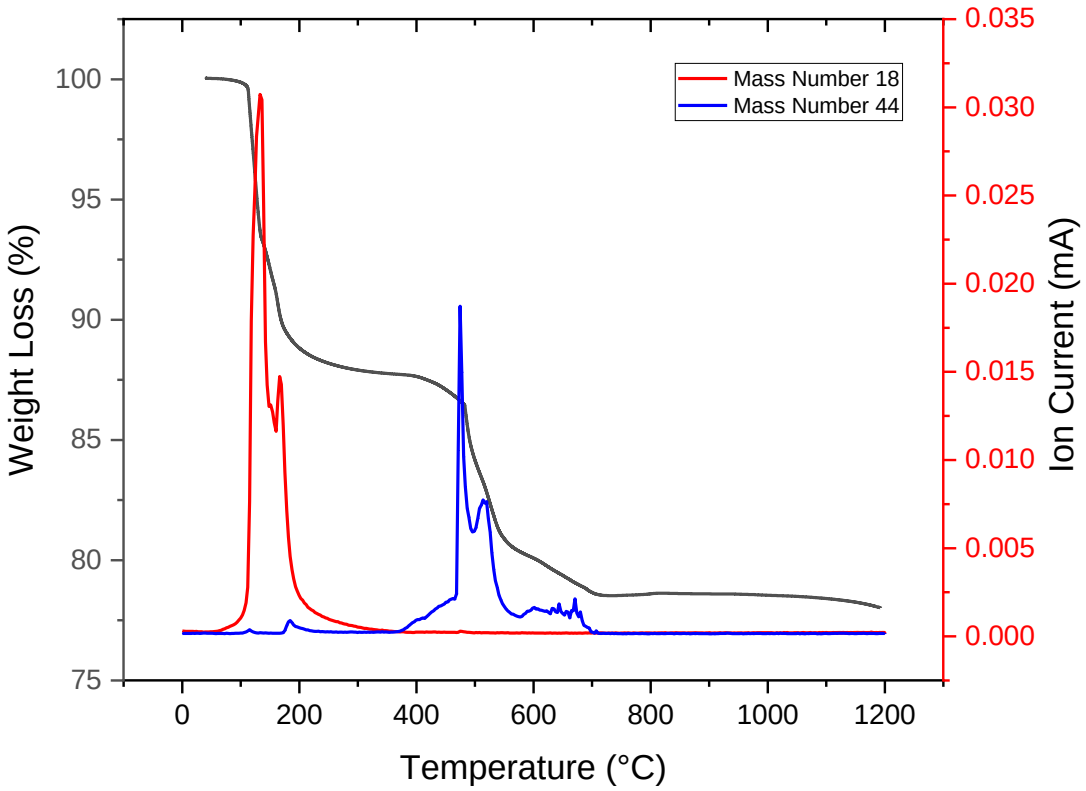

Figure 4.2. Mass spectrometer intensities (red and blue lines) for major emissions from MW glass batch relating to weight loss (grey line) of the batch, weight loss = ■ , AMU 18 = ■, AMU 44 = ■

In figure 4.2 the MS signals show that the MW batch loses predominantly those with an atomic mass of 18 and 44 relating to H_2O and CO_2. The emission of H_2O at 130 °C and 168 °C corresponds to the same peaks in the DTA suggesting this initial mass loss under 300 °C mostly relates to H_2O loss. The water loss in this section is significant and relates to not just atmospheric moisture loss from batch materials but also the loss of physiosorbed water from hygroscopic boric acid (H_3BO_3) drying[207]. In MW glass 29.29 wt% of the batch is H_3BO_3 and theoretically 12.80 wt% of that is lost (43.70 % of the total boric acid mass) as water during the decomposition reaction:

$$2H_3BO_3 \xrightarrow[Dec.\ 150\,^{\circ}C]{} 3H_2O + B_2O_3$$

This equates closely to the 11.92 % mass loss seen in the batch TG trace therefore the majority of this emission in due to boric acid. The CO_2 peaks in the mass spectrometry graph very closely match the position of the weight losses at 400 – 700 °C which is a 9.05 % total mass loss. The total contribution to mass from carbonates in the batch is 24.18 % and the mass of carbon dioxide loss assuming

complete decomposition is 11.83 %. This is greater than the actual mass loss of 9.05 % we see around this temperature which indicates either not all of the carbonate raw materials are decomposing, carbon is incorporating into the glass structure or carbon dioxide is being entrained in the glass as bubbles rather than emitting to atmosphere. The major peaks at 483 °C, 530 °C and minor peaks at 651 °C from the MS can be assigned to CO_2 and matched with the DTA peaks at these temperatures. These correspond to $NaCO_3$ and Li_2CO_3 thermally decomposing in the MW batch. The earlier peak at 483/530 °C is likely to be $NaCO_3$[208] and above that the minor peaks around 600 – 700 °C are Li_2CO_3[201] based on comparisons with literature.

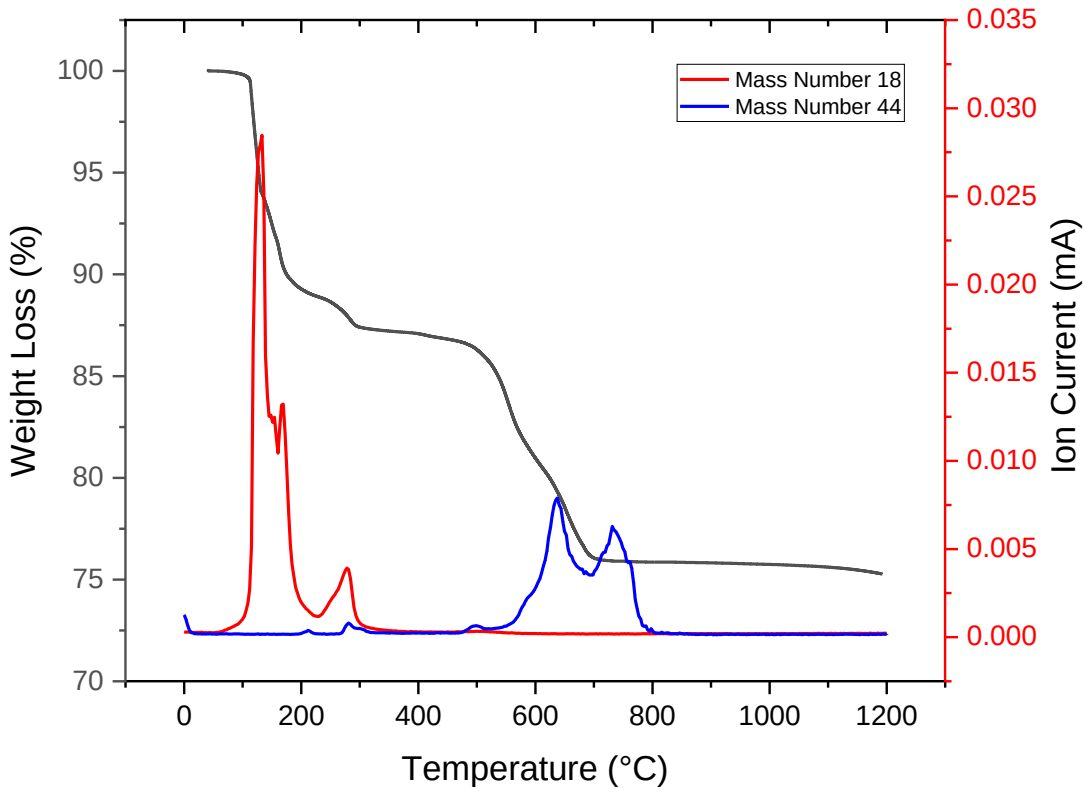

Figure 4.3. Mass spectrometer intensities (red and blue lines) for major emissions from CaZn glass batch relating to weight loss (grey line) of the batch, weight loss = ■, AMU 18 = ■, AMU 44 = ■

In CaZn batches the same H_2O peak is seen (figure 4.3) at 130 °C and 168 °C and as a boron containing batch we can assume the same reaction is occurring here where boric oxide is forming from the acid. The only difference in the AMU 18 MS is at 284 °C where another evaporation/decomposition reaction occurs separate to MW also appearing as endothermic peaks in the DTA and relating to a stepwise

mass loss by TGA. This is due to the aluminium containing reagent material being $Al(OH)_3$ and releasing H_2O by the following reaction:

$$2\mathrm{Al(OH)_3} \xrightarrow[dec.\ 284\,^{\circ}\mathrm{C}]{} 3H_2O + Al_2O_3$$

Carbon dioxide loss is seen at 500 – 800 °C with two distinct peaks at 632 °C and 732 °C maintaining that two (or more) separate decomposition reactions occur. Breaking down the distinct areas of mass loss in the TGA trace of the CaZn batch reactions we can see 4 steps relating to 4 different events. The first 11.14 % at 100 – 200 °C as we have discussed is likely drying of the raw materials and decomposition of boric acid, calculated losses of water (see table 4.2) from boric acid equate to 13.22 % of the total mass of the batch. The second step was a 1.79 % reduction at 200 – 300 °C comparing closely to the calculated 1.62% loss of water from Al(OH). The third step gradient at 425 – 582 °C represents a 5.20 % loss of mass from the sample, given literature and degree of loss this can be assigned to carbon dioxide evolution from sodium carbonate. The final step 582- 725 °C makes up the losses from the remaining carbonates (Li_2CO_3/$CaCO_3$) (table 4.2).

		Mass Loss (%)		
Step	Temperature Range	Measured	Calculated (H_2O/CO_2)	Decomposition Assignment[37,201,209,210]
1	100 – 200 °C	11.14	13.22	H_3BO_3
2	200 – 300 °C	1.79	1.62	$Al(OH)_3$
3	425 – 582 °C	5.20	4.44	$NaCO_3$
4	582 – 725 °C	5.69	4.50/3.43	Li_2CO_3/$CaCO_3$

Table 4.2. CaZn batch mass losses from distinct sections of the TGA plot

4.5 Characterisation of Base Glass

Now we understand the thermal events of the batch reactions we can investigate the details of the fritted resultant glass product.

4.5.1 Crystal character of base glass compositions

Figure 4.4 shows any crystalline nature of the base glasses, however, upon lower heating temperatures the material either remained in batch form or heavily crystallised into multiple phases. In addition, the high melting temperature (1400 – 1450 °C) required for SLS and CAS glasses would

significantly volatilise any components and therefore was not considered a good candidate glass to continue studies on. For reference, in section 2.4 we covered the temperatures at which caesium (900 – 1000 °C)[159], iodine (600 – 695 °C)[134] and chlorine (800 – 1000 °C)[20] are likely to become volatile. Borosilicate base glasses are much better suited to nuclear waste incorporation and were continued with as candidate glass host, these are shown in table 4.1.

The experiments completed show that there is crystallisation of SiO_2 (cristobalite) even dwelling the batch materials at 1300 °C for 2 hours. Applying this to thermal treatment in the nuclear industry, glasses need to flow easily to pour into containers safely and reduce blockages. These properties

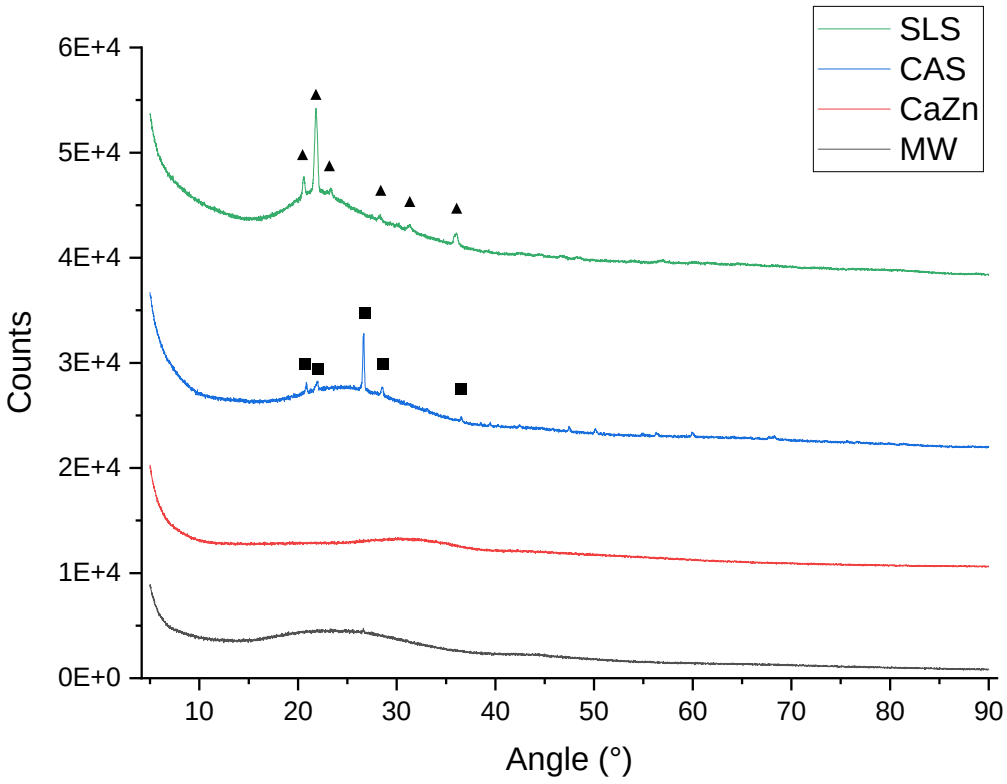

Figure 4.4. XRD comparison of base glasses MW, CaZn, calcium aluminosilicate (CAS) and soda lime silicate (SLS) melted at 1150 °C ▲= SiO_2 (cristobalite phase ID: 04-007-2134), ■ = SiO_2 (quartz phase ID: 00-033-1161).

would not be desirable for a radioactive waste glass and therefore CaAlSi glasses were decided against for continuing with further testing. MW and CaZn glasses were both found to be X-ray amorphous melting at 1150 °C for 2 hours with a heating rate of 10 °C/min (see figure 4.1) and were not too viscous to be poured from a crucible to a mould. These two glasses were the best candidate glasses in

our set for continuing future experiments with given that they could more suitably be used to melt at lower temperatures, load waste and pour sufficiently.

4.5.2 Density of base glass compositions

Density measurements showed that MW had a density of 2.45 g/cm^3 and CaZn 2.58 g/cm^3. This is consistent with literature as MW matches closely as similar borosilicate glasses[211] are calculated to have a density of 2.45 g/cm^3. The same can be shown for CaZn with a reference density[212] of 2.56 g/cm^3. Part of the base glass development was understanding these systems in greater detail. TG-MS on the batch and fritted glasses highlights important properties such as the glass transition temperature and for the batch reagents when certain components melt. All of these were completed under air, however, there was little difference in nitrogen atmosphere. In addition, if there are any volatilisation events from the batch/frit independent of any additives/wastes then we need this information as a baseline to identify any other losses.

4.5.3 Thermal analysis of base glass compositions

The TGA/DTA trace in figure 4.5 compares MW and CaZn glasses as they are remelted up to 1200 °C. Mass loss of the glasses over this period are fairly similar and are low (1.45 % for MW and 0.64 % for CaZn). Some of this could be from the frit taking moisture from ambient air, however, no 18 AMU mass intensities were found in the MS (no peaks appeared in the MS) and the main mass loss was seen above 800 °C, far above the normal drying temperature. This suggests that another mass loss event is occurring above 800 °C most likely boron/sodium derivatives. This would also explain the slightly larger mass loss seen in MW as it contains less stabilising elements such as zinc and aluminium. From the DTA we can calculate glass transition and melting temperature of the glasses. MW has a glass transition of 502 °C, a second at 649 °C with a melting temperature of 795 °C whereas CaZn has a lower temperature of glass transitions and melting at 497 °C, 625 °C and 750 °C respectively. Boron, sodium and calcium are known to reduce both of these temperatures in glass systems therefore we

are likely seeing these effects in CaZn glasses. These elements interact and interrupt the glass network to reduce the average bond strength throughout the structure reducing T_g and T_m.

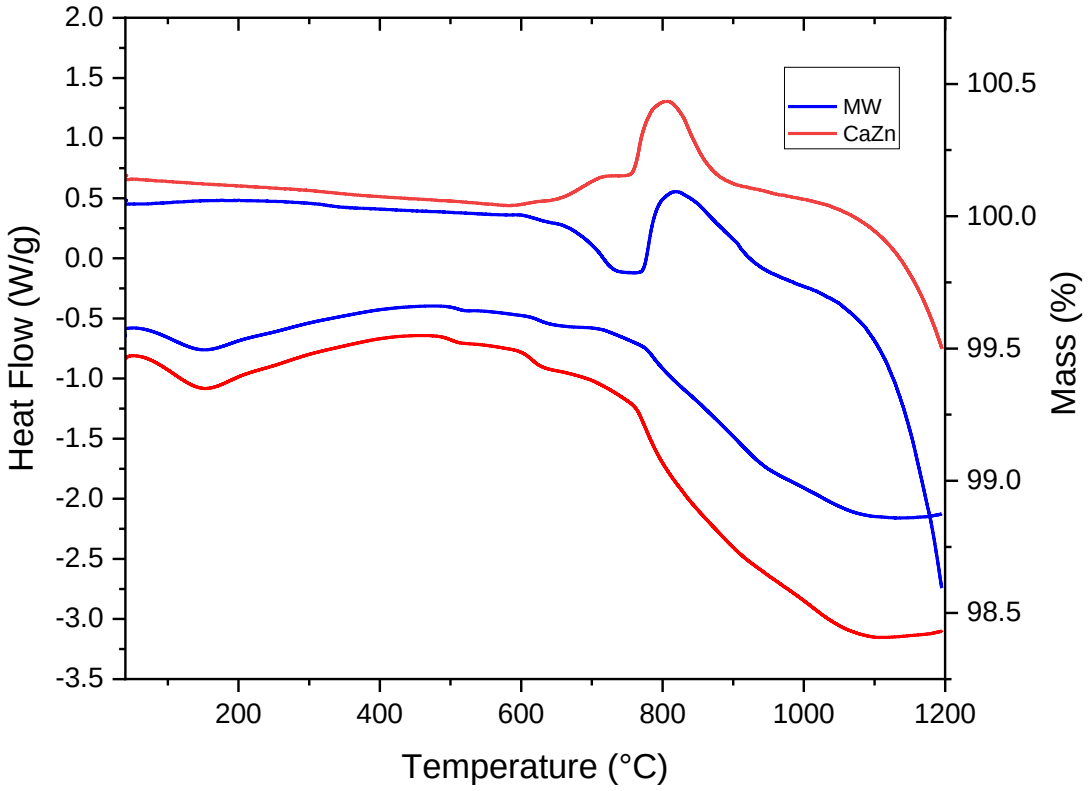

Figure 4.5. TGA (top) and DTA (bottom) trace of MW and CaZn glasses remelting

4.6 Glass selection

Glass Properties			
Glass	Density (g/cm^3)	T_g (°C)	T_m (°C)
MW	2.45	502	800
CaZn	2.58	497	775

Table 4.3 Summary of MW and CaZn base glass properties

Discussions with field experts and looking at the temperatures used in most vitrification plants (1000 – 1150 °C), SLS and CAS were considered to require operating temperatures that are too high[111] for practical use. This is based on the knowledge that crystallisation occurred at 1400/1450 °C in both glass products (figure 4.4) and these temperatures are significantly higher than 1150 °C or lower than is generally used in the nuclear industry. Therefore continuing through this chapter we use MW and CaZn as our base glasses and for any derived glasses we developed in section 4.7 properties in table 4.3.

4.7 Borosilicate Glass Modifications

The first modification attempted was to reduce the silica content in both MW and CaZn base compositions and increase the other components proportionally. Pre-melting, silica content was adjusted between 50 wt% down to 0 wt% (tables 4.4 & 4.5) and all the batches heated at 10 °C/min to 950 °C and dwelled at maximum for temperature 2 hours.

	Target Composition (wt%)						
	MW	**0% SiO_2**	**10% SiO_2**	**20% SiO_2**	**30% SiO_2**	**40% SiO_2**	**50% SiO_2**
SiO_2	61.75	0.00	10.00	20.00	30.00	40.00	50.00
B_2O_3	21.88	57.19	51.47	45.75	40.03	34.31	28.59
Na_2O	11.05	28.88	25.99	23.11	20.22	17.33	14.44
Li_2O	5.33	13.93	12.54	11.14	9.75	8.36	6.97

Table 4.4. Target composition for MW glass alterations between 0 wt% and 50 wt%

	Target Composition (wt%)						
	Ca/Zn	**0% SiO_2**	**10% SiO_2**	**20% SiO_2**	**30% SiO_2**	**40% SiO_2**	**50% SiO_2**
SiO_2	47.6	0.00	10.00	20.00	30.00	40.00	50.00
B_2O_3	23.40	44.66	40.16	35.73	31.26	26.79	22.33
Na_2O	8.60	16.41	14.77	13.13	11.49	9.85	8.21
Al_2O_3	4.20	8.02	7.21	6.41	5.61	4.81	4.01
CaO	6.00	8.02	7.21	6.41	5.61	4.81	4.01
Li_2O	4.20	11.45	10.31	9.16	8.02	6.87	5.73
ZnO	6.00	11.45	10.31	9.16	8.02	6.87	5.73

Table 4.5. Target composition for CaZn glass alterations between 0 wt% and 50 wt%

The maximum silica content in this series (50 wt%) slightly goes above the base glass composition for CaZn with 47.6 wt% being the original silica concentration, however, this is not the case for MW. As can be seen in tables 4.3 and 4.4 proportionally all the other components eg. (B_2O_3, Na_2O) increase in concentration as the silica is substituted out. These glasses were analysed for their qualitative melting properties (ease of pouring, observed crystallisation or discolouration) and also measured by XRD to determine crystal character that the samples had (if any). For most of the glasses in the series a clear, easily poured product was found, in figure 4.6 we can see there is little change in the colour/clarity. It is worth noting in the photos that the bright white colour in the 0 %wt SiO_2 is the glare from the backlight reflection used on the strain viewer and doesn't represent any crystallisation in the sample.

In addition, some of the samples either did not pour from the crucible due to high viscosity or cracked during cooling so the appearance may be changed in these samples.

0 wt% SiO_2	10 wt% SiO_2	20 wt% SiO_2	30 wt% SiO_2	40 wt% SiO_2	50 wt% SiO_2

Figure 4.6. MW and CaZn glass reducing silica content, Top row MW glasses, Bottom row CaZn

In particular, the cracked sample for the MW 30 wt% and highly viscous CaZn 50 wt% sample were difficult to pour, demonstrating that viscosity lowers with decreasing silica content in both MW and CaZn glasses CaZn 50% wt% SiO_2 was impossible to pour from a crucible at 950 °C and all the 0 wt% SiO_2 borate glass pouring with a similar viscosity more akin to water. Figure 4.6 at a surface level shows the crystallisation that occurs in CaZn glasses above 30 wt% SiO_2 where small white particles appear dispersed throughout the samples. By XRD these crystallisation events were shown to be from SiO_2 quartz (figure 4.8) decreasing in intensity as the silica concentration decreases, reflections disappearing at 30 wt% SiO_2. This correlates with what was observed visually as this is when white crystals were seen in the glass/glass-ceramics in the CaZn series. Other than this there were no other

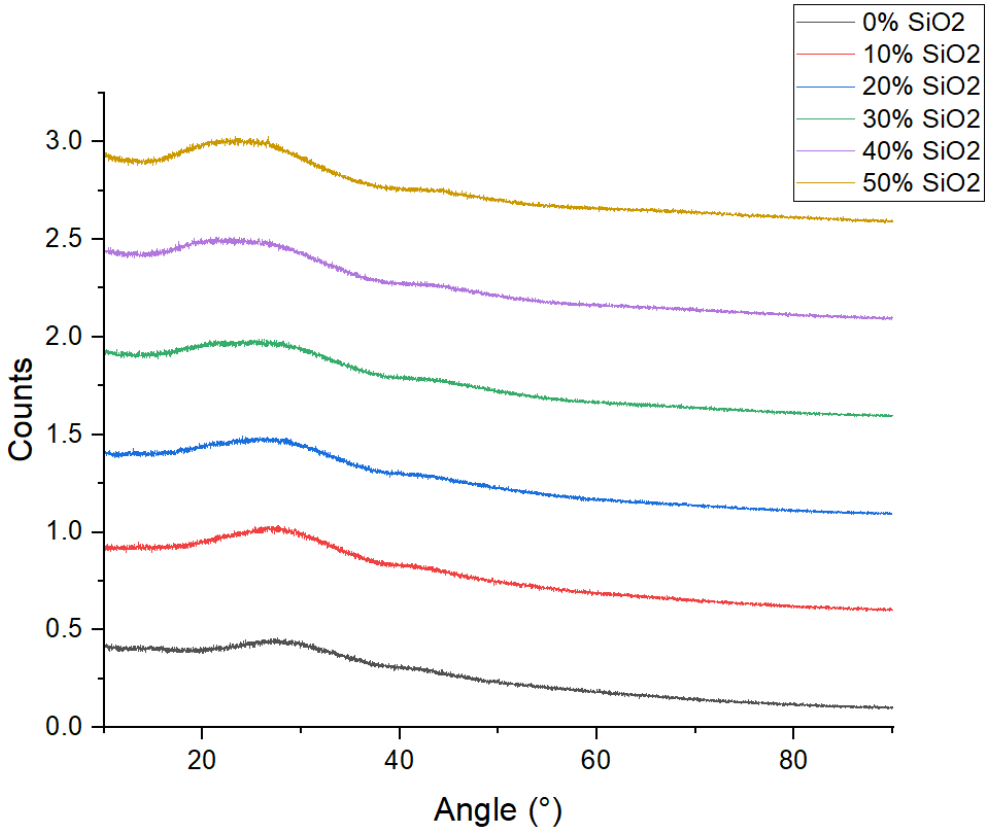

Figure 4.7. XRD pattern of MW glasses with varying concentrations of silica. Melted at 950 °C.

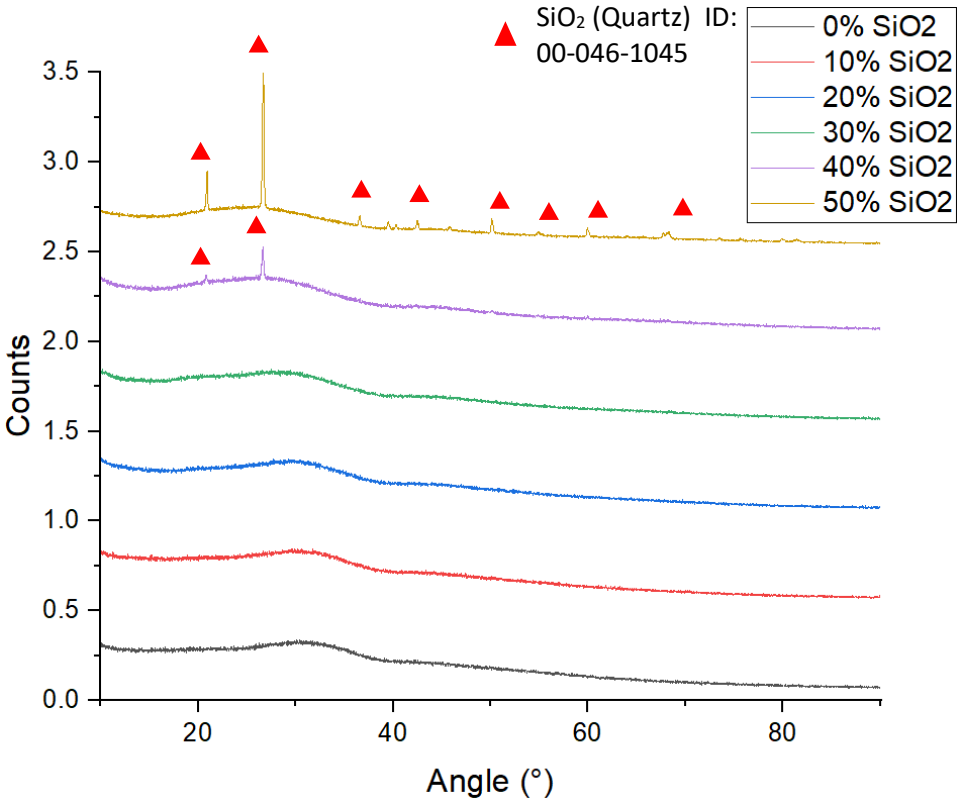

Figure 4.8. XRD pattern of CaZn glasses with varying concentrations of silica. Melted at 950 °C.

peaks in the XRD patterns for either the MW or CaZn glasses the other remaining pattern only shows the large amorphous hump that is representative of non-crystalline solids (figure 4.7). This suggests the products from these experiments were largely amorphous glasses even down to silica free glasses where the main glass former is boron rather than a mix of silica and borate units modified by sodium/lithium/calcium etc. This could have interesting implications for the nuclear industry if other glass systems with lower melting temperatures could be used, volatility could be reduced, CO_2 from power generation reduced and crucible/tank corrosion reduced. However, the occurrence of crucible corrosion on alumina crucibles used in this study did increase dramatically for the samples that contained no silica. Figure 4.9 shows the crucible after pouring the liquid glass and it can be seen that a deep melt line is visible where the molten glass interfaces with the air, crucible and molten glass. This could be concerning for use of this glass system if the molten glass is in contact with any corrodible material, especially ceramic based refractories as they are most comparable to the alumina crucible.

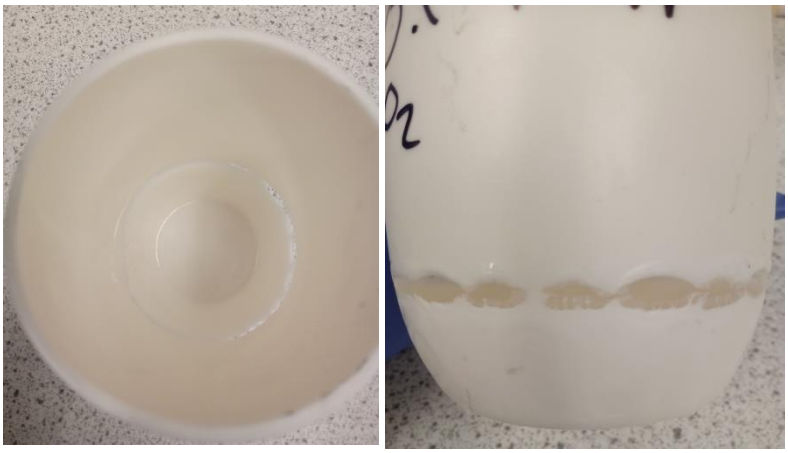

Figure 4.9. Crucible corrosion visible on alumina crucibles after melting MW 0 %wt SiO_2 compositions at 950 °C for 2 hours.

For the fritting of glass batches for larger scale production in the laboratory we needed to ensure that the melting temperature is correct to reduce alumina contamination from dissolution of the crucible and to reduce any unnecessary volatilisation of the original glass composition (e.g. Boron, Sodium). The corrosion seen in MW 0 %wt SiO_2 batch to glass preparation clearly indicates the melting temperature is too high. The highly fluid liquid glass has more of an impact on the corrosion of the crucible and for that reason adjusting the melting temperature before melting large batches was a

priority to produce effective base research glasses. Of the series of compositions in tables 4.3 and 4.4 4 were selected (2 from MW and 2 from CaZn) to continue with (alongside the original MW and CaZn glasses) based on crystallisation behaviour and glass structure. Borate glasses are different structurally so interesting to investigate for volatility and nuclear waste incorporation applications, reduced silica would provide an insight into the role of silica compared to silica free/full silica frits. For these reasons the 0 % SiO_2 and 30 % SiO_2 glasses were selected from each set as the candidates for production and refining. These four glasses were then melted between 600 and 950 °C to determine the correct temperature to produce a suitable end product, this was achieved qualitatively by observing viscosity and crystallisation of the melt upon pouring. Table 4.6 shows the quality of the glass upon pouring for all four glasses.

Glass	**Melting Temperature (°C) (2 hr dwell)**				
	600	**700**	**800**	**900**	**950**
MW 0 wt% SiO_2	X (partially glassy)	✓	✓	✓	✓
CaZn 0 wt% SiO_2	X	X (partially glassy)	✓	✓	✓
MW 30 wt% SiO_2	X	X	X (partially glassy)	✓	✓
CaZn 30 wt% SiO_2	X	X	X (partially glassy)	✓	✓

Table 4.6. Glass quality over 600 – 950 °C melting temperatures based on viscosity and observed crystallisation of the end product. (✓ = amorphous glass, x = crystalline non glass)

Both the silica free glasses had a much lower effective melting temperature than the silica containing systems due to the silica content increasing the viscosity and reducing the amount of dissolved components at those temperatures. In table 4.5, comparing the two silica free glasses, however, we see that MW produce amorphous glass at a lower temperature than CaZn. This is most likely due to the boron oxide content (which has a lower melting temperature than lithium carbonate and sodium carbonate) being higher in MW whereas CaZn substitutes 12 wt% of the B_2O_3 in the structure for calcium carbonate, zinc oxide and aluminium oxide. These reagents will increase the melting temperature of the whole bulk resulting in unmelted parts of the batch or significant crystallisation at temperatures higher than without those reagents. In the case of these glasses the effect is around

100 °C between the two, however, when the silica content is higher the changes are a lot less pronounced. At 30 %wt SiO_2 the two glasses were observed to react similarly with MW and CaZn, viscosity of the pouring appearing the same and the glasses forming crystalline components (SiO_2) at a similar temperature. This was the case until 900 °C where a sufficiently glassy product was formed from batch reagents for both glasses at 30 wt% SiO_2. The results of this work were that the future operating temperatures for production of these fritted glasses from batch materials were better known and all future materials would be melted at 700, 800 and 900 °C for MW 0 wt% SiO_2, CaZn 0 wt% SiO_2 and both 30 wt% SiO_2 compositions respectively.

TGA of these base glasses (figure 4.10) demonstrates the lower melting temperature of both the MW and CaZn base frits with silica substituted completely out.

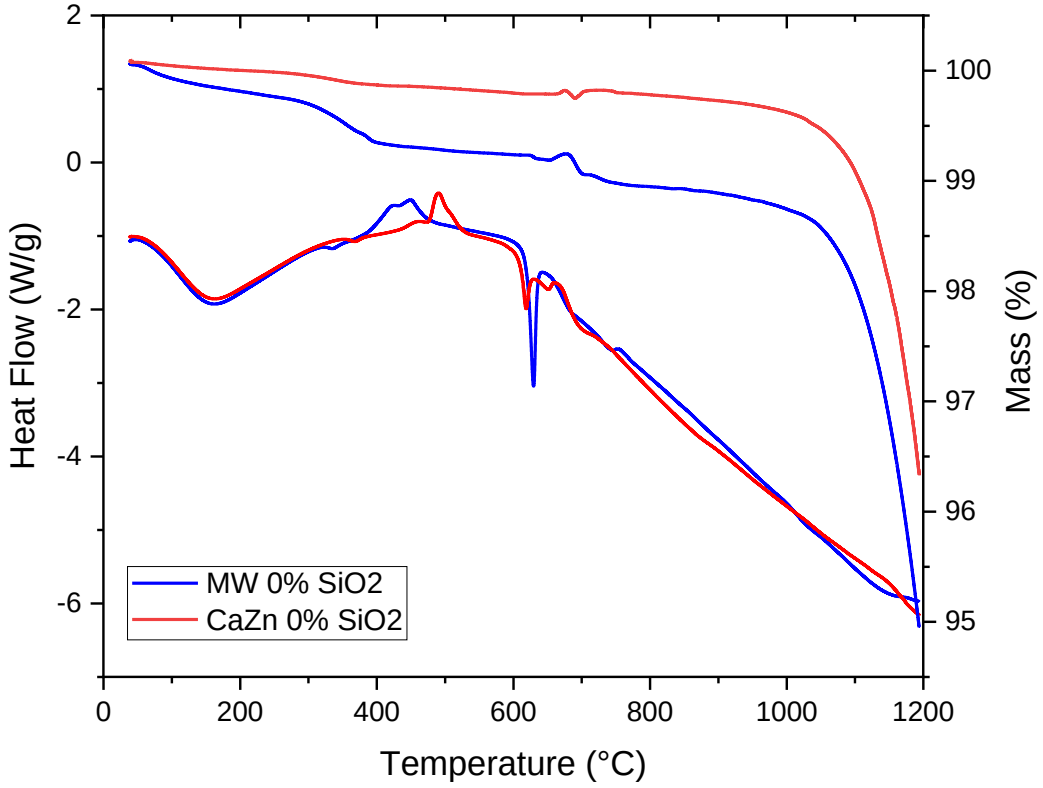

Figure 4.10. TGA (top) and DTA (bottom) trace of 0% SiO_2 MW and CaZn glasses

From the DTA the T_g of these fritted glasses are considerably lower than the original MW and CaZn compositions due to the low silica and increased boron content. For the 0% SiO_2 MW T_g was 328 °C

and for 0% SiO_2 CaZn 357 °C. The 0% SiO_2 CaZn composition is 29 °C higher than the MW because the boron content is lower and the concentration of aluminium/zinc is raised likely lowering the quantity of NBOs in the glass system. Both systems however, had a similar melting temperature with major melting event occurring at 618 – 628 °C although CaZn seemed to have another endothermic event at slightly higher temperature (651 °C). An exothermic event appears on both traces at 433 and 489 °C for 0% SiO_2 MW and CaZn respectively which likely corresponds to crystallisation of borate species. Mass loss is larger for MW at 5.10 % than for CaZn at 3.74 %, in the MS gas analysis no m/z ions were detected which indicates mass loss of a high temperature condensate above the temperature of the heated line (180 °C). These are likely to be boron or sodium containing as the most volatile agents in the glass melt and given the noticeable 268 – 408 °C step weight change.

4.8 Summary

In this section we have explored the melting behaviours, thermal properties and crystallisation of 4 different base glasses (SLS, CAS, MW, CaZn) and selected suitable glasses for further trials in following chapters. We have also developed new glasses which can be evaluated for volatilisation properties and ILW incorporation (section 4.7). These experiments give a wide baseline of measurements that allow us to compare and utilise these glasses when added to with waste or volatile elements.

TGA of MW and CaZn shown in figure 4.5 (section 4.5.3) shows the weight loss up to 1200 °C totalling 0.5 wt% for CaZn and 1.3 wt% for MW both very minor losses which can be used in future calculations. The most volatile element in these compositions is boron or sodium and these are likely responsible for these minor losses. The other contribution could be from moisture however no H_2O was detected in MS therefore this will be small. MW may lose more than CaZn because of the zinc and calcium content in CaZn which as we have discussed may provide a more stable environment for retention. It can be seen in figure 4.5 that there is a raise in mass at 825 °C which is likely an instrumental error as this does occur in both glasses separately at the same temperature. Other explanations for this could

include a buoyancy change in the material as the glass accepts and emits bubbles of gas into its liquid state or reactions of some glass components with oxygen over the melt.

The modified glasses were low silica variants which showed low crystallisation between 800 – 950 °C and these have potential for new nuclear waste glasses. They have a lower melting temperature compared to MW, CaZn, SLS and CAS and they are silica deficient so will have the a capacity for silica containing wastes. One negative of these glasses are their (high temperature) corrosive nature which could reduce the lifespan or refractory/crucible/metal containers the glass is being melted in (see figure 4.9. When melted at 950 °C (below the recommended CaZn melting temperature of 1150 °C) properties of CaZn lower silica variants did show crystallisation at 40 wt% which is below to the base glass composition (47.6 wt%) and this should be taken into account in future measurements as CaZn when melting at lower temperatures as crystallisation of quartz will occur.

Moving into chapter 5 we will use the data from this section to choose glasses that will be most appropriate for research into volatilisation. MW and CaZn will be at the forefront of these experiments as the UK's current waste glass of choice and a second new composition '0% SiO_2 CaZn' will be investigated as a high boron alternative (section 4.7) to these glasses based on the melting temperature (table 4.5) and crystallisation work found in figure 4.8. CaZn variant was chosen because the zinc and calcium content is likely to be able to accept ILW at higher loadings than MW and the UK only uses CaZn for this reason for vitrification. The 0% silica variant was chosen because the silica free nature has the opportunity to accept high levels of waste and also reduce volatility (in section 2.4 we discussed the volatility reducing influence of boron).

Chapter 5 Caesium, Iodine and Chlorine Incorporation in Glasses

5.1 Introduction

In the previous chapter we found that MW and CaZn (composition in table 4.1) were the selected glass types for this study and that a modified high boron glass 0% SiO_2 CaZn (composition in table 4.4) was a suitable candidate for continuing trials. It is in this chapter that we take these three glasses forward to explore their volatilisation and retention properties.

The incorporation of three elements (Cs, I and Cl) were investigated at different temperatures and in three glass systems, MW, CaZn and CaZn 0% SiO_2. Given the impact and state of contaminants highlighted in section 1.2 the raw materials used as Cs, I and Cl sources in this study were Cs_2CO_3, NaI and NaCl depending on the experiment these were added to the frit or batch to study losses of the key element. To give a basis to compare our measurements to we will first look at the raw materials and their reaction to high temperatures without glass reagents being added. Then we will move to discuss the thermal behaviour results from glasses doped with the element of interest in each section.

5.2 Methodology

To determine the incorporation of the three key elements in this study (Cs, I and Cl) 5 analytical techniques were utilised, TGA, DTA, MS, XRF and pyrolysis with active tracers. As the first three (TGA, DTA, MS) are all within the same instrument and procedure these have been grouped into one section for convenience. Raw material analysis was completed by TG-MS and DTA to understand the differences that occur when glass frit is added.

Retention properties were determined by the addition and mixing of powdered frit glass with a suitable agent, Cs_2CO_3, NaI, NaCl and then heating. TG-MS and DTA analysis was performed by mixing 0, 5 and 10 wt% of the agent (added as weight of the element post decomposition) and then a small

sample (~20 mg) of the mix added to a TGA crucible and heated to 1200 °C at 10 °C/min. The off-gases for the heating were captured by transfer through heated line to MS detector which gave information about temperature at which agents volatilised. Caesium and chlorine did not appear in the MS as they condensed in the heated line due to the vaporisation temperature being lower than the heated line temperature.

XRF measurements in this section are undertaken to understand the dependence of temperature on the volatilisation of Cs, I or Cl. 20g of dried glass powder was added with 1 wt% of the element and melted in a furnace for 2 hours each sample varying temperature between 800 – 1200 °C. Each sample was weighed and doped individually they were not mixed in a large batch and a portion taken. This glass was then cooled, powdered and analysed by XRF. This sample set was called the t=0 series as this is the initial state of glass. The experiments were taken further to extend the duration of melting by 2 hours and these samples were designed as t=2h. To complete this the process was repeated but using the glass powder from the previous experiment.

The materials were also investigated by using active tracers in a pyrolysis melting furnace and capturing any resultant gases in solution. Volatilisation was analysed using the active ^{137}Cs or ^{129}I capture from pyrolysis method (see section 3.3.6). 20 g samples of powdered glass were doped with 1 ml of water solution containing 20 bq ^{129}I or 10 bq ^{137}Cs and then heat treated to 950 °C for 2 hours any emitted gases were captured in solution and counted for radioactivity. The difference in radioactive between the start (added to glass) and end (captured in solution) gives us our total retention factor. 950 °C was chosen as the temperature for these measurement as it was the upper limit for the instrument.

5.3 Caesium

5.3.1 Raw Material

Cs_2CO_3 is the only carbonate used out of the three reagents and therefore has an expected carbonate decomposition at lower temperatures.

This can be seen in figure 5.1 at 202 – 255 °C where a 32.5 % mass loss is observed to be corresponding to a 246 °C endothermic thermal event in the DTA which is volatilisation of CO_2. This occurs by the following thermal decomposition reaction leaving Cs_2O remaining and losing mass as CO_2:

$$Cs_2CO_{3\,(s)} \rightarrow Cs_2O_{(s)} + CO_{2\,(g)}$$

The theoretical mass loss of this reaction is 14 % with the remaining 86 % relating to Cs_2O solid, this is quite a lot lower than the observed 32.5 % loss seen in the TGA in figure 5.1. As Cs_2CO_3 is a highly hygroscopic material this is likely coupled with mass loss of water as well as CO_2 during this temperature range despite the material being dried as discussed in section 5.2.

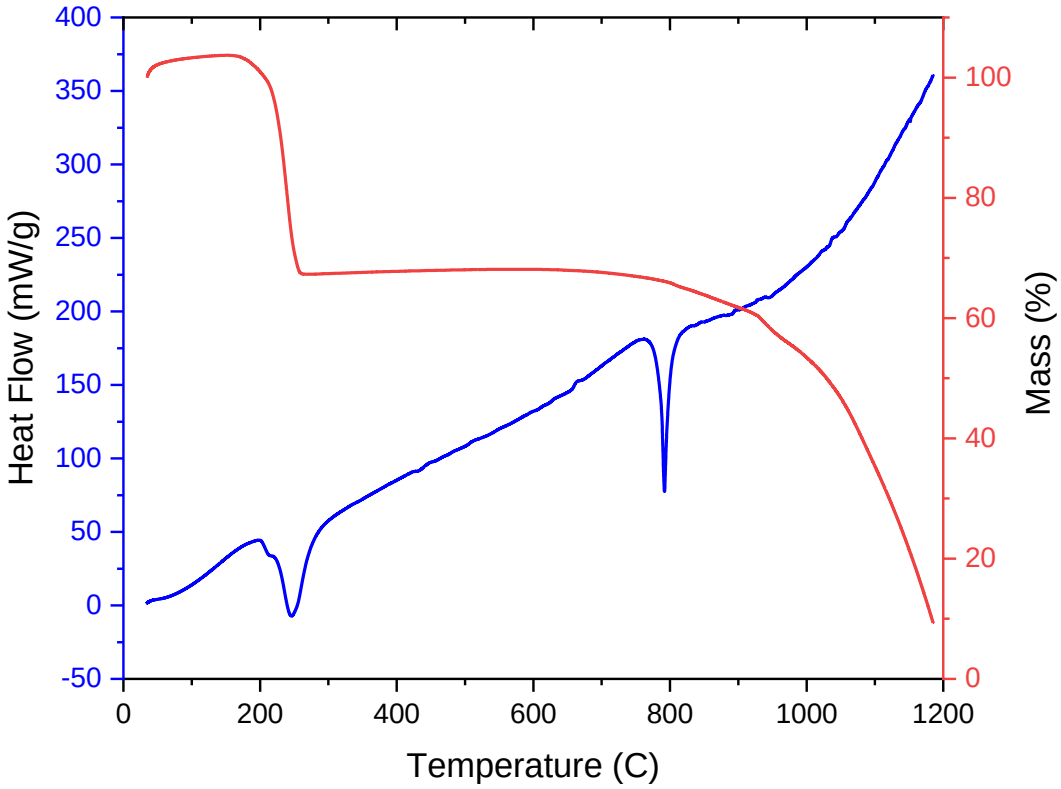

Figure 5.1. TGA and DTA trace of Cs_2CO_3 raw material, Red = Mass %, Blue = Heat Flow

This is corroborated by a shoulder peak in the DTA at 215 °C that is a response from water however the major response in the DTA at this temperature is from degradation of the raw material emitting CO_2. This is key information for storage and transport of Cs_2CO_3 as a raw material being added to batches/frits because a true accurate weight of the material can only be achieved if the sample is dried sufficiently. The second and final event in the heat flow graph is a sharp endothermic event at 792 °C

which corresponds to a melting event from the Cs_2O product of the thermal decomposition reaction. This closely matches literature[213] which show liquidus temperature of Cs_2O to be ~775 °C which is the same as the onset of the heat flow peak. As the material reaches its liquid state volatilisation increases dramatically, 55.1 % of the remaining mass is lost as a gaseous emission above 792 °C increasing in rate of loss as the temperature increases. The MS showed no gas m/z ions above 792 °C when this mass loss occurred suggesting that the off-gas from this process condenses rapidly before reaching the MS detector.

5.3.2 MW Base Glass

5.3.2.1 TG-MS and DTA

Caesium was added to MW glass frit in varying quantities and analysed by TGA, MS and DTA, compositions shown in table 5.1. Figure 5.2 shows the variation of mass loss comparing the base glass, 5 and 10 wt% additions of caesium added as Cs_2CO_3. As we have seen previously MW glass frit itself loses a small amount of mass (1.45 %) and Cs_2CO_3 loses 87.8 % of its mass over the 0 – 1200 °C temperature range.

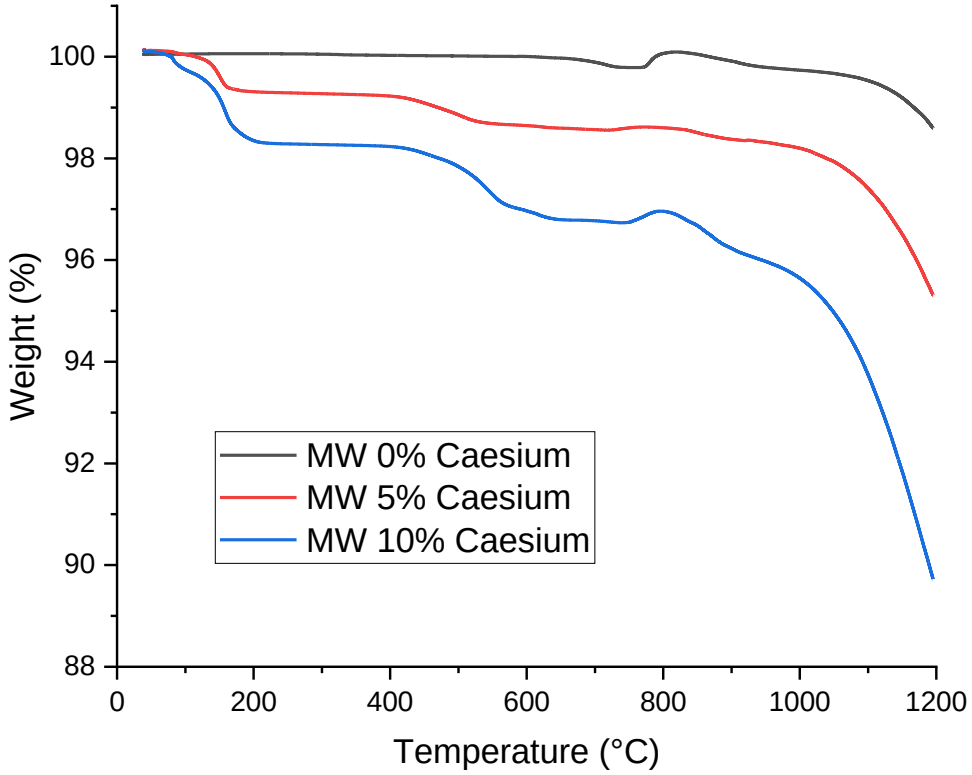

Figure 5.2. TGA trace of MW glass frit with 0, 5 and 10 wt% caesium addition as Cs_2CO_3

For the 5 % caesium sample the end weight at 1200 °C is 95.3 %, the base mass loss from the MW glass is 1.36 % (proportionally factored by the total mass of MW) therefore the total contribution from caesium carbonate is 3.34 %. Given that the starting material made up 5.92 % (equal to 5 % Cs content) of the starting mass we can see that 56.4 % of the Cs_2CO_3 is lost during the TG analysis. When increasing the proportion of caesium to 10 % we can see the final mass is at 89.7 % after analysis, 9.01 % of the total mass loss contribution from caesium carbonate when substituting the loss from the base glass (figure 5.2). Heat flow changes can be found in appendix A.

	Composition (wt%)		
	MW	**+ 5 wt% Cs**	**+ 10 wt% Cs**
SiO_2	61.75	58.66	55.58
B_2O_3	21.88	20.79	19.69
Na_2O	11.05	10.4975	9.95
Li_2O	5.33	5.054	4.79
Cs_2CO_3	-	5.00	10.00
Total	100.00	100.00	100.00
Melt Temp (°C)	1150		

Table 5.1 Table of MW glass compositions used for reference in section 5.3.2

This is understandably higher than the 5 % caesium addition because of the increased content of the volatile caesium compound. When we compare the percentage of the caesium in both samples we can observe that percentage loss of caesium carbonate is 76.4 % (11.8 % of total mass is Cs_2CO_3, 10 % of which is mass from caesium). We can then assume as the caesium loading increases the proportion of caesium lost from the melt environment also increases for the MW glass system. This could be due to the liquid glass melt and caesium phases not dissolving in each other fast enough to overcome the volatility of the liquid caesium oxide. 10% caesium overcomes the solubility limit of the most borosilicate glasses and therefore an immiscible liquid Cs_2O phase is likely occurring at higher temperatures and a higher proportion of that is being lost as a gas rather than dissolving into the MW glass structure. In the DTA there is a delayed effect of caesium carbonate thermal decomposition which can also be seen in the stepwise mass changes in the TGA. The initial loss at 72 – 207 °C can also be seen in the Cs_2CO_3 TGA-DTA trace in figure 5.1, however, this starts earlier likely due to the loss of water from any unintended moisture on the powdered glass frit. The CO_2 loss is at a similar

temperature in the raw material, since the glass has not transitioned at all there are little differences between the two systems at this temperature. As the samples heat to 564 °C another carbon dioxide loss is seen at the same time as the glass is melting. This is theorised to be either entrained carbon dioxide in the glass releasing or unreacted Cs_2CO_3 dissolving in the glass as Cs_2O therefore releasing CO_2. Any mass loss above this is undetected by MS and by extension in these batches the majority is likely to be Cs_2O boiling, this is also corroborated by the increase in this high temperature loss as caesium content is increased.

5.3.2.2 Temperature Dependence

The effect of temperature on the volatility and glass composition of caesium in MW glass is investigated in this section. This will be as Cs_2CO_3 is added to MW fritted glass powder and remelting glasses already containing Cs_2O. We will also look at the changes in density of the resultant glasses and mass loss all of which will be over the temperature range of 800 – 1200 °C. Firstly we will discuss the addition of Cs_2CO_3 to MW frit composition. Figure 5.3 shows the final composition of the glasses after heating at their respective temperatures with the addition of Cs_2CO_3 to make up 1% total caesium in the final batch assuming no volatilisation. As the temperature increases to 1200 °C Na_2O does not change in relative concentration and B_2O_3 also shows little change, although at the higher temperatures there is a slight trend towards a decrease in B_2O_3 concentration.

Silica content did appear to increase, this is due to the other glass components decreasing in mass content and proportionally silica appearing to be at a higher concentration. Caesium content trends downwards from 0.745 % to 0.511 % with a maxima at 900 °C of 0.944 % Cs_2O. This is consistent with TGA where at higher temperatures more volatilisation of caesium occurs.

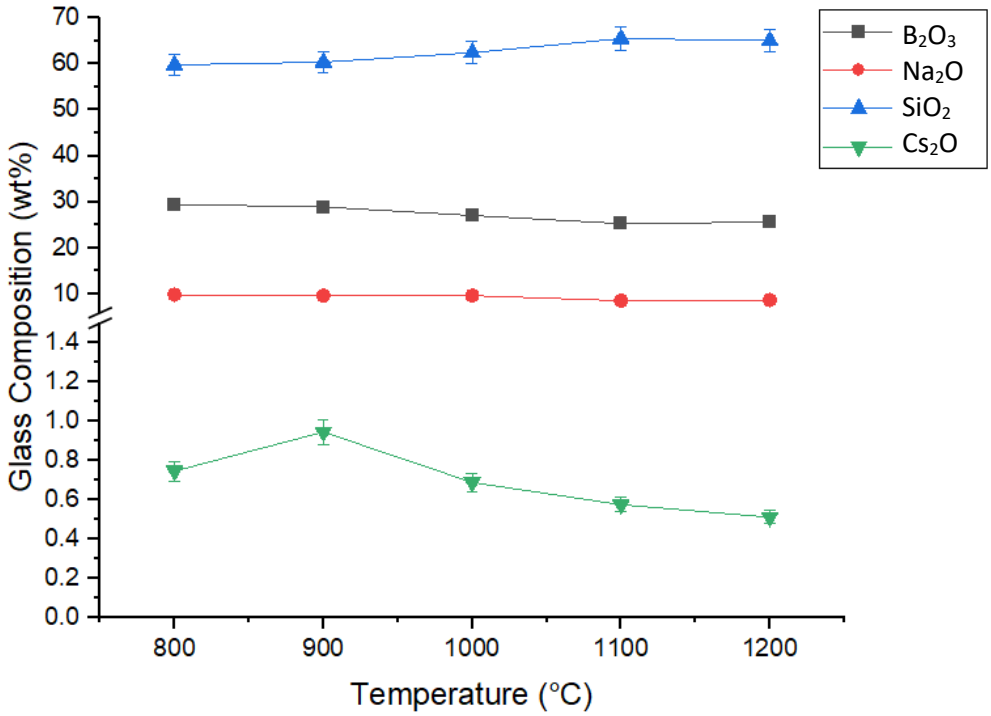

Figure 5.3. Change in glass content (analysed by XRF) of MW between 800 – 1200 °C with the addition of 1 % Caesium (as Cs_2CO_3) added to fritted MW glass (t=0)

The crystal character of the material changed depending on the temperature at which the sample was treated. The original MW glass was amorphous as we have previously shown, however, upon addition of caesium carbonate and treatment at 800 °C the material devitrifies and forms crystalline phases (figure 5.4). The main devitrification product was silicon oxide making up approximately 77 mol% of the total crystalline material. Silica makes up a large proportion of the MW glass system and therefore is a likely element to crystallise out of the glass. The thermal analysis of MW glass (figure 4.10) does not show a significant crystallisation peak in the heat flow by itself which indicates either a minor crystallisation event or that the addition of Cs_2CO_3 changes the behaviour. The Cs_2CO_3 has a distinct effect on the XRD pattern at 800 °C as the presence of cesium boron silicate shows that caesium has begun to interact with the softened glass. This material makes up the remaining 23 mol% approximately at 800 °C. When the temperature is increased to 900 °C most of the crystal character has gone, however, a small peak remains from the strongest SiO_2 (Phase ID 01-075-8320) intensity at 26.6 ° 2θ. Asides from these temperatures the other three products are amorphous from 1000 –

1200 °C. When caesium is added previously to a batch to make a glass containing a final composition with 1 wt% caesium the subsequent losses are different to when raw material is added to glass frit separately. Figure 5.5 shows the effect of temperature on glass content when remelting this system for 2 hours.

Most elements of this glass system remain constant throughout the temperature range with a small increase in silica content towards the higher temperatures and a slight lowering of Cs_2O content at the 900 – 1100 °C compared to the original glass. The base glass (at temperature = 0 °C) contains 0.88 wt% Cs_2O which reduces to a minimum of 0.60 wt% at 1000 °C, however, the concentration increases above this temperature.

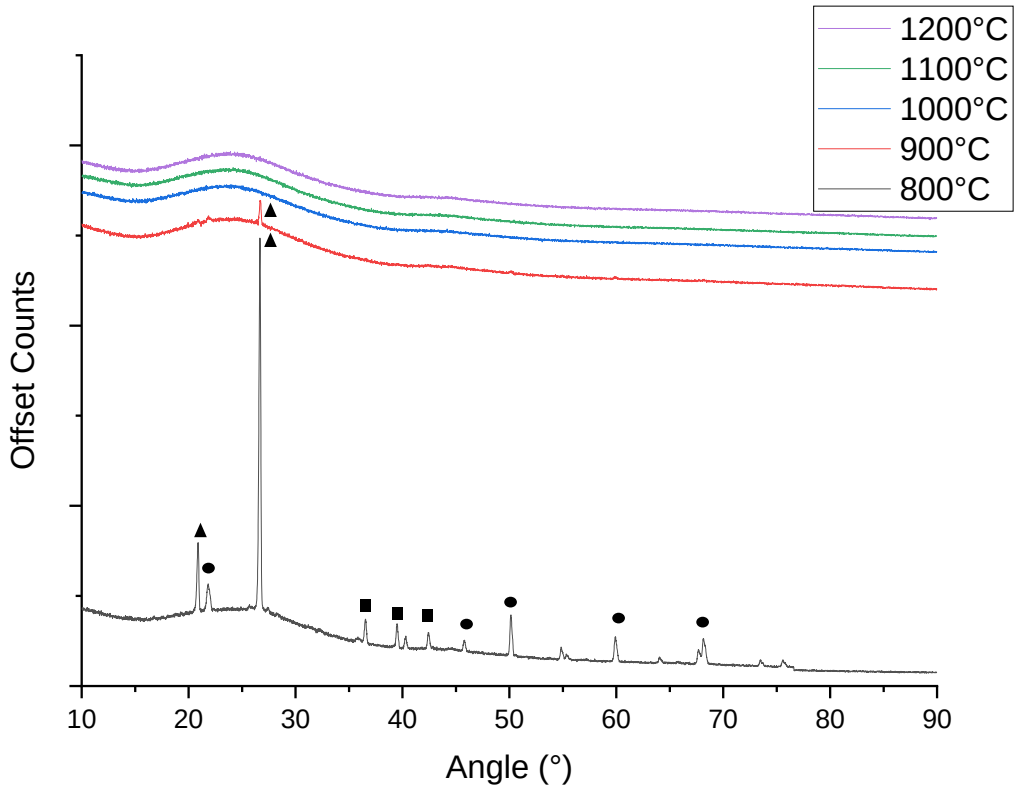

Figure 5.4. XRD pattern of MW frit remelted at 800 – 1200 °C with the addition of 1 % Cs added as Cs_2CO_3. ▲ = SiO_2 Phase ID 01-075-8320, ■ = SiO_2 Phase ID 04-013-7117, Cs0.85 (B1.29 Si1.71 O5.77) ● = Phase ID 01-070-8065

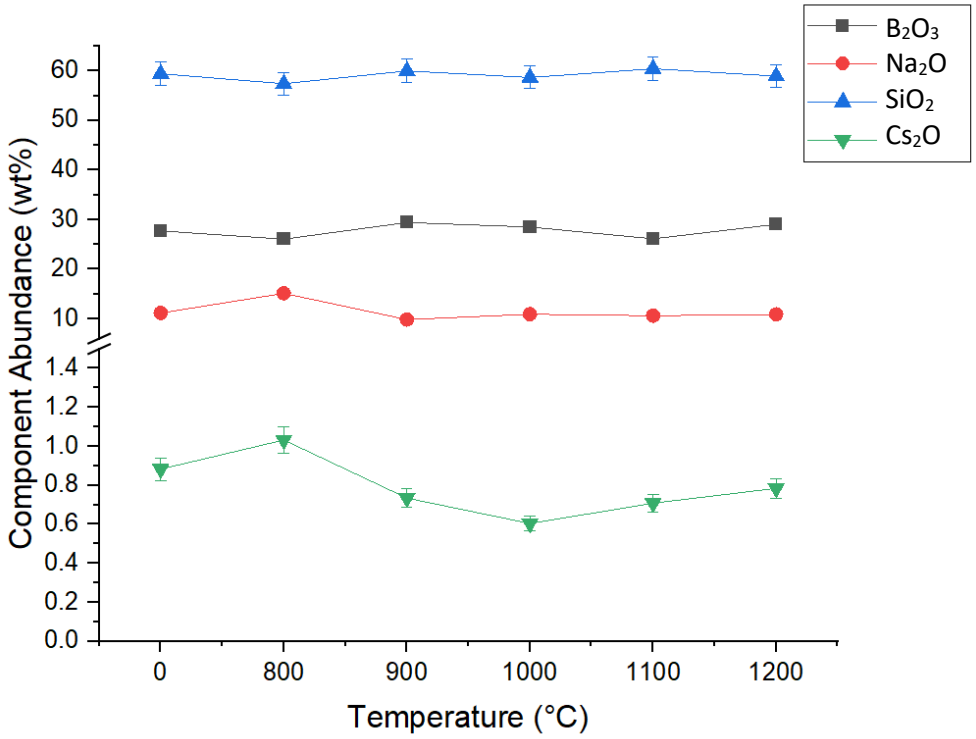

Figure 5.5. Change in glass content (analysed by XRF) of MW incorporated with 1 wt% Cs_2O remelted for 2 hours between 800 – 1200 °C (t=2h)

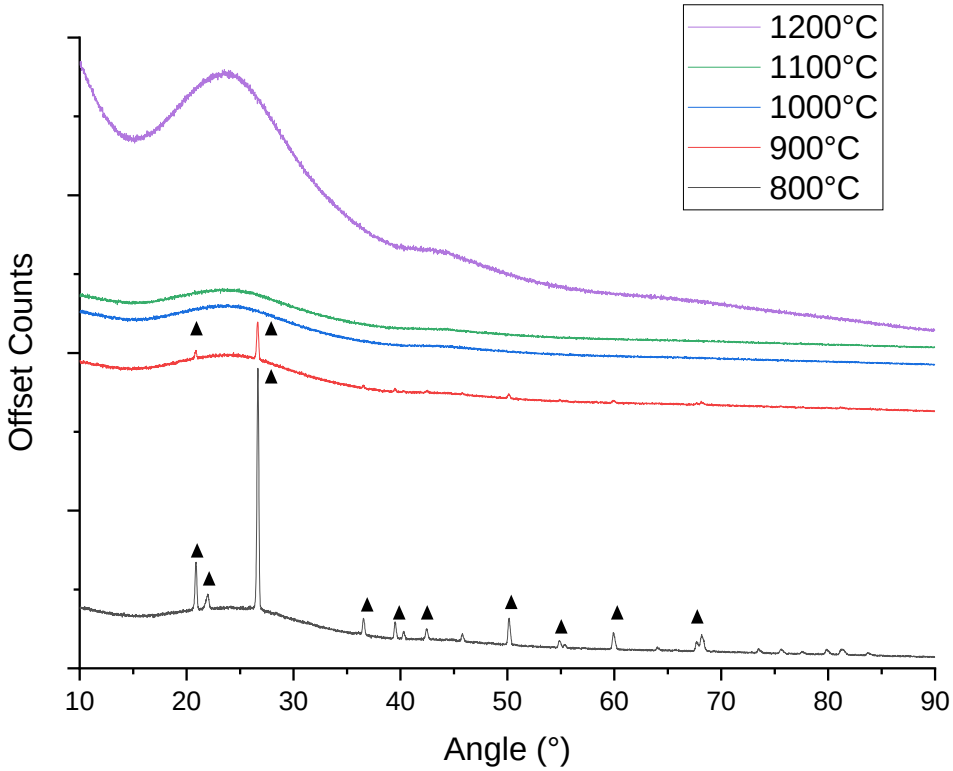

Figure 5.6. XRD pattern of MW frit remelted at 800 – 1200 °C with the addition of 1 % Cs added as Cs_2CO_3. ▲ = SiO_2 Phase ID 01-075-8320

The crystal character of the samples over the 800 – 1200 °C temperature range is very similar to the glass frit plus Cs_2CO_3 system (figure 5.4) showing the same SiO_2 peaks for the same 800 and 900 °C samples. We can assume the same devitrification is occurring in the MW glass as it is heated at 800 and (less intensely at) 900 °C.

Density was also affected by either the temperature / caesium additions as the glass is either remelted with Cs_2CO_3 (t=0) or with caesium already in the glass network (t=2h). Density trend (figure 5.7) is very similar for both glass systems from the base glass we see a trend downwards with both the 800 °C and 900 °C and then a large increase for the remaining 1000 – 1200 °C samples to a density either around or larger than the original base glass. Although the trends are similar the density was reduced for the samples already containing caesium in their structure (t=2h) especially at 900 °C where we see a minimum of 2.30 g/cm^3, the lowest in the series. The average of the final three points are 2.4650 and 2.4444 g/cm^3 very similar to the starting MW base glass density of 2.45 g/cm^3 indicating there is likely little density changes upon the remelting of these systems at 1000 – 1200 °C. The t=0 system is slightly higher in density on average, the change is more significant at a lower temperature with only 0.0206 g/cm^3 separating the averages of t=0 and t=2h at 1000 – 1200 °C.

This data does show a change in sample density at the same temperature at which crystallisation / devitrification occurs. The change in density therefore is due to lower density crystals forming in the glass increasing as the glass is purely remelting at 1000 – 1200 °C.

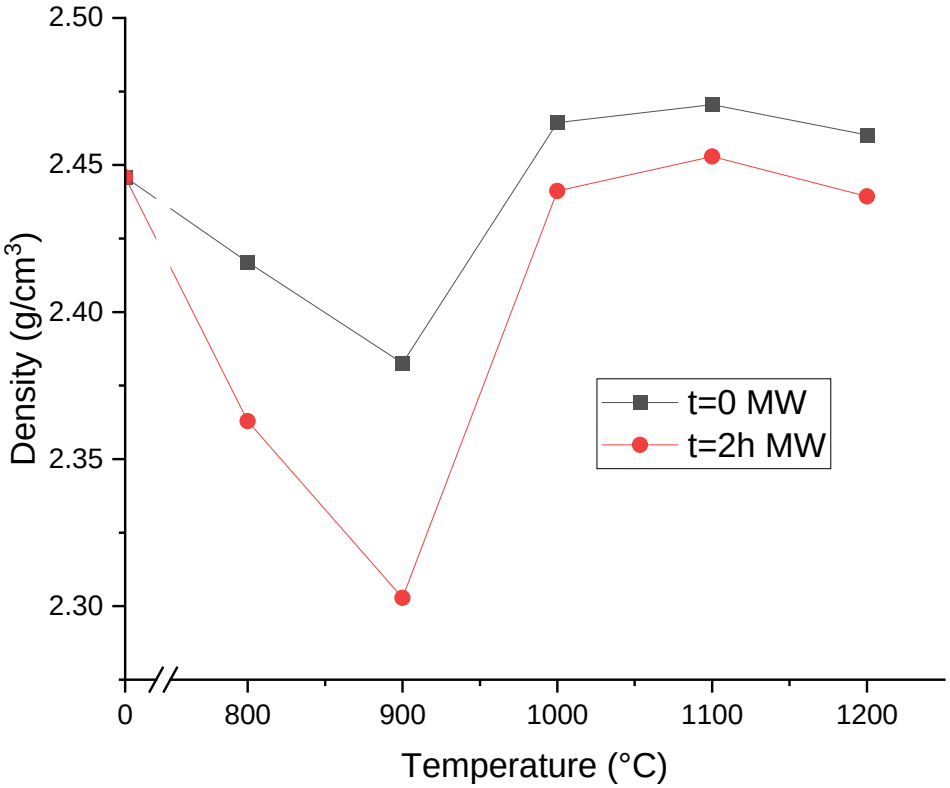

Figure 5.7. Effect of heat treatment temperature (800 – 1200 °C) on density of MW glass systems, t=0 remelted with Cs_2CO_3 and 1 wt% caesium already in the glass network. Error bars represent +/- 0.001 g for each measurement over an average of three samples which is smaller than the points.

5.3.3 CaZn Base Glass

In this section we discuss the caesium volatility from CaZn base glass series added as caesium carbonate to frit, fritted glass already containing Cs_2O and also ^{137}Cs added as a radioactive tracer.

5.3.3.1 TG-MS and DTA

To CaZn frit Cs_2CO_3 was added to make 5 and 10 wt% Cs content and analysed by TG-MS and DTA, composition shown in table 5.2. Figure 5.8 shows the TGA data for this series of experiments compared to the CaZn base glass without any caesium additions. Mass loss was larger for caesium

containing samples similar to MW glass and expected, due to the carbonate decomposition and volatility of caesium already seen in MW glass systems.

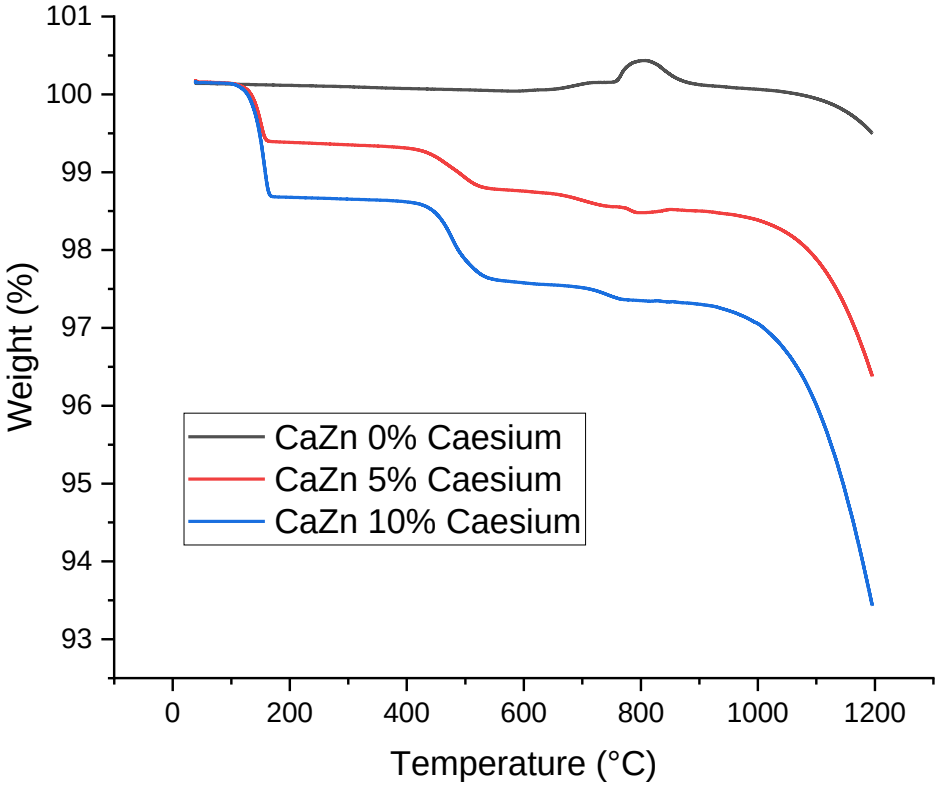

Figure 5.8. TGA trace of CaZn glass frit with 0, 5 and 10 wt% caesium addition as Cs_2CO_3

The total mass loss from these glasses is less when compared to the MW system (which was one motivation for continuing with CaZn glasses for pyrolysis experiments) and trended on increasing caesium content in a similar manner. The total mass loss for the 5 and 10 Cs wt% is 3.62 and 6.56 wt% respectively, weight percentage of Cs_2CO_3 in these samples was 5.92 wt% and 11.80 wt% respectively. The mass loss of base CaZn glass is 0.63 % and therefore substituting this away from the total mass loss we can assume the mass loss contribution for Cs_2CO_3 to be 2.99 wt% (5 wt% Cs sample) and 5.93 wt% (10 wt% Cs sample). As a percentage of the total mass loss 50.51 wt% is from Cs_2CO_3 at 5 wt% Cs loading and 50.25 wt% is from Cs_2CO_3 at 10 wt% Cs loading. Compared to MW glass the total mass loss is much lower (50.25 compared to 76.40 wt%) for the 10 wt% sample and slightly lower for the 5 wt% sample (50.51 compared to 54.40 wt%).

	Composition (wt%)		
	CaZn	**+ 5 wt% Cs**	**+ 10 wt% Cs**
SiO_2	47.6	45.22	42.84
B_2O_3	23.4	22.23	21.06
Na_2O	8.6	8.17	7.74
Al_2O_3	4.2	3.99	3.78
CaO	6	5.7	5.4
Li_2O	4.2	3.99	3.78
ZnO	6	5.7	5.4
Cs_2CO_3	-	5.00	10.00
Total	100.00	100.00	100.00
Melt Temp (°C)	1150		

Table 5.2 Table of CaZn glass compositions used for reference in section 5.3.3

The TGA data in figure 5.8 shows us major mass loss events over the temperature range the first one being at 105 – 170 °C where a 0, 0.776 and 1.481 wt% mass loss step is seen for each of the 0, 5 and 10 wt% caesium samples respectively. These are the CO_2 and moisture losses seen in the caesium carbonate material in figure 5.1 also visible in the MW TGA in section 5.1.2.1. We see a mass loss relating to more CO_2 emission (from MS) at 426 – 550 °C in both caesium containing samples. This is also seen in the MW variant of this graph and the losses can be attributed to the same factors, these are CO_2 from unreacted Cs_2CO_3 as the glass melts and entrained CO_2 in the glass frit releasing as the sample melts. Above 800 °C a major mass loss is seen for all three samples increasing as the caesium content increases. Given that no m/z ions appear in the MS above this temperature this can be assigned to the boiling of Cs_2O from the liquid glass and a minor loss from molten B_2O_3 both condensing before reaching the MS detector.

5.3.3.2 Temperature Dependence

The effect of temperature on caesium loss from CaZn is investigated for both 1 wt% Cs_2CO_3 added to powdered glass (t=0) and remelting of glass containing 1 wt% Cs.

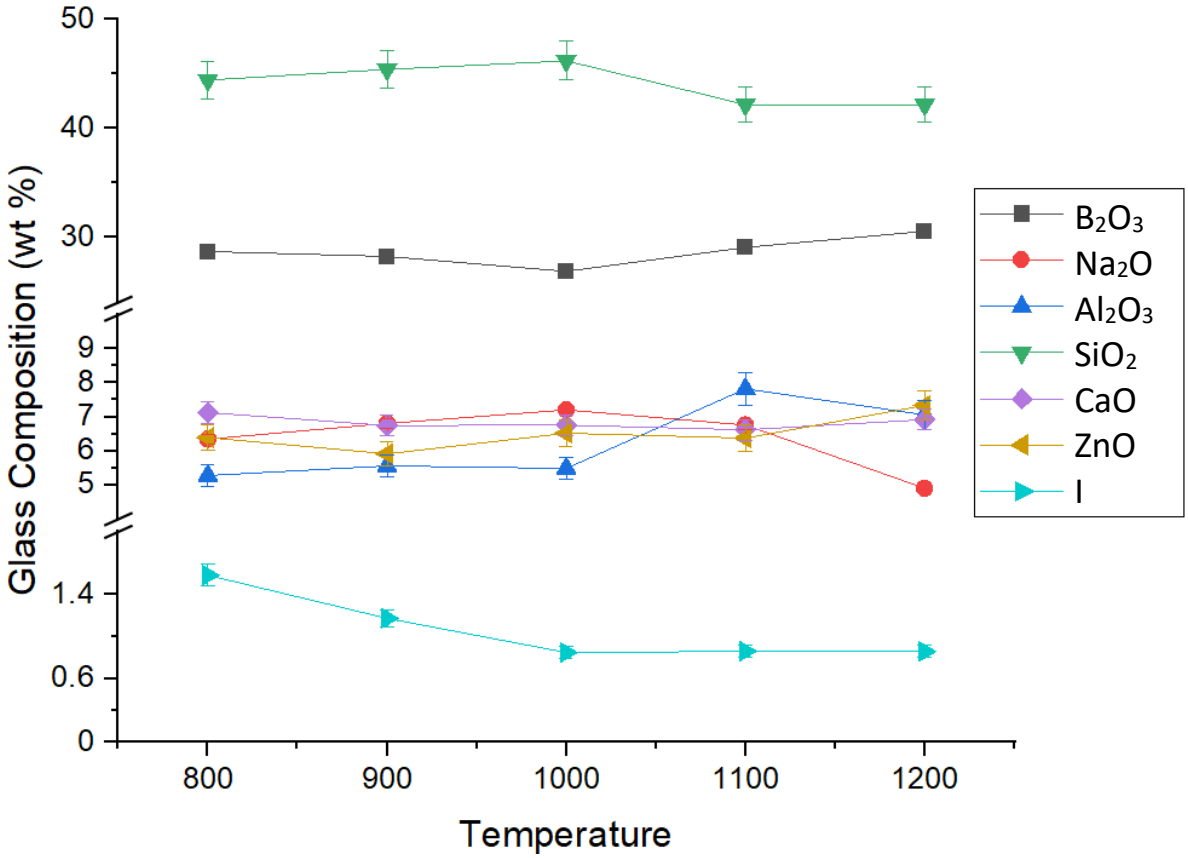

Figure 5.9. CaZn powdered glass frit heated between 800 – 1200 °C with the addition of Cs_2CO_3 to add 1% Cs (t=0)

Firstly, the t=0 series from 800 – 1200 °C shows the loss (or gain) of material percentage weight of all major glass components and caesium. This can be seen in figure 5.9 where a trend in most glass components remains constant, however, at higher temperatures the Al_2O_3 content increases by ~ 1 wt% in the system which is likely due to alumina from the crucible dissolving into the glass, this would also happen more at higher temperatures (as is discussed in section 2.2 and 4.3.1) as the glass liquid becomes more corrosive. There are a few other changes in increasing Na_2O content and a slight shift downwards in SiO_2 which may occur because of the alumina content increasing or the caesium content reducing. One of the most interesting results is the consistent caesium loss from 1.58 to 0.86 wt% Cs_2O. There are two key take-away points from this, CaZn retains more in general at all temperatures

compared to MW and the volatilisation trends downwards changing very little between 1000 – 1200 °C and the majority of the reduction occurring at 900 and 1000 °C. Higher temperatures increase volatilisation of caesium in this system, however, above 1000 °C we see little change, although if the temperature was increased above 1200 °C caesium content would likely reduce further. From the maximum at 800 °C a 45.5 wt% loss of Cs_2O can be seen at 1200 °C. This correlated with the mass loss seen from TGA data in 5 and 10 wt% caesium CaZn glasses where 50.25 and 50.51 wt% Cs_2O is observed at 1200 °C for a similar heating time.

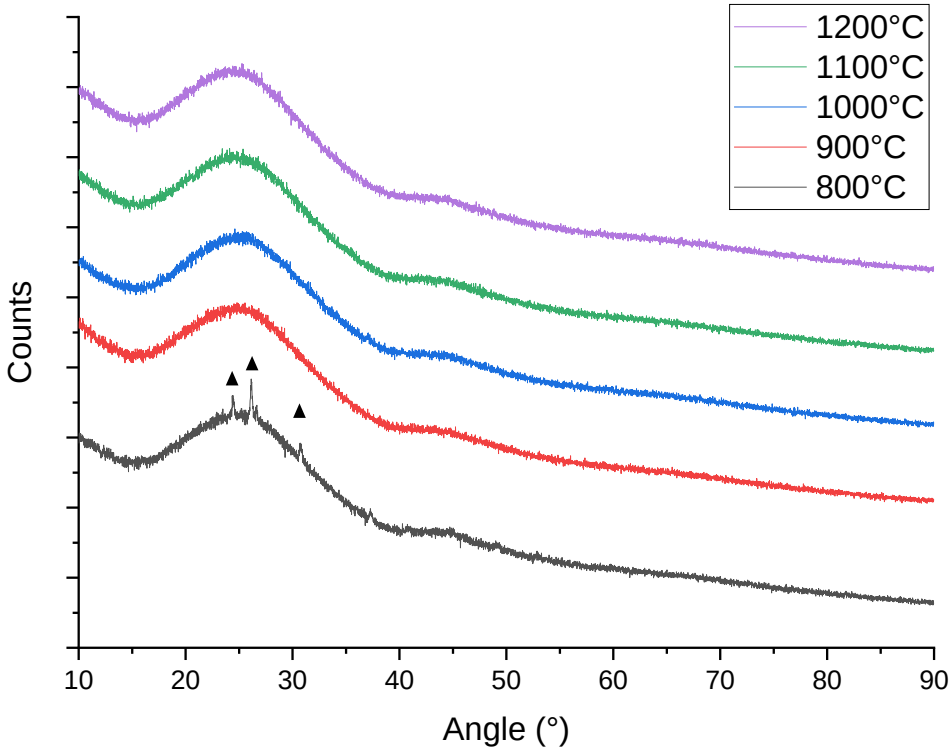

Figure 5.10. XRD data of CaZn glass with the addition of 1% Cs as Cs_2CO_3 melted at 800 – 1200 °C (t=0) ▲ = $Cs_8Al_8Si_{16}O_{48}$ Phase ID 01-075-8320

Some crystallisation is seen in these samples, however, significantly less than for MW glasses. As CaZn is remelted with Cs_2CO_3 we can see that at 800 °C the XRD shows peaks at 24, 26 and 31 ° 2θ. These are not very intense when compared with the background and the MW temperature dependence XRD data (figure 5.4). When assigning the peaks at 800 °C in figure 5.10 we see that there are a few minor intensities which can be assigned to a leucite named caesium aluminium silicate ($Cs_8Al_8Si_{16}O_{48}$). This

shows a difference in MW and CaZn, MW devitrifies without caesium incorporation into the crystal phase whereas CaZn forms a caesium containing leucite product.

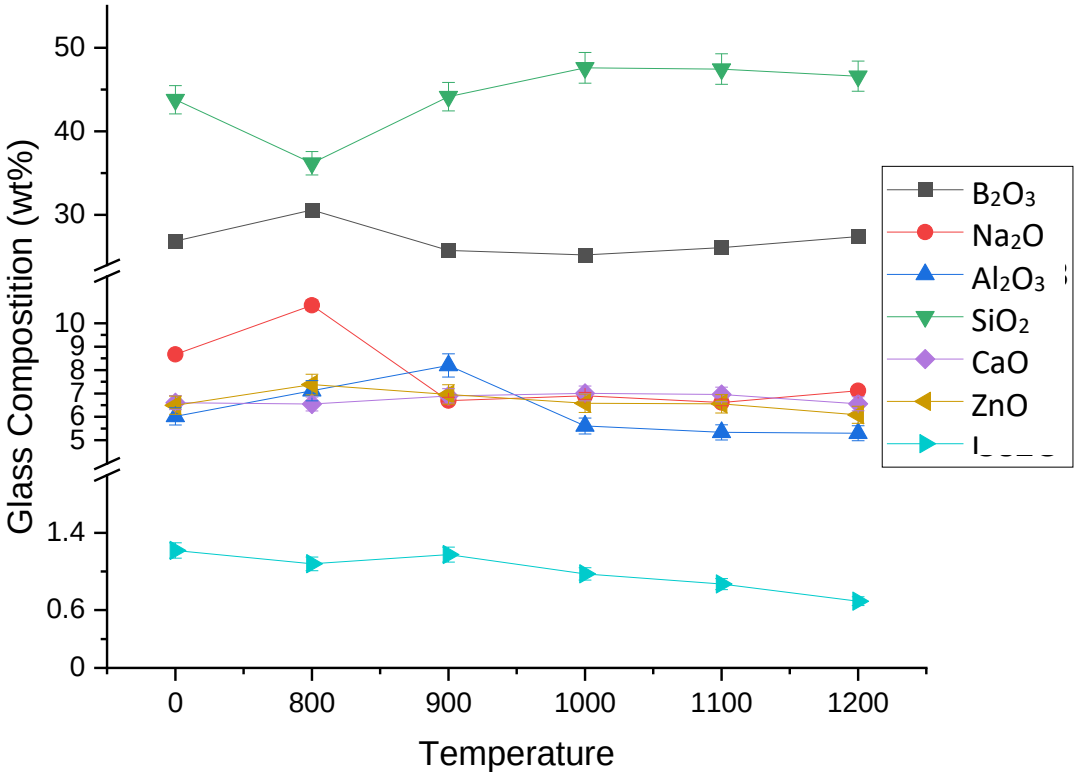

Figure 5.11. Change in glass content (analysed by XRF) of CaZn incorporated with 1 wt% Cs_2O remelted between 800 – 1200 °C

When incorporated in the glass structure caesium volatility appears to trend down to a minor degree and at a linear rate. The graph (figure 5.11) starts with around half the caesium concentration. It shows that there is a change in caesium concentration over a 2 hour dwell between 800 – 1200 °C for glasses containing caesium. Compared to when loading caesium into CaZn glass (figure 5.9) the reaction is similar in amplitude at 1200 °C, however, the drop in caesium concentration happens at an earlier temperature (1000 °C) when added as Cs_2CO_3 to frit. There are some issues with the data in figure 5.11 as Na_2O content at 800 °C seems to increase by ~ 2 wt% which may be due to experimental error in the melting process or XRF analysis, in addition we see a raised Al_2O_3 content at 900 °C which is from alumina crucible corrosion. Despite this, useful data on caesium loss can be determined from this graph. The maximum percentage loss of caesium is seen at 1200 °C and is 56.6 %. This is comparable to the percentage mass loss seen in TGA analysis (figure 5.8) and temperature

dependence graph (figure 5.9) of Cs_2CO_3 added to CaZn frit. The two systems are likely comparable at higher temperatures as the glass softens and is able to release caesium from the liquid glass system, however, at lower temperatures we have less liquid glass and therefore either no state change for the caesium material incorporated in the glass or no interaction between the Cs_2CO_3 or Cs_2O and the solid glass. The material not interacting with the glass more readily volatilises at lower temperatures as the energy required to transition to gaseous state is lower in the raw material (or thermally decomposed raw material) compared to the glassy form of Cs_2O. There was no significant crystallisation observed (figure 5.12) in any of the CaZn t=2h samples (twinned with the samples in figure 5.10). There are minor Bragg peaks which closely resemble SiO_2 however these are poorly resolved as they are very weak and amorphous portion of the graph covers most of these

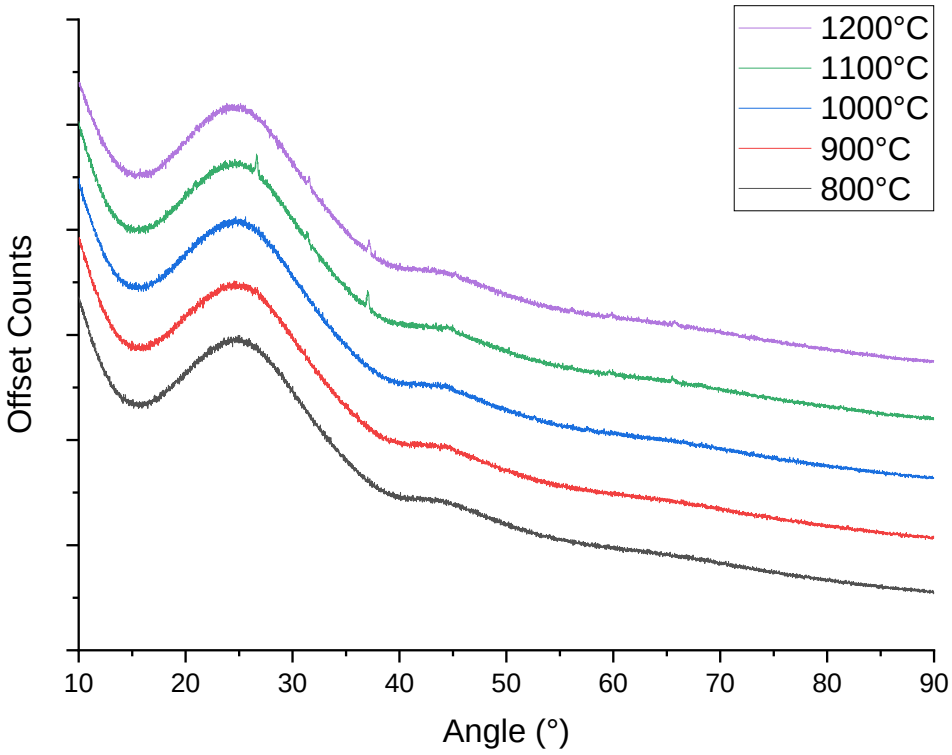

Figure 5.12. XRD data of CaZn glass containing 1% Cs as Cs_2O remelted at 800 – 1200 °C (t=2h)

Figure 5.12 shows that, by XRD, the samples in the series between 800 – 1200 °C were completely amorphous. This is different to MW glass which was seen to devitrify at 800 and 900 °C. This could indicate that CaZn is a better glass for wasteforms in nuclear waste applications as it more thermally stable and less prone to devitrification which could present an issue if crystallising out radioactive

waste components. This is also seen in the t=0 CaZn series where less crystallisation occurs compared to MW.

Density of the two CaZn glass series we have discussed is variable in a similar manner to the MW density changes seen in section 5.1.2.2. Figure 5.13 illustrates the density reduction from both systems (t=0 and t=2h) at 800 °C and the minor reduction at 900 °C for the glass system (t=2h).

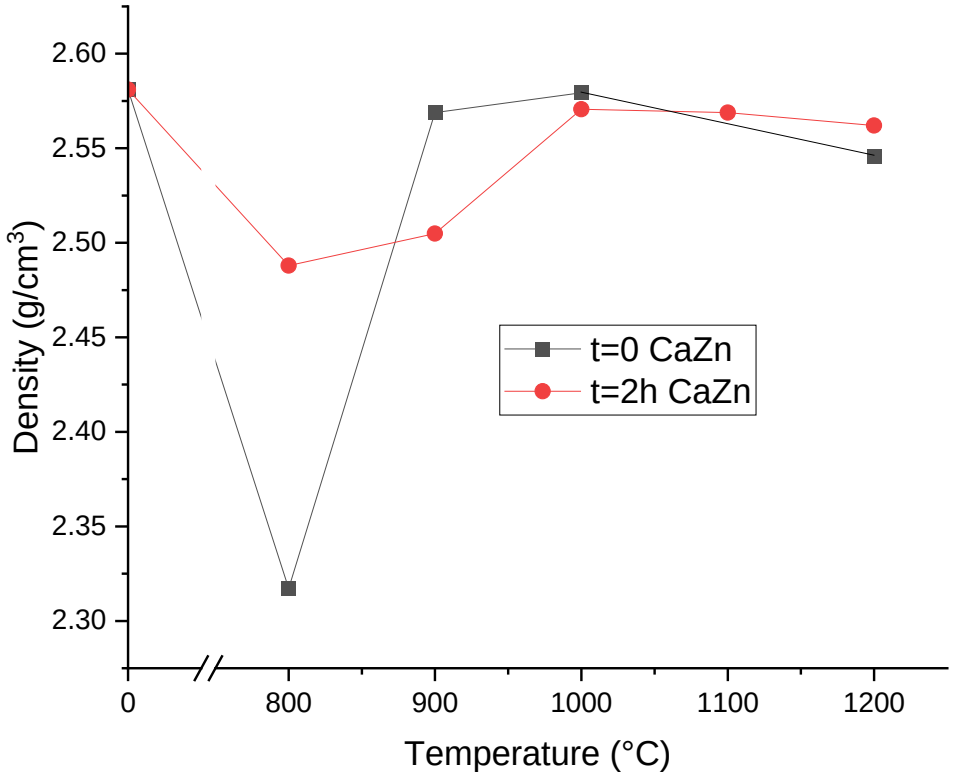

Figure 5.13. Effect of heat treatment temperature (800 – 1200 °C) on density of CaZn glass systems, t=0 remelted with Cs_2CO_3 and 1 wt% caesium already in the glass network. Error bars represent +/- 0.001 g for each measurement which is smaller than the points.

The large drop in density of 0.2638 g/cm^3 at 800 °C observed in the t=0 CaZn glass is also the only sample in that series that showed signs of crystallisation. Above 800 °C, density returns to the same (or similar) as/to the base glass (2.5810 g/cm^3). The materials formed are less dense than the glass structure and therefore effect the density of the material as a whole. The t=2h glasses (which showed no crystallisation from 800 – 1200 °C) do have dedensification of ~0.1 g/cm^3 at 800 and 900 °C, less so

than the t=0 CaZn series at the same temperatures. The density reduction is an effect seen in an earlier section (figure 5.7, section 5.3.2.2) and coincides with crystallisation products. This could be a result of lower density $Cs_8Al_8Si_{16}O_{48}$ phases dispersing throughout the glass matrix.

5.3.3.3 Pyrolysis and Active Tracers

This section discusses the use of a radioactive ^{137}Cs tracer to determine volatility properties of CaZn glass and compare radioactive caesium with non-active caesium. Only one sample relates to purely to CaZn glass the others will be revisited later in chapter 6 when we discuss waste loaded samples. We will compare this with the standard gamma activity from 1 ml of the dopant solution.

The standard had an activity of 10.84 Bq +/- 0.6 over an average of 3 samples this can be classed as 100% retention as the sample was not heated in the furnace, activities can be compared to this and given a percentage retention based on this. The standard was a good estimation of the added activity as the working solution was created from a more concentration solution to add 10 Bq/ml.

Figure 5.14 Image of CaZn base glass post pyrolysis at 950 °C spiked with 10 Bq ^{137}Cs

The CaZn base glass upon heating to 950 °C for 6 hours had a gamma activity of 8.19 Bq +/- 0.51 comparing this to the standard we can calculate that this glass retained 75.55 % of the ^{137}Cs after heat treatment. This quite closely matches the mass loss of caesium seen in the temperature dependence study for CaZn where 63.92 % of the caesium added was seen to volatilise (using an average of the 900 and 1000 °C readings to estimate 950 °C). This comparison could show that active and inactive caesium samples are closely related in terms of volatility, however, this is only one sample and more will be discussed later to ascertain the validity of this statement.

5.3.4 0% SiO_2 CaZn Base Glass

In this section we discuss the caesium volatility from CaZn glass series adjusted pro-rata to contain 0 wt% SiO_2 doped with radioactive ^{137}Cs tracer to frit, composition shown in table 5.3.

	Composition (wt%)	
	0% SiO_2 CaZn	**+ Cs Tracer**
SiO_2	0.00	0.00
B_2O_3	44.66	44.66
Na_2O	16.41	16.41
Al_2O_3	8.02	8.02
CaO	8.02	8.02
Li_2O	11.45	11.45
ZnO	11.45	11.45
Cs_2CO_3	-	Trace
Total	100.00	100.00
Melt Temp (°C)		950

Table 5.3 Table of 0% SiO_2 CaZn glass compositions used for reference in section 5.3.4

5.3.4.1 Pyrolysis and Active Tracers

Similarly to the previous section 5.1.3.3 there is only one sample which is defined by this category, this system is the most investigated under the pyrolysis net, however, these all include waste additions or atmosphere modifications and will be discussed in a following section.

Figure 5.15 Image of 0% SiO_2 CaZn base glass post pyrolysis at 950 °C spiked with 10 Bq ^{137}Cs

The sample under discussion in this section is a 10 Bq ^{137}Cs doped glass heated in pyrolysis instrumentation for 6 hours at 950 °C. The activity of this sample after heating was found to be 7.51 Bq +/- 0.44. Compared to the standard activity of the tracer (10.84 Bq +/- 0.6) the remaining activity in the sample after heat treatment was 69.28 %. This is less than the retention seen in CaZn glass (75.55 %) which can tell us about the role of silica in caesium retention. From this data it likely that that silica has a positive effect on the retention of caesium although this will also be discussed further

in later sections. The appearance of this sample (figure 5.15), however, is much clearer than the CaZn glass in figure 5.14 perhaps due to less crystallisation upon cooling of the sample.

5.4 Iodine

5.4.1 Raw Material

Sodium iodide has no thermal decomposition step, however, there are still thermal events to discuss. Figure 5.16 shows very little change in the mass and properties of the NaI material below 646 °C, above that temperature the changes are more dramatic.

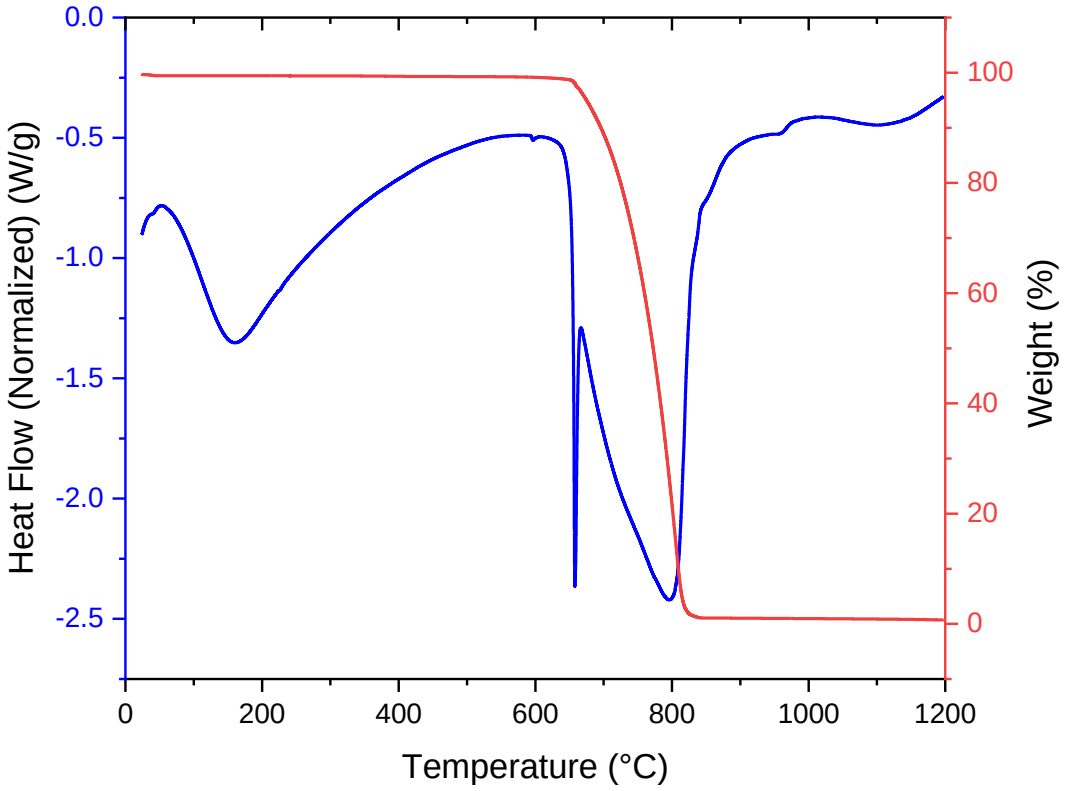

Figure 5.16. TGA and DTA trace of NaI raw material, Red = Mass %, Blue = Heat Flow

Firstly we see a sharp endothermal peak at 658 °C in the DTA analysis of NaI which represents the melting of the material, in literature shown to be 651 °C experimentally[214]. Directly after this melting event a significant loss of mass is seen of 97.5 % of the total with 2.5% of the mass remaining afterwards. This large drop occurs over a short temperature range of 650 – 842 °C which could be below the softening/melting point of some of the glass systems used in this study. In the MS data (figure 5.17) it can be seen that the only volatiles for this period is m/z 127 (minor) and 254 (major).

The 254 m/z peak was stronger by a factor of 5 than the 127 peak. Using this data we can ascertain that the off gas from this emission is I_2 with I^- minor fragments detected by MS. There were no NaI (m/z = 150) peaks detected therefore it is unlikely the sample boiled and more likely a reaction with oxygen occurred to decompose NaI to I_2 and Na_2O:

$$2NaI_{(s)} + \frac{1}{2}O_{2\,(g)} \rightrightarrows Na_2O_{(s)} + I_{2\,(g)}$$

The detection of I_2 and associated fragments was found to be after the main mass loss peaking at 810 °C with an onset at 653 °C. This may be due to a lag in the system between species making their way to the detector and the sample being heated.

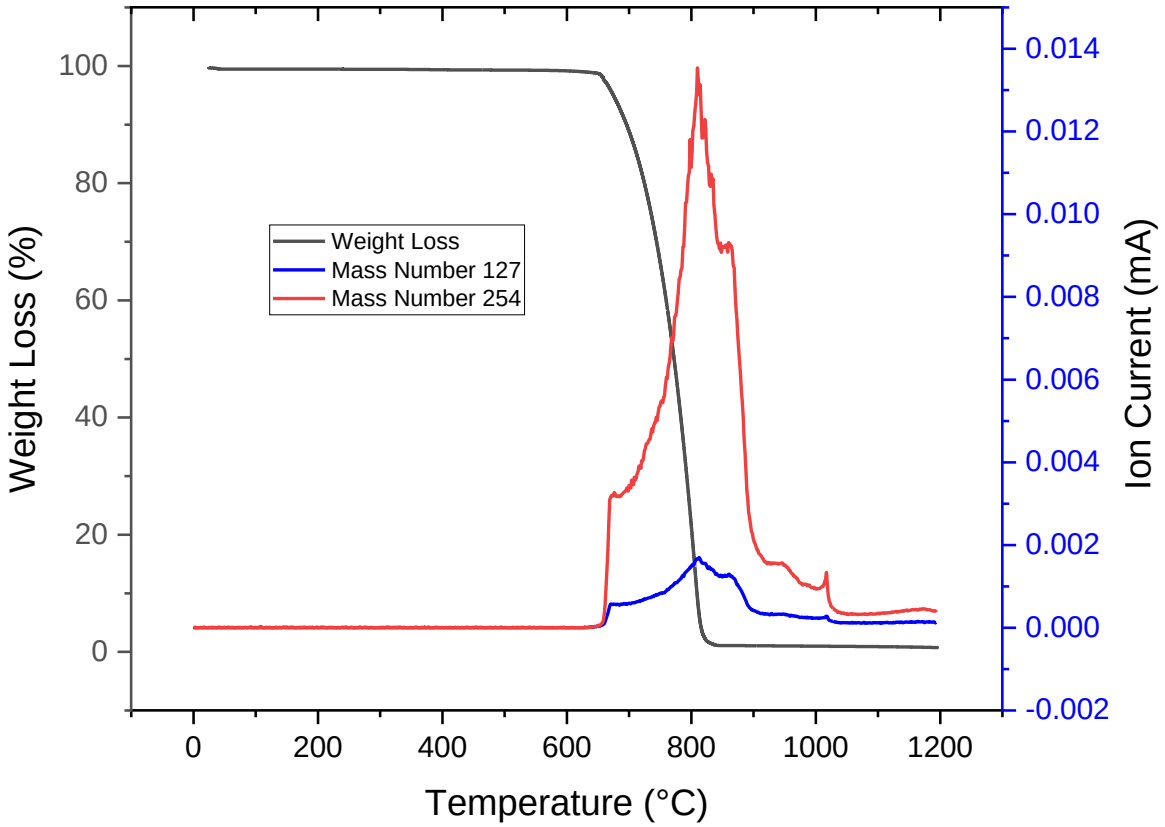

Figure 5.17 MS intensities of AMU 127 (blue) and 254 (red) whilst heating of the raw material NaI over the temperature range 0 – 1200 °C, weight loss added for comparison.

5.4.2 MW Base Glass

5.4.2.1 TG-MS and DTA

This section discusses the MW base glass and its response to temperature and sodium carbonate/zinc oxide/iodine additions analysed by TGA, DTA and MS. Firstly we look at the effect of temperature on addition of 1, 5 and 10 wt% I added as NaI to fritted MW glass.

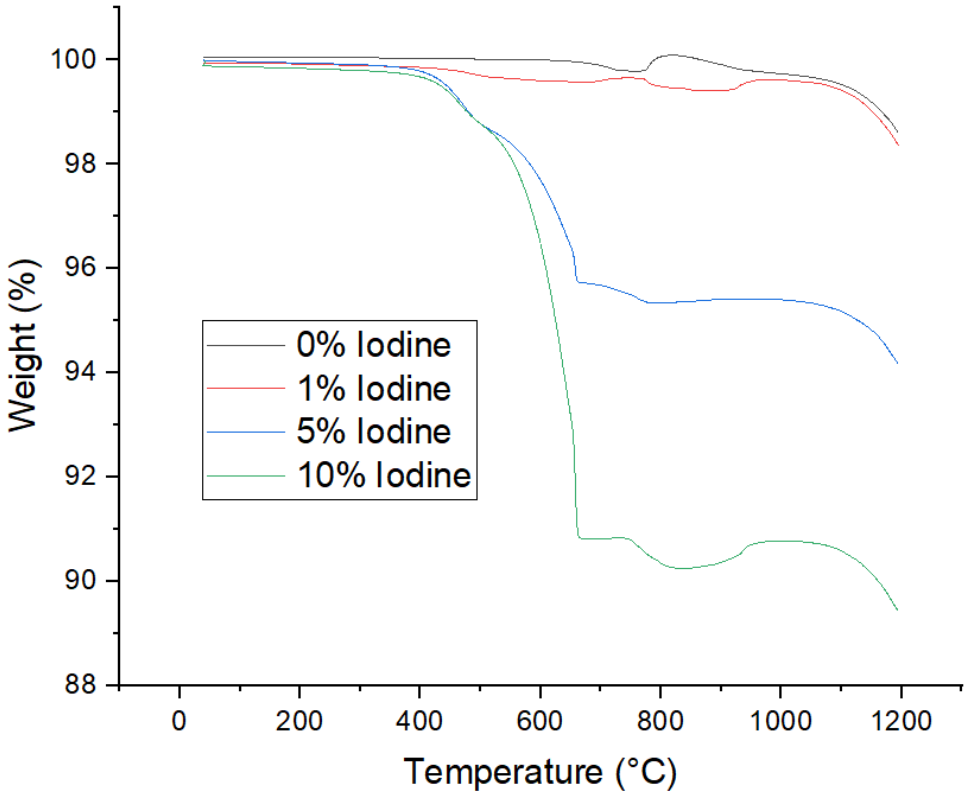

Figure 5.18 TGA trace of MW base glass with additions of 1, 5 and 10 wt% iodine added as NaI

As we have already seen iodine is a very volatile element and the majority of it is lost when heating NaI raw material up to 1200 °C. In the MW glass system (figure 5.18) we can see a similar effect where a significant proportion of the total mass is lost at one certain temperature. The temperature at which this occurs does not change between 1, 5 and 10 wt% in MW glass and this change does not occur in the base glass therefore is attributed to NaI addition. The onset of the loss is at 385 °C for all iodine containing samples and the range is also consistent from 385 – 674 °C. The raw material showed a similar loss, however, the temperature at which this occurs is higher at 650 °C with a range of 650 – 842 °C (figure 5.14). It is possible we are observing a dissolution step before NaI volatilisation where

liquid/solid NaI is dissolving in liquid MW glass instead of thermally decomposing. Once dissolved in solution the volatilisation properties may be very different to in the raw material alone.

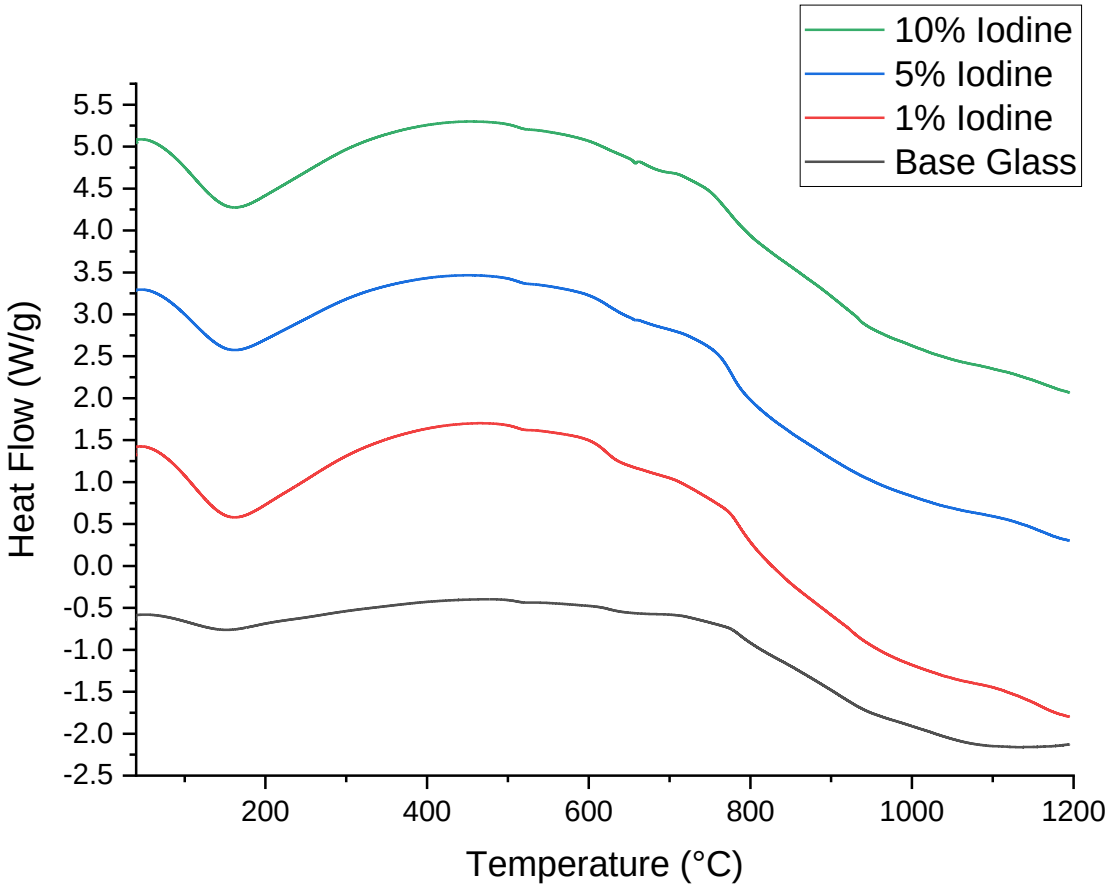

Figure 5.19 DTA data of the MW base glass with additions of 1, 5 and 10 wt% iodine added as NaI

The glass transition temperature over this range of iodine additions doesn't vary much from the base glass or over the series, the value remains at around 510 °C. The only other variation in the DTA trace is the more pronounced reduction in heat flow at 622 °C after the main mass loss occurs in the iodine doped glass samples. In figure 5.18 it can be observed that there are two main step changes in weight, more evident in the more concentrated iodine doped glasses. Looking from left to right we see the first change beginning at 406 °C and changing gradient at 535 °C, the second event occurring at 535 – 674 °C. Total mass loss over the whole temperature range for each glass is 1.45 wt%, 1.57 wt%, 5.84 wt% and 10.49 wt% for MW base glass, 1% I, 5% I, 10% I respectively. The weight change at 406 °C is not observable in the 1 wt% iodine sample because of the low mass loss, there is a mass loss over the whole period between 406 – 674 °C but no distinct gradient change. The first shift in mass at 406 –

535 °C in figure 5.18 is 1.28 and 1.19 wt% for 5% and 10% iodine samples respectively. These are very similar and therefore loss may be due to the MW glass rather than the iodine addition, this also explains why this initial loss decreases upon increasing iodine content as there is less MW glass frit proportionally in the higher iodine concentration samples. Unlike the caesium experiments using the TG-MS there are noticeable m/z ions detected in the MS portion of the data relating to iodine.

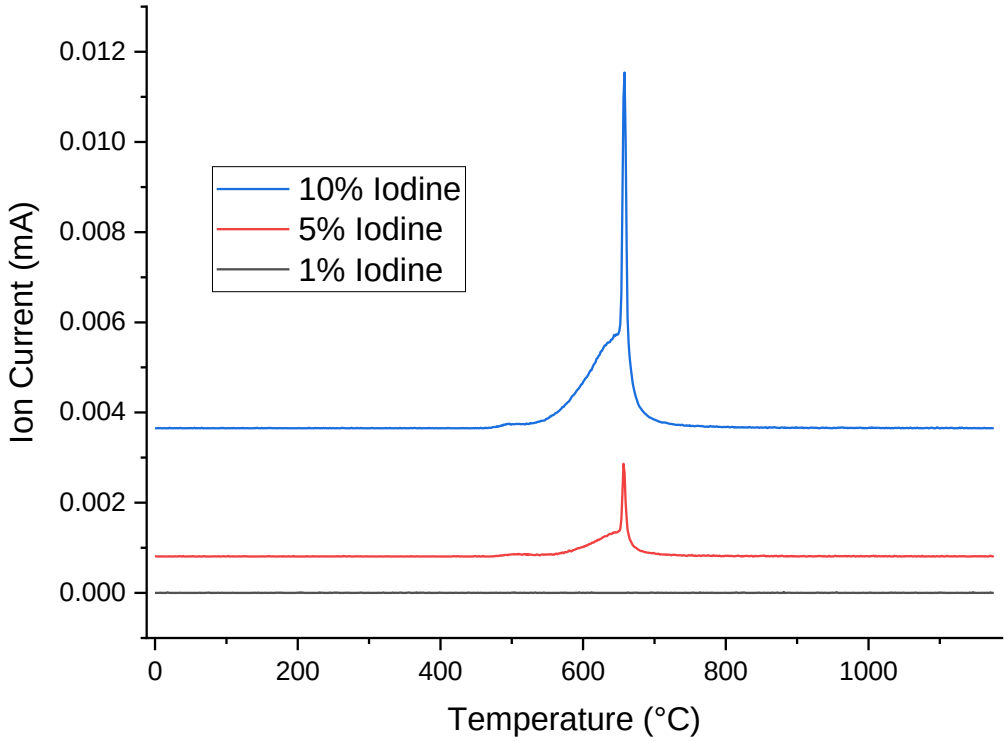

Figure 5.20 Mass spectrometry of gas emissions from 1, 5 and 10 wt% iodine doped as NaI onto MW fritted glass heated between 0 – 1200 °C, showing m/z ion 254 AMU (I_2) intensity. I^- traces are directly proportional to the displayed data.

Ions detected by MS were AMUs 127 and 254 which are assigned to I_2, 127 being present as a fragmentation product of the MS process (with expected isotopic distribution, see appendix B). No other peaks were present including 18 (H_2O) and 44 (CO_2). In figure 5.20 we can see that the emission peaks at 658 °C with an onset at 552 °C. The peak that appears in both 5 and 10 % iodine samples is very sharp with a broad shoulder beforehand almost identical other than in intensity. Size of the less intense peak from the 5 % iodine sample is 25.98 % of the intensity of the 10 % iodine peak (3.85 times). This could be showing that iodine is retained better at lower concentrations due to the

solubility limit of the glass being reached. It is also worth noting that all iodine volatilised as I_2 as both I^- and I_2 are directly proportional showing I^- is a fragment of I_2 ionisation in the MS instrument.

Now we understand what gaseous products form from this glass melt we can estimate the mass losses from the TGA and compare them to NaI completely dissociating.

Based on the reaction of:

$$2NaI_{(s)} + \frac{1}{2}O_{2\,(g)} \rightarrow Na_2O_{(dissolved)} + I_{2\,(g)}$$

We can calculate that for every gramme of NaI added 0.85 g of iodine gas (I_2) would be produced assuming complete decomposition. This translates to a mass loss of 80.4 % if this reaction includes the addition of oxygen. Comparing this to TG data in figure 5.16 the percentage mass loss of the total associated to iodine in 1, 5 and 10 % samples is 0.12 , 4.39 and 9.04 % after substituting the contribution from MW glass. As a percentage of the total sodium iodide added the samples show the following losses 10.16, 74.34 and 76.54 % for 1, 5,and 10 wt% iodine samples respectively. At 1 % iodine in MW the lowest loss of iodine is seen over the temperature range this is seen in the MS data also where no peak appears for any iodine containing gas species. This might suggest the solubility limit for this glass system for iodine being closer to 1 % iodine as we see a lot less volatilisation in this sample.

In these group of experiments, we also attempted to see the effect of sodium and zinc on volatility of iodine. This was completed by additions of 5 wt% of the additive and 5 wt% iodine (added as NaI) and analysis by TG-MS. The TGA trace in figure 5.21 shows that there is little difference between the samples and there is no improvement in the retention of iodine upon the addition of either sodium or ZnO. The MS data in figure 5.22 does show a more intense ion current for the m/z ion 254 (relating to I_2) in zinc and sodium doped samples, however, this increase is not large, and the peak position / shape does not change from the doped base glass. CO_2 (AMU 44) loss was found to be at 600 °C and only present in $NaCO_3$ samples (appendix C).

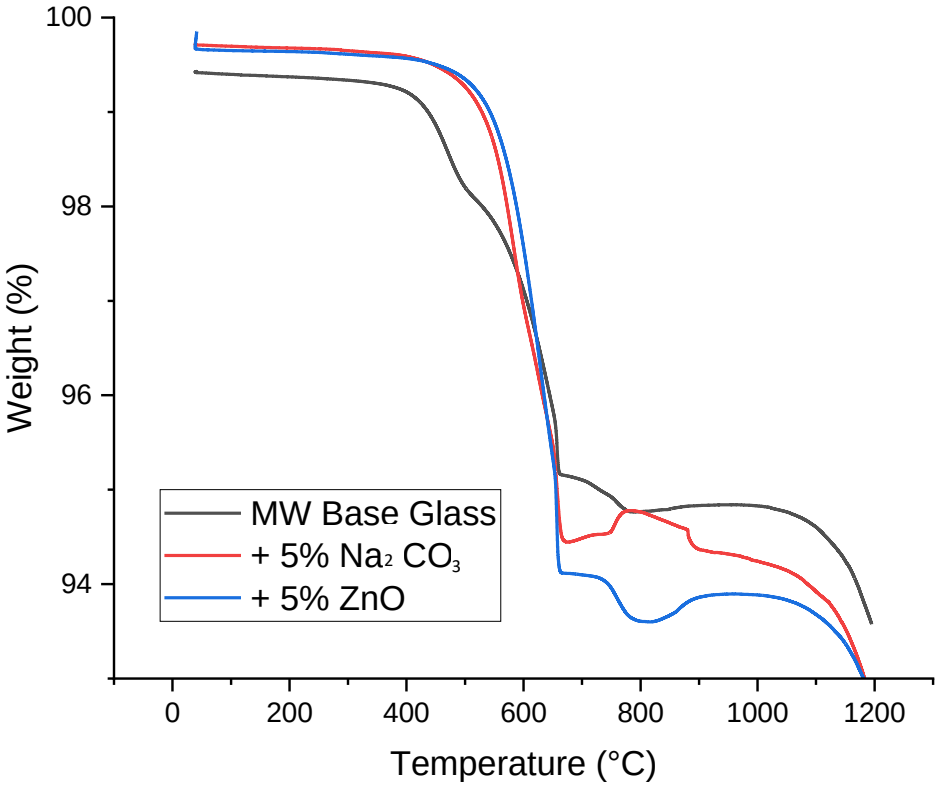

Figure 5.21 TGA trace showing the weight change of MW base glass, MW + 5% Na_2CO_3, MW and MW + 5% ZnO all with the addition of 5% iodine added as sodium iodide between 0 – 1200 °C

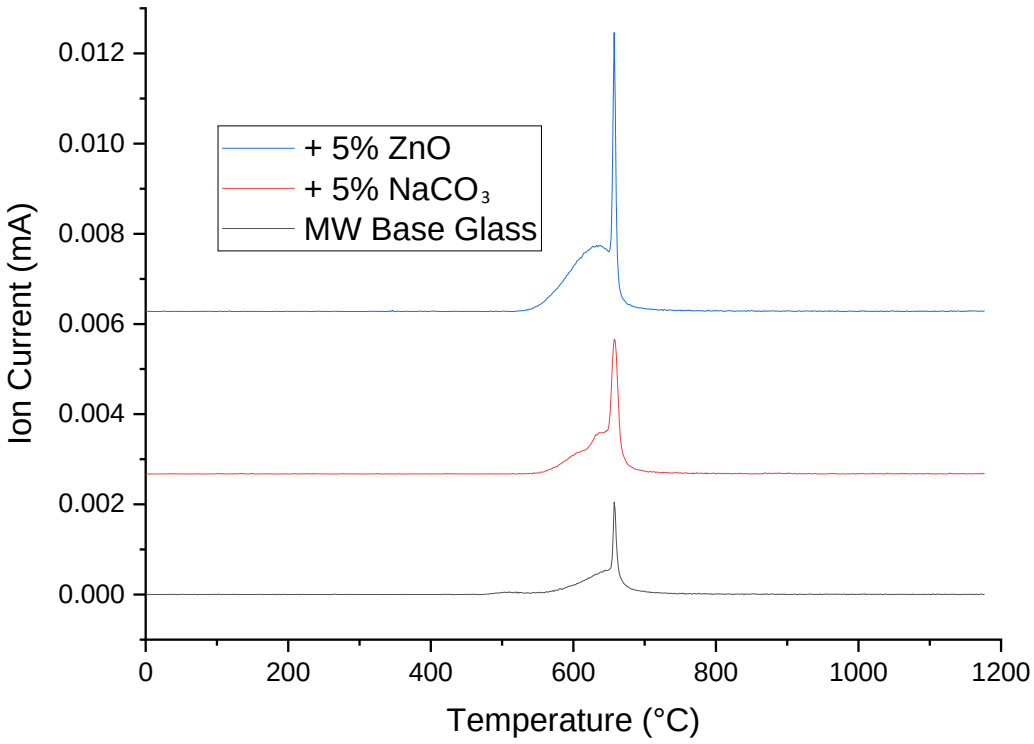

Figure 5.22 Graph of MS data from AMU 254 (I_2) for samples MW base glass, MW + 5% Na_2CO_3, MW and MW + 5% ZnO all with the addition of 5% iodine added as sodium iodide between 0 – 1200 °C

5.4.2.2 Temperature Dependence

In this section we discuss the effect of temperature on MW glass composition with the addition of 1 % iodine (as NaI) to either the glass frit as raw material (t=0) or remelting glass containing 1 % iodine in its structure (t=2h).

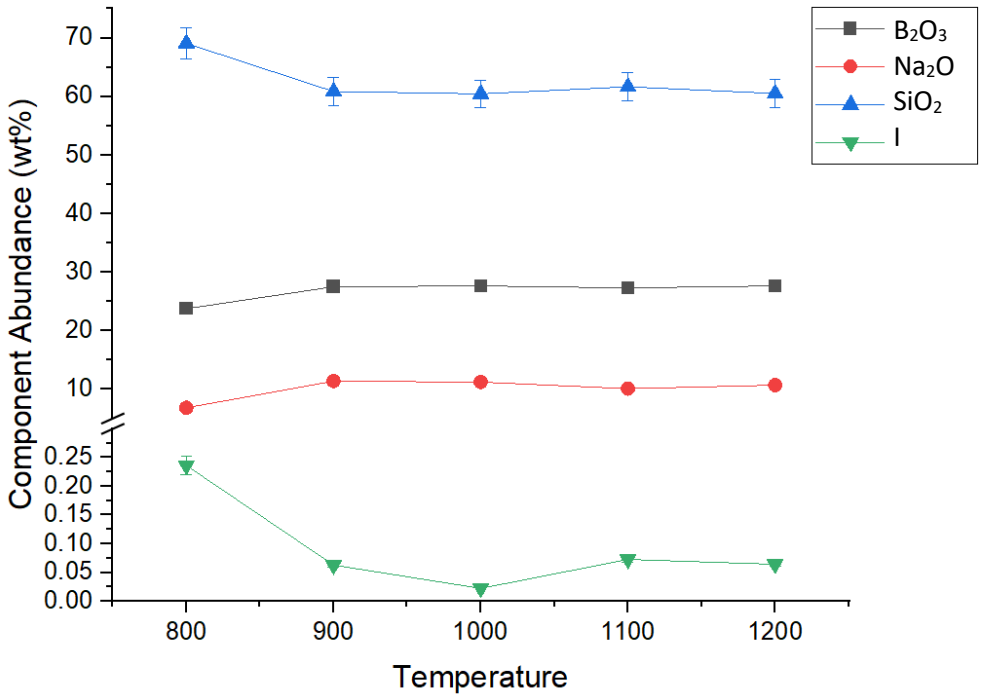

Figure 5.23 The effect of temperature on glass composition of MW with addition of 1 % iodine (added as NaI) from 800 – 1200 °C (t=0)

The graph in figure 5.23 shows the change of iodine concentration in the glass with temperature from the t=0 series. At 800 °C 0.24 wt% iodine remains in the end product after 2 hours, significantly less than the added 1% iodine. The iodine content in the product greatly reduces at 900 °C averaging at 0.06 +/- 0.004 wt% and not varying much from this value. This is consistent with the TGA data in figure 5.16 which shows a distinct drop in iodine content at 658 °C in very small (15-25 mg) and more concentrated samples. In the 1% iodine doped sample around 10 % iodine loss is seen in the TGA data, however, over 2 hours of heating this effect could be compounded to the loss we see in figure 5.23.

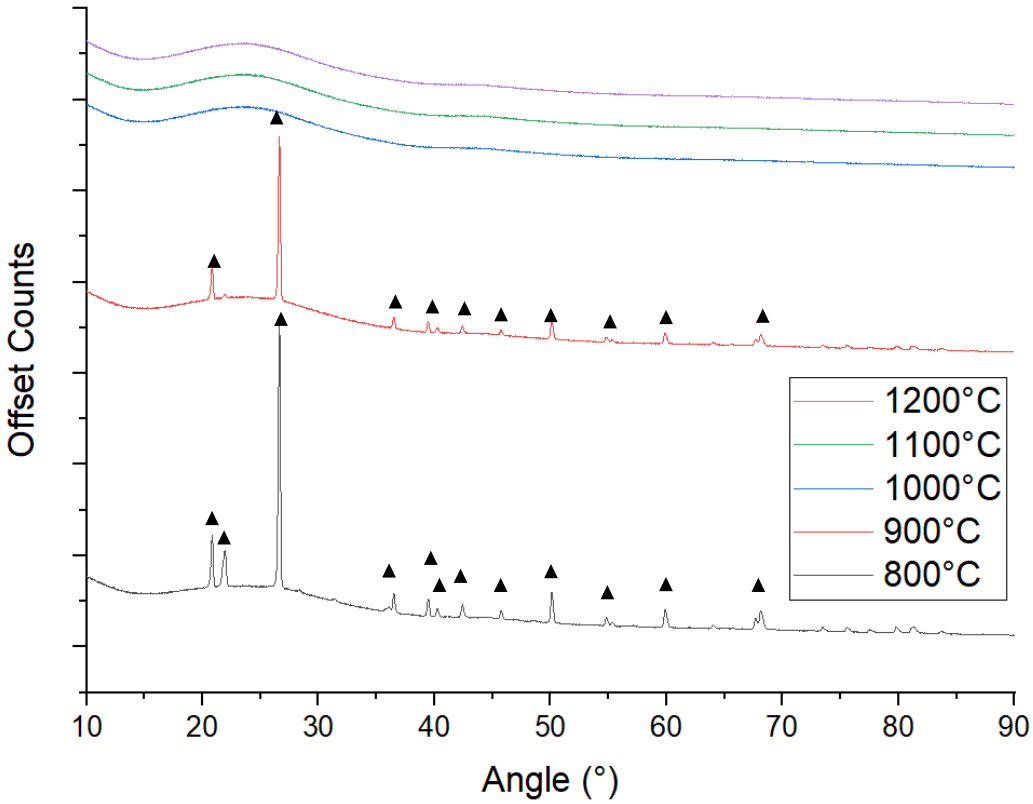

Figure 5.24 XRD data of MW glass added with 1% I as NaI (t=0) melted at 800 – 1200 °C. ▲ = SiO_2, Quartz (Phase ID: 01-075-8320)

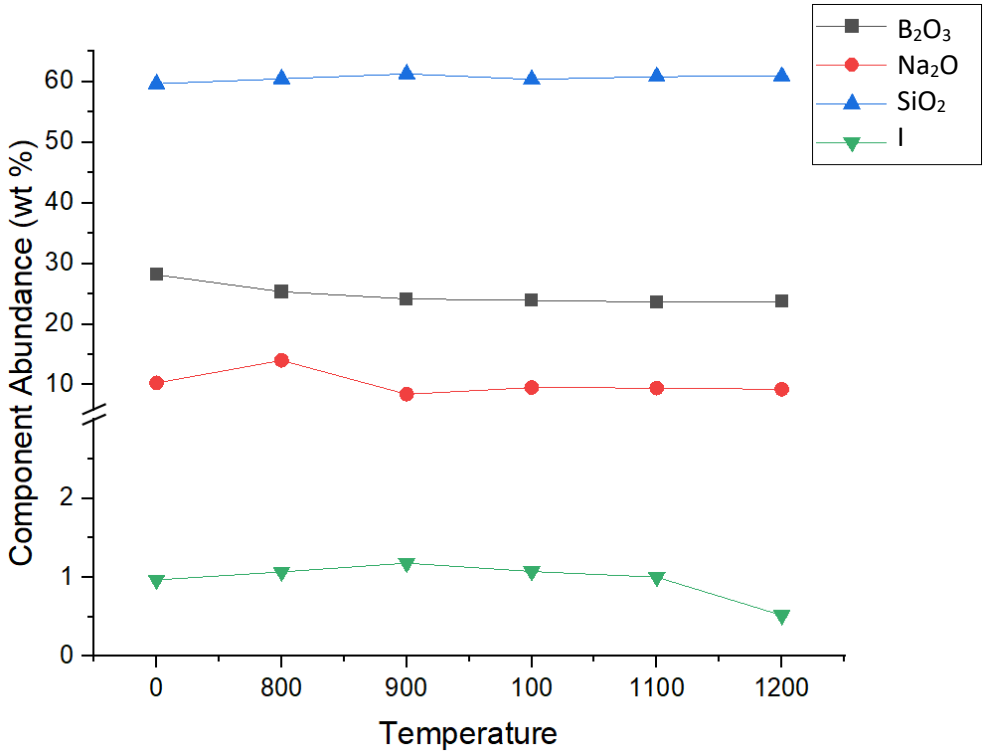

Figure 5.25 Change in glass content (analysed by XRF) of MW incorporated with 1 wt% iodine remelted between 800 – 1200 °C (t=2h)

Another large difference between comparing the two sets of data is surface area : volume ratio which is larger for the 600 µl TGA crucibles (3.25:1) compared to the 80 ml crucibles used in the temperature dependence work (1.57:1) which would increase the volatilisation in TGA samples compared to other experiments. Other glass contents varies only at the 800 – 900 °C silica content does reduce slightly between 800 and 900 °C in tandem with sodium and boron content increasing. Over the remaining 900 – 1200 °C there is little change in glass composition over the period.

Crystal character in the t=0 series also changes over the temperature range, seen in figure 5.24, where there is peaks seen in the XRD patterns for 800 and 900 °C samples. After analysis this was shown to be assigned to SiO_2 (quartz) . The pattern does not change other than a disappearance of a peak at 22 ° 2θ, intensity of the other peaks reduce in from 800 to 900 °C which could be an indication of concentration of these crystals reducing as the sample is heated. This devitrification was also seen in the other caesium containing temperature dependence series and since there is no iodine containing crystal species in this graph we can assume iodine has either been lost or incorporated into the glass. There are implications for the use of this system to incorporate iodine and caesium at temperatures below 1000 °C in the nuclear industry as the devitrification of a glass is undesirable in wasteforms.

When remelting glass containing iodine (t=2h) we see a very different reaction to temperature. In figure 5.25 we can see that there is little change in most glass components other than iodine which has a noticeable decrease at higher temperatures. At 1200 °C the concentration of iodine in the glass is 0.52 wt%, compared to the average of the previous 5 samples (1.06 wt%) this represents a large drop. This only occurs at 1200 °C suggesting that at this temperature volatilisation of iodine starts to increase dramatically. Interestingly the glasses between 0 and 1100 °C did not show any loss from the original glass without heating which shows that the resultant glass containing iodine is quite stable more so than the NaI raw material added to MW glass. Over this series (t=2h) the crystallisation behaviour is rather similar to the t=0 series where crystallisation of the product occurs if the sample is heated to 800 °C, however, in the remelting experiments (figure 5.26) the 900 °C sample does not

show any peaks by XRD. The peaks appearing at 800 °C are the same as the t=0 series assigning to SiO_2 (as quartz). This indicates that this crystallisation is likely from the devitrification of the MW glass rather than from the iodine raw material or the iodine in the glass. At 900 °C (and higher) the crystallisation no longer occurs and the products are amorphous.

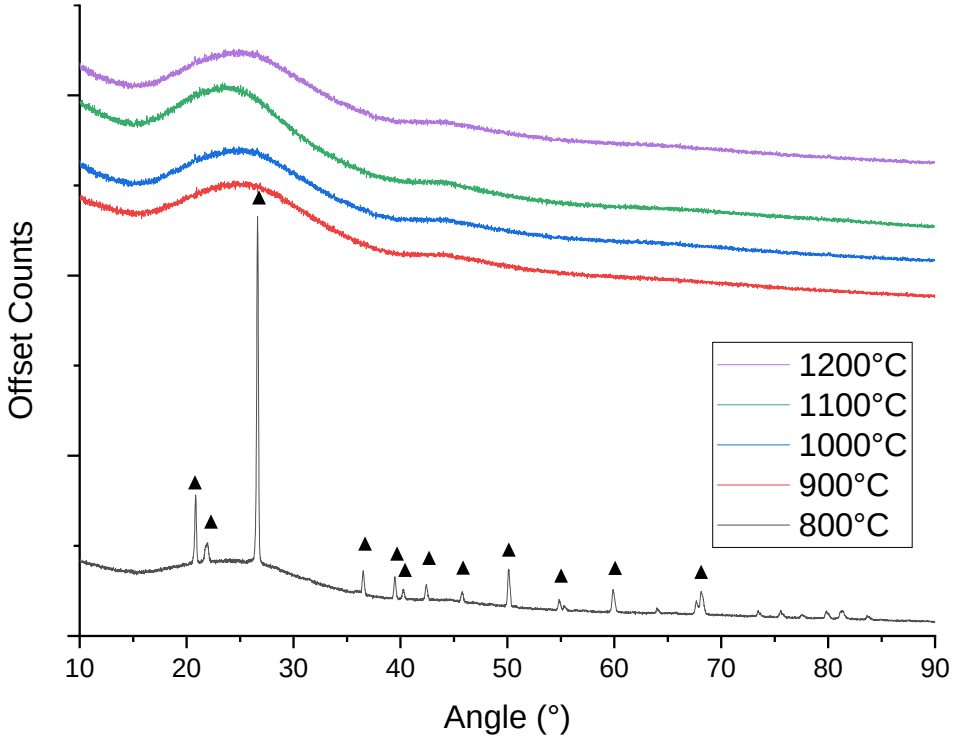

Figure 5.26 XRD data of MW glass containing 1% I (t=2h) remelted at 800 – 1200 °C. ▲ = SiO_2, Quartz (Phase ID: 01-075-8320).

Density of the products follows a similar trend to the caesium containing temperature dependence measurements. At lower temperatures where crystallisation occurs due to devitrification of the MW glass system we also see a drop in density. This is evident in both t=0 and t=2h series in figure 5.27 where the remelted glass containing iodine (t=2h) drops to its lowest value at 800 °C 2.3283 g/cm^3 and recovers back to 2.5283 g/cm^3 at 900 °C which is also the temperature at which we see a change in crystal character to becoming amorphous (figure 5.26). The t=0 samples added with NaI have crystallisation at 800 and 900 °C seeing also a decrease in density at the same temperatures (2.3506 and 2.3114 g/cm^3) recovering at 1000 °C to 2.4600 g/cm^3 similar to that of the original glass (2.4459 g/cm^3). Another notable occurrence in this data is the apparent densification of the t=2h samples at

900 – 1200 °C an average of the 2.53 g/cm^3 occurs, compared to the base glass this is higher (2.45 g/cm^3).

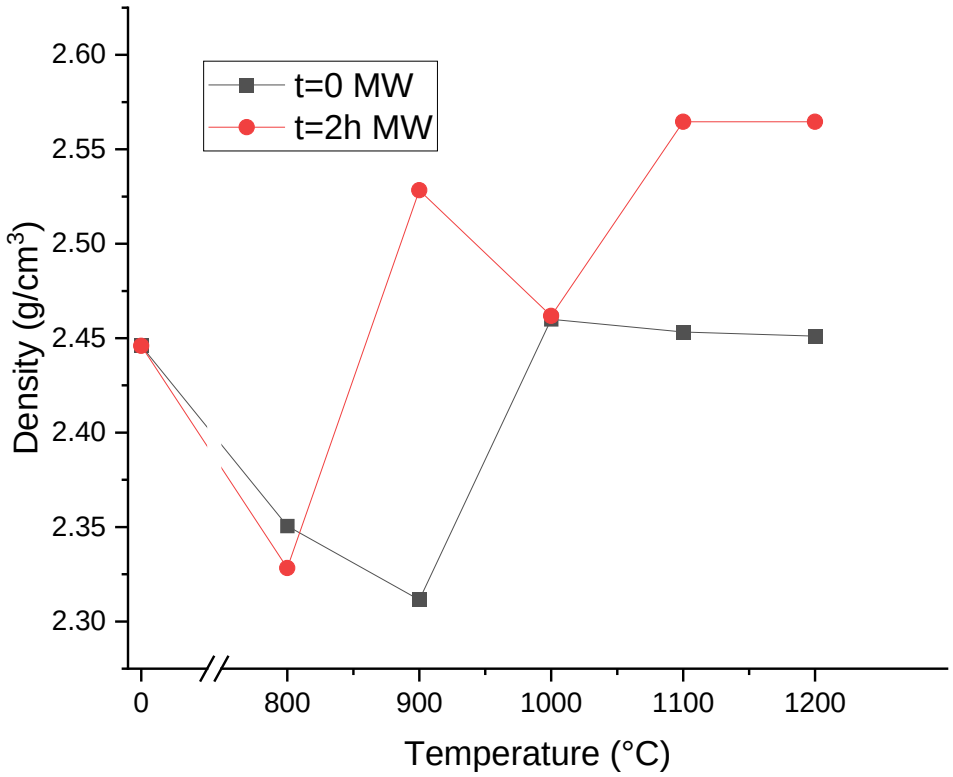

Figure 5.27 Effect of heat treatment temperature (800 – 1200 °C) on density of MW glass systems, t=0 remelted with NaI and 1 wt% iodine already in the glass network. Error bars represent +/- 0.001 g for each measurement which is smaller than the points.

The increase in density above the original value of 2.45 g/cm^3 seen in figure 5.27 when remelting MW at 900, 1100 and 1200 °C could be because of void filling of the original glass from welting and reforming. However, the same does not occur to the same extent in caesium containing MW glasses (figure 5.7) suggesting iodine is refining the density at higher temperatures. More investigations are needed to clarify this point.

5.4.3 CaZn Base Glass

We will now shift to discussing the properties of CaZn glass by analysing the TG-MS, DTA and XRF data looking the effect of temperature and concentration on the gas emissions from CaZn glass when doped with NaI or when glass contains iodine incorporated previously.

5.4.3.1 TG-MS and DTA

TGA, DTA and MS data is analysed at differing iodine concentration (0, 1, 5 and 10 wt%) over a temperature range of 0 – 1200 °C and a heating rate of 5 °C/min. In addition, the doping of CaZn with sodium carbonate and zinc oxide is demonstrated and the effects on iodine retention found. Firstly, the effects of iodine concentration on volatility are shown by TGA in figure 5.26. CaZn Base glass has a mass loss (over the conditions previously mentioned) of 0.63 wt% therefore this will be substituted from the total mass loss from the iodine doped samples to estimate iodine percentage mass loss. Total mass loss over up to 1200 °C for each sample is 1.499, 5.046 and 10.907 % in 1, 5 and 10 % iodine samples respectively. After substituting for intrinsic CaZn weight change this reduces to 0.869, 4.416 and 10.277 % for 1, 5 and 10 % iodine CaZn glasses, an estimation of the iodine loss in the samples.

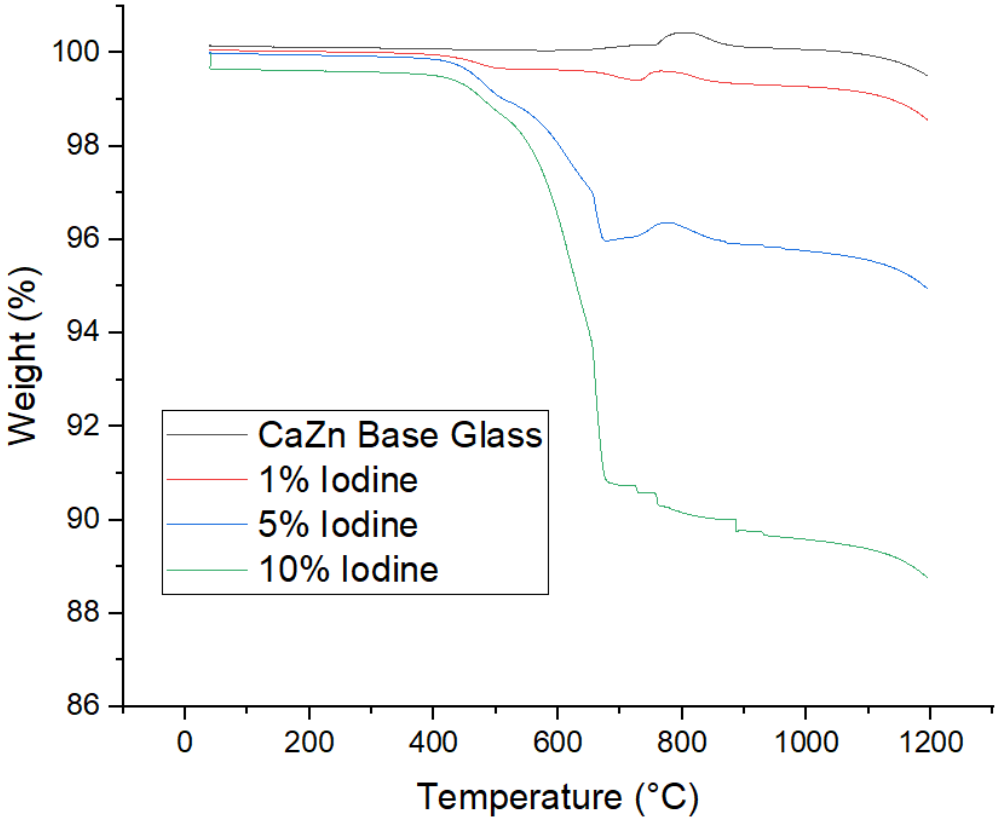

Figure 5.28 TGA trace of CaZn base glass with additions of 1, 5 and 10 wt% iodine added as NaI between 0 – 1200 °C

This indicates that there is significant iodine loss when heated up to 1200 °C, the more concentrated 10 % iodine sample appears to lose 100 % of the iodine added whereas when the concentration lowers the percentage of iodine loss decreases. For 1 and 5 % iodine doped samples 86.90 and 88.32 % of the

iodine is lost to volatilisation. This data shows that for when the solubility limit for the glass is overcome by a large amount iodine is more likely to volatilise from the glass melt. DTA data from these samples (0, 1, 5 and 10 % iodine) is shown in figure 5.29 and illustrates the differences in heat flow over 0 – 1200 °C.

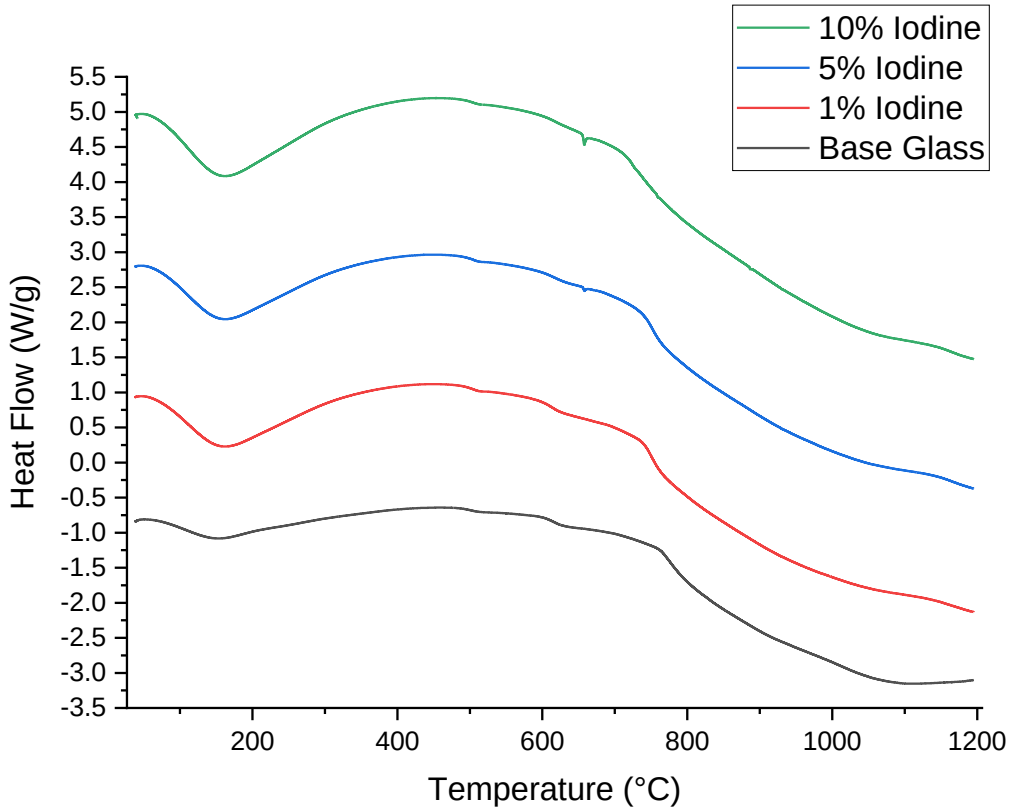

Figure 5.29 DTA data of the CaZn base glass with additions of 1, 5 and 10 wt% iodine added as NaI

Few differences are seen between the base glass and the iodine doped samples, glass transistion temperature remains constant and the final tail is of similar shape and location. The onset of the tail at 750 °C does occur at a slightly lower temperature for the iodine containing samples but the change is not large (~20 °C). An endothermic peak occurs at 658 °C only in 5 and 10 % iodine spiked samples which can be assigned to the melting of sodium iodide as we see the same peak occur in the raw material in figure 5.16 and an increase in intensity of this peak occurs with increasing iodine concentration. Volatilisation of I_2 gas (AMU 254) can be seen in the MS data (with the expected 127 I^- fragment) in figure 5.30. Similarly to the MW glass system (figure 5.20) we see a no detection of m/z

ion 254 or 127 in the 1% iodine sample and an increase in intensity for these units over 5 and 10 % doped. The major peak for iodine gas detection is at 660 °C for both 5 and 10 % iodine, when compared to MW this is a very similar emission (658 °C). One main difference is the shape of the peak, other than the shoulder at 624 °C (which is similar) there is a more pronounced minor shoulder at 513 °C which does not appear in the MW MS frits at the same iodine concentrations. In addition, there are two small peaks at 725 °C and 753 °C in the highest concentration 10 % iodine material which doesn't appear in any other of the MS graphs.

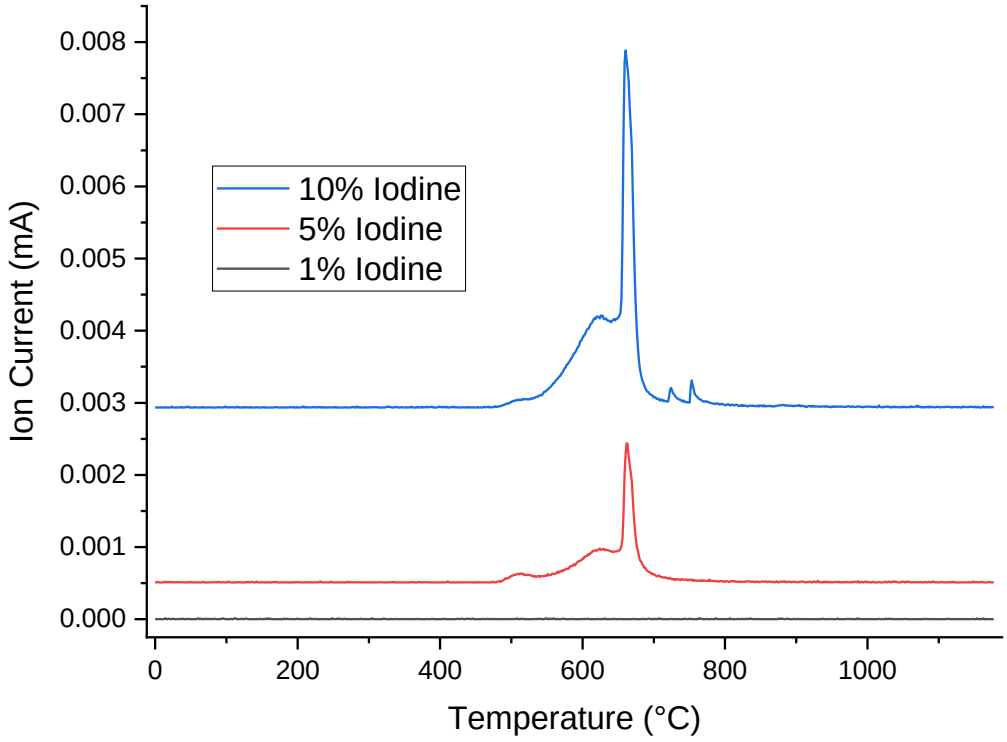

Figure 5.30 Mass spectrometry of gas emissions from 1, 5 and 10 wt% iodine doped as NaI onto CaZn fritted glass heated between 0 – 1200 °C, showing m/z ion 254 AMU (I_2) intensity

The solubility limit of iodine in MW and CaZn is likely very similar given that there is no iodine detection and less mass loss in 1 % iodine samples. When the 5 % iodine spiked sample is adjusted in content with sodium and zinc oxide we see a change in mass loss and iodine volatilisation. Figure 5.31 is a graph of the weight change in CaZn glass with 5% ZnO or Na_2CO_3 all with the addition of 5 % iodine. There is a clear increase in mass loss upon sodium carbonate addition, however, this is due to sodium carbonate decomposition at 580 °C (when carbon dioxide appears in MS (appendix D)), this is also seen by a gradient shift in the TGA at 615 °C where carbonate decomposition ends and iodine

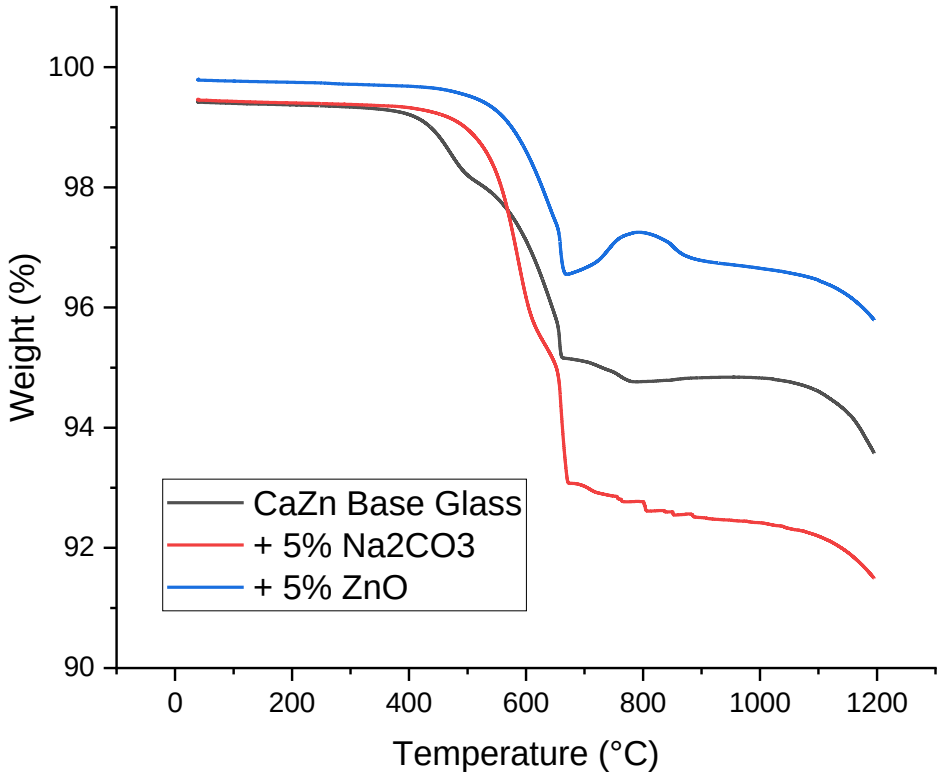

Figure 5.31 TGA trace showing the weight change of CaZn base glass, CaZn + 5% Na_2CO_3, CaZn and CaZn + 5% ZnO all with the addition of 5% iodine added as sodium iodide between 0 – 1200 °C

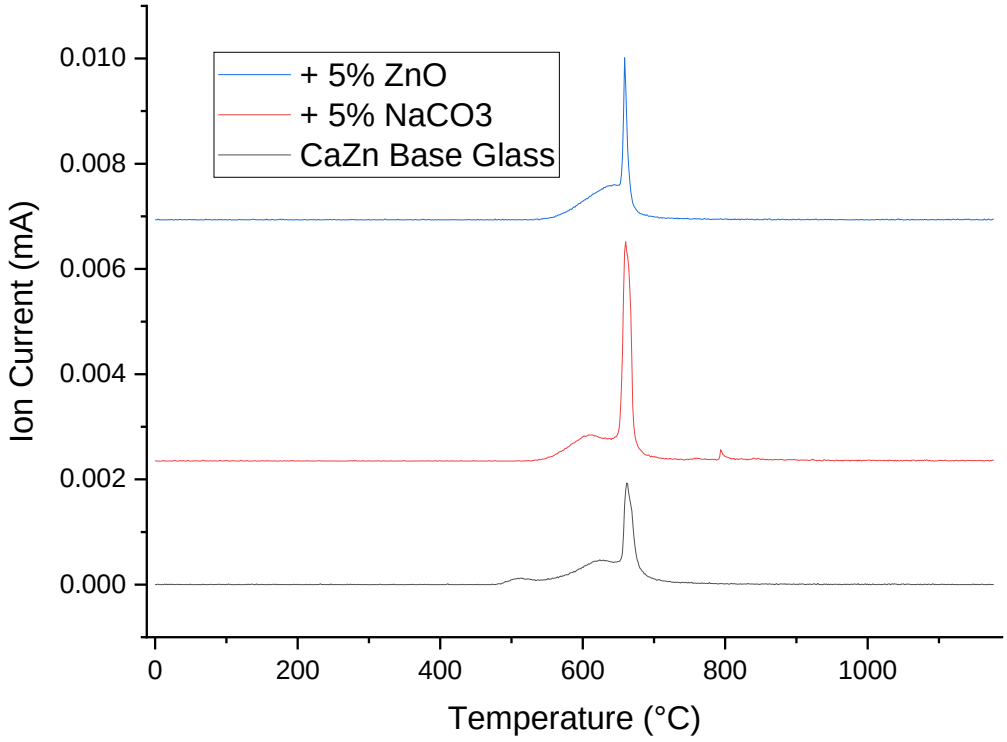

Figure 5.32 Graph of MS data from AMU 254 (I_2) for samples CaZn base glass, CaZn + 5% Na_2CO_3, CaZn and CaZn + 5% ZnO all with the addition of 5% iodine added as sodium iodide between 0 – 1200 °C

volatilisation begins. Discounting carbon dioxide the mass loss of the Na_2CO_3 added sample has a very similar mass loss and therefore sodium has less of a role in iodine retention. Zinc oxide has a positive effect on retention of iodine, the base glass with 5 % iodine is 5.05 % whereas with 5 % ZnO the mass loss changes to 4.00 %. The MS data (figure 5.32) shows all samples contain AMU 254 (I_2) the most intense being from sodium carbonate and the other two samples having very similar intensities.

5.4.3.2 Temperature Dependence

The effect of temperature on iodine volatility or retention in CaZn glass is determined by the heat of the glass from 0 – 1200 °C with both fritted glass spiked with sodium iodide raw material (t=0) and glass containing iodine already in its structure.

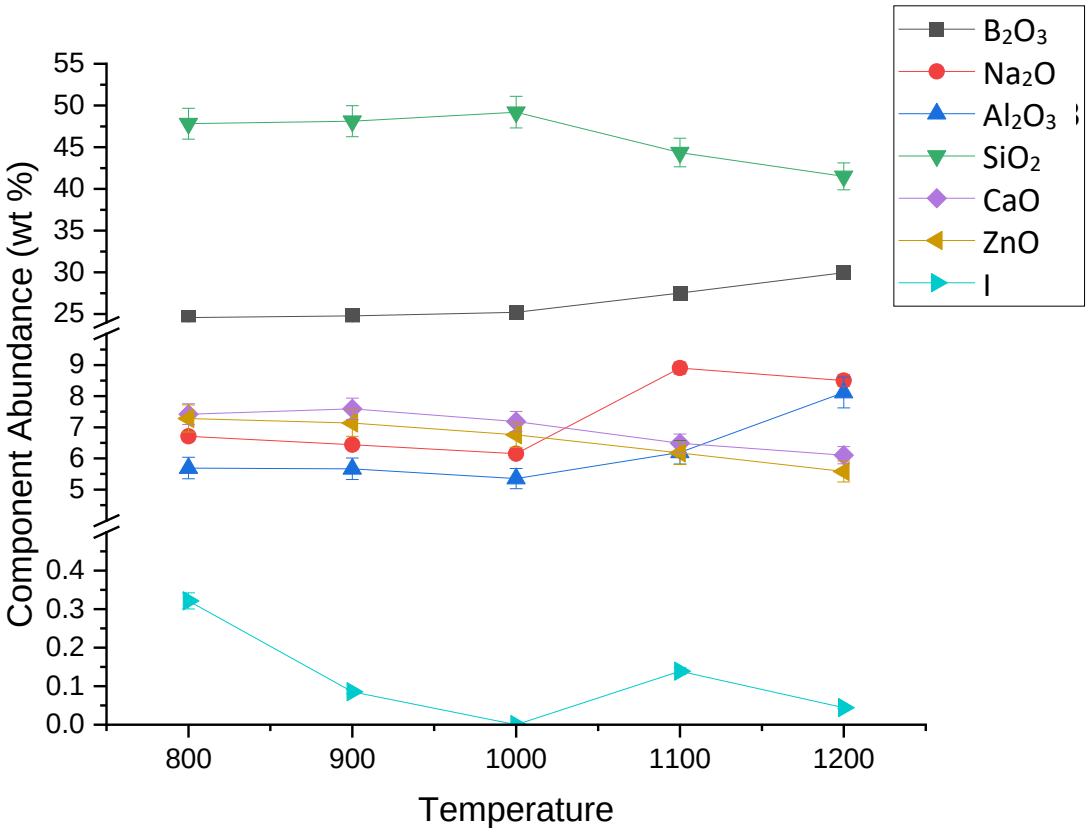

Figure 5.33 The effect of temperature on glass composition of CaZn with addition of 1 % iodine (added as NaI) from 800 – 1200 °C (t=0)

The loss of iodine can be clearly seen in figure 5.33 from 800 – 1000 °C. At 800 °C the content of iodine in the glass is 0.3215 wt% reducing rapidly over the 800 – 1000 °C period to 0.09 wt% at 900 °C and with no iodine being detected at 1000 °C. After 1000 °C however, we do see some fluctuation in the

composition of the glass, this may be due to aluminium contamination from the crucible because at 1100 and 1200 °C there is an increase in aluminium content that may be creating more error in the system whilst being analysed by XRF. This is the likely cause of the decrease in silica content, the increase in boron / sodium content and the slightly unpredictable iodine at these higher temperatures. This is due to the proportional change in weight percent. Iodine content at 1100 °C is likely anomalous effected by high alumina contamination from crucible dissolution which artificially changes other results. No crystallisation of the end product from these experiments was seen in the heat treated sample as can be seen in figure 5.34 from 800 – 1200 °C, all samples appeared XRD amorphous. This shows that iodine had very little impact on the devitrification of CaZn frit, the caesium temperature dependence series shows a similar trend (figure 5.10).

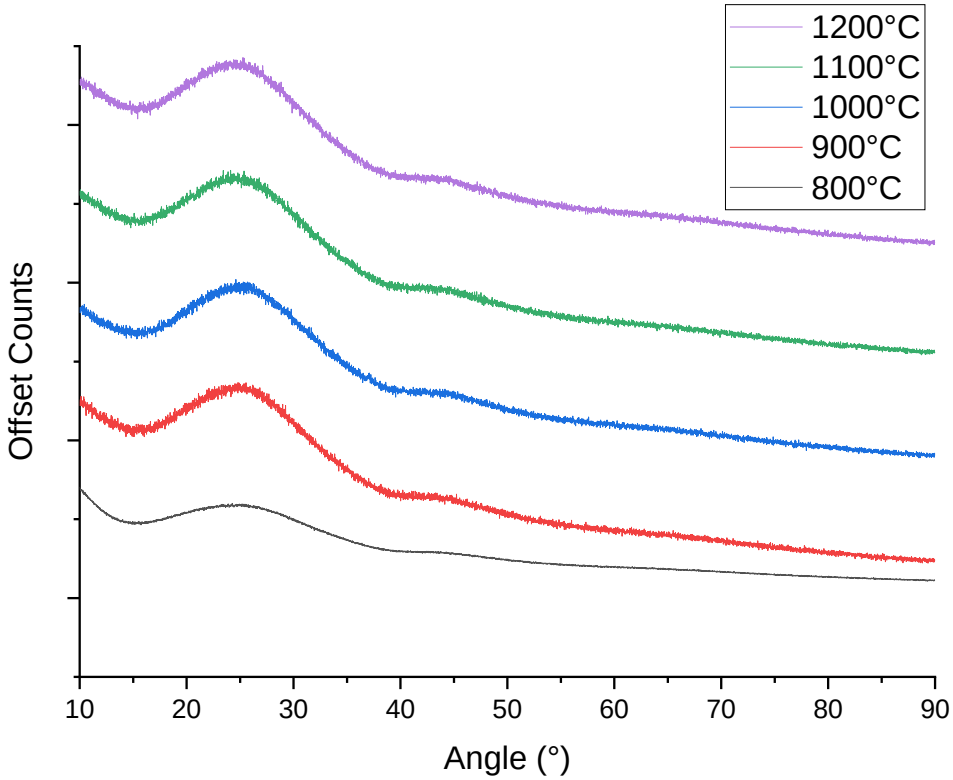

Figure 5.34 XRD data of CaZn glass added with 1% I as NaI (t=0) melted at 800 – 1200 °C

MW glass self devitrifies at 800 °C without any additional agents (figure 5.22), however, CaZn either doesn't produce any crystalline products (figure 5.34) or incorporates into the crystalline product (figure 5.10).

Remelting of the glass (t=2h) has very different volatilisation properties to raw material added to glass as we have seen previously. Figure 5.35 shows the effect of temperature on CaZn glass content in iodine containing glasses remelted between 800 and 1200 °C. Similarly to other systems the concentration of iodine remains higher and stable at 0 – 800 °C (1.36, 1.41 wt% iodine), after, iodine content slowly decreases as the heat treatment temperature increases. This loss is poorly linearly over the 0 – 1200 °C temperature range with a r^2 value of 0.87 and a slope of -0.21. The linear trend of iodine loss from the t=2h series is very different to the t=0 series where no linear trend is observed. However, the concentration at 1200 °C of the t=2h graph is still very low compared to the starting concentration, at 1200 °C 0.27 wt% representing a 80.17 % loss in iodine content from the original glass. Other glass components do not vary much or with a particular trend, however, there is a slight increase in boron, sodium and aluminium content at 1200 °C likely in response to the decrease in iodine content. At 800 °C there is an anomalous point from sodium where the Na_2O concentration decreases suddenly. XRD data of the series shows that the glasses/products are amorphous at all heat treatment temperatures (0 – 1200 °C).

The density is also affected by the heat treatment temperature for both t=0 and t=2h series. At lower temperatures the density reduces, at 800 °C we see the minimum density for both t=0 and t=2h of 2.4817 and 2.3589 g/cm^3 respectively (figure 5.37). This density recovers back to a value like that of the original base glass (2.5633 g/cm^3 = base glass, 2.5516 g/cm^3 = t=0, 2.5470 g/cm^3 = t=2h) after the drop at 800 °C. The density then stabilises for the t=0 series, the t=2h samples, however, do start to decrease trending down as the temperature increases.

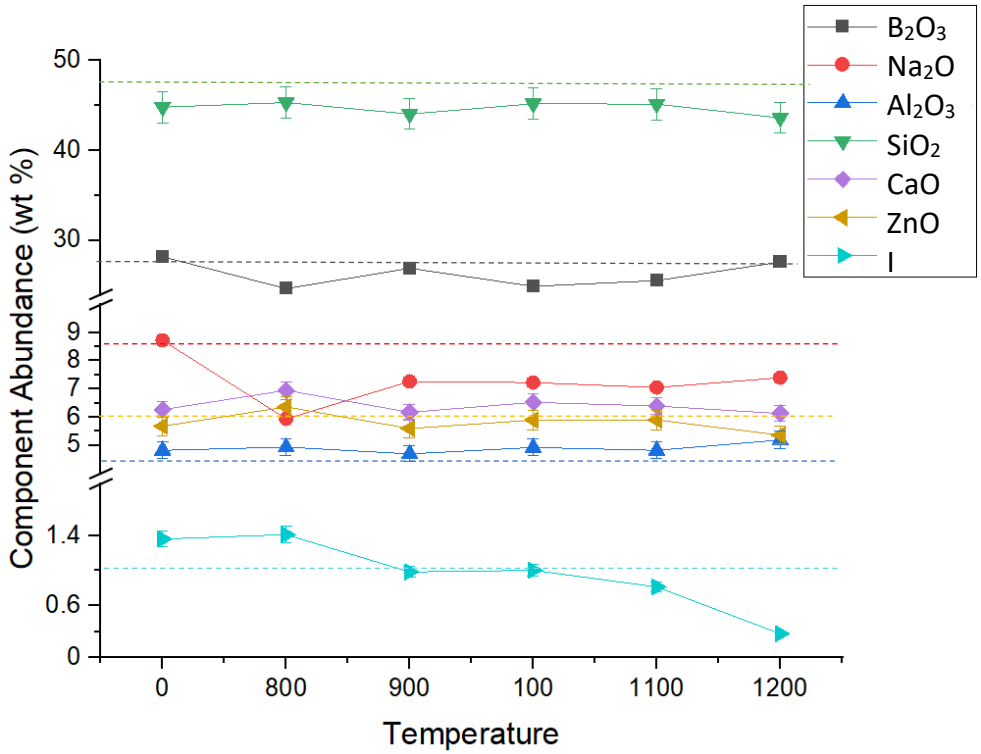

Figure 5.35 Change in glass content (analysed by XRF) of CaZn incorporated with 1 wt% iodine remelted between 800 – 1200 °C (t=2h). Dashed lines indicate expected composition.

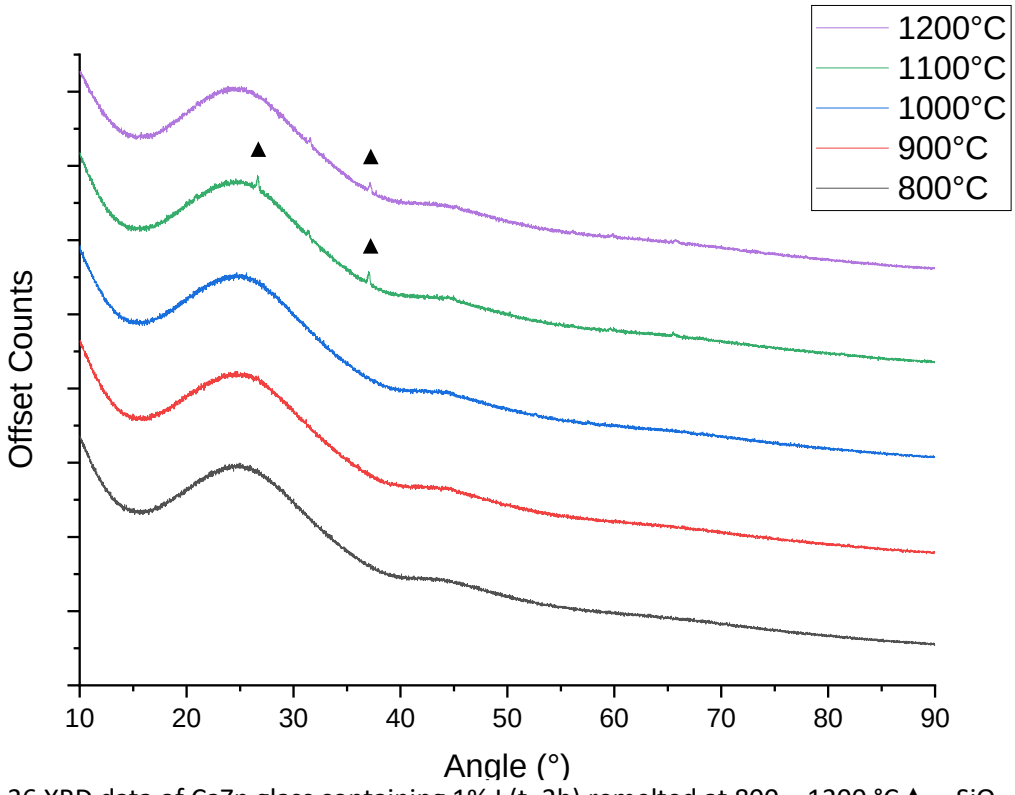

Figure 5.36 XRD data of CaZn glass containing 1% I (t=2h) remelted at 800 – 1200 °C▲ = SiO_2, Quartz (Phase ID: 01-075-8320)

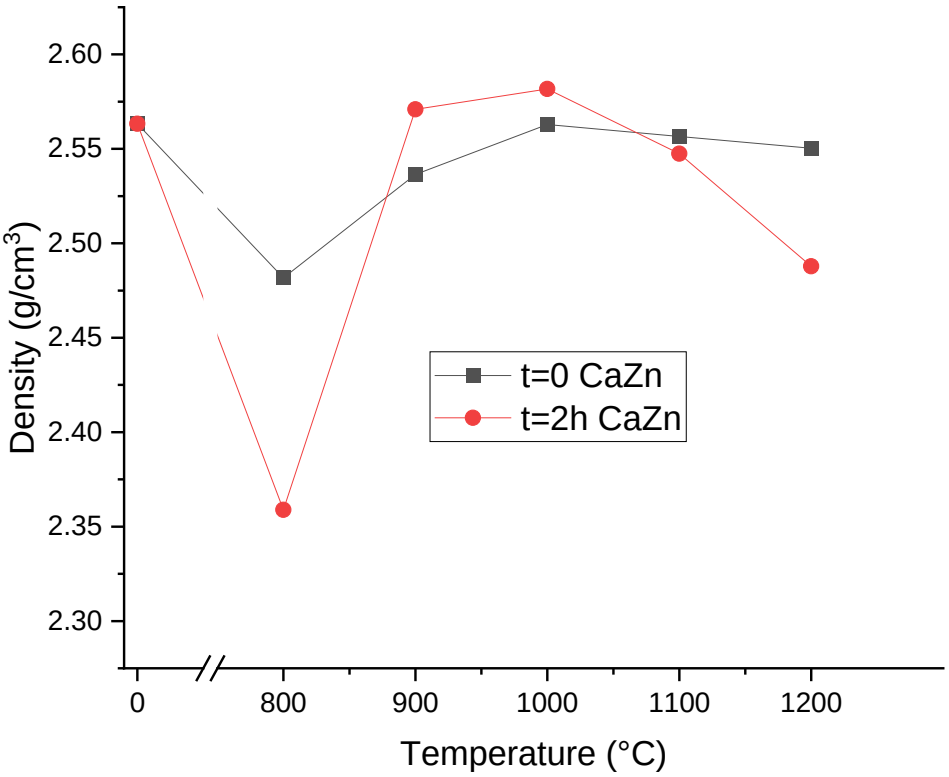

Figure 5.37. Effect of heat treatment temperature (800 – 1200 °C) on density of CaZn glass systems, t=0 remelted with NaI and 1 wt% iodine already in the glass network (t=2h). Error bars represent +/- 0.001 g for each measurement which is smaller than the points.

5.4.3.3 Pyrolysis and Active Tracers

We will discuss the results from radioactive tracer experiments as gases from CaZn glass heat treatments with ^{129}I solutions spiked on are captured in solutions and analysed for activity. Only base glasses and alterations are examined in this section, activity trials of the effect of waste loading if experimented upon in section 6.4.2.1.

Figure 5.38 Image of CaZn base glass post pyrolysis at 950 °C spiked with 10 Bq ^{137}Cs

The standard activity of ^{129}I added is 19.17 Bq/ml which is added as 1 ml of solution to the CaZn glass. After 2 hours of heating CaZn glass the capture solution contained 389.56 counts/minute of activity

given the mass counted and the mass of the sample we can calculate the activity of the capture solution to be 21.12 +/- 0.52 Bq. The mass of the tracer added for this sample was 1.021 g and therefore we can calculate the total expected activity of the tracer to be 19.58 Bq. Dividing the two activities we can find a percentage recovery of the tracer in the solution, found to be 107.88 +/- 2.74 %. This indicates that all of the tracer in the sample moved into the capture solution and therefore the loss from the glass melt was 100% (or retention was 0%). Given that the heating temperature was at 950 °C and the system is comparable to the t=0 temperature dependence series the data from active tracers is consistent with (t=0) furnace experiments where close to all of the iodine was lost.

5.4.4 0% SiO_2 CaZn Base Glass

5.4.4.1 TG-MS and DTA

For 0% SiO_2 CaZn glass the samples were heated between 0 – 1200 °C and analysed by TGA, DTA and MS doped with 5 % iodine added as NaI to ascertain volatilisation properties and the effect of iodine on glass properties, if any. Firstly, we shall look at the mass loss of iodine containing and iodine free 0% SiO_2 CaZn frit from TG analysis shown graphically in figure 5.39. Mass loss is high in iodine containing samples as has been seen in previous experiments where iodine is lost as I_2 gas during heating (seen in figures 5.16, 5.18). In these samples we can see a comparison between the base glass (0 % SiO_2 CaZn) and 5 % iodine spiked base glass. The 5 % spiked sample had a total mass loss of 7.99 wt% significantly higher than the base glass which had a mass loss of 3.73 wt%. Subtracting the base glass losses from the weight change in the 5 % iodine doped sample we can estimate the iodine loss from the sample.

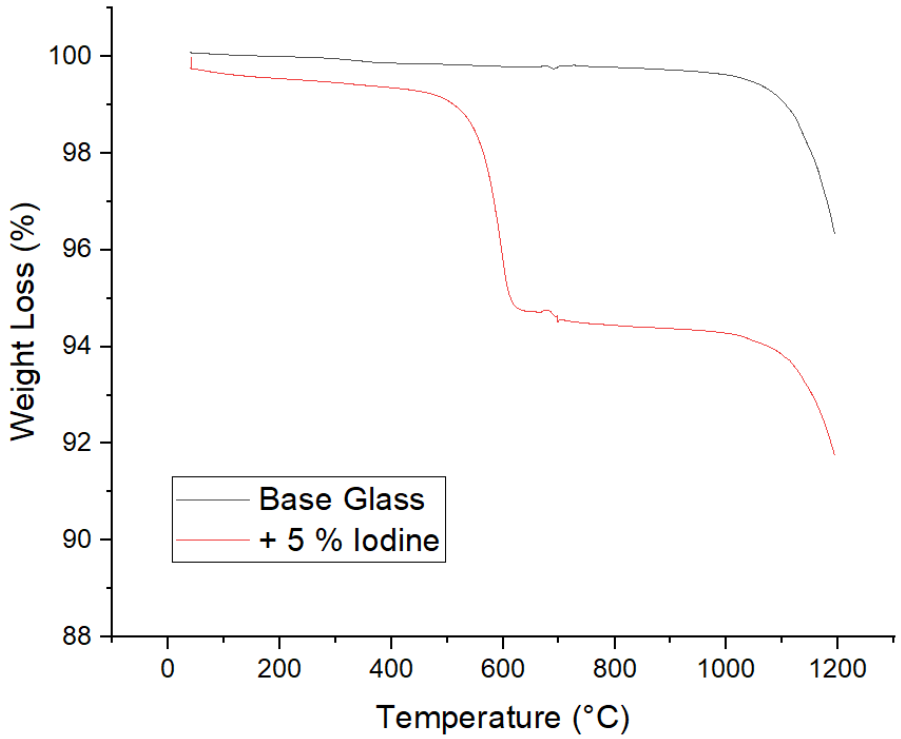

Figure 5.39 TGA trace of 0% SiO_2 CaZn base glass with additions of 1, 5 and 10 wt% iodine added as NaI between 0 – 1200 °C

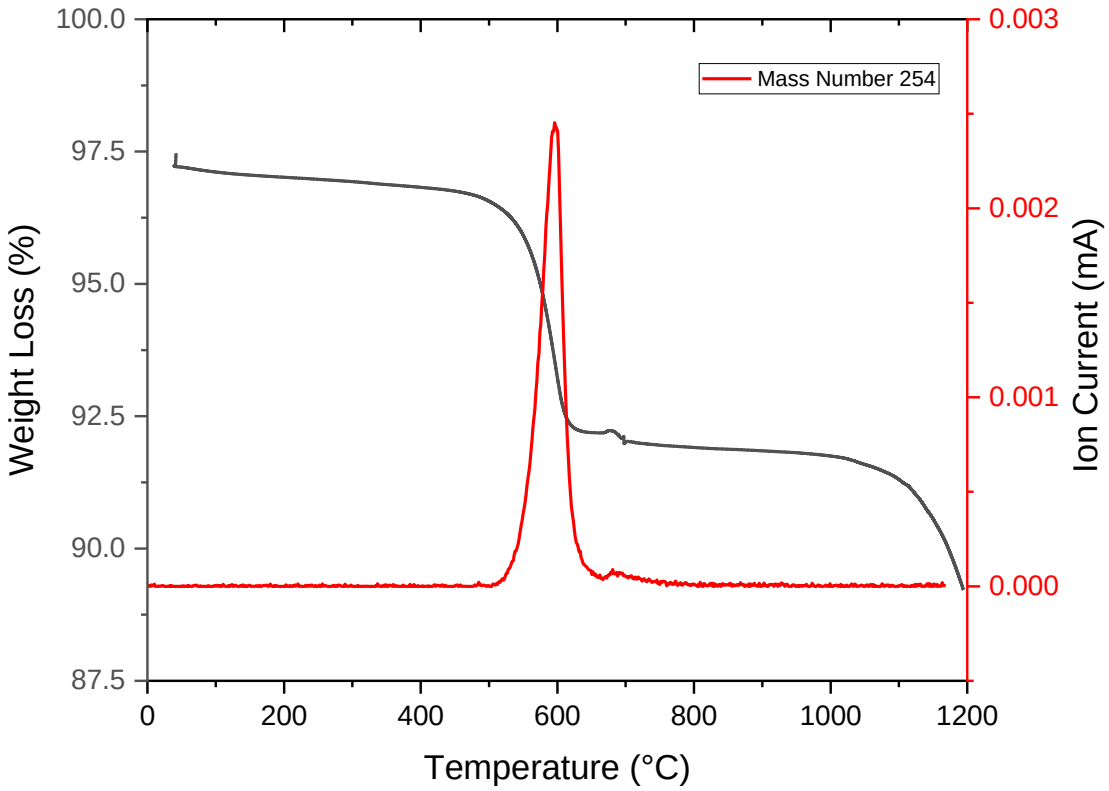

Figure 5.40 Mass spectrometry detection trace of AMU 254 from 0% SiO_2 CaZn glass spiked with 5 % iodine as NaI, weight loss from TGA trace added for comparison.

This results in a 4.26 wt% estimated iodine loss (85.12 % of the added mass), a minor retention increase compared to standard CaZn doped with the same concentration which loses 4.42 wt% iodine (88.32 % of the added mass). Two distinct weight reductions are seen in the TGA at 462 – 697 °C and above 1036 °C the higher temperature loss being present in the base glass as well. The 462 – 697 °C is therefore due to the loss of iodine or caused by the addition of NaI.

This is confirmed by the MS portion of the study (figure 5.40) where mass number 254 (I_2) was detected at 510 – 663 °C, this was the only major peak over the temperature range from 0 – 1200 °C. A minor peak for AMU 254 does also occur 686 °C likely from volatilisation after the dissolution of NaI into liquid glass or from iodine condensing/moving slower through the heated line and having a delayed response in the MS. The major mass loss event occurs at the same temperature at the MS emission and therefore the loss event can be assigned as gaseous I_2 loss.

The DTA data can be seen in figure 5.41 and illustrates the thermal events that occur in the doped (5% iodine) and un-doped 0% SiO_2 CaZn glass. The figure shows a comparison with the original glass frit and looking at each individual peak position there appears to be very little difference between the two. The same strong crystallisation peak appears, melting and glass transition temperatures do not vary significantly because the base glass has not interacted with the sodium iodide at those temperatures. The only main difference is a weaker doublet endothermic event at 607 °C. Given that

this is the same temperature at which iodine volatilises in this system it is likely that this event is combining with the volatilisation event we see at 610 °C in the base glass.

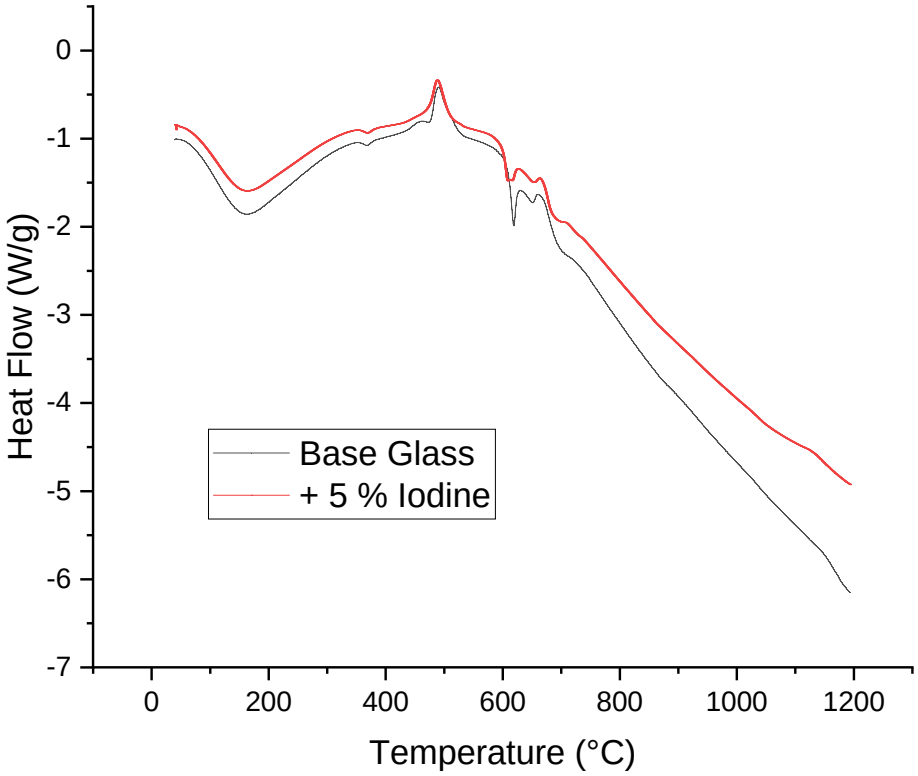

Figure 5.41 DTA trace of 0% SiO_2 CaZn base glass and with the addition of 5% iodine between 0 – 1200 °C

5.4.4.2 Pyrolysis and Active Tracers

Active tracer ^{129}I was used to track the volatilisation of iodine from 0% SiO_2 CaZn powered glass frit upon heating to 950 °C. 2g of the base glass in this section was spiked with 19.174 Bq of ^{129}I in 1 ml of 0.5 % NaI solution. The capture solutions after heat treatment for 2 hours contained 367.7 +/- 2.48 counts per minutes of activity over an average of 3 samples this is calculated to 19.54 +/- 0.49 Bq of activity. Using the added activity and mass of spiking solution we can find the percentage recovery for these samples; this was found to be 101.28 +/- 2.96 %. This shows that all of the active iodine is lost at 950 °C after 2 hours similar to data in shown in the previous section from TG analysis of the glass system and in CaZn base glass (section 5.2.3.3). The glass (figure 5.42) appears clear and colourless in the quartz crucible with no evident visible signs of crystallisation.

Figure 5.42 Image of the resultant 0% SiO_2 CaZn glass from 2 hours of heating at 950 °C

Additionally, one more trial was completed on this glass system to determine whether a 'carrier' was needed in the spiking solution. A spiking solution containing 19.174 Bq of ^{129}I was added as 1 ml in solution with water without 0.5 wt% iodine like conducted in the previous experiment. This was found to volatilise significantly less than the sample with carrier. 17.97 +/- 0.46 Bq of activity were found in the sample relating to a 95.82 +/- 2.51 % active iodine loss. This might indicate that samples low in iodine content could have reduced volatilisation compared to samples containing even small concentration of iodine (>0.5 wt%), however, the change is not large. Because of this disparity it was agreed that future experiments would be completed with 'carrier' (0.5 wt% NaI) added.

5.5 Chlorine

5.5.1 Raw Material

As the chlorine raw material is fully understood in literature research into the thermal properties of the raw material was not undertaken. For reference, Broström et al[215] describes mass loss of NaCl beginning 810 °C accelerating in rate above this temperature.

5.5.2 MW Base Glass

5.5.2.1 TG-MS and DTA

This section will cover the TGA, DTA and MS data from MW glass with no modifications other than the addition of chlorine to 1, 5 and 10 wt% added as NaCl. Chlorine is a volatile element at temperatures usually used in glass making so it is expected we will see losses of this element probably as HCl or Cl_2 gas.

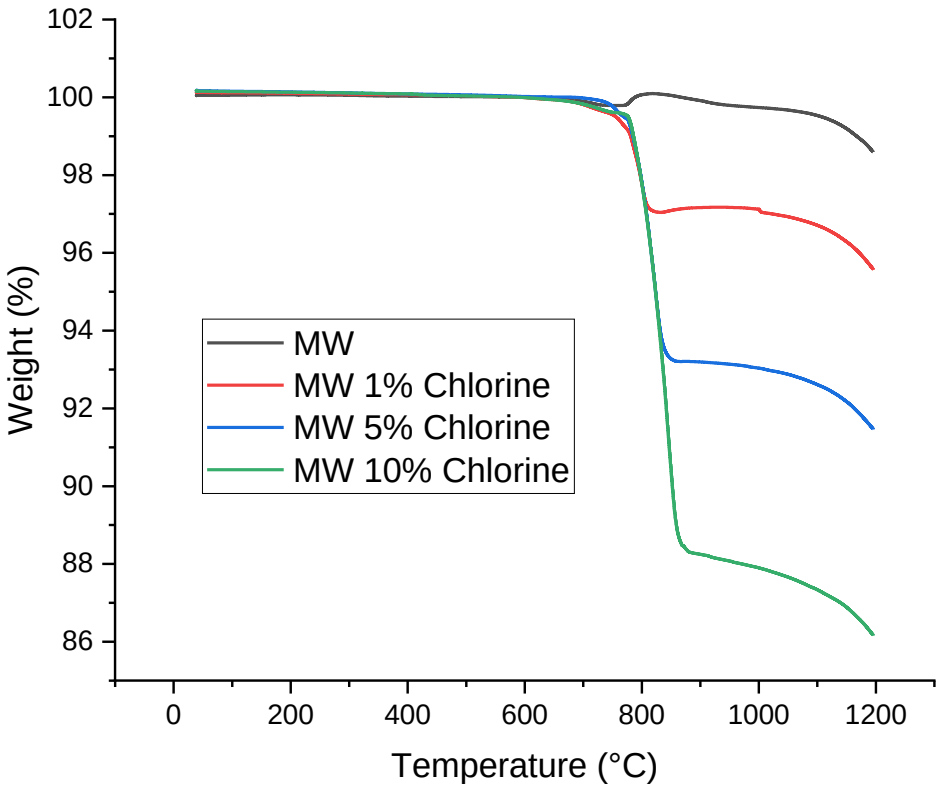

Figure 5.43 TGA trace of MW base glass with additions of 1, 5 and 10 wt% chlorine added as NaCl, baseglass with no NaCl addition included for reference

The graph in figure 5.43 shows that we see a large weight change consistently at 712 – 880 °C in all samples. The total mass loss of MW base glass without any additives is 1.45 wt%, when adding chlorine, the mass loss becomes 4.55, 8.70, 13.96 wt% respective of 1, 5, 10 wt% chlorine samples. Subtracting the loss contributions from the MW glass these values become 3.10, 7.25, 12.51 wt%

respective of 1, 5, 10 wt% chlorine samples. Curiously this is more mass loss than the added chlorine and therefore one of a few effects must be occurring:

- Chlorine catalysing boron mass loss from MW glass, sodium dissolving into the glass matrix
- Sodium volatilisation from NaCl

The majority of the mass loss in the chlorine containing samples over the whole temperature range from 0 – 1200 °C was found at 712 – 880 °C, an effect not seen at all in the MW baseglass TGA. This indicates that chlorine was responsible for mass loss at these temperatures whether by volatilising as chlorine containing compounds or accelerating glass component volatilisation. In any case it is likely that due to this large mass loss that most chlorine is lost over the temperature range 0 – 1200 °C when added to glass frit. This is indicative of the solubility limit of chlorine in MW glass being very low, particularly problematic for nuclear wastes containing high amounts of PVC or other chlorine sources. Speciation of the off-gas from this TGA experiment (analysed by MS) detected no peaks from any AMUs including CO_2, H_2O, Cl_2, Cl^-, NaCl or HCl (all predicted volatile products).

Whilst there were no species detected by the MS in any of the samples there was a large mass loss seen and that must relate to an emission. Given this, chlorine species must condense or deposit readily upon cooling from ~ 800 °C down to the 300 °C in the heated line connecting the furnace and detector. The thermal events tracked by DTA (figure 5.44) show that there is a large endothermic peak at 795 °C for all chlorine containing samples. This grew in intensity upon increasing chlorine content. Towards the more concentrated 5 and 10 % chlorine samples a new, sharp, endothermic peak appears at 778 °C. None of these appear in the DTA trace for the base glass and therefore must be dependent on chlorine addition. The occurrence of this coincides with the temperature at which major mass loss is seen in the TGA in figure 5.43, the broad endothermic peak in the DTA can be assigned evaporation because of this. The sharp endothermic peak at 778 °C can be assigned to the melting of NaCl raw material after which the liquid/solution rapidly evaporates. The melting event is overshadowed by the broad evaporation event in the MW glass with 1 % chlorine added.

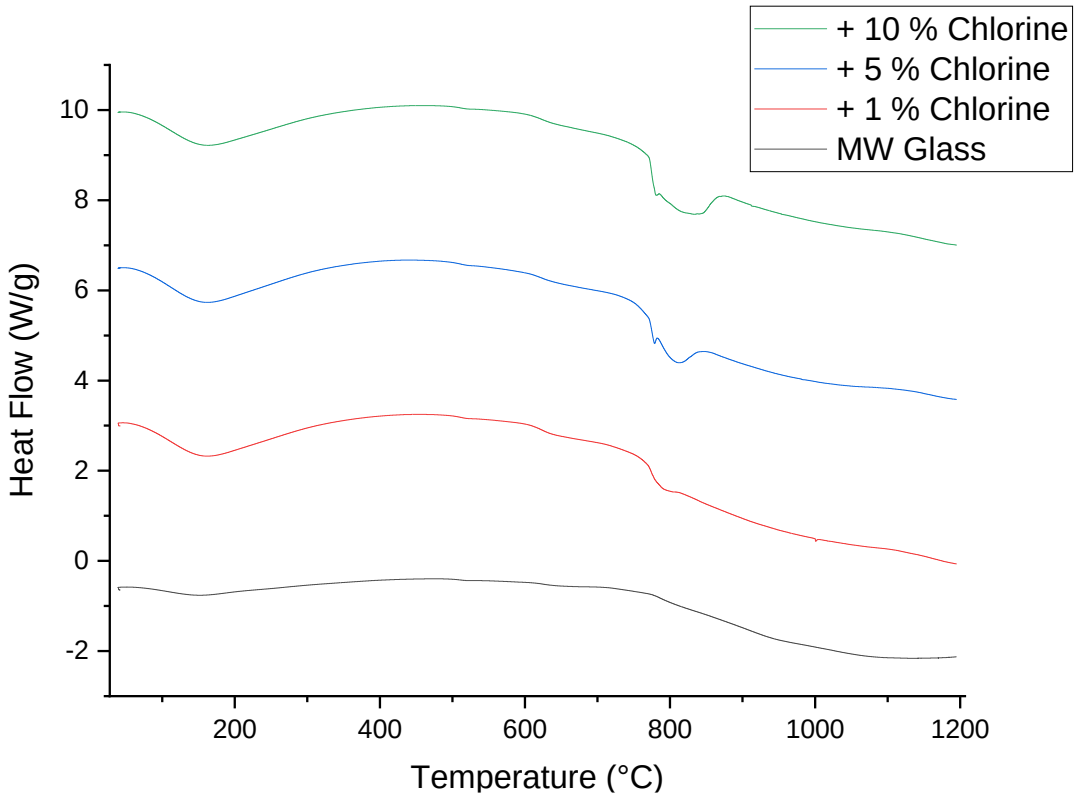

Figure 5.44 DTA data of the MW base glass with additions of 1, 5 and 10 wt% chlorine added as NaCl baseglass with no NaCl addition included for reference

5.5.2.2 Temperature Dependence

In this section we discuss the effect of temperature on MW glass composition with the addition of 1 % chlorine (as NaCl) to either the glass frit as raw material (t=0) or remelting glass containing 1 % iodine in its structure (t=2h). Firstly we will look at the composition of the glass frit heat treated with NaCl raw material added (t=0) between 0 – 1200 °C. Figure 5.47 shows the trends in this series between 0 – 1200 °C. MW glass components (SiO_2, B_2O_3, Na_2O) do not vary much in this range of temperatures remaining consistent in XRF measurements. Chlorine content, however, appears to change reducing in content initially and increasing at 1100 °C to fall again afterwards at 1200 °C. A trend is seen in the first three points from 800 – 1000 °C beginning at 0.26 wt% and ending at 0.04 wt% chlorine. However, including the 1100 °C result changes these and makes the trend non – linear. This point is most likely anomalous and if discounted the data shows a downward trend of retention dependant on increasing temperature. At and above 1000 °C this could show that chlorine is mostly volatilised in this system rather than incorporating into the MW glass structure. A similar effect has

been seen in iodine containing samples when added directly to frit. This might suggest that waste additions to fritted glass containing chlorine or iodine could be harder to incorporate into glasses at higher temperatures.

Crystallisation behaviour of the MW glass added with 1% chlorine (as NaCl) was very similar to previous XRD data from caesium and iodine doped glasses (figure 5.24). Similar SiO_2 deflections are seen and are not present in the 1000 °C pattern which indicates again that MW glass devitrifies at 800 and 900 °C regardless of caesium, iodine or chlorine addition. The patterns (shown in figure 5.46) can be assigned to SiO_2 (quartz) (major component) and ~ 5% NaCl only at 800 °C (minor component). Quartz has the same assignment given to the iodine containing samples (figure 5.24) and the same Bragg peaks appear in the caesium containing t=0 graph as well (figure 5.4).

In the t=2h series, glass containing 1 % chlorine is remelted at 800 – 1200 °C. We see little change in the glass content excluding chlorine, SiO_2 and Na_2O content does appear to rise by ~1-2 wt% and B_2O_3 conversely reduces by the same amount. Given the larger quantities of these components proportionally this variation is not significant. Chlorine on the other hand does change a large amount proportionally to itself. This is evident in figure 5.47 with initial chlorine concentration beginning at 0.517 wt% in the base glass reducing to 0.11 wt% at 1200 °C. The reduction over this period is poorly linear with a slope of -0.03 and a r^2 value of 0.837. If the anomalous point is discounted the slope of this chloride trend is less than seen in the t=0 series (figure 5.45) therefore temperature could have less of an effect on chlorine volatility in remelting of glasses already containing chlorine (t=2h).

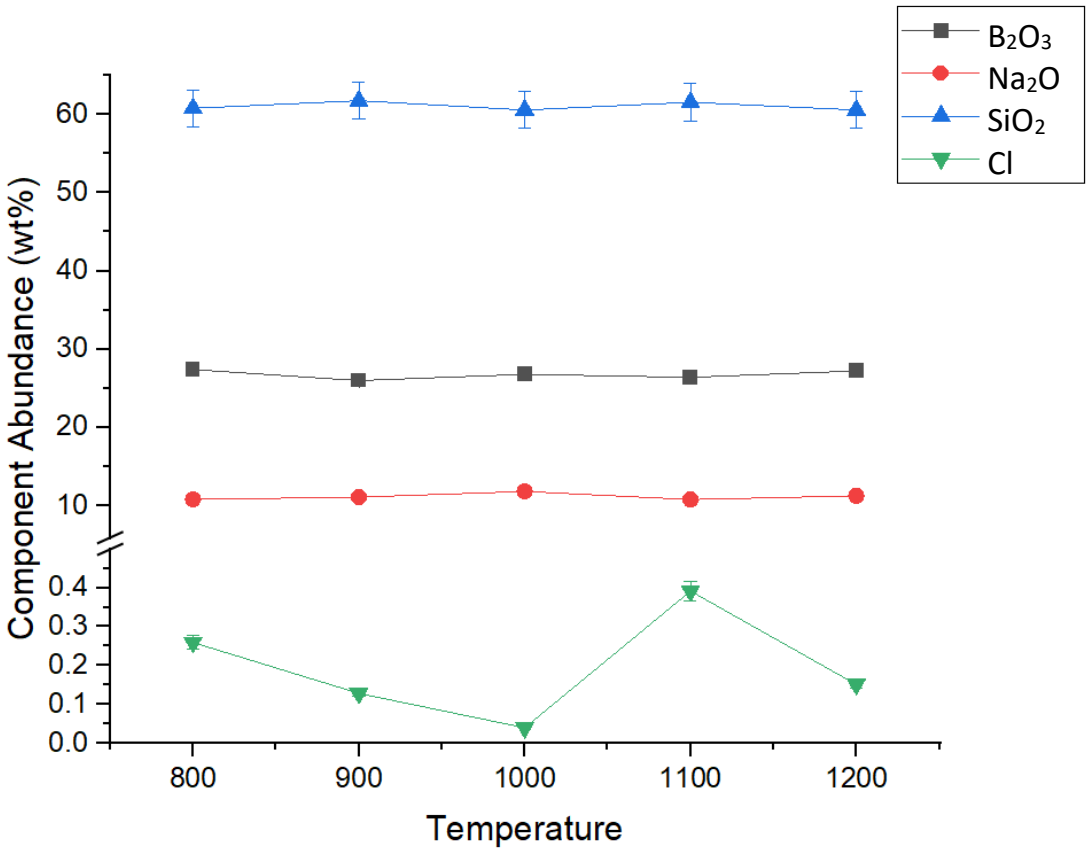

Figure 5.45 The effect of temperature on glass composition of MW with addition of 1 % chlorine (added as NaCl) from 800 – 1200 °C (t=0)

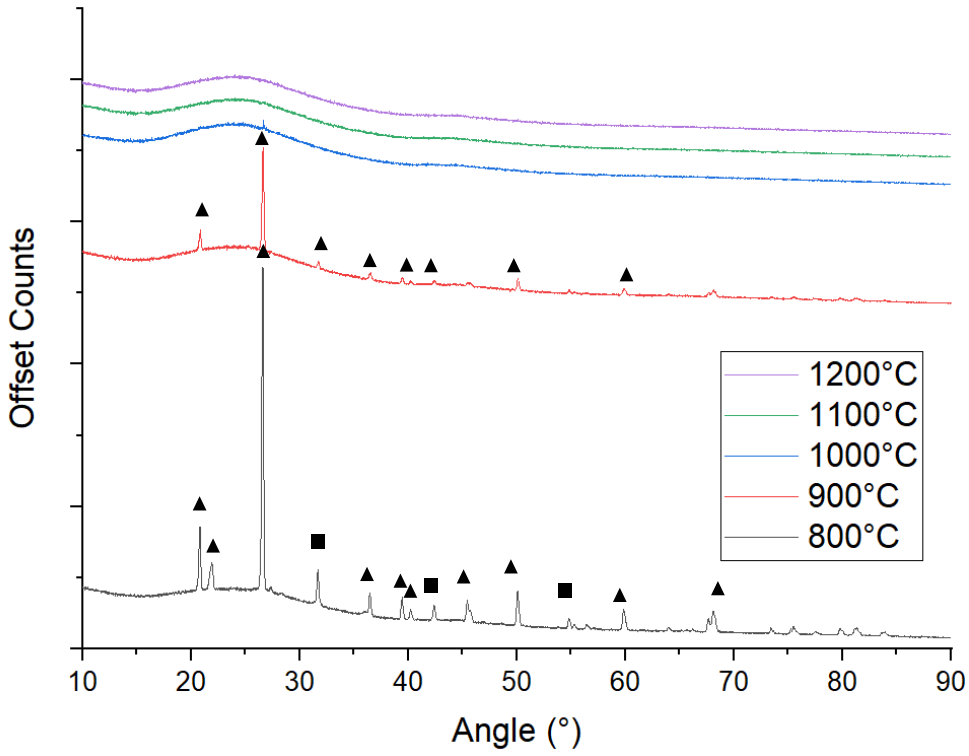

Figure 5.46 XRD pattern of MW frit melted at 800 – 1200 °C with the addition of 1 % Cl added as NaCl. ▲= SiO_2 Quartz (Phase ID: 01-075-0443), ■ = NaCl Halite (Phase ID: 01-080-3939) (t=0).

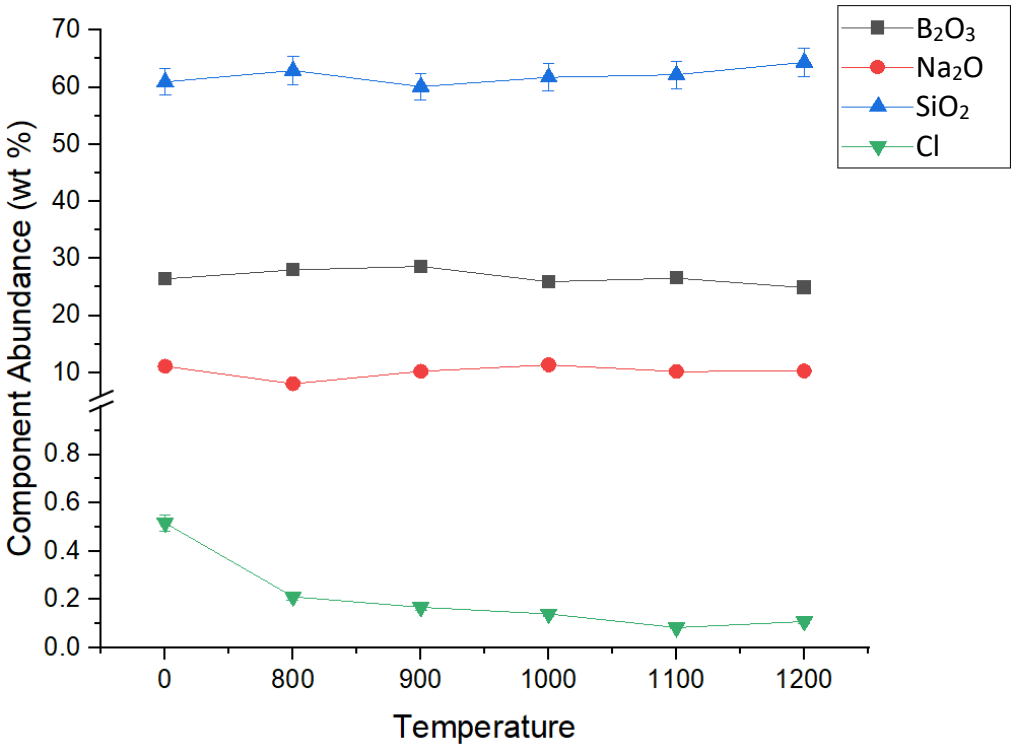

Figure 5.47 Change in glass content (analysed by XRF) of MW incorporated with 1 wt% chlorine remelted between 800 – 1200 °C (t=2h)

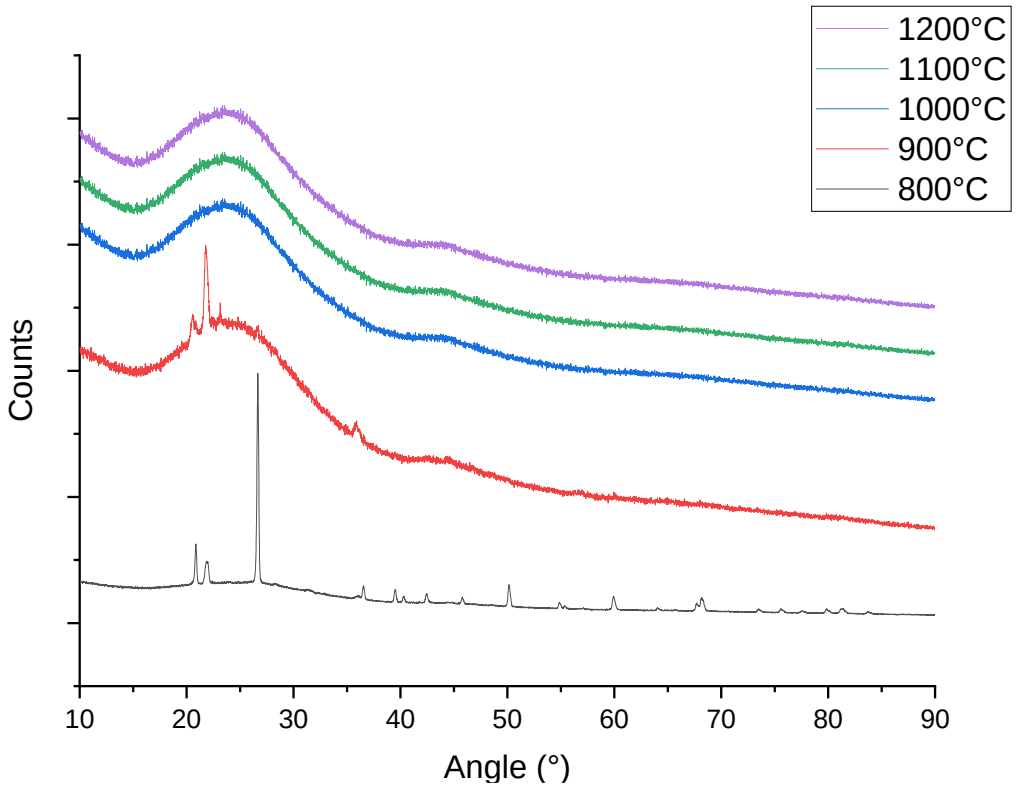

Figure 5.48 XRD data of MW glass containing 1% Cl (t=2h) remelted at 800 – 1200 °C. ▲= SiO_2 Quartz (Phase ID: 01-075-0443)

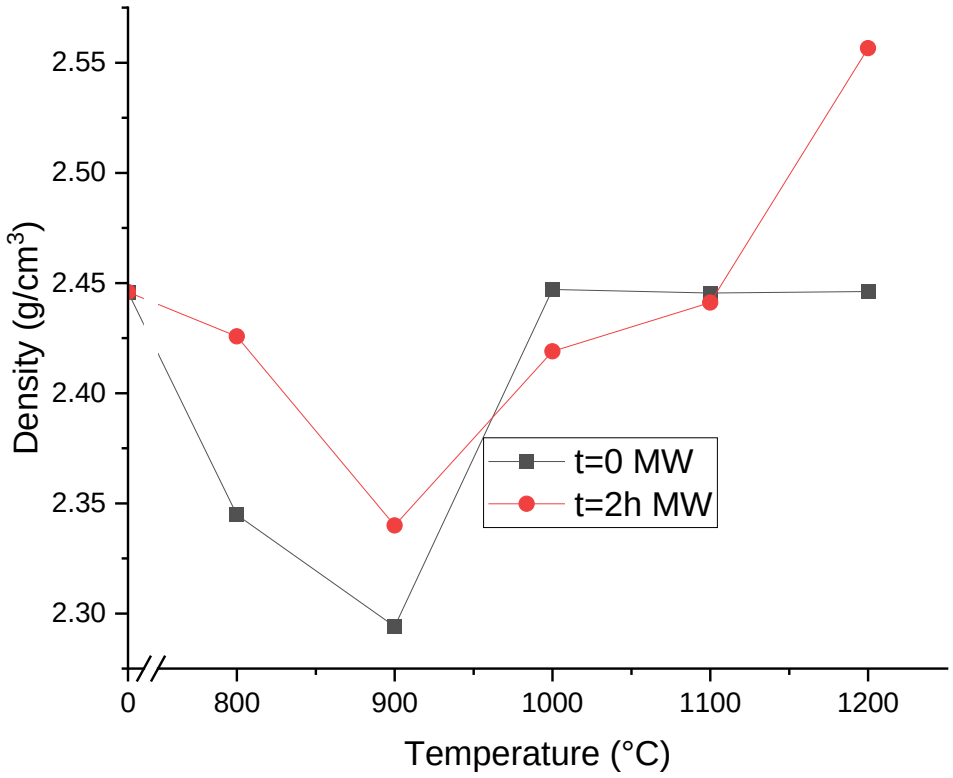

Figure 5.49 Effect of heat treatment temperature (800 – 1200 °C) on density of MW glass systems, t=0 remelted with NaCl and 1 wt% chlorine already in the glass network. Error bars represent +/- 0.001 g for each measurement which is smaller than the points.

The crystal character in the t=2h samples (figure 5.48) at 800 °C show a crystallinity from the same source as found in the t=0 series seen in figure 5.48 which was assigned to SiO_2 (as quartz). The major Bragg peak at 27 °2θ almost completely disappears from 800 – 900 °C possibly as a result of diffraction patterns showing preferred orientation for another phase of quartz crystal effected by sample preparation. This is the silica in the MW glass devitrifying at 800 °C, however, in the t=2h series this only occurs at 800 °C –900 °C and doesn't extend to the 1000 °C samples. This could show that chlorine added to frit does influence the devitrification of MW glass.

Density (figure 5.49) appears to produce similar density readings with increasing heat treatment temperature over the temperature range 0 -1200 °C for both t=0 and t=2h glass. Original MW glass density is 2.4459 g/cm^3 reaching a minima point at 900 °C for both groups with a density value of 2.2941 g/cm^3 for t=0 and 2.3399 g/cm^3 for t=2h series. The reduction begins at 800 °C, however, at

1000 °C the density recovers for both glass systems stabilising at 2.4722 g/cm^3 for the t=0 system and increasing furthur to 2.5566 g/cm^3 for the t=2h glass at 1200 °C.

5.5.3 CaZn Base Glass

5.5.3.1 TG-MS and DTA

In a different glass the behaviour of chlorine retention/volatilisation changes. The CaZn network is discussed here with the addition of chlorine to 1, 5 and 10 wt% (as NaCl) and heated between 0 – 1200 °C analysed by TGA and DTA. As seen in figure 5.50 CaZn frit loses more mass upon the addition of chlorine for all samples (1, 5 and 10 wt% Cl) increasing with chlorine content added. This culminates in one major step weight change for all chlorine containing samples at 694 – 887 °C, very similar to MW glass. Similarities also exist with the MW and CaZn glass with the quantity of mass loss over the samples. In CaZn glass we see a total mass loss of 2.21, 10.70 and 13.34 wt% for 1, 5 and 10 wt% Cl

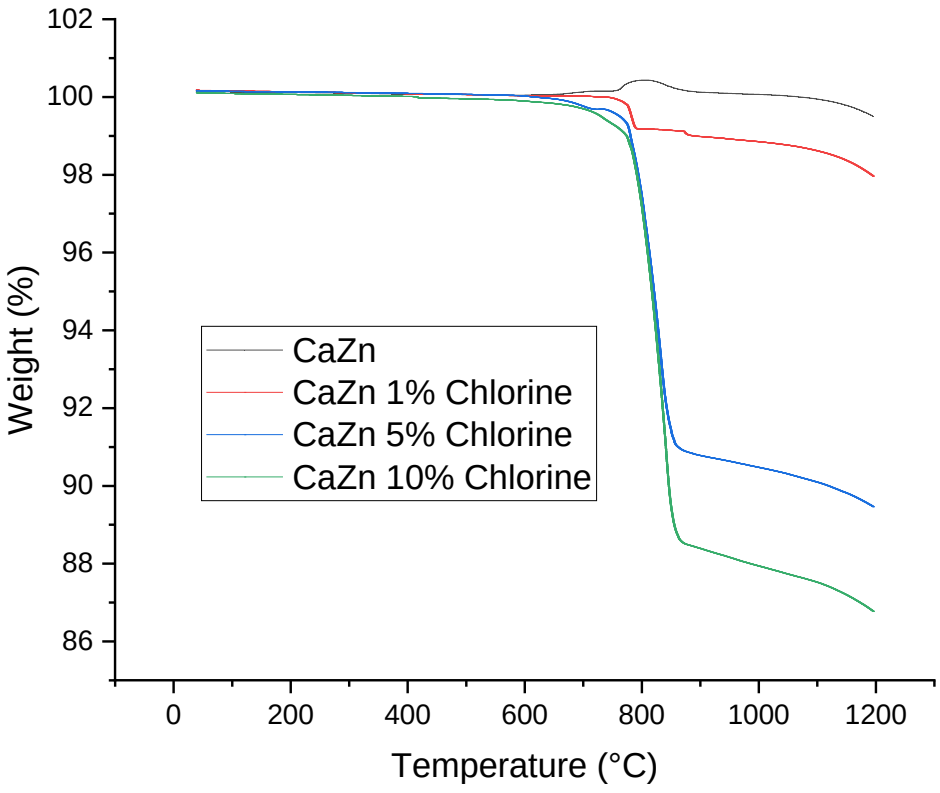

Figure 5.50 TGA data of the CaZn base glass with additions of 1, 5 and 10 wt% chlorine added as NaCl from 0 – 1200 °C

respectively. The original base glass loses 0.647 wt% over the 0 – 1200 °C temperature range and therefore the influence from NaCl would be 1.56, 10.05, 12.69 wt% for 1, 5 and 10% Cl samples.

DTA of the same glasses with chlorine doping shows that a large endothermic peak at 783 – 860 °C grows in amplitude upon increasing chlorine concentration (figure 5.51). This occurs at the same temperature at which we see mass loss in the TGA and therefore can be assigned the volatilisation of a chlorine containing species. This also explains the increase in magnitude upon increasing additive concentration. There is an additional endothermic peak at 775 °C appearing with the 5 % and 10 % chlorine concentrated samples which relates to the melting of NaCl raw material, this increases in size proportionally upon the addition of more chlorine. Glass transition temperature does not change significantly with addition of NaCl up to 10 wt% chlorine, NaCl is likely not interacting with the glass structure below the glass transition temperature because this value does not vary.

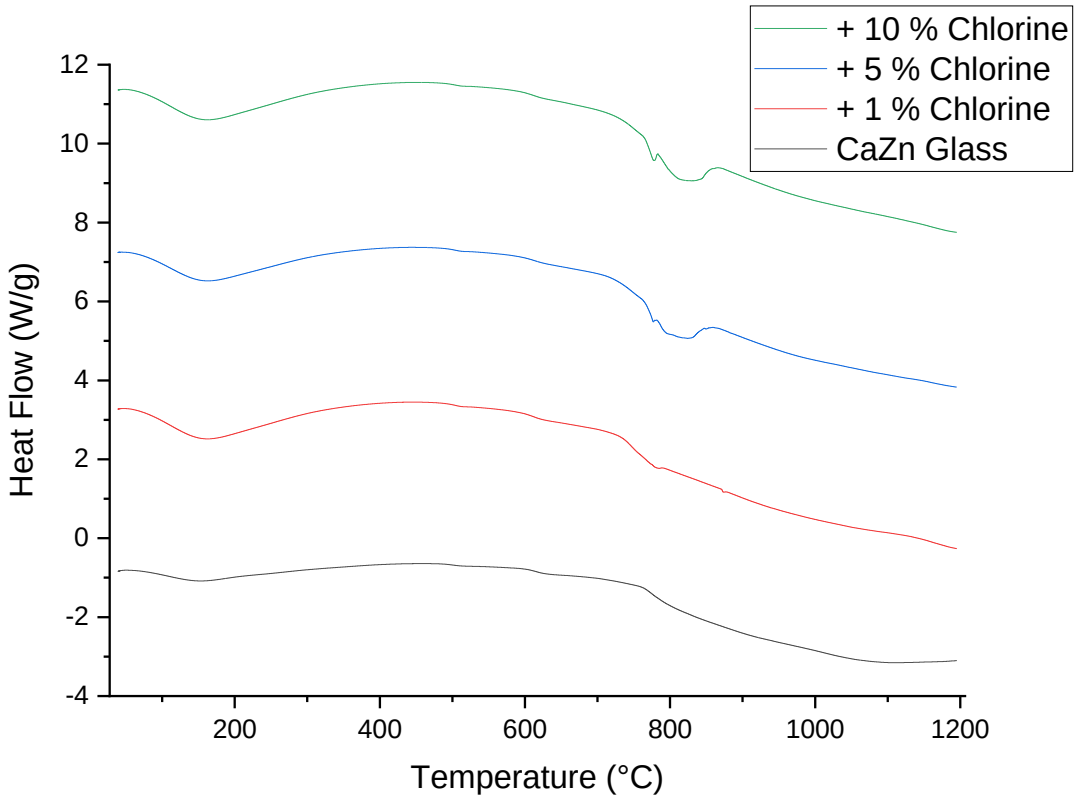

Figure 5.51 DTA data of the CaZn base glass with additions of 1, 5 and 10 wt% chlorine added as NaCl from 0 – 1200 °C

5.5.3.2 Temperature Dependence

The effect of temperature on chlorine volatilisation is discussed from 800 – 1200 °C in two CaZn glass systems with the addition of NaCl. Firstly, we will look at the CaZn glass with added NaCl (t=0) raw material to 1 % Cl content. Glass content contributions from CaZn change very little over the 800 - 1200 °C temperature range explored in this study (figure 5.52), the main changes in these components are at 800 and 1200 °C where silica content lowers and boron content increases both by ~3 wt%. Most other components other than chlorine do not change much other than Na_2O which rises at 1200 °C by ~3 wt% proportionally not a significant change. Chlorine on the other hand does change significantly, particularly at 800 – 900 °C. When heat treating the sample at 800 °C, chlorine is found to have a concentration of 0.5688 wt% in the glass, glass/ceramic system. This reduces to 0.041 wt% at 900 °C, a significant change (93.28%) from the concentration at 800 °C. Chlorine has been seen in other glass (MW) systems to be almost completely lost at 1000 °C therefore in the CaZn system this seems to happen earlier at 900 °C. This might suggest that CaZn glass is poorer at retaining chlorine than MW glass.

The XRD patterns of these heat treatment products can be seen in figure 5.53 from 800 – 1200 °C. The crystal character of these samples are mostly amorphous over the whole temperature range, however, at 800 °C there are two small peaks, overshadowed mainly by a large amorphous hump, but still present. These are assigned by HiScore plus software to the material halite, a sodium chloride crystal. The differences between these samples and MW samples are significant, there is only little crystallisation in CaZn at 800 °C with the addition of chlorine, in MW glass there are very intense peaks at 800 °C (figure 5.48) and minor peaks at 900 °C.

When NaCl is already incorporated into the glass structure the volatilisation properties are different. In the t=2h series chlorine content remains higher over the temperature range compared to the t=0 samples (figure 5.54). This effect has been shown in MW glass and for iodine containing samples where glasses containing the halide in the glass structure retains much more over the 2 hour

remelting/heating period compared to added halide salt to frit. Initially the CaZn glass frit used in this portion of the study contained 0.36 wt% chlorine analysed by XRF. After heating this glass at 800 °C for 2 hours the resultant product contained 0.18 wt% chlorine by mass. This reducing trend in chlorine content follows down with fair linearity (r^2 = 0.731, slope = -0.05) as the temperature increases to a final reading of 0.11 wt% at 1200 °C. The data here is consistent with other trends shown previously, when incorporated in a glass halide content from iodine and chlorine reduces slower that if added to frit. Oxides in this glass system do not vary significantly over the temperature range. There is variation in a few points (Na_2O at 800 °C and Al_2O_3 at 1200 °C), however, these are likely to be anomalous as they do not follow any other trends.

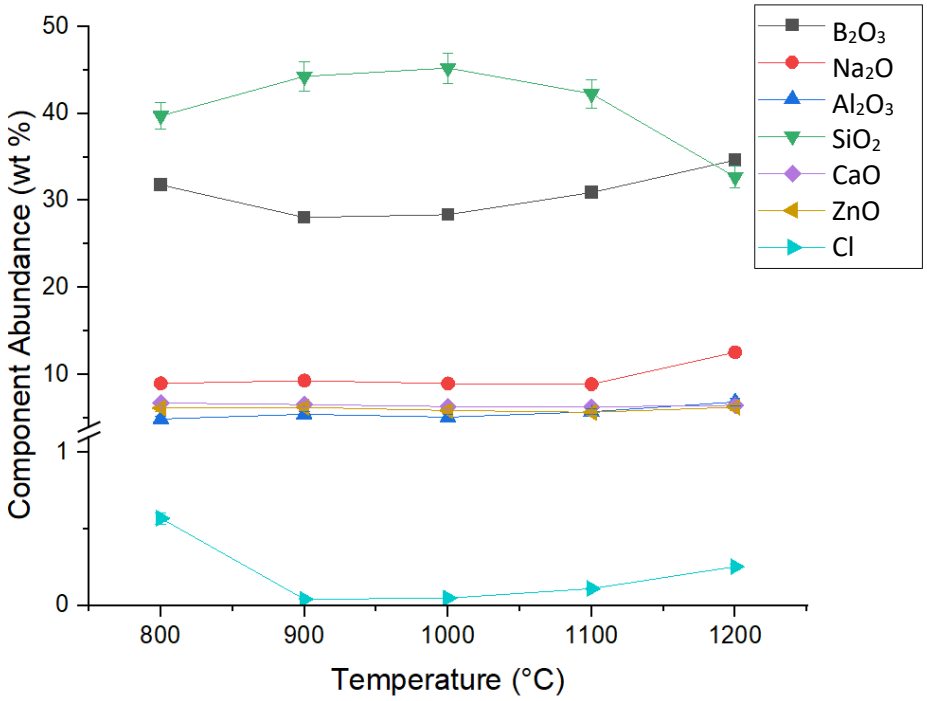

Figure 5.52 The effect of temperature on glass composition of MW with addition of 1 % chlorine (added as NaCl) from 800 – 1200 °C (t=0)

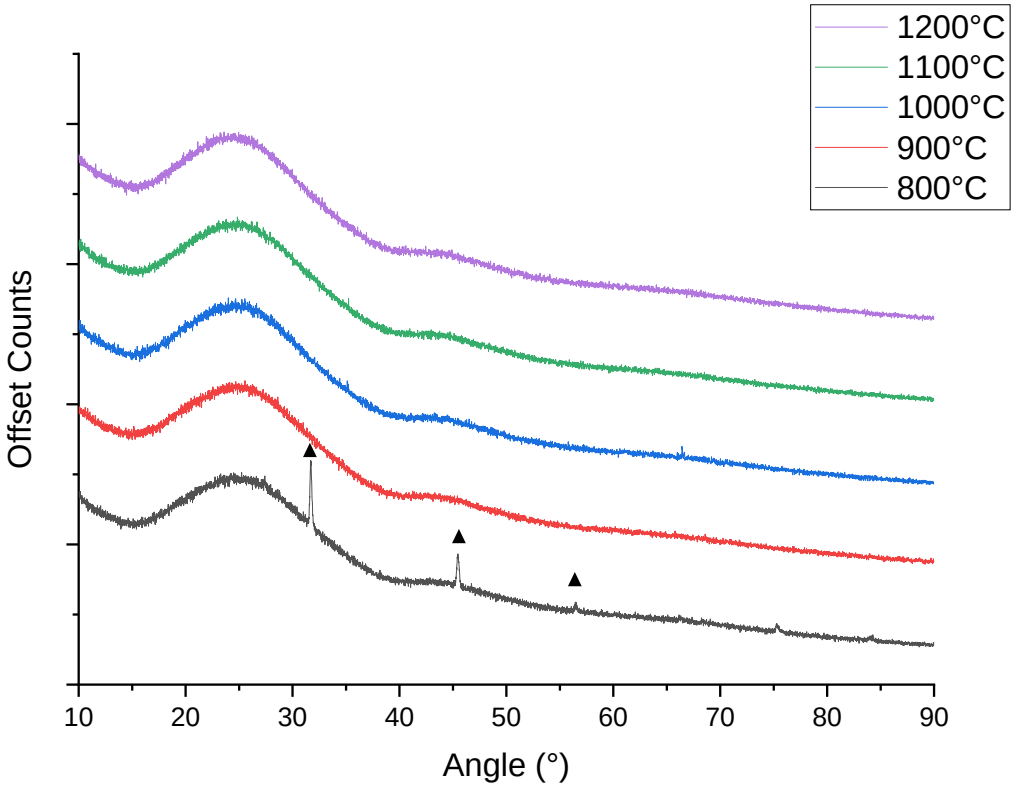

Figure 5.53 XRD pattern of CaZn frit melted at 800 – 1200 °C with the addition of 1 % Cl added as NaCl. ▲= NaCl Halite (Phase ID: 01-071-4661) (t=0)

XRD data of the t=2h series in figure 5.55 shows that the lower temperature heat treated samples in the range had crystalline behaviour primarily relating to SiO_2 as quartz. This appears at 800 °C with intense peaks reducing to minor peaks (20.5 and 21.8 ° 2θ) at 900 °C. The major peak at 26.67 ° 2θ contributed to from quartz does not appear in the 900 °C sample, however, indicating this crystallisation hasn't occurred at higher temperatures. At the same temperature at which we see crystallisation appear we also see a decrease in density (figure 5.56). The original base CaZn glass in this case has a density of 2.5633 g/cm^3 this reduces to 2.4623 and 2.2697 g/cm^3 at 800 °C for t=0 and t=2h the minimum for each set of samples. Density then stabilises for the t=0 series to an average of 2.5547 g/cm^3 over the final 4 samples from 900 – 1200 °C. The other series (t=2h) also has the density recover, however, this happens at 1000 °C with the increase beginning at 900 °C and stabilising at a lower value (2.456 g/cm^3) than that of the original base glass.

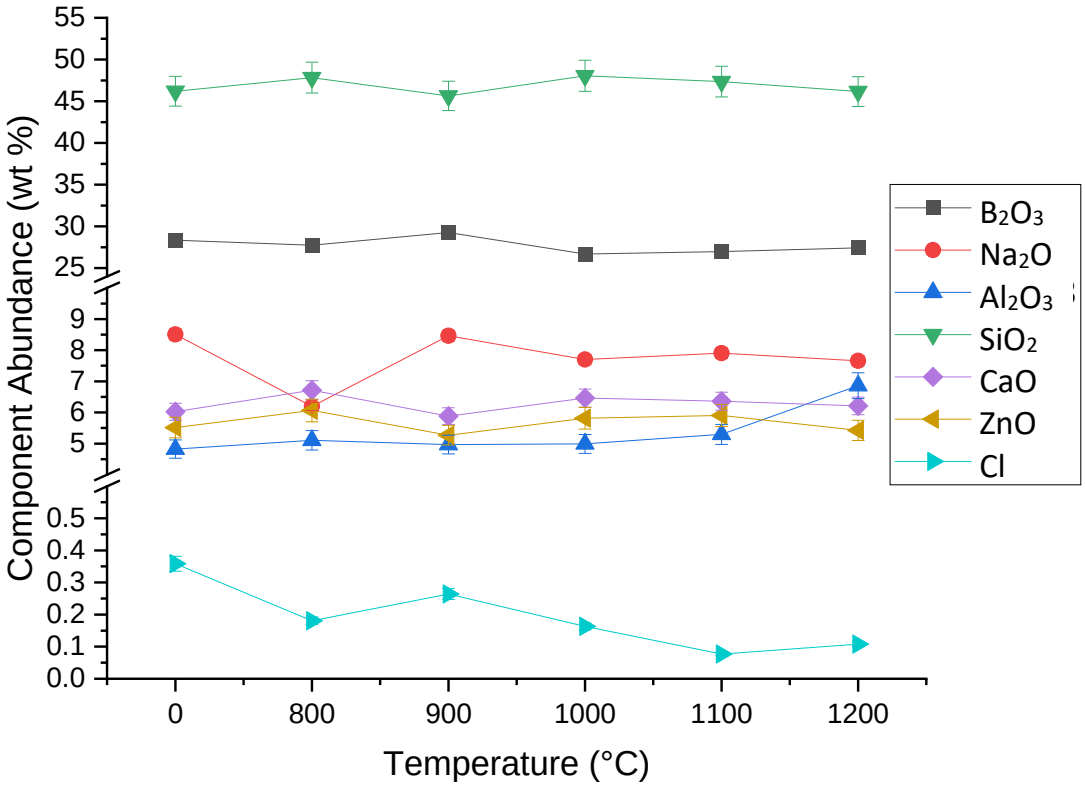

Figure 5.54 Change in glass content (analysed by XRF) of CaZn incorporated with 1 wt% chlorine remelted between 800 – 1200 °C (t=2h)

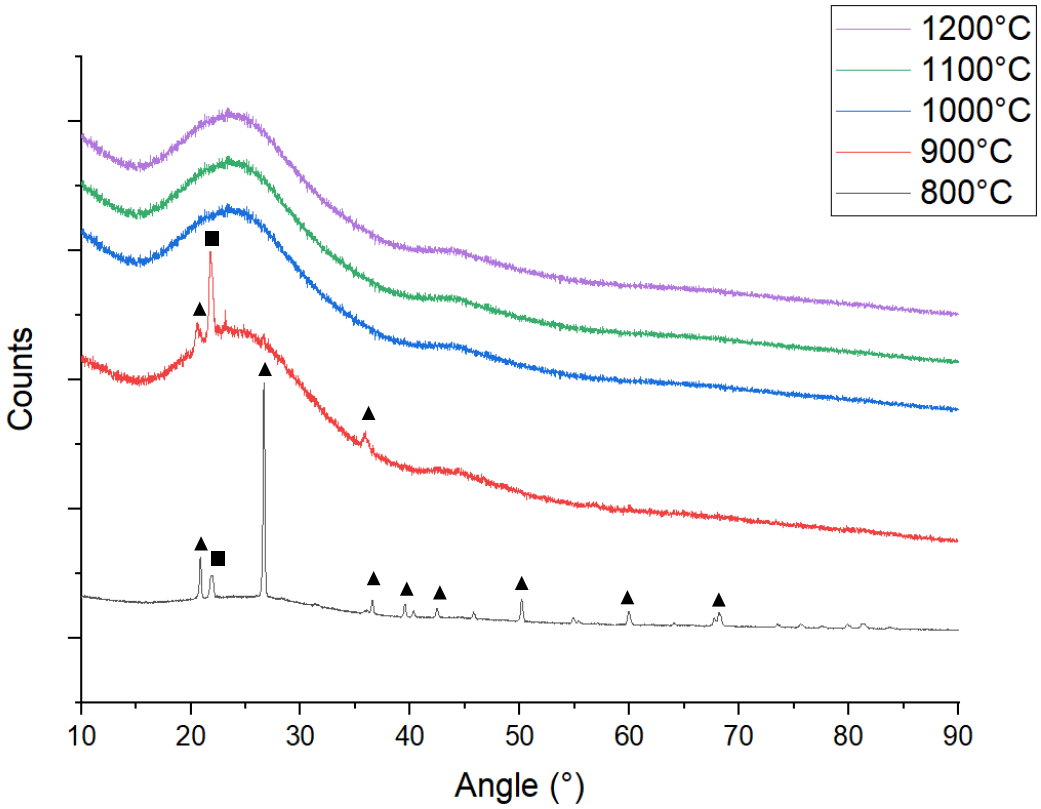

Figure 5.55 XRD data of CaZn glass containing 1% Cl (t=2h) remelted at 800 – 1200 °C ▲= SiO_2 Quartz (Phase ID: 01-070-3755), ■ = $Li_2B_4O_7$ (Phase ID: 01-086-5516) (t=2h)

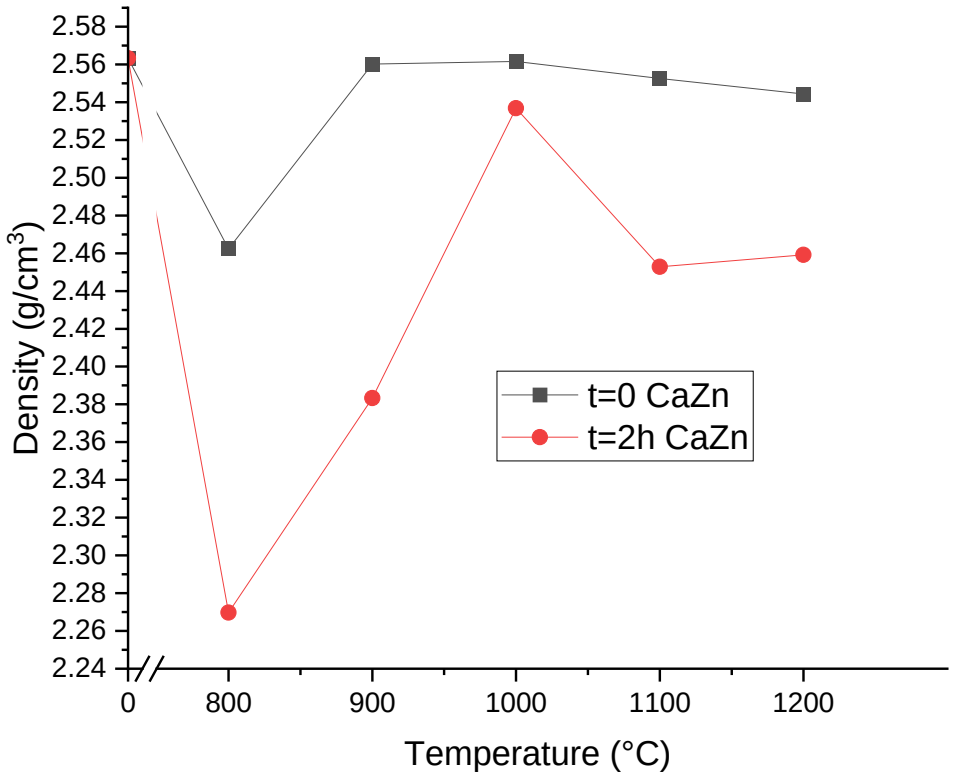

Figure 5.56 Effect of heat treatment temperature (800 – 1200 °C) on density of MW glass systems, t=0 remelted with NaCl and 1 wt% chlorine already in the glass network. Error bars represent +/- 0.001 g for each measurement which is smaller than the points.

5.5.4 Pyrolysis and Active Tracers

Originally the pyrolysis work conducted at Southampton included chlorine testing and analysis. Initial experiments with inactive chlorine in a NaCl solution to spike samples with 1 % Cl by mass showed that the corrosion on the quartz crucible and tube were too dramatic to continue with the experiments. Four chlorine experiments were conducted on 0 wt% SiO_2 CaZn base glass in an attempt to reduce the corrosion and produce results that did not either dissolve the crucible or damage the work tube of the instrument.

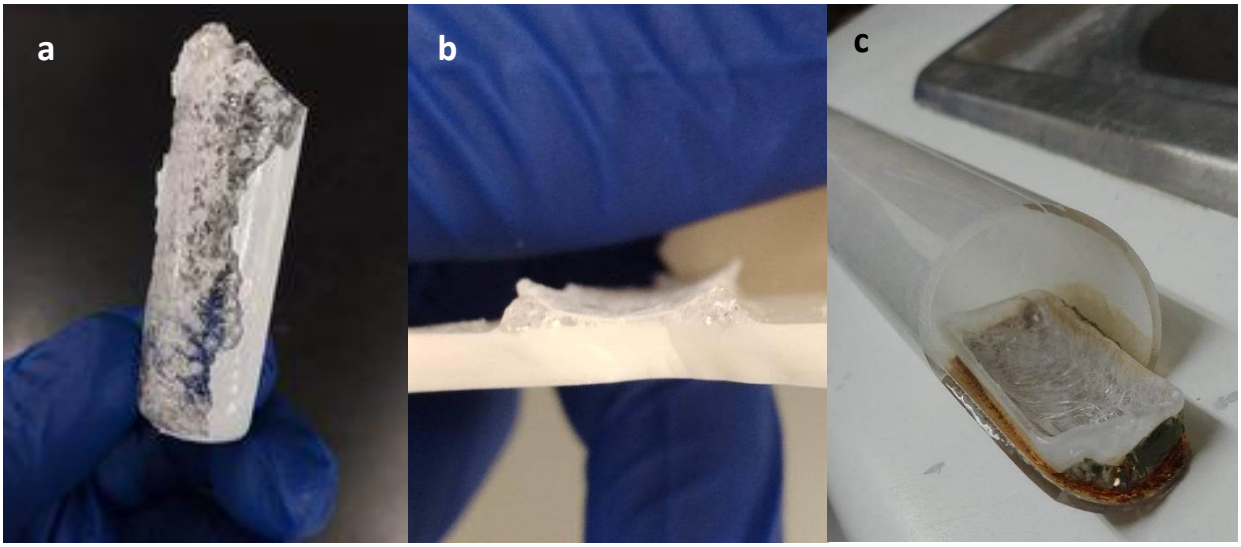

Figure 5.57 Images of crucible corrosion from chlorine containing samples. a) Crucible completely corroded by glass/NaCl. b) Leaking of the crucible and fusing to the working tube. c) Fusing of a sample to the working tube of the pyrolysis instrument, nickel liner used to protect tube.

The type of corrosion that occurred can be seen in figure 5.57, the base of the crucible was almost completely digested by the glass and sodium chloride combination. This caused it to fuse to and damage some of the work tubes and invalidate the samples. Attempts were made to protect and encapsulated the sample by using nickel liners and alumina crucibles, these didn't protect or produce valid samples. The nickel liner is visible in the sample in image 5.59 c) and it can be seen that this did not function as intended because the glass sample has corroded through the liner as well and fused to the work tube. For these reasons chlorine experimentation by pyrolysis was abandoned and more focus was directed at caesium and iodine testing.

5.6 Summary

To conclude this chapter we have explored the volatilisation of caesium, iodine and chlorine from multiple glass systems and seen the effect of temperature on those glasses. Firstly, we can compare the temperature dependence data for each set of experiments, dopant added to frit and heated (t=0) and remelting of glass containing the dopant (t=2h).

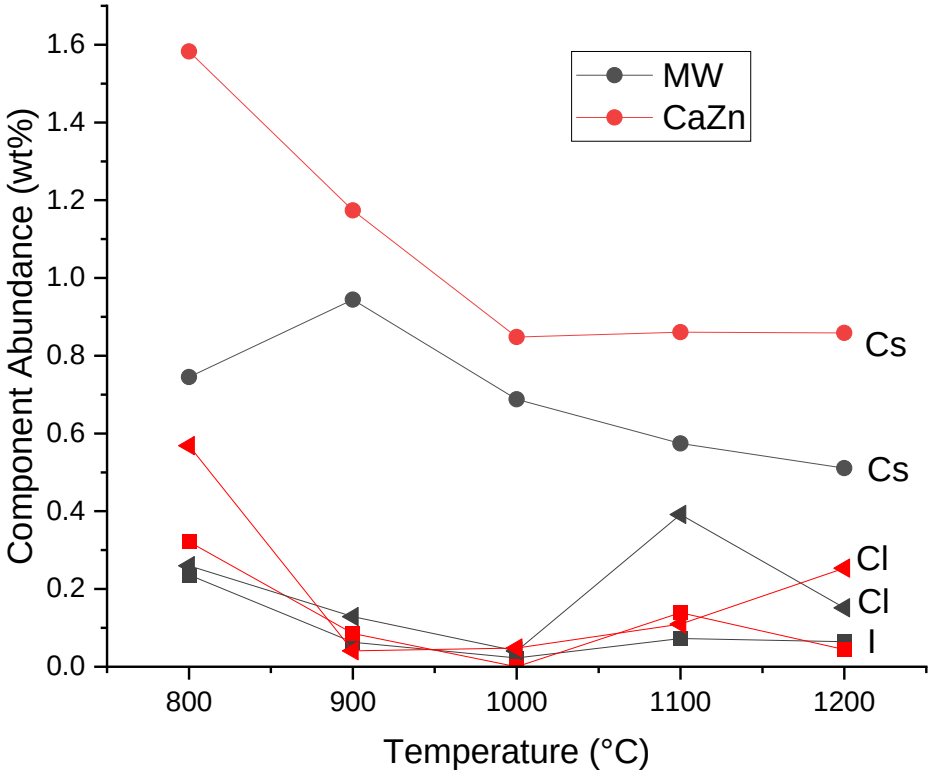

Figure 5.58 The effect of temperature on dopant glass content of MW and CaZn with addition of 1 % of the additive (Cs, I or Cl) from 800 – 1200 °C (t=0). Grey = MW, Red = CaZn, ● = Caesium, ▶ = Chlorine, ■ = Iodine

Overall retention of each element is different, caesium in both t=0 and t=2h retains better than the halides I and Cl. The caesium ion is acting as a network modifier and incorporates into the glass structure much more readily than negatively charged halide ions. The halides I and Cl have very similar retention profiles over the temperature range (figure 5.58). The characteristic trait of the halide trend is that most of the content is lost by 1000 °C with only a minimal quantity remaining in the resulting glass. Looking at the glass rather that the element we can see that CaZn base glass retains caesium better than MW for samples at 800 °C. The target composition was 1 wt% and therefore the glass which is closest to this value can be considered to have performed better in retention. In t=2h samples (figure 5.59) the change is less dramatic, however, CaZn remains better at retaining the caesium and comparable to MW at retaining iodine and chlorine. The trends show that the change between the two glass systems is quite small in the t=2h system. In this figure it can also be seen that chlorine retains very poorly compared to both caesium and iodine in both glass systems.

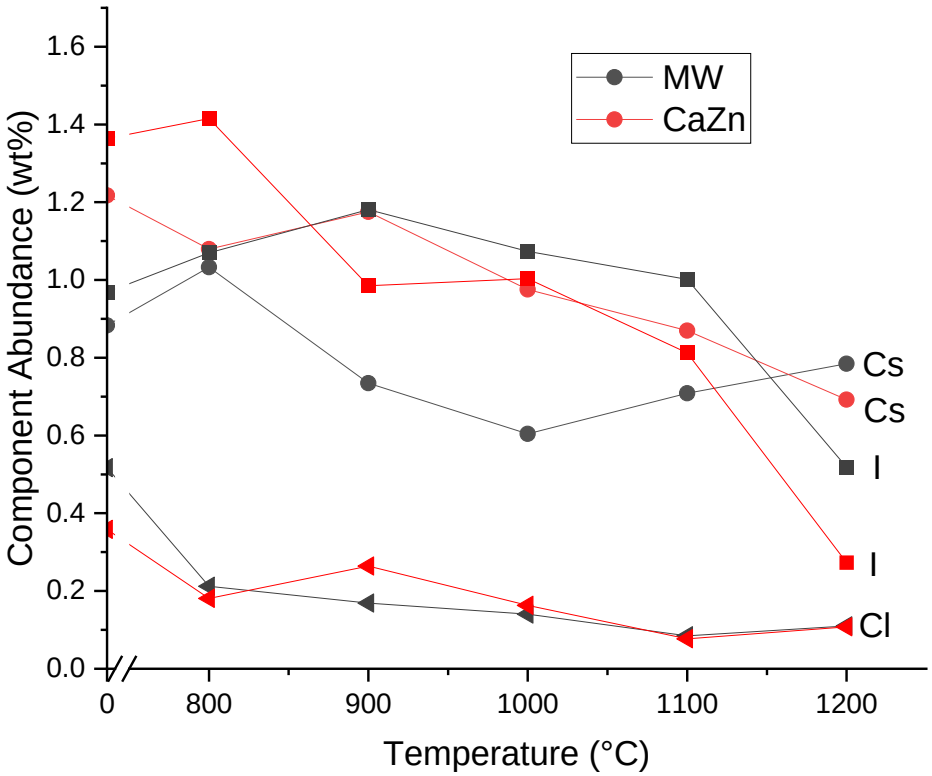

Figure 5.59 The effect of temperature on dopant glass content of MW and CaZn containing 1 % of the additive (Cs, I or Cl) from 800 – 1200 °C (t=2h). Grey = MW, Red = CaZn, ● = Caesium, ▶ = Chlorine, ■ = Iodine

Previous experiments completed on base glasses MW, CaZn and 0 wt% SiO_2 variants are considered, comparing the retention properties of each. For caesium, iodine and chlorine, CaZn base glass generally lost less mass in TG-MS studies than MW glass in doped and undoped glasses (table 5.4). The onset and location of the mass loss event did not change between glass systems (e.g. figures 5.2 and 5.8, 5.18 and 5.28) which indicates this is largely dependent on the raw material added rather than the glass system. The temperature at which this occurs was below the temperature at which raw material is interacting with the glass for iodine and caesium. For chlorine measurements the volatilisation event was at ~810 °C which is 200 °C above the melting temperature of each glass.

Glass Type	Element	Base Glass (%)	5 wt% Dopant (%)	10 wt% Dopant (%)	Gradient Shift Mid-Point (°C)
MW	**Cs**		4.70	10.30	503
	I	1.38	5.84	10.49	452
	Cl		8.70	13.96	810
CaZn	**Cs**		3.62	6.56	507
	I	0.63	5.05	10.91	449
	Cl		10.05	13.34	811

Table 5.4 Total mass loss from 0 – 1200 °C at 5 °C/min in MW and CaZn base glass for all elements and the midpoint temperature of the mass change event associated with the dopant.

The MS data from the base glasses could only detect gas emissions from iodine bearing samples due to the heated off-gas line temperature being too low to carry caesium and chlorine species to the detector. This is also why caesium and chlorine TG-MS measurements are more limited as when this was discovered we ceased experiments with those elements so as not to damage the instrument. Table 9.2 outlines the temperatures at which iodine emission was at its highest. A few important points can be taken from this data. Firstly, all 1 wt% iodine doped samples had no emission detected by MS which indicates that the lower concentration samples do emit less. Secondly, the temperature at which emission was detected was very similar between all glass types which means the glass structure is having little impact on in this system and the likely occurrence is that the majority of NaI is volatilising before the glass frit has softened.

Glass Type	1 wt% Dopant (°C)	5 wt% Dopant (°C)	10 wt% Dopant (°C)
MW	No Peak	658	658
CaZn	No Peak	660	660
0% SiO_2 CaZn	No Peak	600	N/A

Table 5.5 Temperature at which peak ion current is found for m/z ion 254 from MS iodine data over different glass systems and iodine (as NaI) doping concentrations.

The relationship of iodine losses to boron content in our data (comparing figures 5.18, 5.28 and 5.39 in section 5.4) are consistent with Cicconi et al[134], a negative relationship is seen in both cases where an increase in boron content in the glass structure represents a decrease in iodine mass loss. In addition, Bell et al[152] saw a sharp decline in iodine $K_{\alpha 1}$ line intensity in feldspar and silicate glasses with the intensity reducing to 0 after 85 minutes.

Glasses showed a consistent trend in density data with respect to temperature. MW and CaZn glasses had a drop in density from the original glass at 800 – 900 °C and a rise above the original 1100 – 1200 °C (e.g figure 5.49). This phenomenon of initial density decrease is likely due to crystallites forming in the glass matrix and creating vacancies in the glass structure which artificially reduces density. Silica (the main crystalline component) has a density of ~2.65 g/cm^3 which should increase the density if dispersed perfectly through the glass however the vacancies created by these formations

will have a much larger impact on the glass density. The raise in density needs more study however as a consistent trend it is clear that this is a result and not simply an error in our measurements. We theorise that the increase is due to boron volatilisation and compositional changes that densify the glass structure or potentially micro crystallisation of silica.

Zhang et al[216] describes the loss of mass from comparable borosilicate glasses and describes a similar trend in T_g to the results shown in section 4.1 and throughout chapter 5 where a reduction occurs upon increasing boron content due to an increased concentration of less substituted boron subunits compared to silica tetrahedra.

Caesium, iodine and chlorine retention decreases with treatment temperature similarly to research by Claude. S.[217] and Ojovan. M.[77]. Furthermore, in Claude's work ^{137}Cs tracers were found to volatilise at a rate of 22.67 % activity/hr using CsCl more than the losses seen in pyrolysis tracer tests (4.08 % activity/hr) conducted in this study on CaZn base glass, this could be an effect from the use of different raw materials. In literature subsequent melts after fusion the rate dropped to 0.059 % activity/hr theorised to be due to the limited rate of diffusion which is the same effect seen in this study as t = 2h samples always had less volatilisation. There is very limited data available for caesium, iodine and chlorine volatilisation from MW and CaZn in literature to compare our data to however this highlights the importance of work such as this and continuing future studies to corroborate these findings. Overall CaZn seems to have less crystallites and higher retention than MW glass at lower temperatures for resistance to devitrification and incorporation of iodine into its structure, the higher proportion of positive charge compensating ions is likely the reason for the improvement.

When comparing chlorine losses they are higher than the added chlorine content analysed by TGA analysis (e.g. figure 5.50) and therefore there is another process happening other than the decomposition of NaCl into Cl_2 or HCl. We have discussed a similar observation in the MW chlorine containing glass. The most likely reason for this is the thermal decomposition of NaCl in air or boiling of the chlorine containing raw material (NaCl), however, the temperature at which this occurs is low

considering the boiling point of sodium chloride is 1465 °C[218]. Another event that could be taking place is a catalysation of glass component mass loss (B_2O_3, Na_2O etc.). There are no peaks for any m/z ions in the MS trace for any samples so the speciation of this loss event is unknown, however, they are likely chlorine containing and have a low dew point (under 180 °C) as they must condense before reaching the MS detector.

Chapter 6 Effect of Surrogate ILW Loading

6.1 Introduction

The previous chapter took an in depth look at glass with the addition of one element however in real application the contaminant will likely be combined with a waste. This chapter will discuss the effects of incorporating waste into MW, CaZn and 0% SiO_2 CaZn glass systems in varying concentrations (0 – 50 wt%). The dependence of incorporation of caesium and iodine on common ILW sources is investigated when subjected to heat treatment from 0 – 1200 °C. The wastes (and additives) investigated are:

- Clinoptilolite – Calcium aluminosilicate ion exchange resin used for removing caesium and strontium from effluent streams
- Corroded Magnox sludge (CMS) – semi liquid waste of corroded magnesium from fuel swarf

These materials (compositions found in table 6.1) were selected based on the literature available regarding the importance and volumes of each waste. Detailed rational for the use of these materials can be found in section 1.3.

	Oxide Content by XRF (wt%)					
	SiO_2	CaO	Al_2O_3	Fe_2O_3	K_2O	MgO
Clinoptilolite	77.60 +/- 3.00	4.10 +/- 0.18	13.11 +/- 0.80	1.47 +/- 0.09	2.66 +/- 0.02	1.06 +/- 0.06
CMS	0.14 +/- 0.005	0.05 +/- 0.002	1.59 +/- 0.10	0.14 +/- 0.008	-	97.89 +/- 5.97

Table 6.1 Oxide content analysed by XRF in clinoptilolite and corroded Magnox sludge raw material.

To investigate the interactions between glass and waste firstly, we look at the effect of particle size so that we may apply a suitable and consistent size throughout the chapters results and load as much

waste as possible. We then move to attempt heat treatment of the waste with glass frit to determine the melting properties of the glass and waste.

Clinoptilolite is used in the nuclear industry for its ion exchange capabilities and therefore any contamination may not be spread across the surface of the particles but instead actually incorporated into the structure particularly in the case of Cs^+ ions. In all our previous measurements caesium has been added as a dopant, in section 6.5 we cover the effect of using clinoptilolite with ions exchanged into its structure. It is worth noting that in previous sections caesium is the only element we have discussed which is compatible with clinoptilolite and therefore in section 6.6 only caesium in discussed in the exchange of clinoptilolite. Caesium was exchanged into the structure of clinoptilolite to determine if this affected the thermal treatment properties. The purpose of these experiments are to determine whether waste stored at Sellafield is better stored as it is currently (exchanged) or washing the material with an ion exchanging inactive agent (non-exchanged).

6.2 Methodology

Firstly, we look at the effect of particle size of the raw materials so that we may apply a suitable and consistent size throughout the chapters results. Before beginning experiments it was important to look at variables that may alter the loading of waste into glasses and therefore the properties of any volatile component. This was completed by the milling the glass material and passing through sieves to control the particle size. We investigated the particle size of the frit and raw materials looking at the properties of the resultant melt and quantity of the waste that was dissolved into the glass structure. CaZn glass was melted into a block and broken into smaller pieces then reduced in size further in a rotary mill for 30 seconds at 700 rpm. The resulting glass powder was then sieved incrementally using sizes 500 – 2500 μm. Two fractions of this glass powder were taken <500 μm and 500 – 2500 μm, these were separated and used for future experiments.

Waste loaded glasses were prepared by the mixing of powdered glasses MW, CaZn and 0% SiO_2 CaZn (compositions found in table 4.1 in section 4.3.1) with clinoptilolite or CMS and heat treating in a furnace at 1150 °C (for non-active experiments) and 950 °C (for active experiments).

In section 6.6 the exchanged clinoptilolite ions is explored by the use of caesium solution washes to absorb Cs^+ ions into the mineral structure. To exchange ions in clinoptilolite raw material with caesium 12.26 g of caesium carbonate was added to 250 ml of water with 100 g of clinoptilolite so that 10 wt% of the exchanged clinoptilolite by weight was Cs^+. The product from this was kept in solution and placed on a hot plate at 80 °C until completely dry to make sure that if any caesium did not incorporate into the structure that it would be dried onto the surface of the material. The material was then mixed and stored in an alumina crucible in an oven at 110 °C too ensure the material remained dry. For volatility testing, the exchanged material was heated

6.3 Particle Size

The 500 – 2500 µm glass powders was remelted first dwelling at 1150 °C for 2 hours with the addition of clinoptilolite between 10 – 50 wt% waste loading. These glasses/products were attempted to be poured into a mould, however, in some of the samples the glass poured and left behind material in the crucible. The 500 – 2500 µm samples all left behind a brown coloured material particularly around the glass/air boundary after pouring. Figure 6.1 a) shows the material remaining in the crucible which is clearly a result of clinoptilolite addition. The thickness and quantity of un-digested clinoptilolite material increases with waste loading. When the same experiment was conducted on the CaZn frit at a particle size of <500 µm the samples completely poured after 2 hours with no material remaining in the crucible. Images of the crucible after pouring the <500 µm samples can be seen in figure 6.1 b) where the crucible is completely clear of brown material. After this testing it was clear that the raw

material and frit should be milled to under 500 µm before testing for consistency and to optimise waste loading.

Figure 6.1 Images of the crucibles after pouring CaZn glasses loaded with clinoptilolite with a particle size of 500 – 2500 µm (a) and <500 µm (b). From left to right 10, 20, 30, 40, 50 wt% waste loading.

6.4 Initial Loading Trials

After determining the particle size of the glass and raw material, the two wastes (clinoptilolite and CMS) were loaded into different glass systems to determine the limit at which crystallisation occurs and the effect on glass content. Clinoptilolite and CMS raw materials were analysed first by XRF and XRD to determine the elemental composition and crystal character of the raw material for comparison. Table 6.1 shows the breakdown of elements in each raw material. Our supplied clinoptilolite is largely an aluminosilicate containing mineral with calcium, potassium and magnesium in the interstitial sites and some iron from impurities in the mineral. Using this data we can assume an empirical formula of $Si_{36.3}O_{50}Al_{6.9}Ca_{2.9}K_{2.2}Fe_1Mg_{0.6}$ for the clinoptilolite used in this study. The CMS simulant used is predominantly magnesium containing with minor influences from iron, aluminium, silica and calcium.

Next, we will discuss the loading of clinoptilolite in 0% SiO_2 CaZn glass without any addition of dopants. Furnace heat treatments were conducted at 1150 °C for 2 hours with the addition of 10 – 50 wt% of the waste. The poured products from clinoptilolite and CMS additions are shown in figure 6.2. Colour change is seen toward the higher end of waste loading for both samples, for clinoptilolite the samples became darker brown in colour upon increasing loading of clinoptilolite. This is due to the iron in the sample causing a colour shift in the glass product. No observable crystallisation occurred in the clinoptilolite samples (figure 6.2a), all samples appeared clear with no particles dispersed throughout the structure. The CMS loaded samples (figure 6.2b) undergo a colour change at 30 – 50 wt% loading starting at translucent and ending at an opaque white material with evident crystallisation on the surface and particles dispersed through the glass.

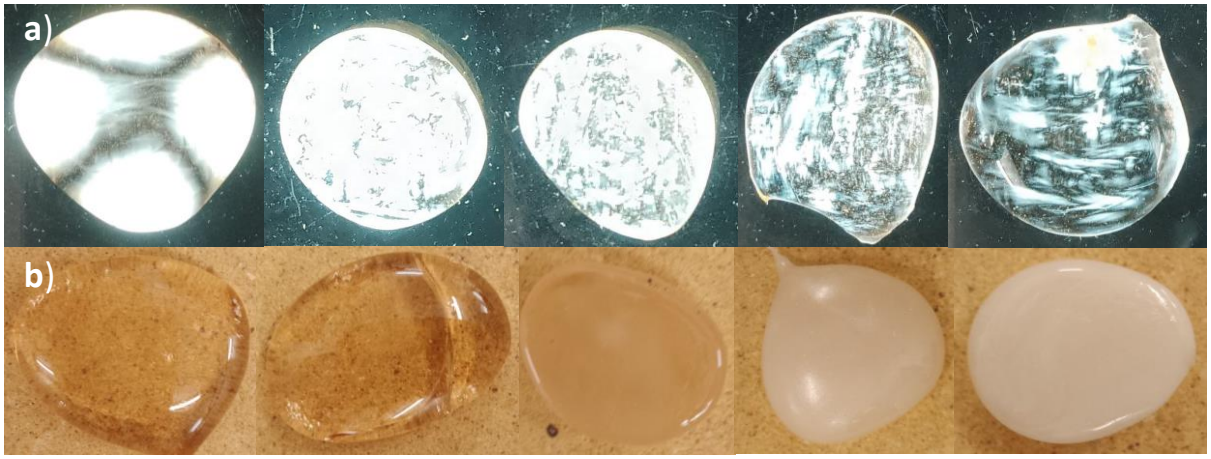

Figure 6.2 Images of glasses/products from waste loaded 0% SiO_2 CaZn glass samples from 10, 20, 30, 40, 50 wt% (left to right). a) Clinoptilolite waste loaded (glare from backlight caused some problems with images). b) CMS waste loading

XRD confirms the observations seen in the glass/products. All clinoptilolite loaded samples show amorphous crystal behaviour by XRD in figure 6.3. The 10 wt% has a small Bragg peak which is likely to be assigned to the major SiO_2 quartz deflection. This result is likely anomalous as all other samples do not show any crystallisation and this is an indication of a procedural error or contamination. This is an incredibly high waste loading for this system. The clinoptilolite material is predominantly composed of silica and aluminium with some minor glass modifying components which allows for the high loading we see into borosilicate glasses. As the glass digesting the clinoptilolite is a borate system the

incorporation of this material essentially brings the composition back up to MW or CaZn concentrations particularly in silica content. CMS is much harder to incorporate as the quantities of glass forming agents in the material are very low (the main component being magnesium). This is evident in figure 6.4 where XRD detected crystallisation assigned to magnesium containing Gahnite ($Mg_{0.35}Zn_{0.65}Al_2O_4$) at 40 and 50 wt% CMS loading into 0% SiO_2 CaZn and a minor secondary $LiMgBO_3$ phase appearing at 50 wt% loading. This is likely responsible for the white colour seen in the images of more loaded samples in figure 6.2b. The minimum loading at this temperature without crystallisation for CMS in this glass system is 30 wt% which remains high compared to standard waste loading used but lower than clinoptilolite due to the high magnesium content.

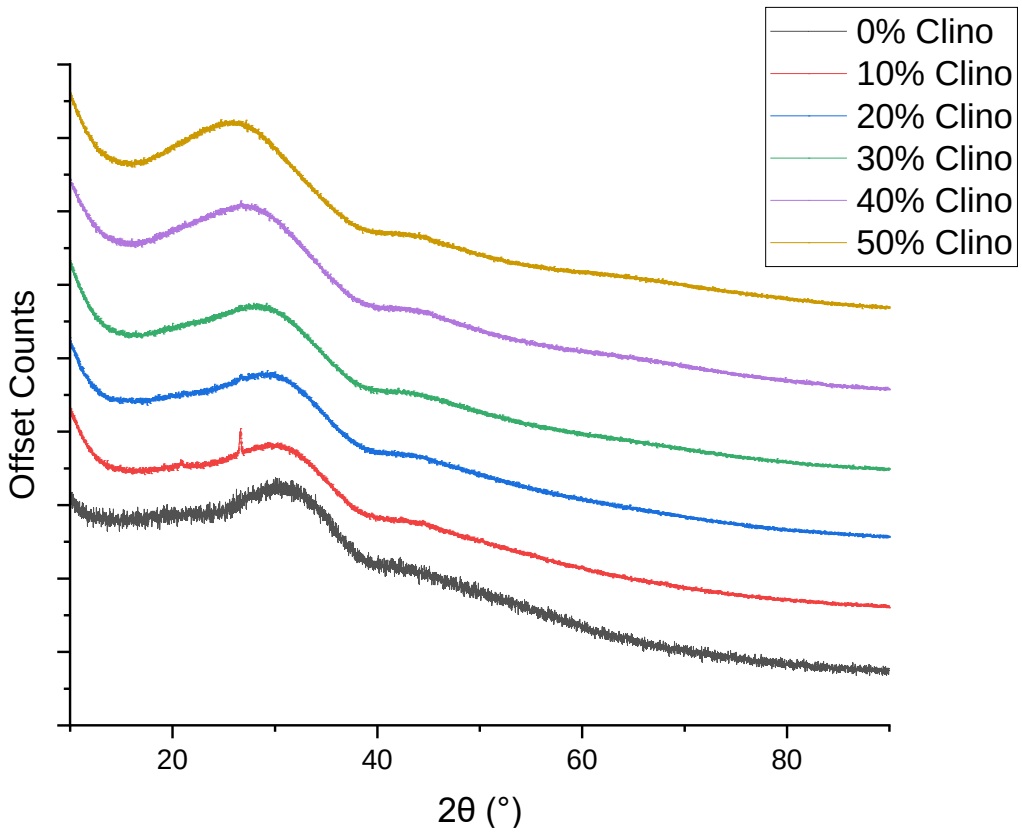

Figure 6.3 XRD patterns of clinoptilolite loaded from 10 – 50 wt% (bottom to top) into 0% SiO_2 CaZn glass

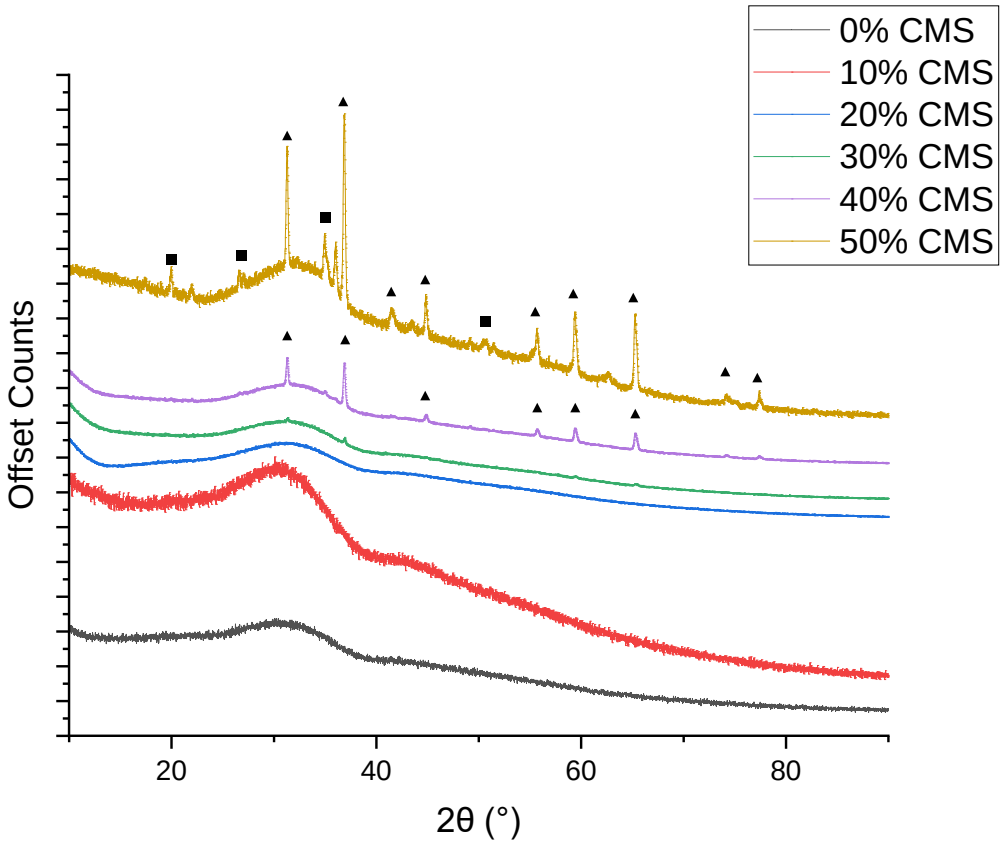

Figure 6.4 XRD patterns of CMS loaded from 10 – 50 wt% (bottom to top) into 0% SiO_2 CaZn glass ▲= $Mg_{0.35}Zn_{0.65}Al_2O_4$ Gahnite (Phase ID: 04-017-1029), ■ = $LiMgBO_3$ (Phase ID: 04-009-5597)

6.4 Effect of Waste on Caesium

In this section caesium volatilisation/retention is investigated in CaZn and 0% SiO_2 CaZn base glasses up to 1200 °C by melting trials, XRF and pyrolysis with active tracers. Clinoptilolite, CMS, xanthan gum, graphite and starch were loaded into the glasses.

6.4.1 CaZn Base Glass

6.4.1.1 Clinoptilolite

This waste was loaded into CaZn glass from 0 – 50 wt%, spiked with caesium and analysed by XRF/XRD after melting in a furnace at 1150 °C and dwelling at the maximum temperature for 2 hours. Active tracers were also used in the pyrolysis instrument with CaZn glass and clinoptilolite to determine the retention of ^{137}Cs at 950 °C. Firstly, we will look at 1 wt% caesium doped CaZn with the addition of 0 – 50 wt% clinoptilolite. In figure 6.5 the XRF data of the resultant glass for this series in seen. As clinoptilolite loading increases in the glass the components from clinoptilolite increase in

concentration. This includes SiO_2 which steadily increases from 43.79 – 57.50 wt%, silicon is the most prevalent element in clinoptilolite raw material therefore this is an expected change to see in the end product. The change is linear with an r^2 of 0.996 and a slope of 2.75 +/- 0.12. Aluminium content remains constant, ~12 wt% on average in clinoptilolite loaded samples, this change is non-linear. Conversely, components that only appear in the glass (B_2O_3, ZnO) linearly reduce with a negative slope in composition over the waste loading, values can be seen in table 6.2.

	R^2 value	**Slope**	**Error (+/-)**
SiO_2	0.996	2.75	0.12
B_2O_3	0.895	-2.22	0.38
ZnO	0.988	-0.654	0.04

Table 6.2 Linearity and gradient of oxide content upon addition of 0 – 50 wt% clinoptilolite

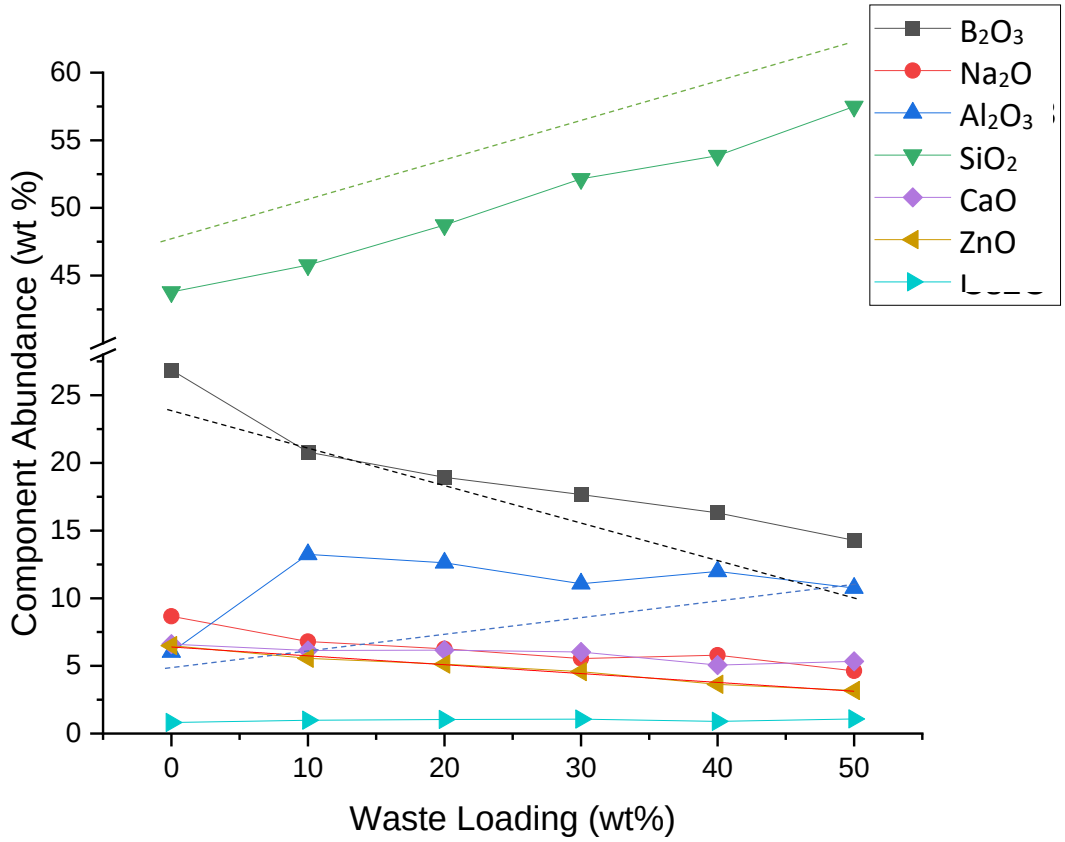

Figure 6.5 XRF concentration data points of CaZn glass/product with the addition of 10 – 50 wt% clinoptilolite all with the addition of 1 wt% Cs added as Cs_2CO_3.

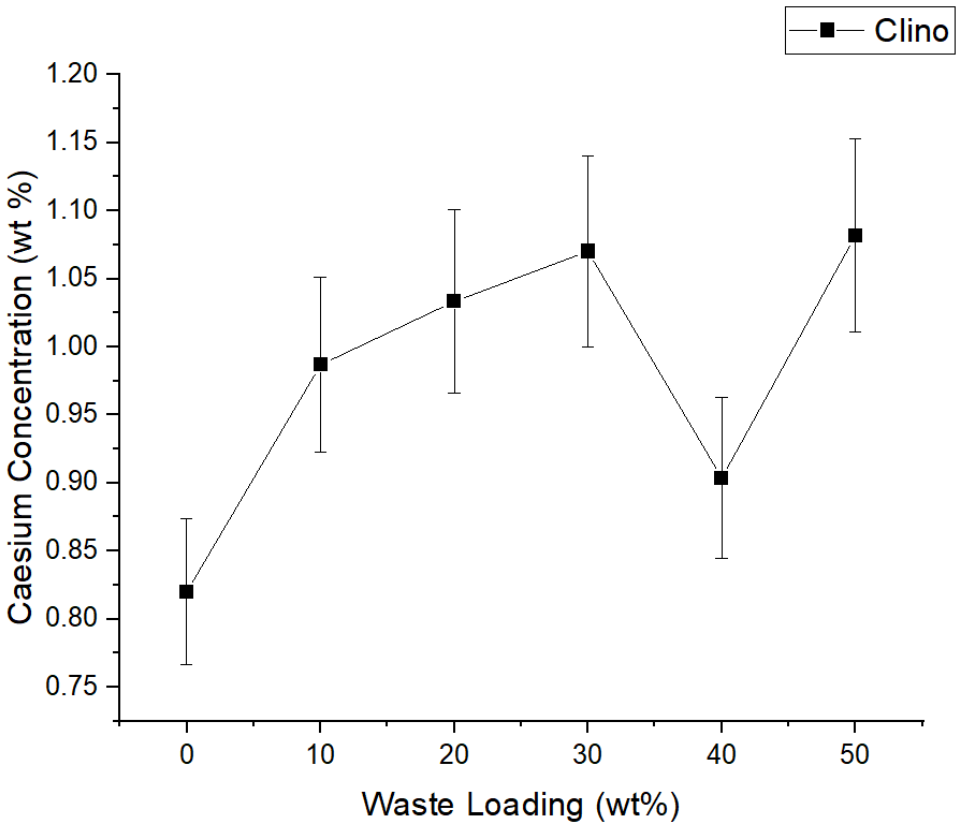

Figure 6.6 Caesium concentration data points of CaZn glass/product with the addition of 10 – 50 wt% clinoptilolite all with the addition of 1 wt% Cs added as Cs_2CO_3.

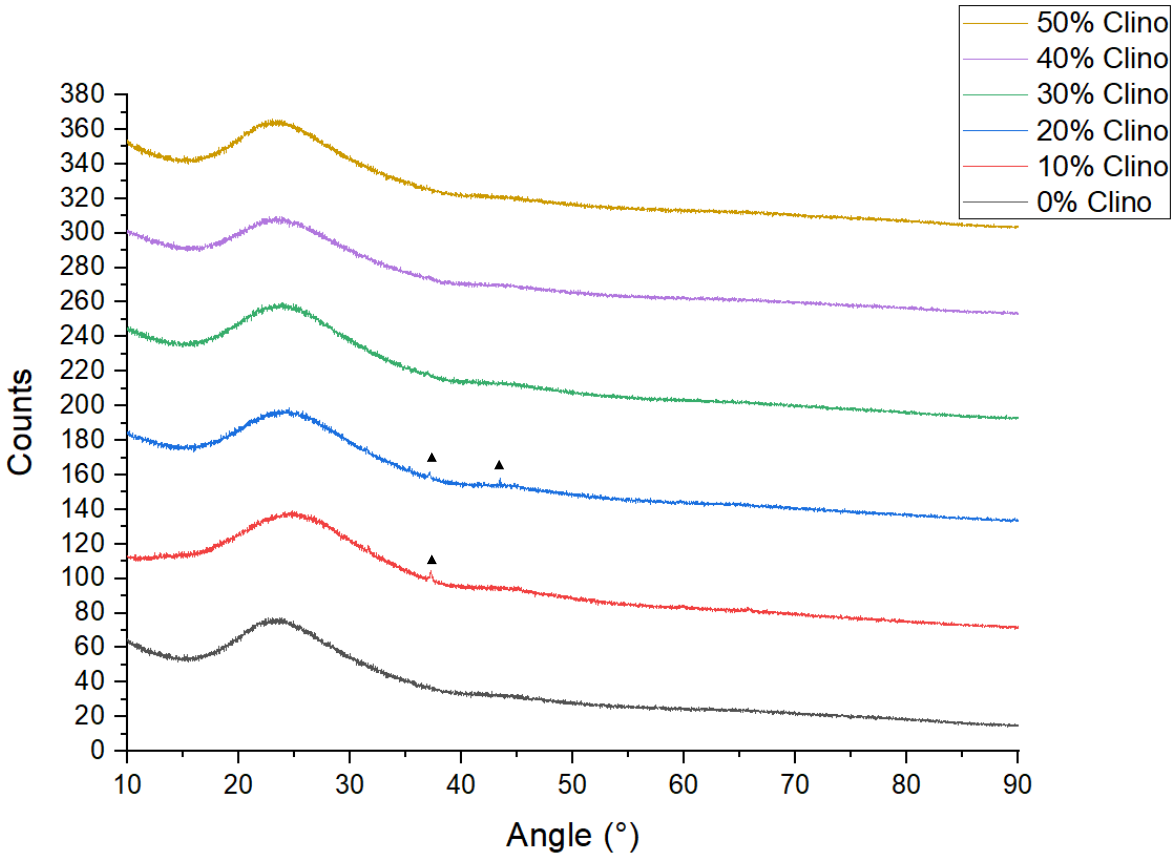

Figure 6.7 XRD traces of clinoptilolite waste loaded CaZn glass with the addition of 1 wt% Cs as Cs_2CO_3 from 0 – 50 wt%. Assignment estimated: ▲= $ZnAl_2O_4$ Phase ID (01-073-1961)

When components are in both the CaZn glass structure and clinoptilolite raw material (eg. Al_2O_3, CaO) we see the concentration plateau and vary much less in the loaded samples. The caesium concentration of the same 0 – 50 wt% loaded clinoptilolite series (magnified in figure 6.6) trends upwards upon increasing clinoptilolite content. There is a slight drop at 40 wt%, however, this does not fit the trendline and is likely anomalous. The starting concentration of caesium with no addition of clinoptilolite is 0.82 wt% which increases to 1.08 wt% upon the addition of 50 wt% clinoptilolite, this is a 24% increase in caesium retention. The products from these experiments appear mainly X-ray amorphous (figure 6.7), however, there was some minor contribution from a zinc aluminium oxide crystal that formed in the 10 and 20 wt% samples. The concentration of these crystals is very low and therefore could be a procedural error from a using a slower cooling rate or from contamination of the samples during powdering of the glass. Above this waste loading no crystallisation is seen by XRD.

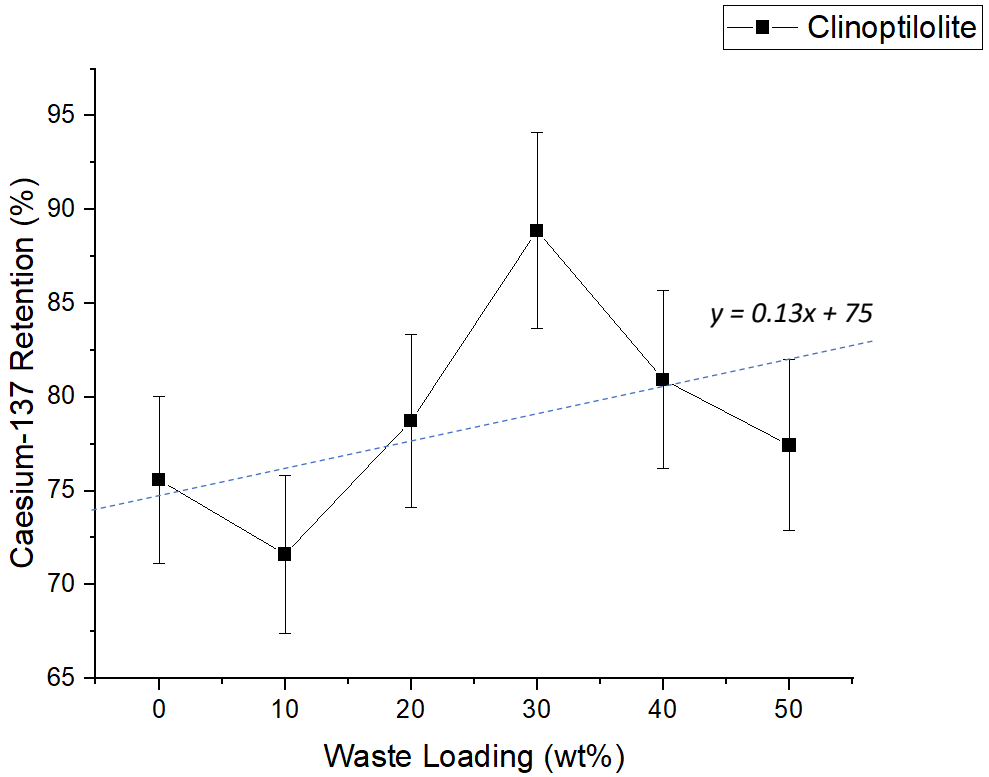

Figure 6.8 Active ^{137}Cs retention in CaZn glass with the loading of clinoptilolite between 10 – 50 wt% analysed by gamma spectroscopy.

Active tracer (^{137}Cs) measurements are similar to caesium retention data we see from XRF. This can be seen in figure 6.8. As clinoptilolite concentration increases ^{137}Cs retains more, increasing to 88.88 wt% at 30 wt% loading from 75.59 wt% in the base glass with no loading. The difference in this data is that

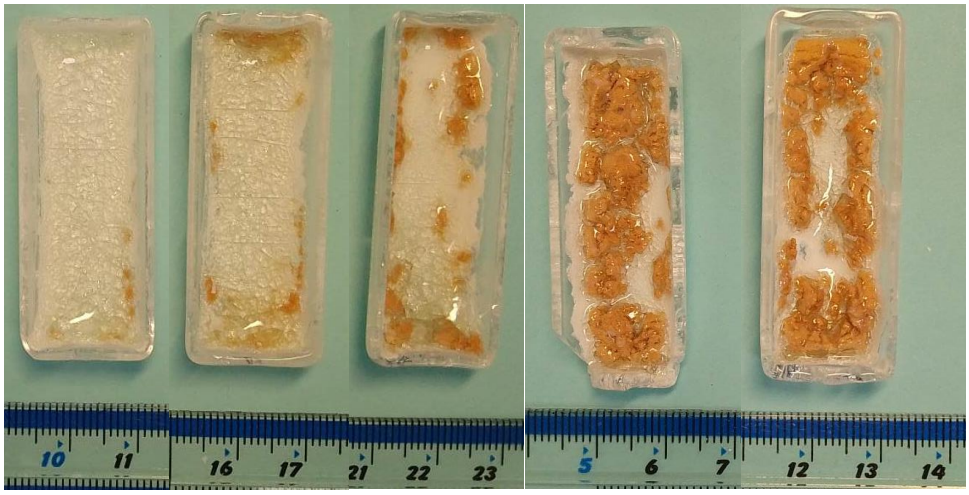

Figure 6.9 Images of clinoptilolite loaded samples in CaZn glass after heat treatment at 950 °C with the addition of 10 Bq of ^{137}Cs. Left to right 10, 20, 30, 40, 50 wt%.

above 30 wt% loading the concentration of ^{137}Cs in the glass seems to reduce again. The differences seen between the two samples may be surface area to volume ratio and sample mass. In the pyrolysis trials the samples use 2g in mass compared to the 20g sample used in the furnace/XRF experiments, the surface area to volume radio is also much larger in the pyrolysis experiments. This could indicate that in smaller samples 30 wt% is the maximum for caesium retention varying clinoptilolite waste concentration. Clinoptilolite could be increasing retention because of higher silica content in the glass structure or due to physical effects from the caesium material binding with the clinoptilolite mineral. It is worth noting however that the reduction in silica in the original base glasses was to incorporate more of the silica containing clinoptilolite waste and therefore a balance is made so that the glass remains amorphous but still has a high concentration of silica.

6.4.1.2 Corroded Magnox Sludge (CMS)

CMS was loaded between 0 – 50 wt% into CaZn glass with the addition of 1 wt% Cs or 10 bq of ^{137}Cs to determine retention. Firstly, the XRF data from glasses melted in the furnaces at 1150 °C shows us that CMS has an overall negative effect on caesium retention (figure 6.10). However, at lower loadings (10 – 30 wt%) the retention of caesium does appear to increase from 0.82 wt% to an average of 1.13 wt%. Retention drops dramatically after 30 wt% to an average of 0.60 wt% under the original retention of the base glass. The values raising above 1 wt% Cs_2O likely represent error associated with

weighing or instability inherent in the boron analysis. The increase in retention must be due to the addition of magnesium into the glass or a physical effect from the absorption of caesium material into the powered waste. Analysis of the XRF data shows that glass/product contents varies as expected (figure 6.11). Components that only occur in the waste increasing linearly, for example magnesium oxide increases linearly with a slope of 7.06 +/- 0.35 (table 6.3).

	R^2 value	**Slope**	**Error (+/-)**
MgO	0.990	7.06	0.35
SiO_2	0.819	-3.52	0.83
Na_2O	0.931	-1.09	0.15

Table 6.3 Linearity and gradient of linear oxide components upon addition of 0 – 50 wt% CMS

As we have seen in section 6.2 CMS can cause crystallisation in CaZn derived glasses and this is the same in CaZn base glass with the addition of caesium. Figure 6.12 shows the crystal products after melting CaZn glass with increasing CMS waste loading. Most of the crystal behaviour is assigned to magnesium silicate with minor fractions of other magnesium containing species (MgO and $Mg_3(BO_3)_2$). This crystallisation does appear at the same loading percentage that we see caesium retention decrease which may indicate a correlation between the two occurrences.

Pyrolysis experiments using ^{137}Cs as a tracer shows that concentration of caesium lowers upon increasing waste loading of CMS (figure 6.13). The retention in the base glass is 75.59% which reduces to a minimum of 56.30% at 50 wt% CMS. The value at 30 wt% is likely to be anomalous as the trend does not fit with this. Compared to the furnace trials based on XRF data in figure 6.10 the retention of caesium is similar at high concentration of CMS and, for 10 – 30 wt% samples, lower in ^{137}Cs retention measured by pyrolysis analysis.

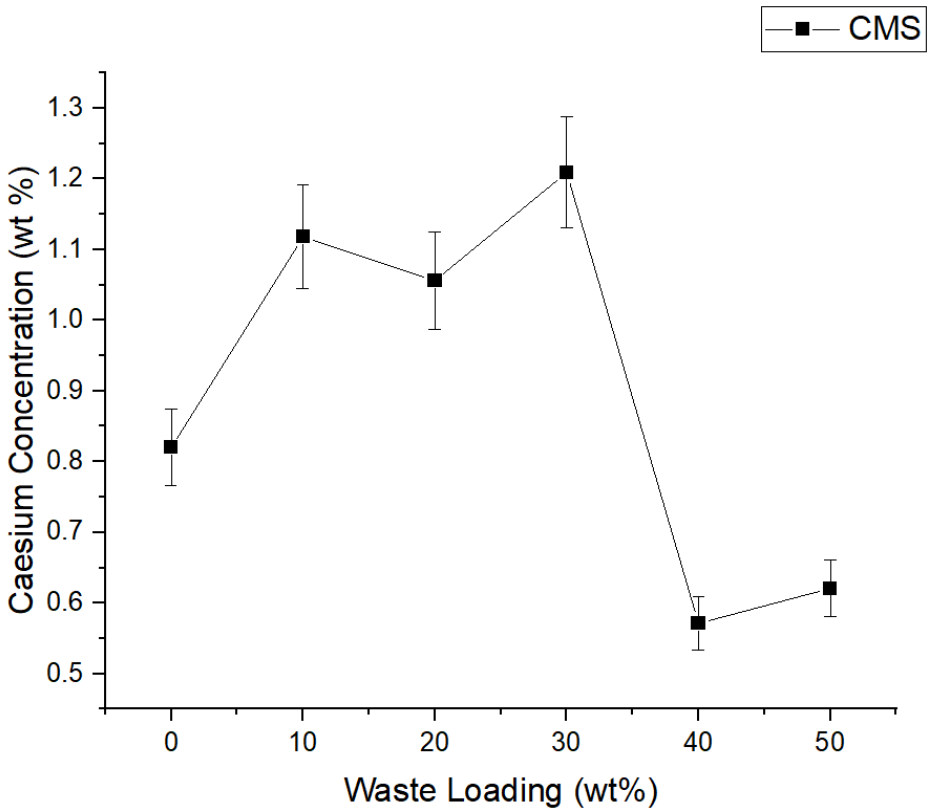

Figure 6.10 XRF concentration data points of CaZn glass/product with the addition of 10 – 50 wt% CMS all with the addition of 1 wt% Cs added as Cs_2CO_3. Data presented as abundance of Cs_2O.

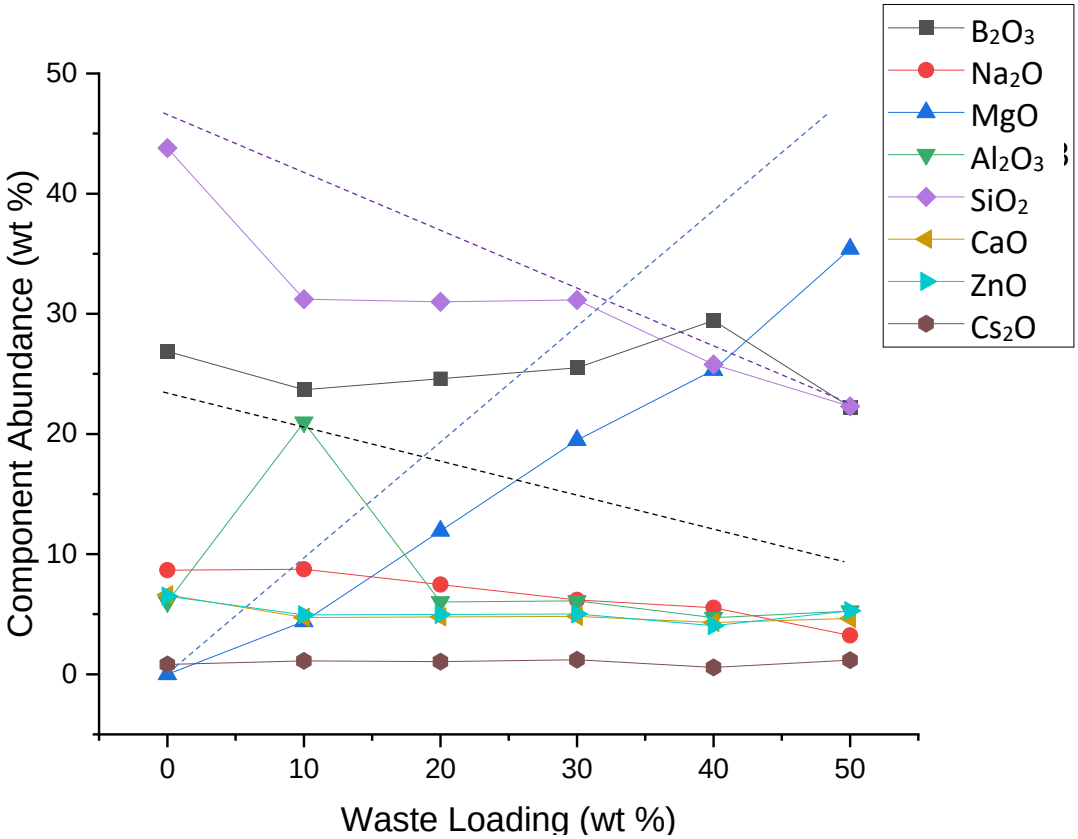

Figure 6.11 Caesium concentration data points of CaZn glass/product with the addition of 10 – 50 wt% CMS all with the addition of 1 wt% Cs added as Cs_2CO_3. Dashed lines indicate expected composition.

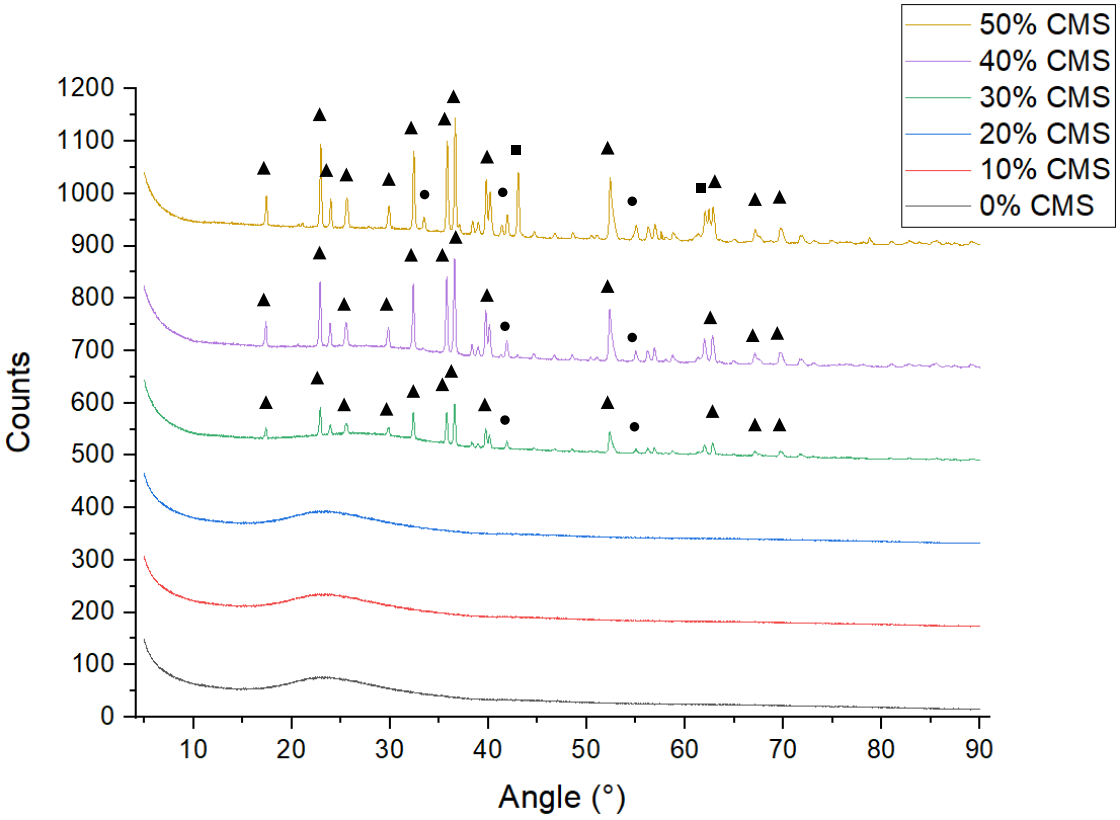

Figure 6. 12 XRD traces of CMS waste loaded CaZn glass with the addition of 1 wt% Cs as Cs_2CO_3 from 0 – 50 wt%. ▲= Forsterite Mg_2SiO_4 (Phase ID: 01-085-1346), ● = Kotbite $Mg_3(BO3)_2$ (Phase ID: 01-073-1541), ■ = Periclase MgO (Phase ID: 04-007-3405).

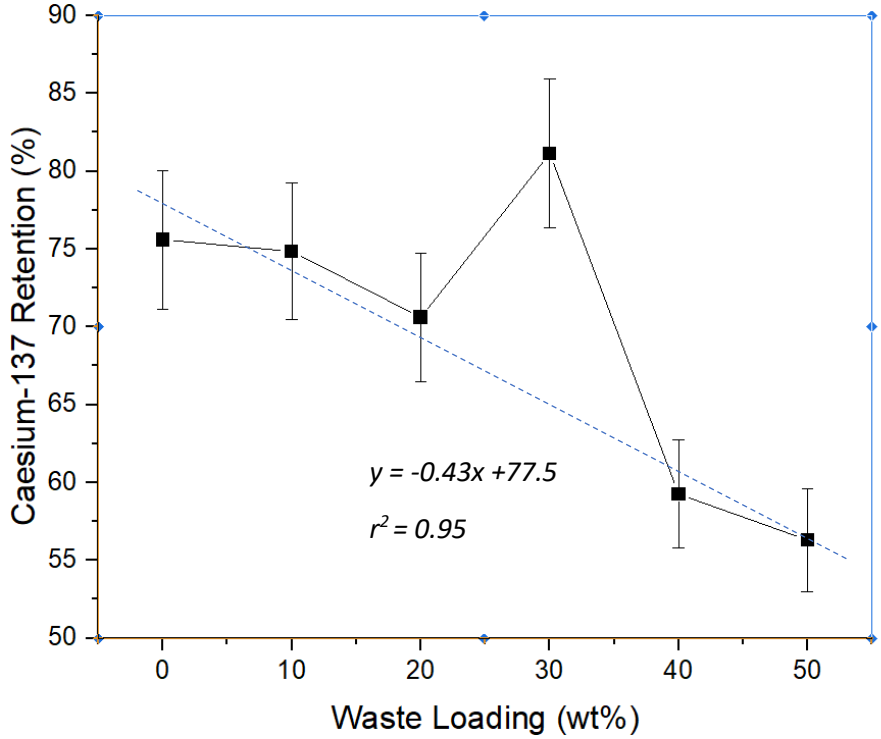

Figure 6.13 Active ^{137}Cs retention in CaZn glass with the loading of CMS between 10 – 50 wt% analysed by gamma spectroscopy. Data presented as abundance of ^{137}Cs.

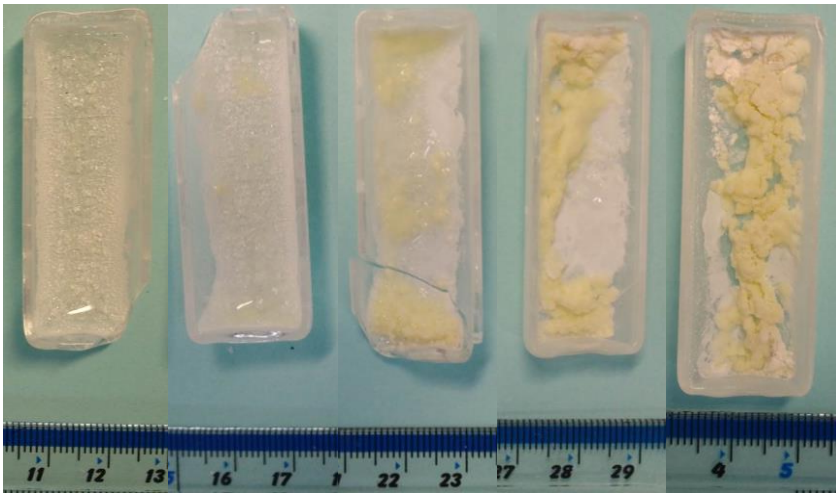

Figure 6.14 Images of CMS loaded samples in CaZn glass after heat treatment at 950 °C with the addition of 10 Bq of ^{137}Cs. Left to right 10, 20, 30, 40, 50 wt%.

6.4.2 0% SiO_2 CaZn Base Glass

6.4.2.1 Clinoptilolite

This waste was loaded into 0% SiO_2 CaZn glass from 0 – 50 wt%, spiked with caesium and analysed. Active tracers were used in the pyrolysis instrument with 0% SiO_2 CaZn glass and clinoptilolite to determine the retention of ^{137}Cs at 950 °C. Figure 6.15 shows the ^{137}Cs retention in this system upon loading clinoptilolite. The graph trends upwards on increasing clinoptilolite waste loading with a high positive gradient of 0.41 +/- 0.09 (r^2 = 0.821). The maximum of this graph is significantly higher than any other previously measured samples at 88.23% when waste loaded with 50 wt%. The data in this figure shows that clinoptilolite could have a positive impact of the retention of caesium (active and non-active), CaZn glass in section 6.3.1 (figure 6.6) shows a similar trend. Silica and alumina content increasing the viscosity may be the reason for this change. Another solution is that caesium maybe be ion exchanging into clinoptilolite and increasing the energy required to dissociate. Figure 6.16 shows discolouration that occurs upon increasing clinoptilolite loading, this is due to the iron in the raw material causing a colour shift as has been seen previously in CaZn glass.

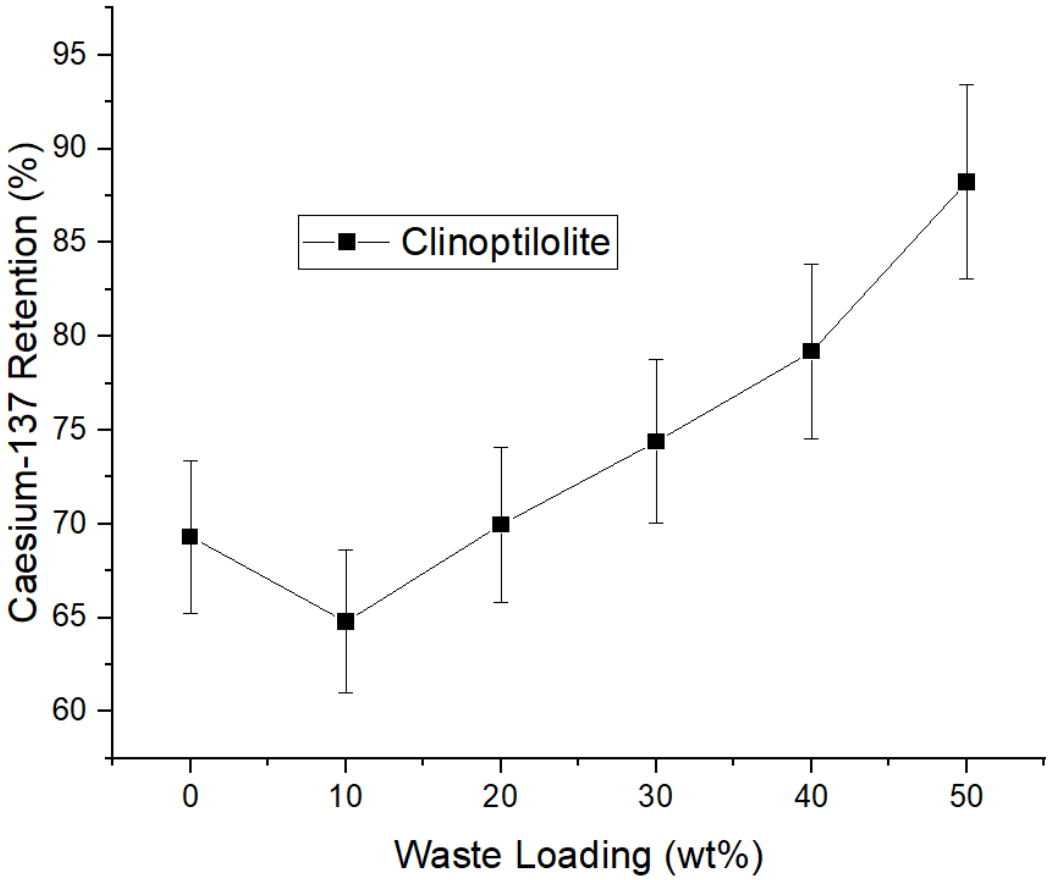

Figure 6.15 Active ^{137}Cs retention in 0% SiO_2 CaZn glass with the loading of clinoptilolite between 10 – 50 wt% analysed by gamma spectroscopy.

Figure 6.16 Images of clinoptilolite loaded samples in 0% SiO2 CaZn glass after heat treatment at 950 °C with the addition of 10 Bq of ^{137}Cs. Left to right 10, 20, 30, 40, 50 wt%.

6.4.2.2 Corroded Magnox Sludge (CMS)

CMS was loaded in the same concentrations, 0-50 wt%, into 0% SiO_2 CaZn glass added with 10 bq caesium as ^{137}Cs and heated to 950 °C. The concentration of active caesium decreases in the samples as more CMS is added therefore the retention of caesium is decreasing. Magnesium added in this form is likely causing the glass to reach the limit of cation incorporation and filling sites that could be taken up by caesium cations. There is also crystallisation that occurs that has been previously shown by XRD, these experiments also showed that the sample had crystallisation products in the crucibles of the resultant product (figure 6.18). Some of the crucibles did break apart upon removal from the furnace, all the sample was recovered, and no spillage occurs, however, the sample has a different geometry when analysed by gamma spectroscopy which increases the error.

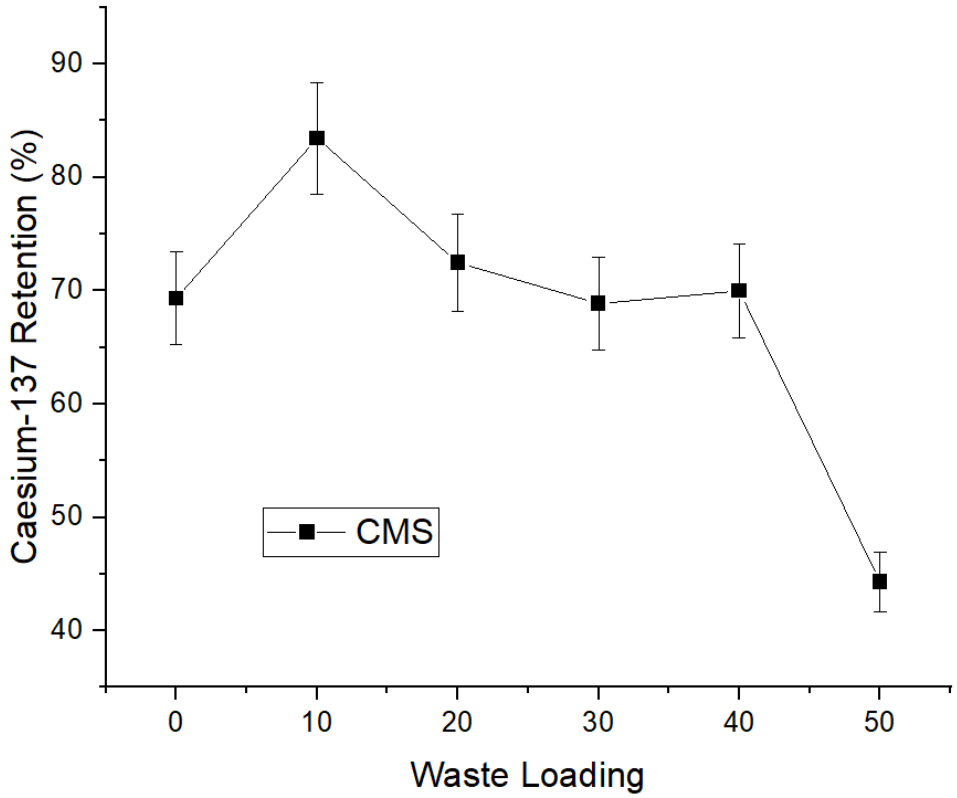

Figure 6.17 Active ^{137}Cs retention in 0% SiO_2 CaZn glass with the loading of CMS between 10 – 50 wt% analysed by gamma spectroscopy.

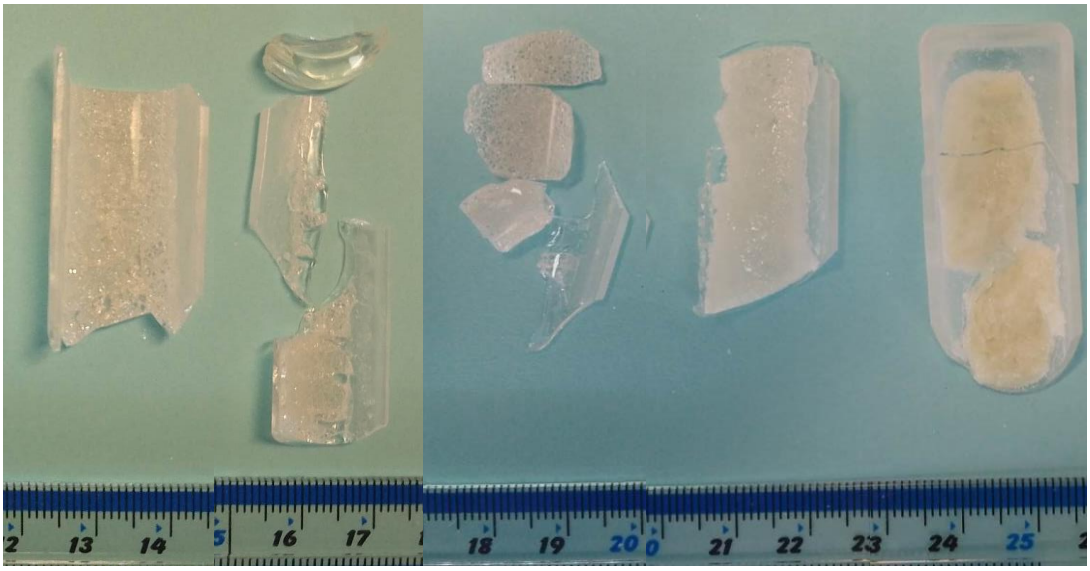

Figure 6.18 Images of clinoptilolite loaded samples in 0% SiO2 CaZn glass after heat treatment at 950 °C with the addition of 10 Bq of ^{137}Cs. Left to right 10, 20, 30, 40, 50 wt%.

The base glass retains 69.31 % ^{137}Cs which reduces to a minimum of 44.30 % at 50 wt% waste loading of CMS other than this large reduction the retention does not change dramatically from 20 – 40 wt% loading averaging at 70.42 % retention. The only other point of note in at 10 wt% loading where the retention increases to 83.43 %.

6.5 Effect of Waste on Iodine

6.5.1 MW Base Glass

Whilst most of the waste loading experiments were completed on CaZn and silica free CaZn base glasses there was a small group of TG-MS trials that investigated in MW base glass. These will be discussed in this section.

6.5.1.1 Clinoptilolite

MW was investigated by TG-MS and DTA with the addition of 10 wt% clinoptilolite and 5 wt% iodine added as NaI. Overall mass loss does not vary much from the base glass upon the addition of even 10 wt% clinoptilolite (figure 6.19), in both measurement the total loss is ~7-8 wt%. The position of the mass loss, however, does appear to change (seen in figure 6.19). The total mass loss over the whole temperature range 0 – 1200 °C is 5.840 and 5.847 % respectively for the base glass and 10 wt% clinoptilolite loaded samples (with 5 wt% I). It is likely that during this period all iodine is lost and

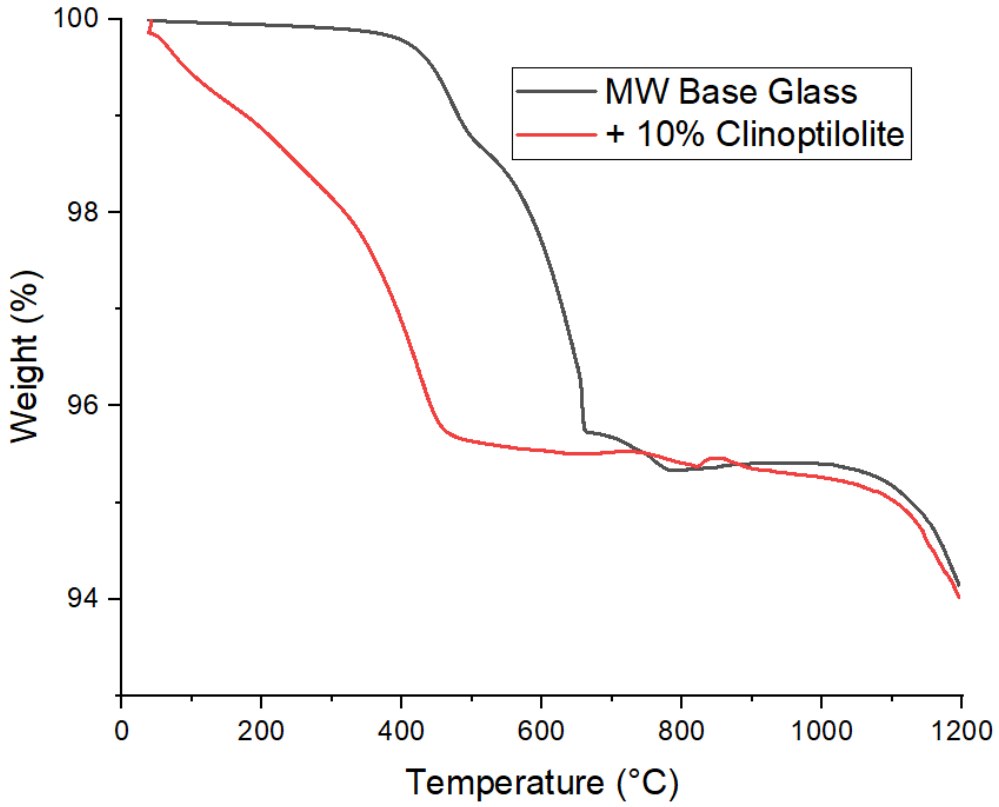

Figure 6.19 TGA data for 5 wt% iodine doped MW glasses with and without the addition of 10 wt% clinoptilolite over the temperature range 0 – 1200 °C

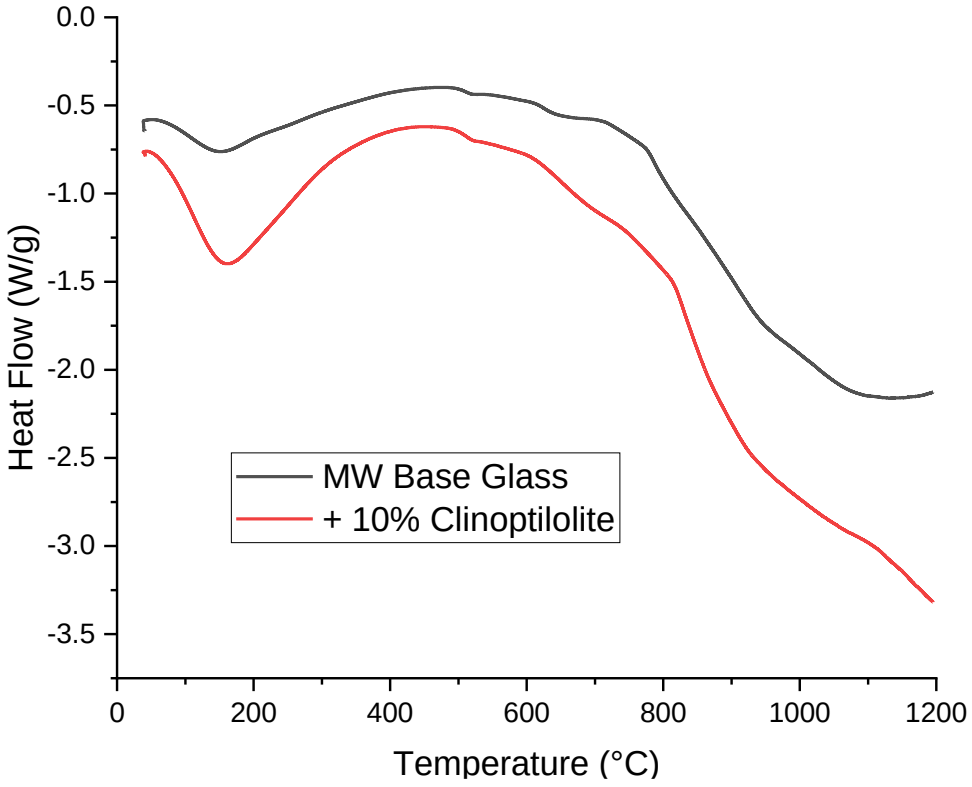

Figure 6.20 DTA data for 5 wt% iodine doped MW glasses with and without the addition of 10 wt% clinoptilolite over the temperature range 0 – 1200 °C

that is why we see little difference between the two samples. The main mass loss event for each sample ends at 471 and 665 °C for the base glass and 10 wt% clinoptilolite sample respectively, this is one large difference as well as the mass loss beginning much earlier than in the base glass. The DTA analysis in figure 6.20 shows very little variation in the two samples. Glass transition (~545 °C) and melting temperatures (~625 °C) do not vary significantly with the addition of clinoptilolite. Mass spectrometry of the samples show that iodine is the only emission (AMU 254 with expected distributions of AMU 127 and 253). The detection of iodine peaks a 657 and 444 °C for 5 wt% iodine doped MW base glass and 10 wt% clinoptilolite addition respectively. The temperature at which emission occurs lowers when clinoptilolite is added, this may be because clinoptilolite is ion exchanging some of the iodine and therefore is retained until higher temperatures allowing for more glass dissolution to occur.

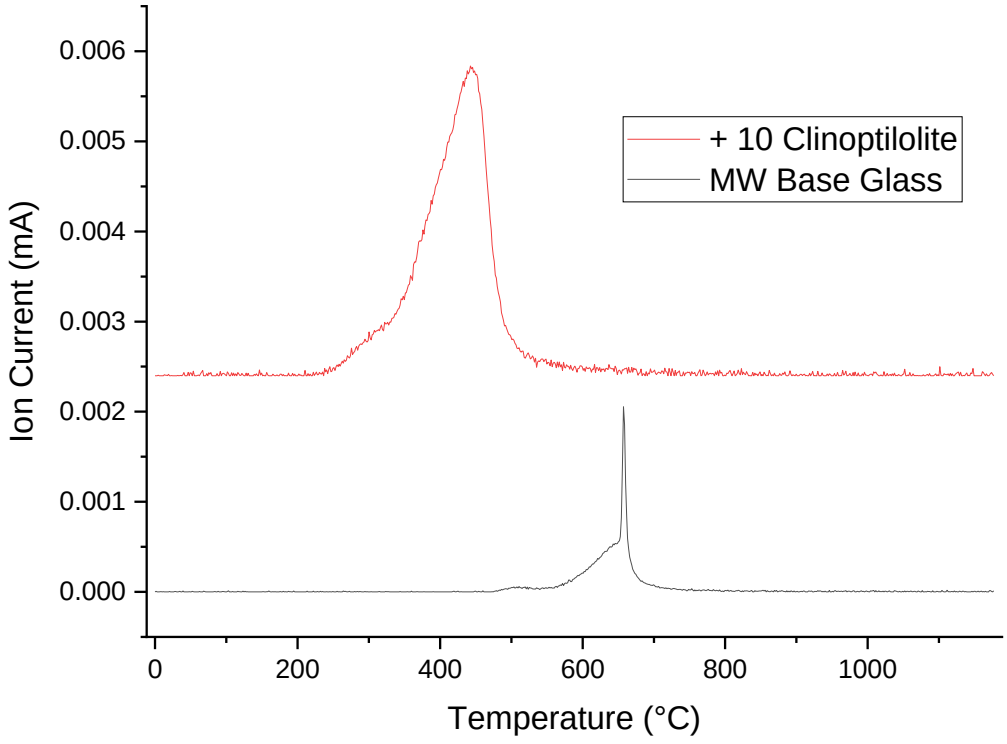

Figure 6.21 MS data traces of 5 wt% iodine doped MW glasses with and without the addition of 10 wt% clinoptilolite over the temperature range 0 – 1200 °C. AMU 254.

6.5.1.2 Corroded Magnox Sludge (CMS)

Thermal analysis of MW glass containing CMS was compared with the base glass traces from TGA, DTA and MS measurements. Firstly, the TG analysis shows us a similar effect to the clinoptilolite additions seen in section 6.4.1.2, however, the mass loss is higher in CMS loaded glasses than the base glass and the loss occurs at an earlier temperature (figure 6.22). The major mass loss event occurs at 295 – 629 °C presumably from iodine which is significantly earlier than the base glass (430 – 665 °C). The trend other than location is very similar even showing a gradient change during the major mass loss. The total mass loss over the whole period of 0 – 1200 °C for the CMS loaded sample is 7.65 % more than the base glass at 5.84 %. All the iodine is lost over this temperature range which should contribute around 5 % mass loss, it is theorised that CMS added is volatilising itself which is contributing to the total mass loss allowing this sample to exceed the 5% threshold.

DTA analysis of these samples only show one major difference, other thermal events such as glass transition temperature and glass melting do not change on initial melting/digestion. The difference is an endothermal peak at 334 °C that only appears in the DTA for the 10 wt% CMS loaded sample. This must be due to the addition of CMS and therefore is likely the melting of the raw material or potentially the volatilisation of iodine at an earlier temperature compared to the MW base glass.

Analysis of the gas emissions by mass spectrometry detects AMUs of 254, 253 and 127 which can be assigned to I_2 isotopes and I^- fragments. Figure 6.24 shows the intensity of AMU 254 over the temperature range 0 – 1200 °C for CMS loaded and non-loaded MW glasses with 5 % iodine.

The peak of this emission is at a lower temperature for CMS loaded MW (485 °C) than MW base glass (657 °C). There is little information from literature to explain this but we theorise that the lowering of emission temperature on the addition of magnesium oxide powder is because of the reduced interaction with softening glass. The iodine is instead adsorbing to the magnesium oxide particles and volatilising rather than interacting with the softening glass. This effect was also seen in clinoptilolite waste additions and it is likely a similar effect that causes the decrease in volatilisation temperature.

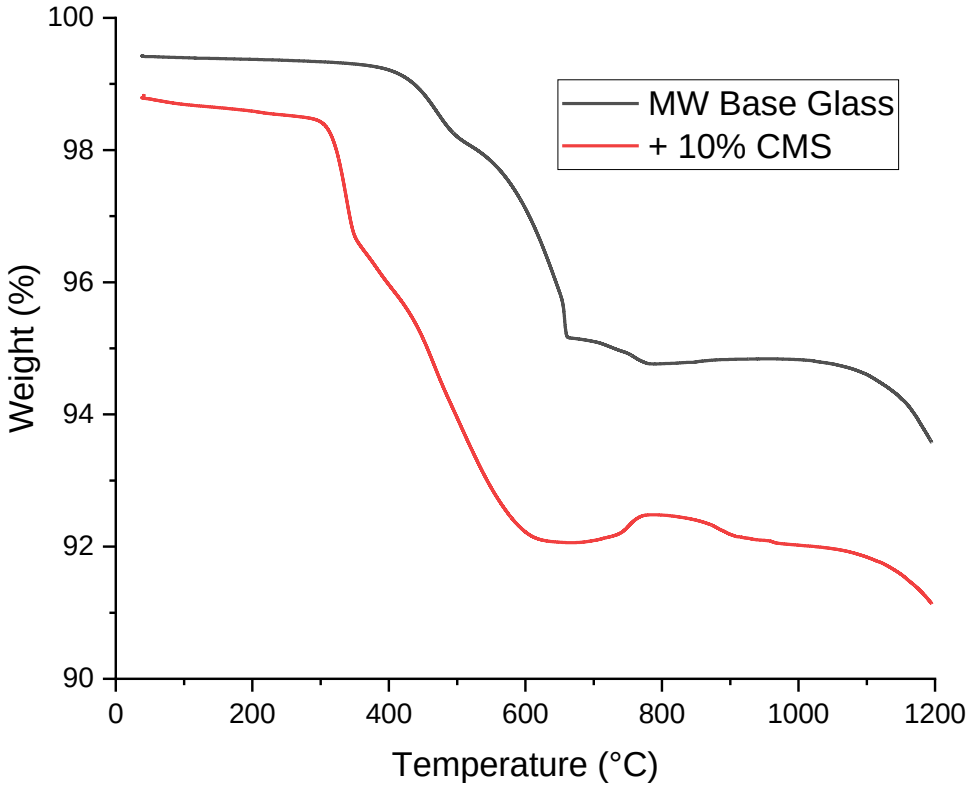

Figure 6.22 TGA data for 5 wt% iodine doped MW glasses with and without the addition of 10 wt% clinoptilolite over the temperature range 0 – 1200 °C

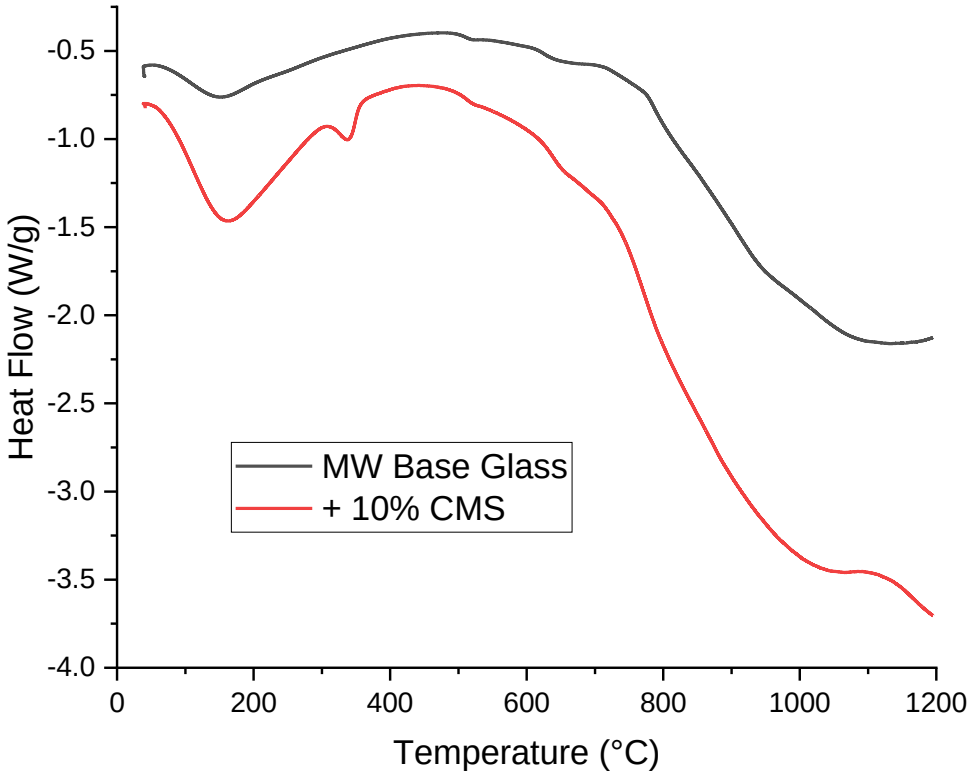

Figure 6.23 DTA data for 5 wt% iodine doped MW glasses with and without the addition of 10 wt% CMS over the temperature range 0 – 1200 °C

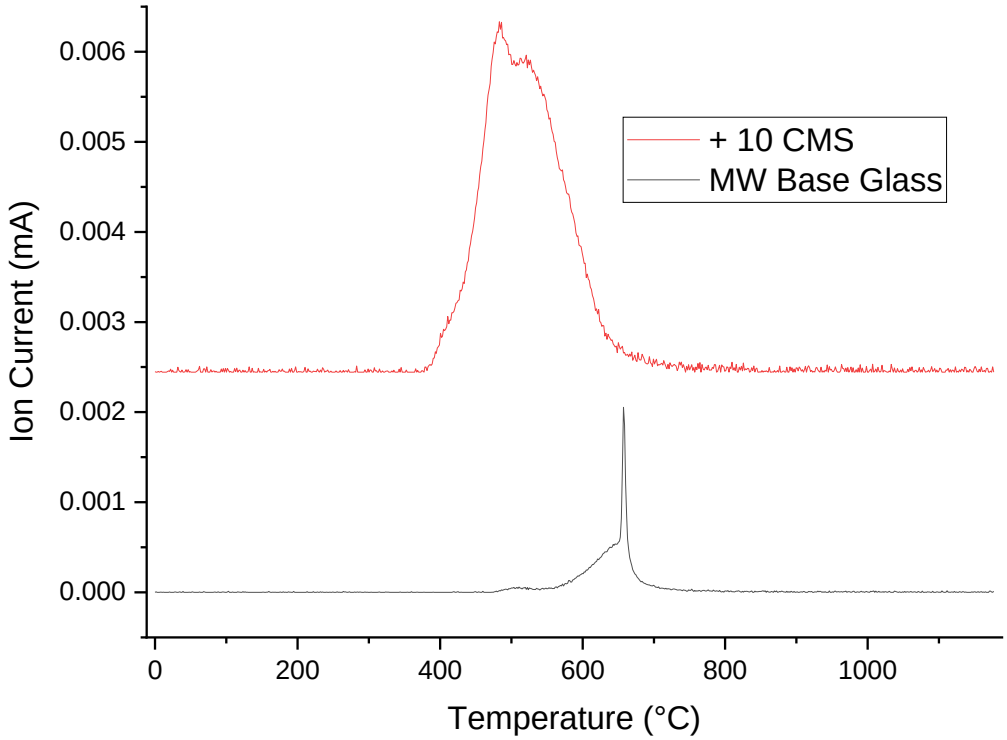

Figure 6.24 MS data traces of 5 wt% iodine doped MW glasses with and without the addition of 10 wt% CMS over the temperature range 0 – 1200 °C. AMU 254.

6.5.2 CaZn Base Glass

6.5.2.1 Clinoptilolite

We have already seen that clinoptilolite can affect the volatility of iodine and caesium in other glass systems, here we will look at the relationship between waste loading of clinoptilolite and volatilisation of iodine from CaZn glass. Firstly, TG analysis was undertaken on samples loaded with 10 wt% clinoptilolite and 5 wt% iodine (figure 6.25). There is a large gradient change seen at 485 °C in the 10% clinoptilolite CaZn sample which begins at a very low temperature (319 °C). The largest changes in mass gradient with respect to temperature have occurred at 436 and 785 °C. The loss at 436 °C is very similar to the trace in the MW glass system for the same additives and previously has been assigned to iodine loss as I_2. In figure 6.26 the DTA data shows the similarities between the clinoptilolite added and clinoptilolite free CaZn glass. The value of T_g is unchanged (525 °C) and most other features and shape are the same when comparing the two, other than some very minor exothermic events that are likely within the error of the instrument.

The MS data in figure 6.27 confirms that the mass loss at 436 °C is from iodine as there was only three AMUs that was detected (127, 253 and 254). The onset and end of the iodine peak in MS is 250 – 510 °C which correspond to the gradient change seen in the TGA. The iodine volatilisation event is at a lower temperature than the base glass (663 °C) which is seen in the MW series also. The comparison of the DTA traces of iodine containing samples seen in figure 6.26 shows very little change upon the addition of clinoptilolite to the CaZn glass, glass transition and melting temperature remain similar. The total mass loss over the whole period for the base glass with 5 wt% iodine is 5.05 % this is increased to 5.87 % in the clinoptilolite loaded samples.

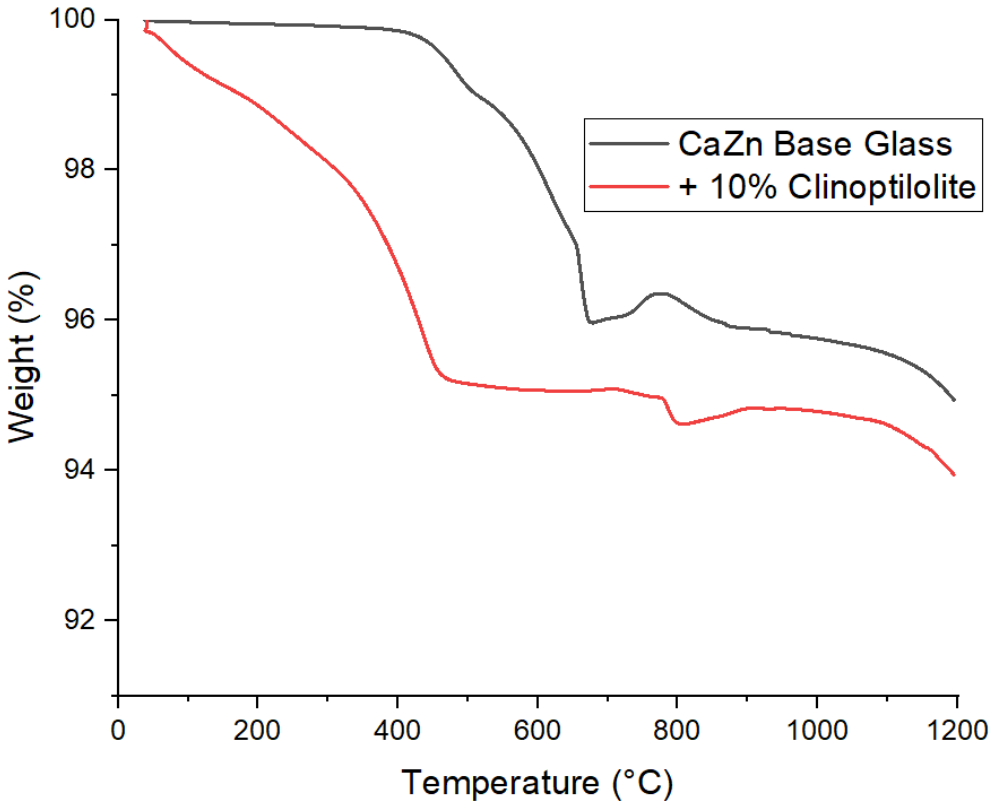

Figure 6.25 TGA data for 5 wt% iodine doped CaZn glasses with and without the addition of 10 wt% clinoptilolite over the temperature range 0 – 1200 °C

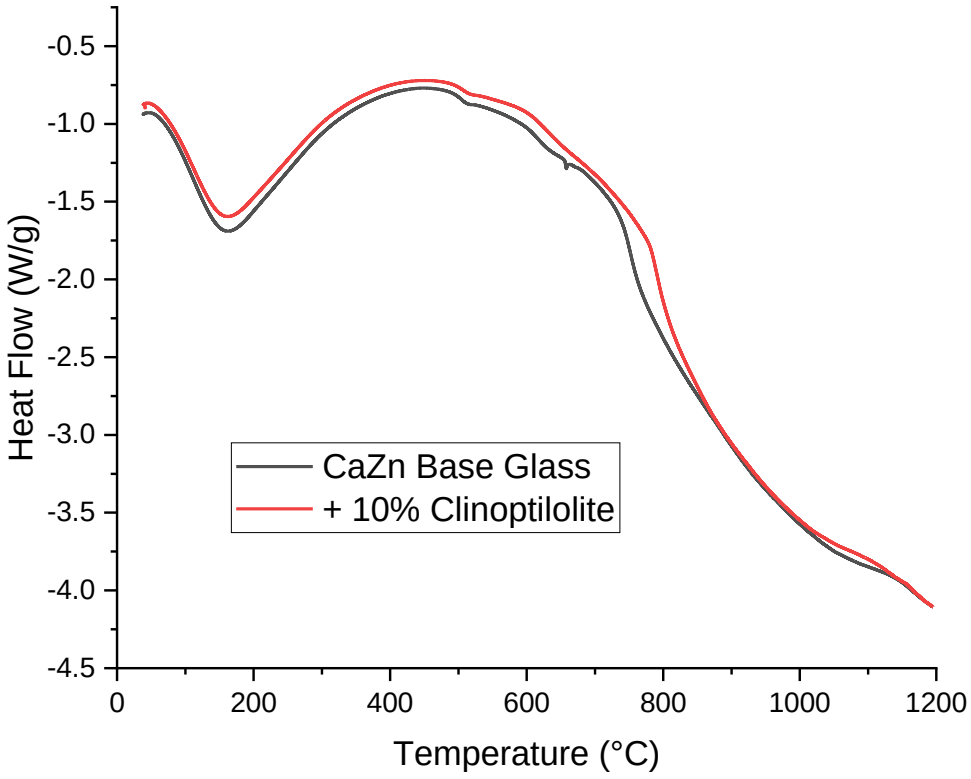

Figure 6.26 DTA data for 5 wt% iodine doped CaZn glasses with and without the addition of 10 wt% clinoptilolite over the temperature range 0 – 1200 °C

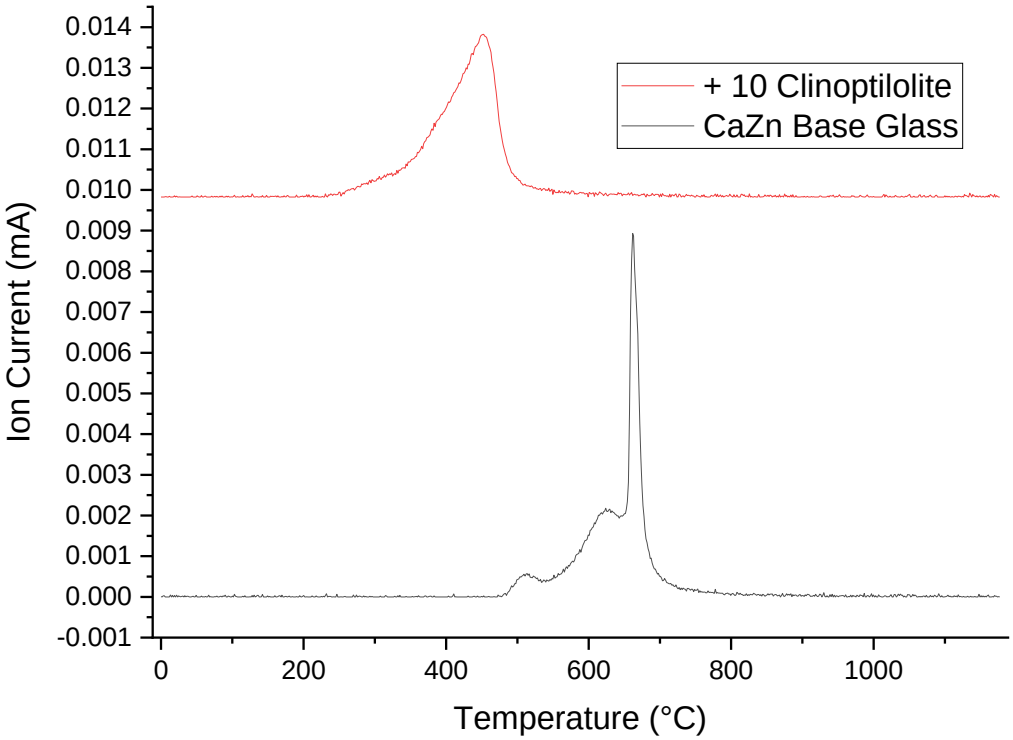

Figure 6.27 MS data traces of 5 wt% iodine doped CaZn glasses with and without the addition of 10 wt% clinoptilolite over the temperature range 0 – 1200 °C. AMU 254.

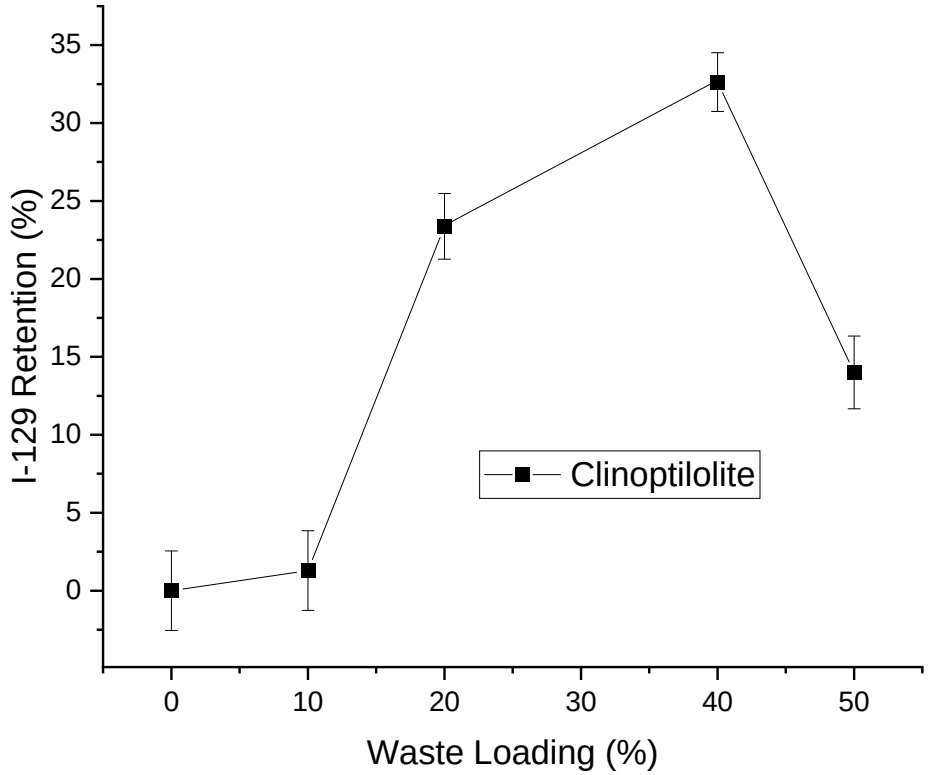

Figure 6.28 Active ^{129}I retention in CaZn glass with the loading of clinoptilolite between 10 – 50 wt% analysed by LSC.

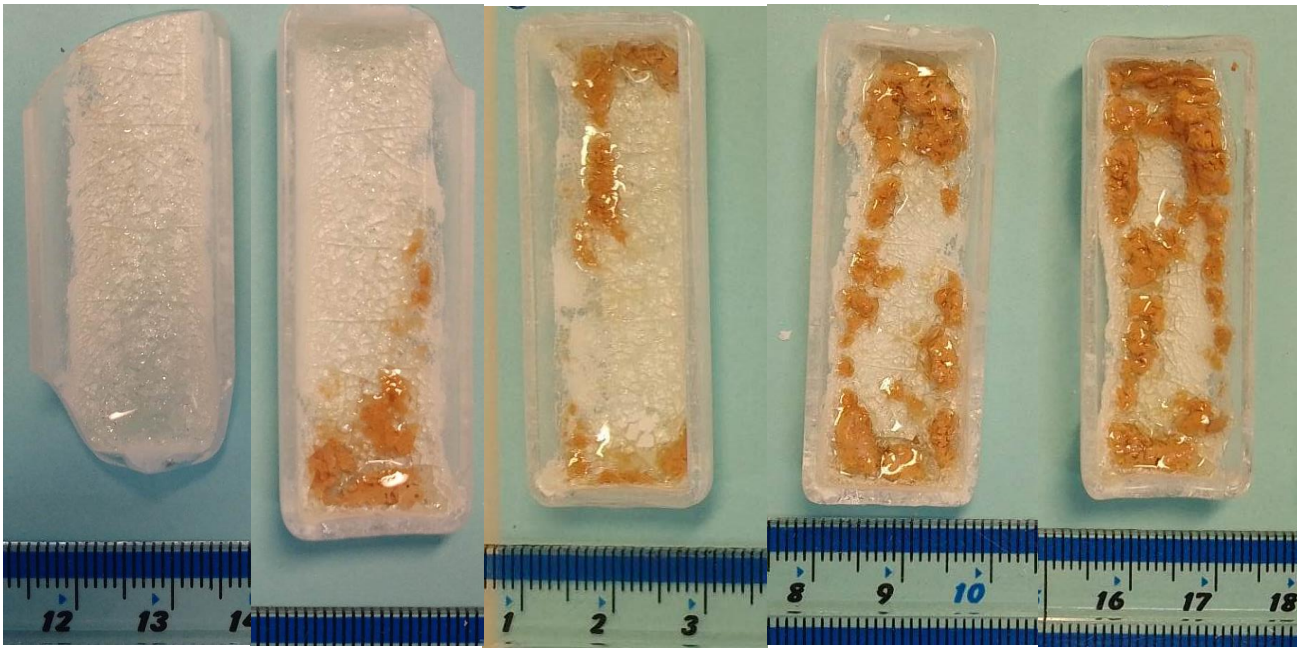

Figure 6.29 Images of clinoptilolite loaded samples in CaZn glass after heat treatment at 950 °C with the addition of 10 bq of ^{137}Cs. Left to right 10, 20, 30, 40, 50 wt%

Active tracers were also used to track the volatilisation of ^{129}I in clinoptilolite containing CaZn glasses between 0 – 50 wt%. Analysis by LSC showed that clinoptilolite increases the retention of ^{129}I from the 0 % retained in the base glass (figure 6.28). The change from retaining nothing to a maximum of 32.63 % at 40 wt% clinoptilolite loading is large and seems conflicting with data shown by TGA where more mass loss was seen when adding clinoptilolite. At 50 wt% loading the retention reduces to 14.00 % which makes the trend non-linear. Images of end products shown in figure 6.29.

6.5.2.2 Corroded Magnox Sludge (CMS)

Thermal analysis of 10 wt% CMS loaded CaZn glass (with 5 wt% I added as NaI) (figures 6.30 and 6.31) showed that there is a significant drop in mass at 295 °C continuing until 651 °C over which 6.73 % of the mass in the sample is lost. The total mass loss for 0 – 1200 °C is calculated to be 7.98 % therefore the majority (84.34%) is lost during the 295 – 651 °C period. Compared to the base glass this amount of weight change is higher due to the CMS addition, the material was measured from a dry state however some of the loss is likely from water or moisture adsorbed during sample preparation (figure 6.33).

The DTA for the same samples (figure 6.31) showed little variation in glass transition and melting from the base CaZn glass to CMS loaded. There is an additional peak in the 10 wt% CMS loaded CaZn sample which does not occur in the CaZn base glass when both are doped with iodine to 5 wt%. This occurs at 341 °C and it present slightly before the major mass loss and H_2O MS detection event. The change is heat flow at this temperature is therefore due to the melting and decomposition of hydroxides in the CMS waste before significant interaction with the glass[22]. Detection of iodine gas (AMU 254) is found to occur in CMS loaded CaZn samples at 515 °C by MS (figure 6.32). The peak in figure 6.36 is broad with the onset of the peak 394 °C ending at 663 °C showing that the iodine emissions are responsible for a portion of the mass loss in the sample. The detection of I_2 in the base glass peaks at 663 °C therefore CMS reduces the temperature at which NaI in converted to I_2.

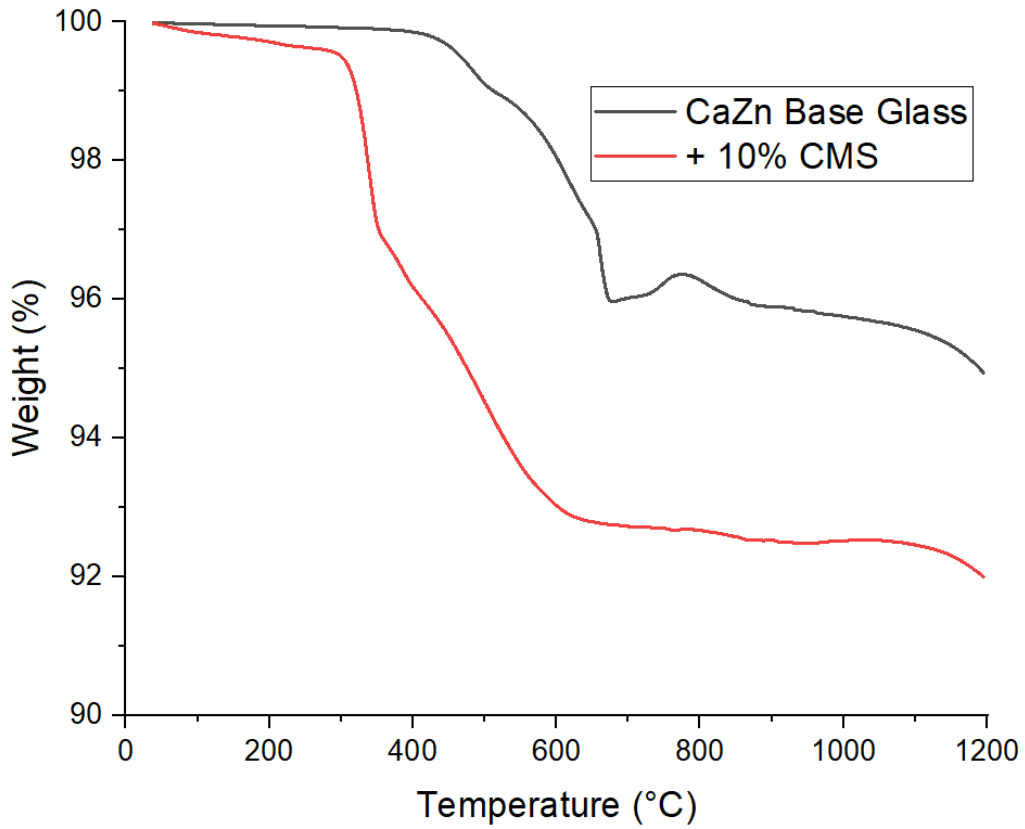

Figure 6.30 TGA data for 5 wt% iodine doped CaZn glasses with and without the addition of 10 wt% CMS over the temperature range 0 – 1200 °C

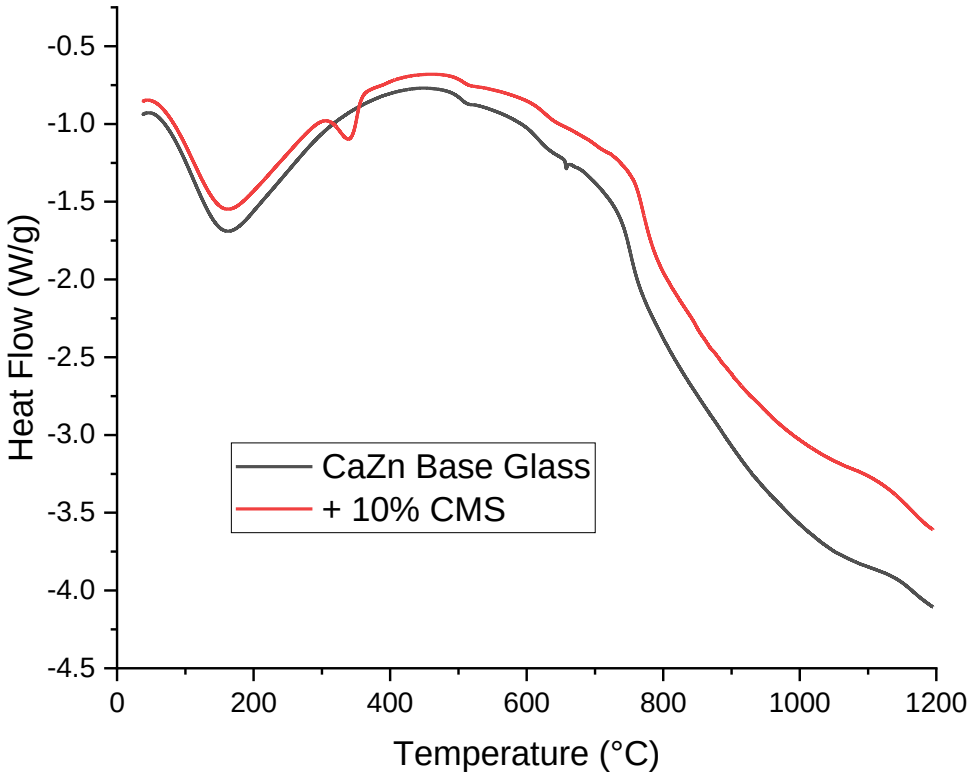

Figure 6.31 DTA data for 5 wt% iodine doped CaZn glasses with and without the addition of 10 wt% CMS over the temperature range 0 – 1200 °C

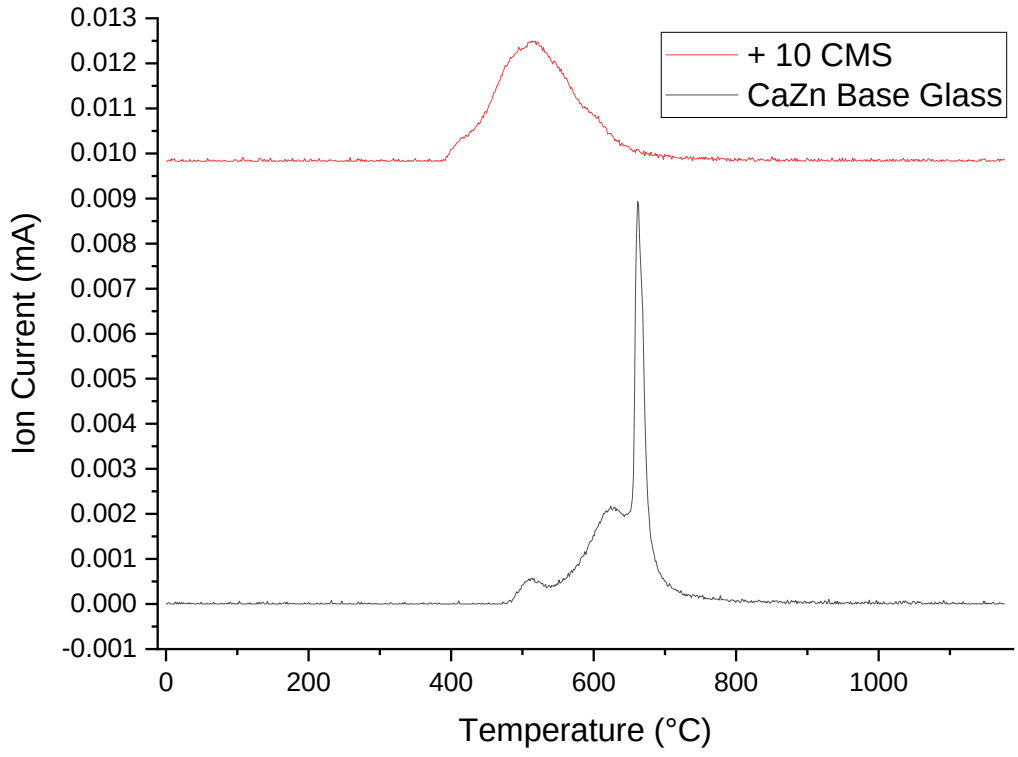

Figure 6.32 MS data traces of 5 wt% iodine doped CaZn glasses with and without the addition of 10 wt% CMS over the temperature range 0 – 1200 °C. AMU 254.

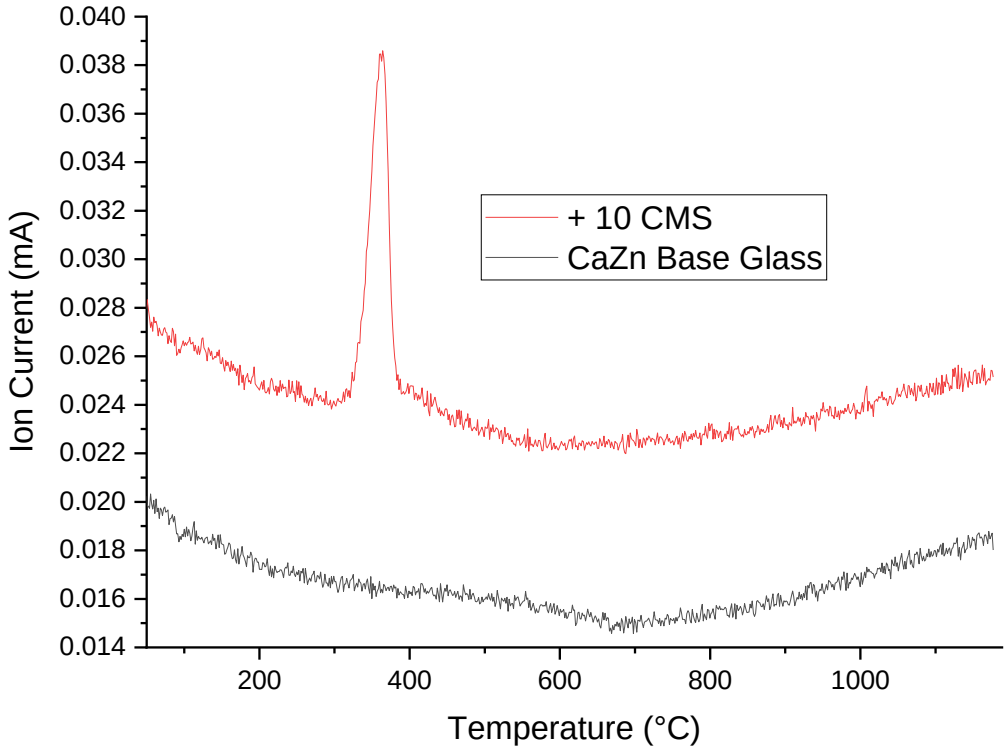

Figure 6.33 MS data traces of 5 wt% iodine doped CaZn glasses with and without the addition of 10 wt% CMS over the temperature range 0 – 1200 °C. AMU 18.

Using active ^{129}I tracers the emission of iodine from CaZn glass was determined with waste loadings of 10 – 50 wt%. Figure 6.34 shows the trend that iodine capture from glass heat treatment follows upon the addition of CMS to the fritted glass. Initially the activity of the capture solutions slightly decreases linearly to 40 wt% indicating a retention increase in the product. The maximum retention of the sample was 4.53 wt% at 40% CMS concentration by weight, however, upon an increase in waste loading to 50 % the capture solutions contained almost all the iodine added indicating a poorer retention of 0.82 wt%. The initial increase in linear with a r^2 of 0.980 and a slope of 0.11. Images of the samples in figure 6.35 shows that some waste in most samples has either recrystallised or not digested whilst heating, particularly the 50 wt% sample that appears to have exposed dry powder from undigested CMS.

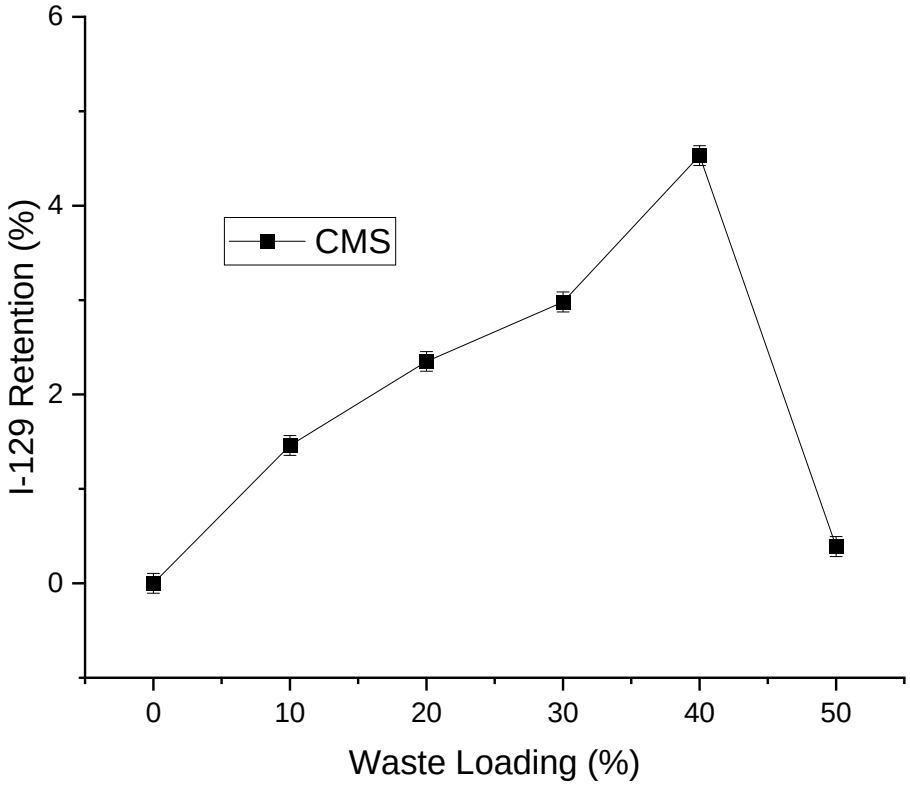

Figure 6.34 Active ^{129}I retention in CaZn glass with the loading of CMS between 10 – 50 wt% analysed by LSC

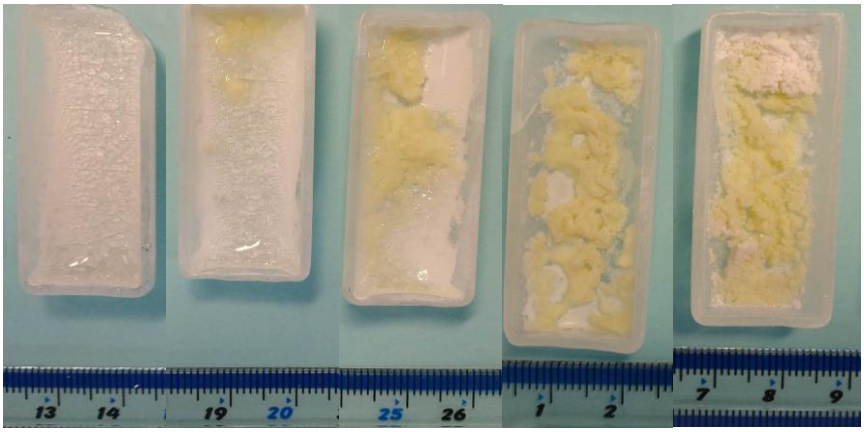

Figure 6.35 Images of CMS loaded samples in CaZn glass after heat treatment at 950 °C with the addition of 10 bq of ^{137}Cs. Left to right 10, 20, 30, 40, 50 wt%

6.5.3 0% SiO_2 CaZn Base Glass

6.5.3.1 Clinoptilolite

The section will focus on the effects of iodine retention on clinoptilolite additions into a different glass system, 0% SiO2 CaZn base glass, analysed by pyrolysis with ^{129}I active tracers. Figure 6.36 shows the change in retention of ^{129}I on 0 – 50 wt% additions of clinoptilolite to the glass melt. In this data we

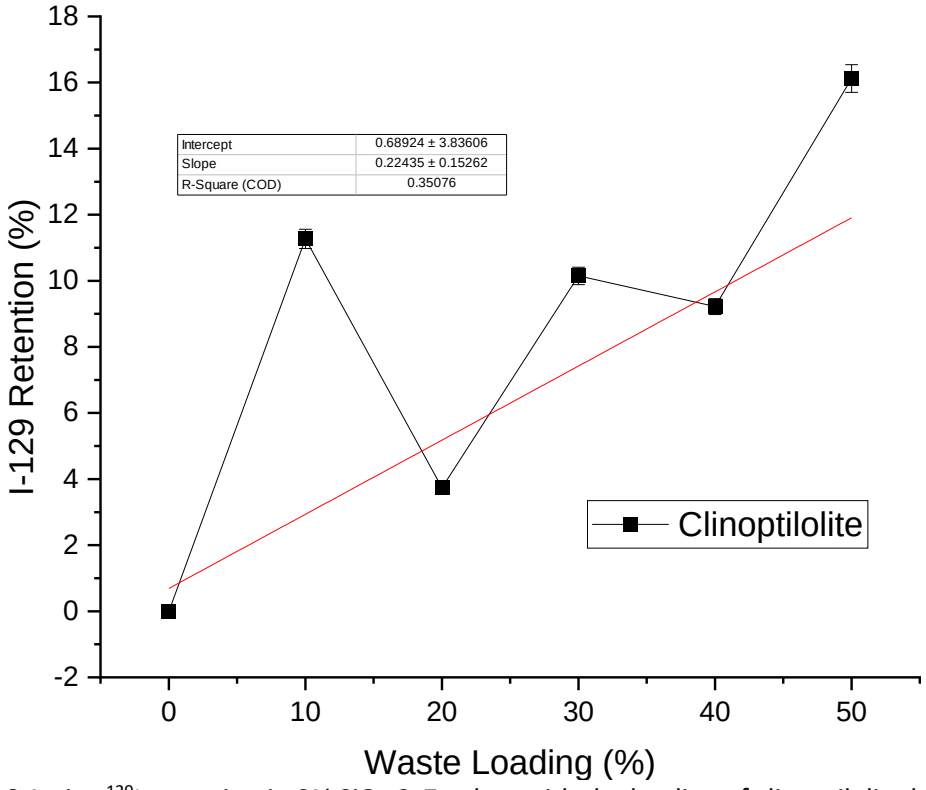

Figure 6.36 Active ^{129}I retention in 0% SiO_2 CaZn glass with the loading of clinoptilolite between 10 – 50 wt% analysed by LSC. Some of the error bars are smaller than the points. Red line represents a linear fit trendline.

can see there is a general positive trend towards more clinoptilolite contributing to more retention in the glass or glass/ceramic system, the maximum (16.12 %) being reached at 50 wt% waste loading. This trend is poorly linear with an r^2 value of 0.351 and a gradient of 0.224 +/- 0.15. We have seen a similar trend CaZn samples (figure 6.28 in section 6.5.2.1) upon clinoptilolite addition, however, the higher waste loadings see the retention decrease again. This changes because of the high boron glass composition, 0% SiO_2 CaZn glass has large differences in structure and silica content compared to MW and CaZn. Silica from the clinoptilolite is likely incorporating into the glass without crystallisation and not creating two phases like is present in the MW and CaZn samples. This can be seen in figure 6.37 where the glass product appears homogeneous in nature with no visible signs of crystallisation. In addition, the forming elements of the glass change during the clinoptilolite addition, boron units are the predominant glass forming element until higher waste loadings where this is overcome by silica tetrahedra.

Figure 6.37 Images of Clinoptilolite loaded samples in 0% SiO_2 CaZn glass after heat treatment at 950 °C with the addition of 10 bq of ^{137}Cs. Left to right 10, 20, 30, 40, 50 wt%

6.5.3.2 Corroded Magnox Sludge (CMS)

In the same glass system CMS has an effect on ^{129}I retention in the system, again analysed by LSC. The trend of this series from 0 – 50 wt% CMS is seen in figure 6.38. The retention appears to increase upon increasing CMS concentration from a minimum of 0 % retention without the addition of CMS to a maximum of 4.67 wt% at a CMS loading of 50 wt%. This trend is linear with an r^2 equalling 0.856 and

a slope of 0.086 +/- 0.018. This is more linear than the clinoptilolite trend for the same glass, however, the retention benefits are lessened for the CMS containing samples. Images of the samples (figure 6.39) show no major unmelted CMS in the sample until 40 wt% waste loading, even these samples appeared single phase although more testing would have to be done to explore this.

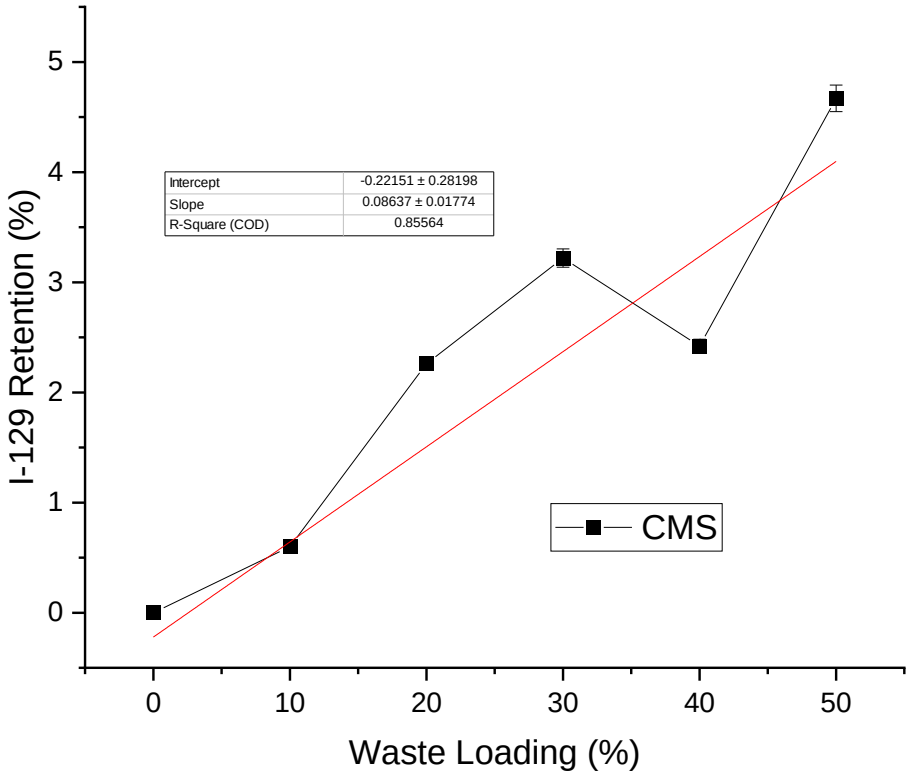

Figure 6.38 Active ^{129}I retention in 0% SiO_2 CaZn glass with the loading of CMS between 10 – 50 wt% analysed by LSC. Red line represents a linear fit trendline.

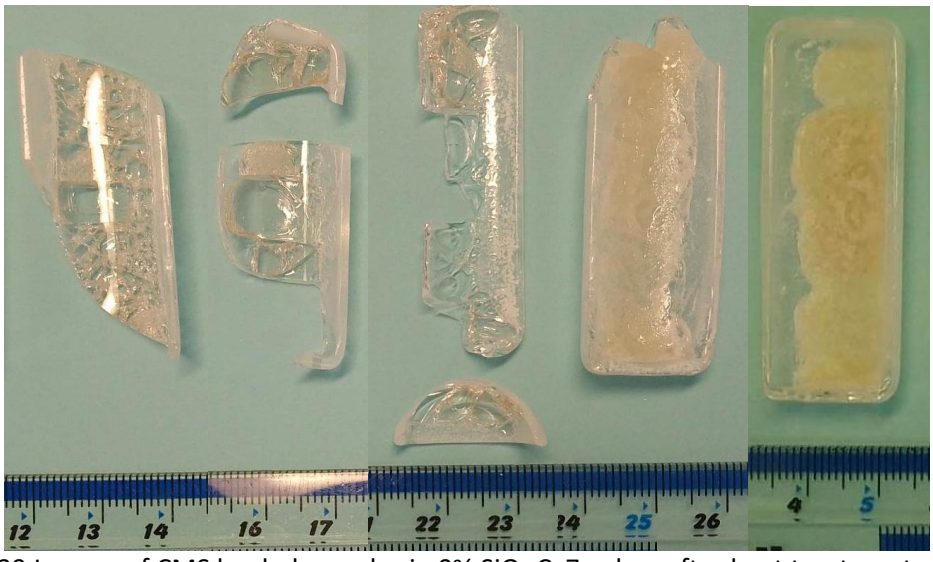

Figure 6.39 Images of CMS loaded samples in 0% SiO_2 CaZn glass after heat treatment at 950 °C with the addition of 10 bq of ^{137}Cs. Left to right 10, 20, 30, 40, 50 wt%. Some samples broke on removal from the furnace work tube.

6.6 Effect of Ion Exchanged Clinoptilolite on Volatility

6.6.1 Ion Exchanged Clinoptilolite

Firstly, to understand the capabilities of the caesium loaded raw material it was heated alone at 1150 °C in an alumina crucible for 2 hours. The resultant material was fused, appeared dark brown in colour and ceramic in texture and hardness. It is interesting that the raw material alone can sinter into a ceramic material as this could shows that there is a potential for clinoptilolite to be heat treated without any glass forming additives. The XRD of the final product (figure 6.40) showed very little crystal character indicating that it was mainly amorphous, however, there were some peaks relating to one crystal phase. The crystalline phase present in the material was found to be caesium aluminium silicate, some minor peaks were dwarfed by a large amorphous hump. This could indicate the crystals in this sample make up a small proportion of the whole amorphous bulk.

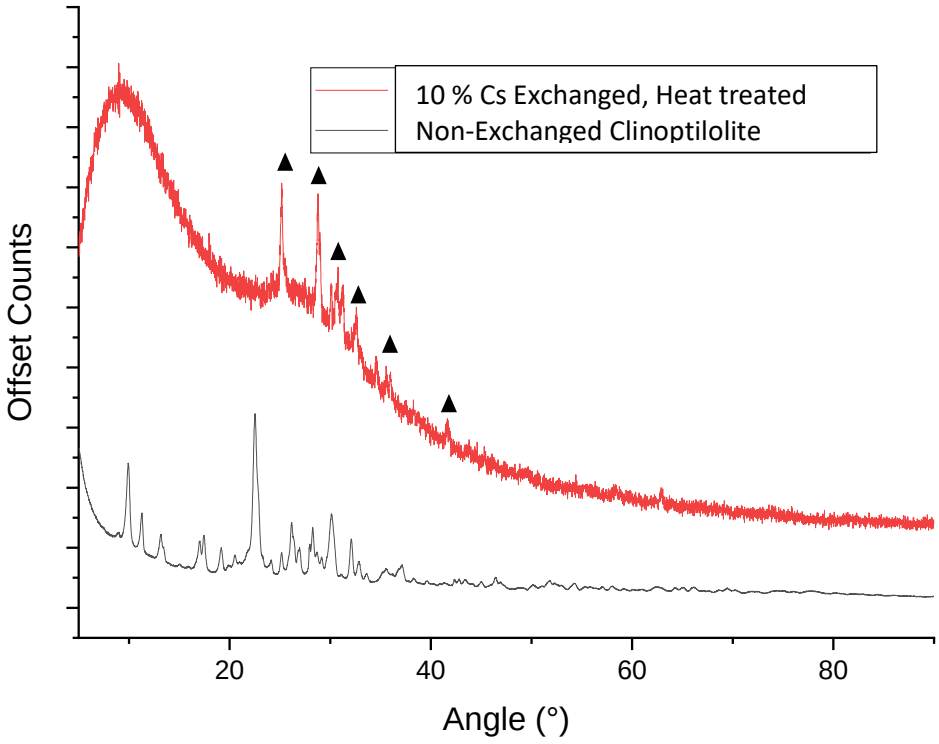

Figure 6.40 XRD trace of 10 wt% Cs exchanged clinoptilolite heat treated at 1150 °C for 2 hours. Crystalline phase ▲= Caesium aluminium silicate, $Cs_{0.804}AlSi_5O_{12}$ (Phase ID: 01-076-8641).

Elemental analysis of the exchanged and non-exchanged samples after heat treatment showed small changes in the composition between the two. The main changes were in the caesium concentration

remaining in the end products, the other elemental components of the material varied very little as the state of the material did not change between samples. Caesium however, was likely in a different state for either sample due to the occlusion method and therefore has different volatility properties. Table 6.4 shows the XRF data from the heat treated exchanged and non-exchanged samples. The caesium content in the end product was higher in exchanged samples (14.47 +/- 0.95 wt%) than in non-exchanged (13.07 +/- 0.86 wt%).

	Component Abundance (wt%)					
	SiO_2	Al_2O_3	K_2O	CaO	Fe_2O_3	Cs_2O
Non-Exchanged	12.38	65.43	2.48	3.81	1.49	13.1
Exchanged	11.83	61.60	2.58	3.85	1.54	14.47

Table 6.4 XRF data of heat treated (1150 °C) clinoptilolite exchanged or doped with 10 wt% Cs added as Cs_2CO_3 (13.5 wt%).

This is likely due to the occlusion method causing the caesium ions to be incorporated into the structure of the clinoptilolite network and requiring more energy to volatilise due to the stability of the ion in the clinoptilolite 'holes'. When in a glass structure however, this effect does appear to differ.

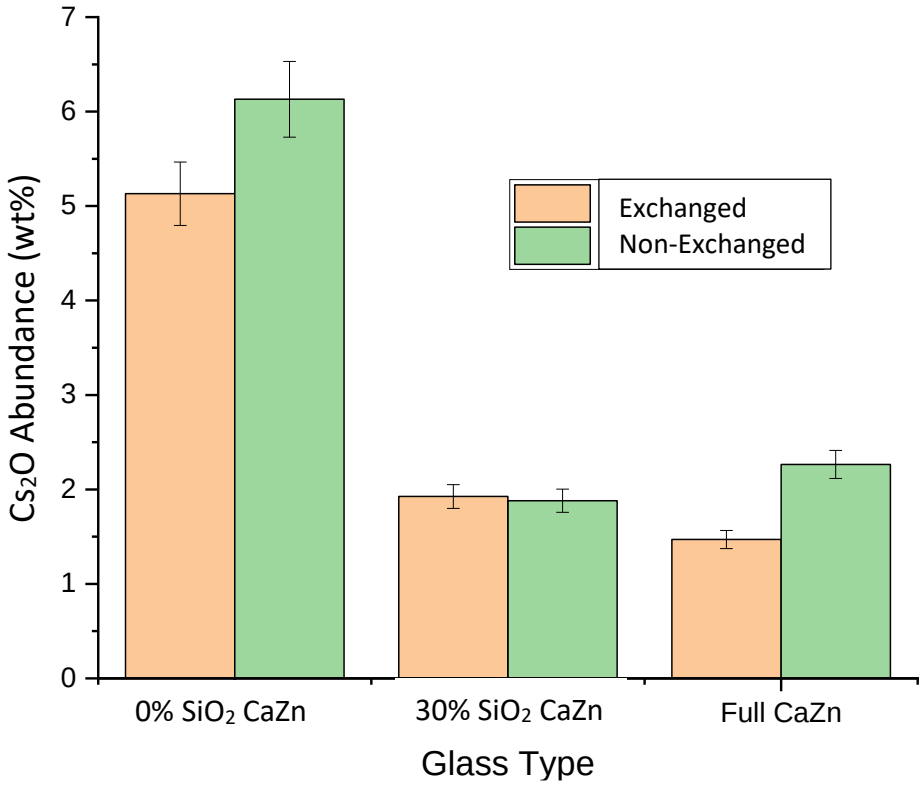

Figure 6.41 Cs_2O concentration by XRF of heat treated (1150 °C) clinoptilolite exchanged or doped with 10 wt% Cs added as Cs_2CO_3 mixed into glass systems 0% SiO_2 CaZn, 30% SiO_2 CaZn and full SiO_2 CaZn at 50 wt% loading (target 5 wt% Cs).

Comparing the caesium concentration in exchanged and non-exchanged clinoptilolite samples heated at 1150 °C (figure 6.41) we see that in borate 0% SiO_2 CaZn modified glass (loaded with 50 wt%) non-exchanged clinoptilolite retains better than exchanged opposite to the effect seen in the raw material. 50 % of the mass of the sample was clinoptilolite (exchanged or not) and the occlusion concentration was 10 wt% Cs therefore 5 wt% of both samples was contributed to by caesium when accounting for the mass of the glass. We do see that in the 0% SiO_2 CaZn glass the concentration raises above 5 wt% which is unexpected however this is theorised to be due to the carbonate loss in this sample whereas the carbonate is washed out during the exchange process in the other sample. Using this we can see most of the caesium has retained in both systems (note that the XRF data shown is for Cs_2O not for Cs alone). The caesium concentration in 30 % SiO_2 glass is very similar between the two clinoptilolite materials after heat treatment and in full CaZn the trend is similar to the 0 % SiO_2 glass variant where non-exchanged retains caesium better. The crystalline behaviour of this series is amorphous by XRD for 30 % and full CaZn (exchanged and non-exchanged) expected based on previous studies into this glass system with similar clinoptilolite loadings. The 0 % SiO_2 CaZn glass with 50 wt% loading did have some peaks in the XRD for both clinoptilolite variants. This was assigned to a leucite structure with general formula $Cs_8Al_8Si_{16}O_{48}$ consistent for both samples, however, the intensity of the peaks associated with this crystal was higher in the non-exchanged sample.

6.7 Summary

Two representative UK ILW streams currently being considered for thermal treatment were investigated, namely CMS and clinoptilolite, with some minor investigations into additives that may be used in the future, Xanthan gum and graphite. These were loaded into three parent glasses, MW, CaZn and 0% SiO2 CaZn.

	Loading at which crystallisation occurred (%)	
Glass Type	CMS	Clinoptilolite
MW	20	40
CaZn	20	40
0% SiO_2 CaZn	40	>50

Table 6.5 Waste loading at which crystallisation occurred by XRD.

The loading at which crystallisation of the end product occurred changed depending on the glass type, seen in table 6.5. The glass type that was able to accept the most waste without peaks appearing in the XRD was the 0% SiO_2 CaZn composition. This is understandable for clinoptilolite waste as the structure contains many glass forming oxides (SiO_2, Al_2O_3) and modifiers (K_2O, CaO) that make it a perfect material for incorporation in borate glass to form a borosilicate network. With sufficient melting time and temperature (2 hrs at 1150 °C) up to 50 wt% loading of clinoptilolite was possible without the sample having crystallisation. CMS loading was also higher in 0% SiO_2 CaZn glass (40 wt%) than the other types (20 wt%). Oxides of magnesium are the primary component of this waste and therefore we can see that magnesium incorporates better into the borate glass than borosilicate glasses. This is likely due to the higher proportion of charge compensating borate tetrahedra which are able to stabilise for Mg^{2+} ions.

CMS has an interesting thermal decomposition effect visible in most TGA traces where gradual mass loss occurs between 250 – 500 °C. This is because of the small proportion of magnesium hydroxide material in the waste decomposing into water and MgO. Literature states a thermal decomposition temperature[219] of 380 °C, during the mass loss event we see in the TGA in figure 6.30. Looking at the MS data from this MW and CaZn samples for detection of AMU 18 (e.g. figure 6.33) we see a large peak at 364 °C from H_2O emission. The likelihood is that $Mg(OH)_2$ in the raw material is undergoing a thermal decomposition reaction and is emitting water contributing to the higher mass loss seen. For waste thermal treatment this should be factored in to weight loss calculations as $Mg(OH)_2$ may contribute to more losses and emission of water.

The effect on retention of iodine and caesium from clinoptilolite loading was positive for most glasses, generally up to its crystallisation limit. This was most noticeable for 0% SiO2 CaZn glass which retained the most at 50 wt% loading after a steady increase in all samples (table 6.6). Clinoptilolite increased the retention of caesium by 13.29 % in CaZn glass and 19.23 % in the 0% SiO_2 CaZn glass with a drop in retention only seen in CaZn where the retention reduced after 30 wt% loading. CMS only had a

minor positive effect for caesium on the 0% SiO_2 CaZn glass and a negative effect for CaZn glass retention reducing by 19.7% over the 0-50 wt% loading period. Iodine volatility, however, did decrease from the addition of CMS ~4.6% for both glass systems.

	Maximum Caesium Retention (%)			Maximum Iodine Retention (%)		
Glass Type	Base	CMS	Clinoptilolite	Base	CMS	Clinoptilolite
CaZn	75.55	75.55	88.88	0	4.53	32.63
Loading (wt%)	0	0	30	0	40	40
0% SiO_2 CaZn	69.28	83.43	88.23	0	4.67	16.12
Loading (wt%)	0	10	50	0	50	50

Table 6.6 Maximum caesium and iodine retention as measured by pyrolysis method (^{137}Cs in product, ^{129}I in captured gas). The loading at which a maximum occurs is denoted under the retention value. MW was not investigated by radioactive tracer method and therefore is not included.

Photos in figure 6.42 show that crystallisation appears only in the exchanged samples, found to be caesium aluminium silicate by XRD. These only occurred in the white spots whereas the brown sections of the bulk for both samples were predominantly amorphous. This data highlights the need for research into thermal treatment of raw clinoptilolite because as a wasteform it may have all the requirements for a stable final wasteform by itself after heat treatment even at lower operating temperatures (950 - 1150 °C). Data indicates a trend based on the oxides donated into the glass from the parent waste.

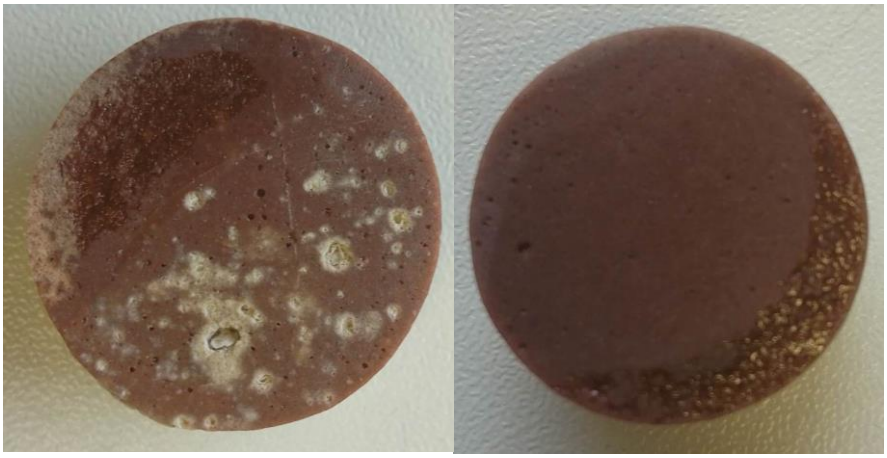

Figure 6.42 1150 °C Heated treated clinoptilolite with 10 wt% caesium added as caesium carbonate either exchanged (Left) or non-exchanged (Right).

For example, Matousek[220] demonstrates an increase in silica content increasing the partial pressure of alkali gaseous species above the liquid melt in models, however, this only occurs noticeably above 1100 °C therefore this effect may not influence the volatility of caesium with silica containing clinoptilolite addition.Guo[221] states that magnesium content has little effect on the primary dissolution of the glass, however, instead increases the viscosity and adds charge compensating Mg^{2+} ions which can allow more additions by balancing the charge from added contaminants. These perform in a similar way to Ca^{2+} ions, however, are less effective. Magnesium contributions from CMS could therefore be the reason why benefits to iodine/caesium retention are seen and using a similar rational, calcium from clinoptilolite. Tan et al[8] also indicates that CMS has a small negative effect on caesium retention and a large negative effect on chlorine at 40 wt% in a similar borosilicate nuclear waste glass. This is similar to our observations as at 40 wt% loading of CMS we see a decrease in retention of caesium and only minor effects below this. The effect of magnesium on the structure of these borosilicate glass systems is primarily on the amount of non-bridging oxygens (NBOs). The forming elements of the glass (SiO_2 and B_2O_3) are reduced in concentration and substituted with MgO and Mg^{2+} ions which cannot glass form. This works essentially as a filler material which reduces the proportion of NBOs and to the extend where any excess magnesium cannot insert into the structure and instead remains as a magnesium crystallite in the liquid glass melt. When cooled the magnesium mineral (dispersed through the glass) crystallises.

Occlusion (or ion exchange) of caesium into clinoptilolite reduced the ability of the glass/clinoptilolite composite to retain the element which opposes our predicted outcome. The initial thinking was that exchanged caesium would require more energy to remove from the structure of clinoptilolite and then subsequently volatilise than compared to caesium dried onto clinoptilolite. This may not be the case, however, because it appears that caesium dissociates from the clinoptilolite structure. This however does have implications for the treatment of this waste at Sellafield. For example, our data in figure 6.41 suggests that, in CaZn glass, ion exchanged clinoptilolite volatilises more than if caesium is dried onto the glass frit.

Chapter 7 Effect of Atmosphere on Volatility

7.1 Introduction

The gas composition above the heat treated glass/waste materials has been shown to have an effect on the composition of the end products (see sections 2.3 and 2.4) and gases emitted. The chemistry of a melting glass for example is affected by the presence of oxygen. Oxygen in some glass/material interactions can act as an oxidising agent which accelerates the rate of decomposition of raw materials and create high temperature crystalline phases. The properties of the glass or ceramic can then be manipulated by changing the atmosphere above the heat-treated material. 'Inert' atmospheres such as argon and nitrogen can be utilised for the purposes of changing the volatilisation properties of a system. In this section we utilise nitrogen gas atmospheres as a candidate for use in the nuclear industry vitrification systems to allow for more control of volatility from high temperature processes.

7.2 Methodology

All the previous measurements/techniques involving heat were completed in air (furnace, pyroliser, TGA). In section 7.3, to understand the effects of oxygen on the glass melt we performed two sets of experiments which were completed with an oxygen free, nitrogen atmosphere. The analyte we will be researching in iodine in both active and inactive forms and there is a small discussion on caesium in its active form (isotope 137). Glasses under investigation were MW and CaZn (compositions found in table 4.1, section 4.3.1) which were analysed by TGA, DTA and MS to determine at what temperature iodine related thermal events took place. These include iodine volatilisation/decomposition temperatures, glass transition temperatures, glass melting temperatures and mass loss. Method for this can be found in section 3.3.5.2, the specific iodine dopant used as an iodine source using this method was NaI which was added to 1.15, 5.77 and 11.53 wt% which equates to 1, 5 and 10 wt% iodine content discounting the contribution from the sodium counterion.

The other glass systems discussed is 0% SiO_2 CaZn (composition found in table 4.4, section 4.7) from which iodine volatilisation was analysed using the active ^{129}I capture from pyrolysis method (see section 3.3.6). 20 g samples of powdered glass were doped with 1ml of water solution containing 20 bq ^{129}I and then heat treated to 950 °C for 2 hours any emitted gases were captured in solution and counted for radioactivity. The difference in radioactive between the start (added to glass) and end (captured in solution) gives us our total retention factor. For samples containing waste, dried clinoptilolite or corroded Magnox sludge was mixed with the powdered glass before doping with iodine. Error was calculated from the radiation counter (liquid scintillation counter) instrument.

Caesium is discussed at the end of the section, however, at this time only the iodine containing samples were run on the TG-MS because of the risks of contamination from caesium and chlorine, however, pyrolysis included ^{129}I and ^{137}Cs.

7.3 Effect of Air and Nitrogen Atmospheres

Firstly, base glass TGA data in shows us that, for iodine doped samples, the total mass loss trend is similar when comparing samples treated under air (figures 5.18, 5.19 (MW) and 5.28, 5.29 (CaZn)) or nitrogen (figures 7.1 and 7.3) and heated up to 1200 °C. Overall the glasses lose slightly more mass overall when under nitrogen (comparison shown in table 7.1).

Conditions and Glass Type with 5% Iodine	Total Mass Loss (%)	Iodine Mass Loss Temperature (°C)	Iodine Mass Loss (%)
Air – MW	5.828	367 - 670	4.071
Air – CaZn	5.046	311 - 682	3.870
Nitrogen – MW	6.913	425 - 960	4.360
Nitrogen – CaZn	6.482	495 - 951	4.734

Table 7.1 Comparison of iodine containing MW and CaZn glasses under air and nitrogen atmosphere.

MW glass still loses more mass than CaZn in total, however, the effect is larger than in air. The most noticeable change is the temperature at which this volatilisation occurs. For the samples heated in air the mass loss event has a steeper gradient and ends at 670/682 °C whereas the nitrogen atmosphere samples finish their slope at 951/960 °C. As can be seen in figure 7.1 and 7.3 there is an interruption during this major mass loss event where the mass seems to rise by ~0.4 wt%, this does not occur in

most samples treated under air however in figure 5.28 there is a similar effect. The peak position is at around 870 °C for all samples under nitrogen other than the CaZn 1 wt% iodine doped which does not appear to show this effect. If the rise in mass is associated with the iodine containing glass samples under nitrogen this could be a result of several effects:

- Re-absorption of iodine containing gases from the melt surface back into the glass structure
- Buoyancy effects from gases rising through the molten glass
- Nitrogen interactions with the glass

Equilibrium should not favour the re-absorption of iodine bearing gas species as the flow of nitrogen should carry the volatile away and reduce the concentration above the melt. However, if the gas flow was not high enough there is the potential for species to interact with the molten glass surface and reincorporate. Buoyancy effects are possible as the gas rises and appears as if the sample has lost more mass, however, this would have to be a very large proportion of the sample for this to occur and we still see this effect in the 1 wt% iodine MW sample therefore this is unlikely. Nitrogen interactions are possible, however, the gas is very inert in the systems we are discussing and it is unlikely that nitrogen is reacting with the glass or iodine. Therefore, we propose a disproportionation reaction that could be occurring by reaction of iodine gas bubbles with the liquid glass system.

$$2NaI_{(l)} + O^{2-}{}_{(l)} \rightarrow Na_2O_{(l)} + I_{2(g)}$$

$$3I_{2(g)} + 3Na_2O_{(l)} \rightarrow NaIO_{3(l)} + 5NaI_{(g)}$$

This includes an iodate species as an intermediate compound which decomposes at a higher temperature into I_2 gas[39]. This could be one explanation as to the increase in mass at 870 °C as volatilised iodine incorporates back into the glass structure temporarily.

DTA analysis produces very different results in nitrogen compared to the air atmosphere samples, there are many extra, small endothermic peaks. Previously, we have discussed DTA data from the samples in air (figures 5.19 and 5.29) which show a mainly smooth transition in heat flow with glass

transition temperature and melting temperatures observable and no other peaks. In nitrogen atmosphere the samples change at 5 – 10 wt% iodine loading in both MW and CaZn glass. The largest and first of the peaks occurs at 657 °C exactly for MW and CaZn glasses at 5 and 10 wt% iodine. Given that it does not change between systems this endothermic event is likely the melting of NaI.

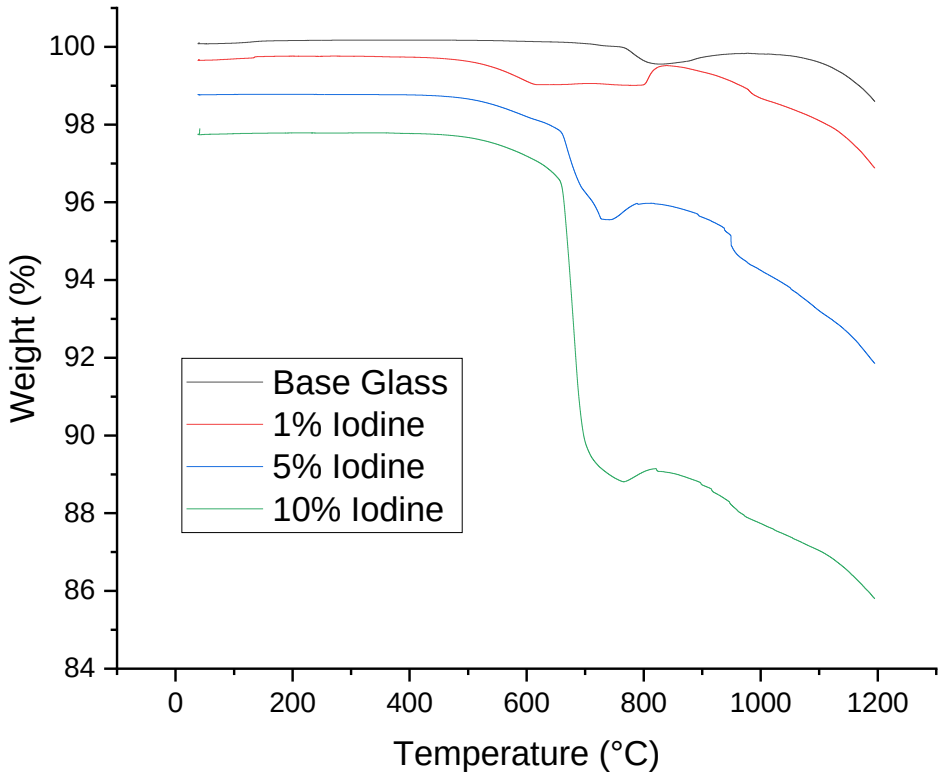

Figure 7.1 TGA trace of MW base glass in heated in nitrogen atmosphere with additions of 0, 1, 5 and 10 wt% iodine added as NaI

The other DTA peaks are small and sharp, in the MW glass these appear at 821 and 950 °C and at 779, 832, 888 and 936 °C in the CaZn glass. Given that these are different between glass systems and only appear in iodine containing samples these thermal events must be related to NaI, I_2 or other intermediate species interacting with the glass. The fact that these peaks occur at higher temperatures indicates that iodine is remaining until later in the heating process. Mass spectrometry data confirms this theory as seen in figures 7.5 and 7.6. The intensity of AMU 254 (I_2) is shown to occur at a much higher temperature than previous measurements for MW (figure 5.18, section 5.4.2.1) and CaZn (figure 5.28, section 5.4.3.1) in air 5 and 10 wt% iodine samples still emitting at 1200 °C in comparison to the samples in air which concluded iodine emission at ~675 °C.

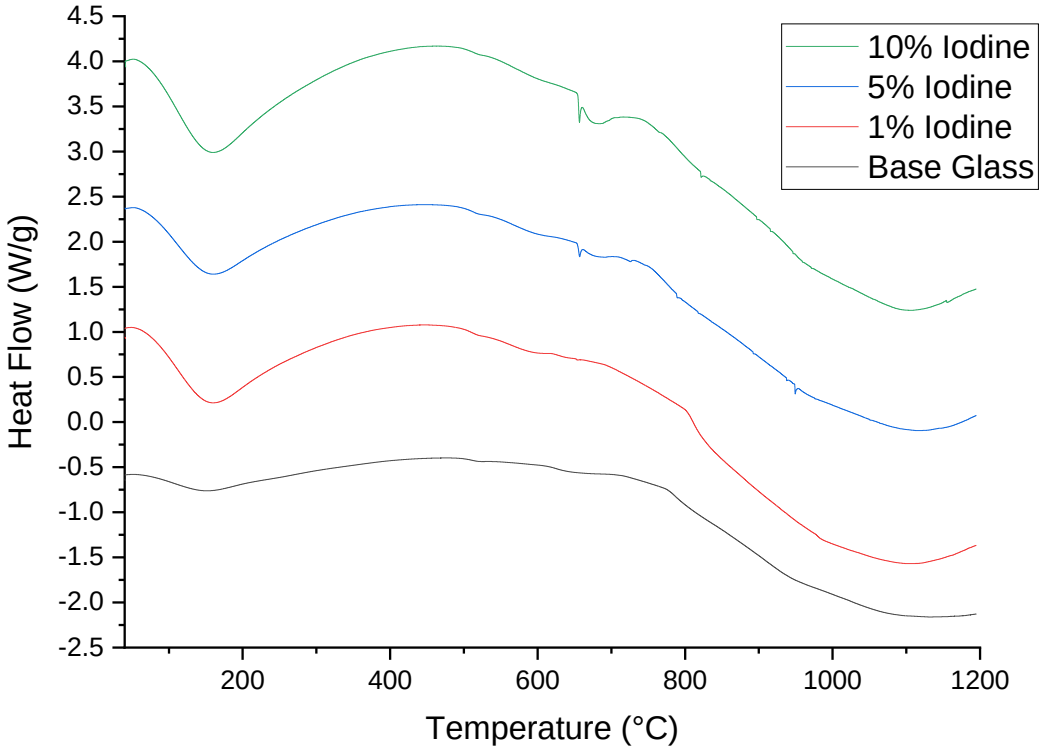

Figure 7.2 DTA trace of MW base glass heated in nitrogen atmosphere with additions of 0, 1, 5 and 10 wt% iodine added as NaI

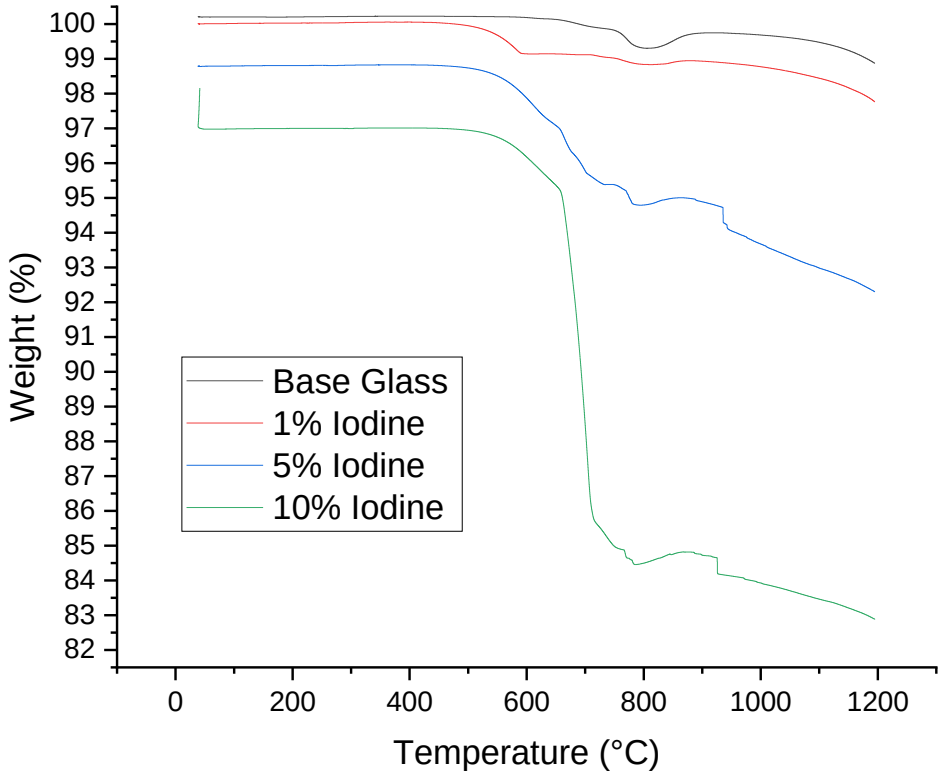

Figure 7.3 TGA trace of CaZn base glass heated in nitrogen atmosphere with additions of 0, 1, 5 and 10 wt% iodine added as NaI

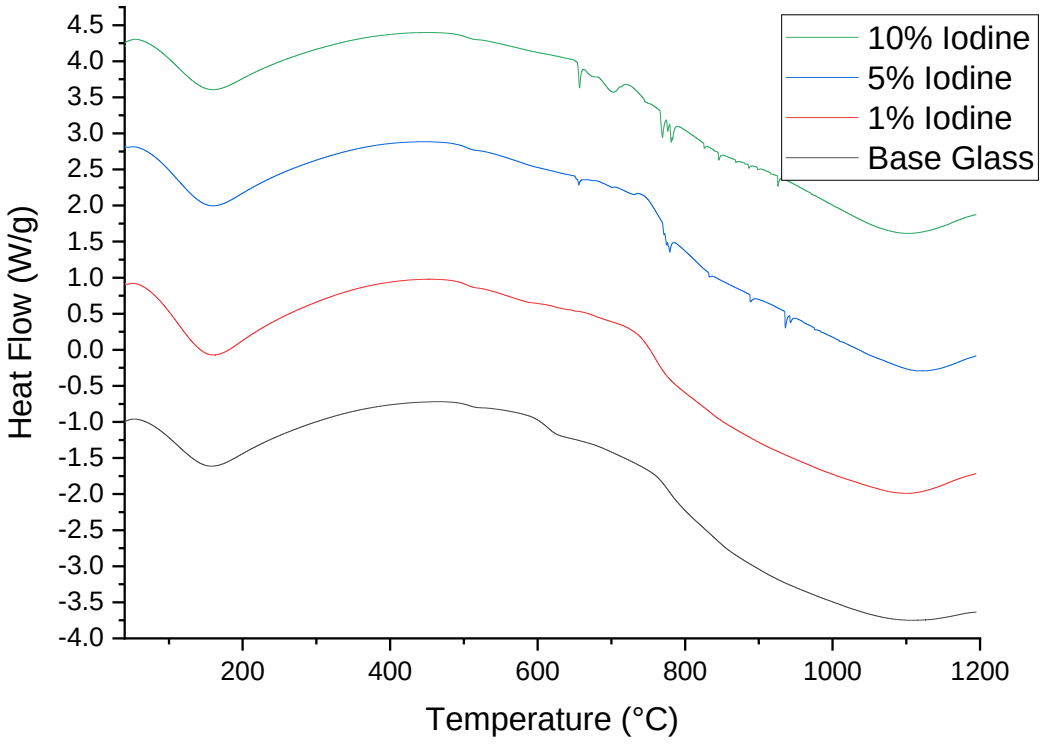

Figure 7.4 DTA trace of CaZn base glass heated in nitrogen atmosphere with additions of 0, 1, 5 and 10 wt% iodine added as NaI

The 1 wt% samples in nitrogen do not have any iodine gas detected likely due to the concentration being below the limit of detection this is seen in previous samples under air. At 5 wt% the emission seems to be low and steady over the period beginning at 925 °C for MW and 665 °C for CaZn with a step increase in CaZn at 921 °C. At 10 wt% the shape changes dramatically, a large peak is present at 700 °C with a shoulder peak at 755 – 775 °C in both MW and CaZn samples. In CaZn another secondary peak occurs at 911 °C likely corresponding to the same event that occurs in the 5 wt% sample. The presence of a higher temperature emission could indicate a more stable iodine compound forming under nitrogen in the glass system and decomposing at a higher temperature.

Next, we will look at the pyrolysis data from samples heated under a nitrogen atmosphere at 950 °C with active ^{129}I and ^{137}Cs tracers and to an inactive concentration of 1 wt%. Iodine bearing samples (figures 7.7) show that nitrogen significantly increases the retention of iodine in all experiments (0 % CaZn base glass, clinoptilolite 20 and 50 wt%, CMS 20 and 50 wt%). The base glass has no retention of

^{129}I, however, under a nitrogen atmosphere retention increased to 73.94%, a large increase compared to all previous measurements. This effect is increased for clinoptilolite containing samples where the increase from air to nitrogen containing samples is 85.06% for the 20 wt% WL sample and 73.80% for 50 wt% WL. The increase is considerably lower but evident in CMS containing samples (4.87 and 21.75 % for 20 and 50 wt% WL respectively).

^{137}Cs retention also improves in a nitrogen atmosphere compared to air (figure 7.8), however, the increase is lower than iodine. The only samples that do not see improvement in retention is the 20 wt% and 50 wt% clinoptilolite loaded samples which remained statistically constant respectively. The base glass increased by 7.66% in nitrogen gas flow less of an effect than seen in the iodine samples. CMS WL saw an improvement of 14.95 and 19.20% for 20 and 50 wt% loading respectively. The increase in retention could be due to a lack of oxidising atmosphere which can facilitate reactions particularly in iodine, for example:

$$2NaI + \frac{1}{2}O_2 \rightarrow I_2 + Na_2O$$

With these reactions not able to take place in a nitrogen atmosphere, oxidation has to occur from the glass system which requires the glass to soften first. This could be the reason the improvement in retention is observed as iodine and sodium from the raw material can begin to incorporate into the glass rather than volatilising before dissolving in the glass structure.

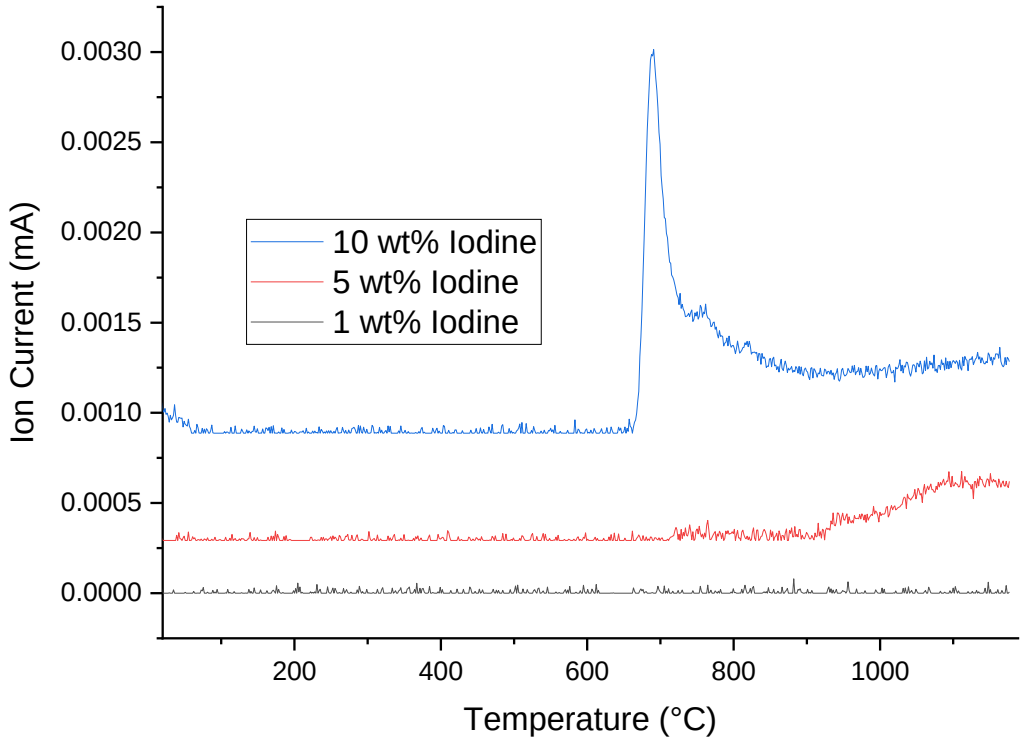

Figure 7.5 Mass spectrometry of gas emissions from 1, 5 and 10 wt% iodine doped as NaI onto MW fritted glass heated between 0 – 1200 °C under nitrogen atmosphere, showing m/z ion 254 AMU (I_2).

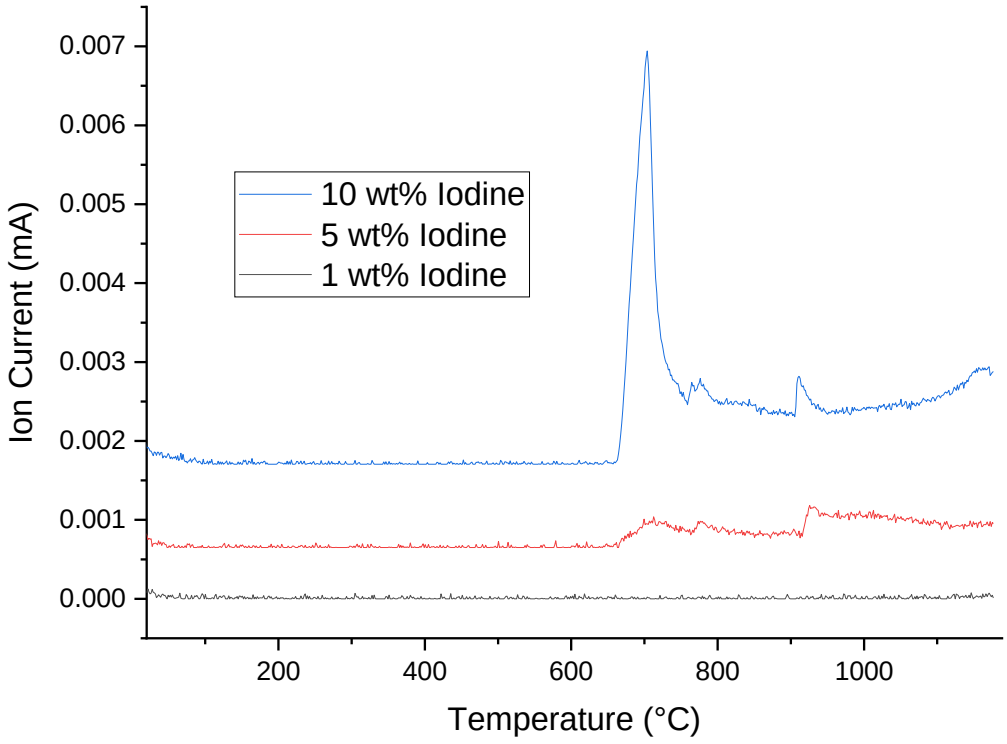

Figure 7.6 Mass spectrometry of gas emissions from 1, 5 and 10 wt% iodine doped as NaI onto CaZn fritted glass heated between 0 – 1200 °C under nitrogen atmosphere, showing m/z ion 254 AMU (I_2).

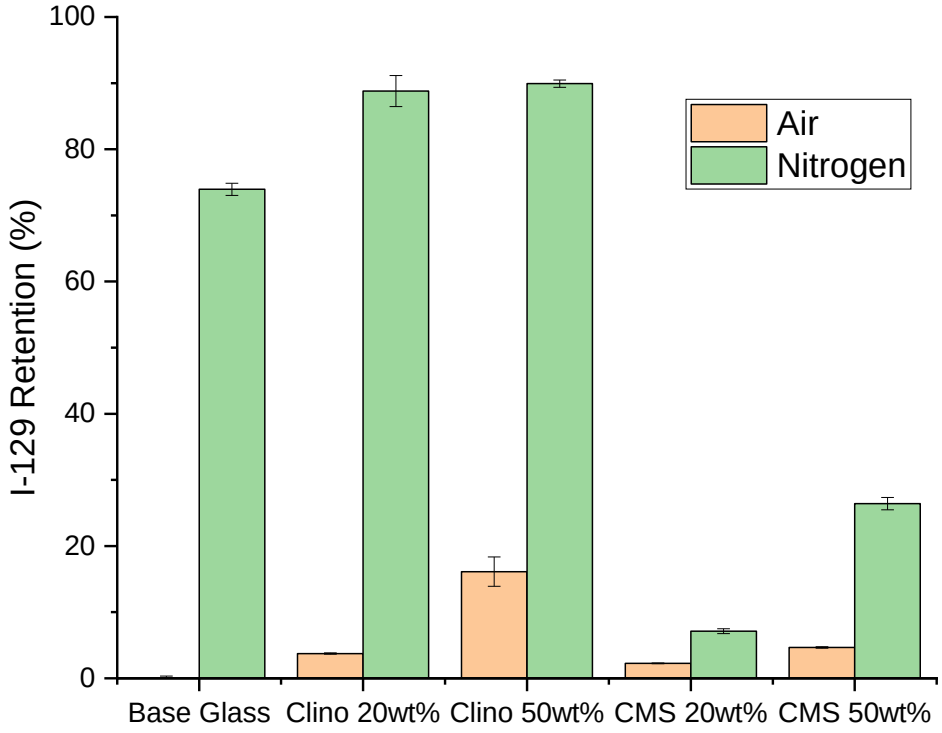

Figure 7.7 Comparison of the effect of air and nitrogen atmosphere on ^{129}I retention in 0% SiO_2 CaZn glass analysed by pyrolysis at 950 °C

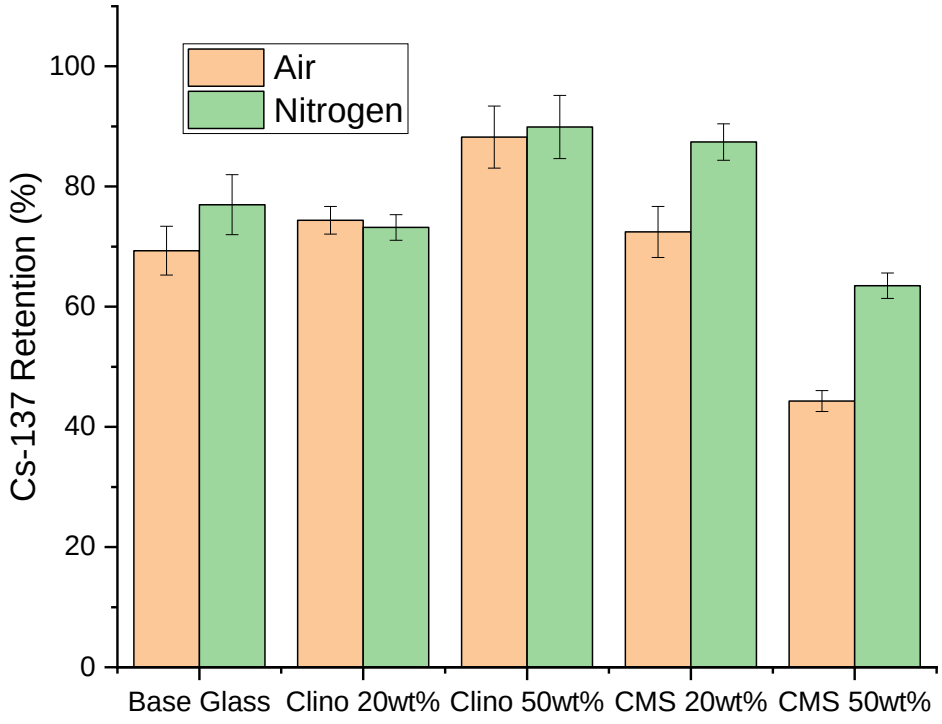

Figure 7.8 Comparison of the effect of air and nitrogen atmosphere on ^{137}Cs retention in 0% SiO_2 CaZn glass analysed by pyrolysis at 950 °C

7.4 Summary

The effect of different atmospheres, in air and nitrogen was investigated for MW, CaZn and 0% SiO_2 base glasses. TG-MS showed that the temperature at which iodine emitted from MW and CaZn glasses was significantly higher (700 – 1200 °C) under nitrogen compared to samples heated in air (550 – 650 °C). Pyrolysis experimentation on 0 wt% SiO_2 showed that the captured ^{129}I from the sample was 73.94% lower than in air compared to nitrogen. Other data showed that improvements (and detriments) from additions of waste were additive to this effect. For example, the 4% positive retention increase of caesium from 20 wt% clinoptilolite CaZn loaded glasses compared to unloaded CaZn are also seen included for retention in nitrogen atmosphere. This has interesting implications for the thermal treatment in the nuclear industry as the potential to decrease emissions of radionuclides is evident, particularly in the case of iodine where the largest increase in retention was seen. CMS loaded glasses do not see as much of a dramatic increase which could be due to the decomposition of magnesium containing species such as $Mg(OH)_2$ readily supplying oxygen to the system and facilitating the NaI decomposition reaction. Alternatively physical absorption of the NaI solution to powdered CMS could prevent the material from interacting with the liquid glass phase and therefore reduce retention.

Xian et al[166] sees a similar influence on iodine retention comparing air and nitrogen atmospheres using a bismuth glass. They showed that for all their glass systems 20 – 50 % more retention is seen in glasses formed at 800 °C. A similar conclusion is drawn in this study; that most iodine volatilisation pathways require (or are catalysed by) oxygen and therefore removing gaseous oxygen from the system interferes with these reactions. This could be applied to other volatile radioactive components to a lesser extent such as metals Cs/Sr/Rb/Tc and other halides Cl/Br.

Chapter 8 Further Discussion and Future Work

There are many implications from the work conducted in this study that apply particularly to the field of nuclear decommissioning of ILW. Firstly, understanding the glass systems was of importance and this study has focussed on the effect of boron and silica content in glasses and how that contributes to crystallisation and volatilisation. The new, high boron, low silica, glass developed in section 4.7 (0% SiO_2 CaZn) was highly studied for thermal and volatilisation properties and this glass out performed MW and CaZn in retention of the three key elements in this study, explained in the summary section 5.6. M *Ojovan et al*[77] also indicated a suppression of caesium volatility by the increase in boron content in line with our findings. This glass is recommended to be taken forward in future trials for development and study.

At a high level our work in chapter 6 shows that thermal treatment is indeed a possible choice for ILW which opens possibilities other than cementation. The pumpable wastes (clinoptilolite and corroded Magnox sludge (CMS)) studied were both able to form amorphous glasses when heated with MW, CaZn and derived glass 0% SiO_2 CaZn. This could be taken further in the future however as the resultant glass durability is unknown and this data would be required to present a case for ILW heat treatment at vitrification plants. 0% SiO_2 CaZn was able to incorporate ~30 wt% more waste in most heat treatments and able to function at a lower temperature (~950 °C). With more research this glass type could make a clear impact in the nuclear ILW inventory by reducing the volume of end waste packages and lowering volatility (from glass chemistry and lower melting temperatures). The limitation of this glass in highlighted in section 4.7 (figure 4.9) where we see that, as a borate glass, this material would be much more corrosive to refractory walls than its predecessors however given the cost reduction of smaller waste packets this may be an option worth considering.

We also present a detailed account of caesium, iodine and chlorine volatilisation the most impactful of which are the dramatic effects of atmospheric changes. The impact of oxygen in the volatilisation of iodine cannot be overstated, in section 7.3 we find that the presence of nitrogen compared to heat treatment in air can have a positive effect of up to 85 %. This is directly applicable to vitrification as a method of controlling emissions not only of iodine but other volatiles in similar groups which will follow a similar reaction pathway such as chlorine and fluorine.

At some data points within the temperature dependence sets in chapter 5 there are anomalous points from aluminium crucible digestion or instrument variation (e.g. figure 5.45) and the variation within these shows that the data may need confirming. Key element concentration can vary as a result which could affect our ability to fit reliable trends to the data. We suggest future work should repeat these in a similar manner with reference to M *Ojovan*[77] in section 19.18.

This study has focussed on the volatilisation of caesium, iodine and chlorine from multiple glass systems with and without clinoptilolite/CMS. There is scope for additional work in the future to be completed surrounding this project. More ILW streams could be studied to give a wider picture of the scope of thermal treatment as a tool for waste immobilisation. These could include but are not limited to:

- Plutonium contaminated material (PCM) including steel drums and packing
- Contaminated concrete
- Contaminated steel building materials (eg. Rebar, piping)

Increasing the field of wastes experimented upon could inform the nuclear industry upon the viability of certain ILWs for heat treatment which might have an effect on cost (reduction of volume), safety (more resilient wasteform) and direction of research.

The retention of three key elements was investigated in this study (Cs, I, Cl). The scope of this could be increased to capture more volatile elements in the nuclear industry. Some other elements that

could be studied are strontium, uranium, plutonium, ruthenium, etc. These have been shown to lose mass after heat treatments[13] and this could benefit the industry to understand these emissions better.

The off-gas rig created at Sheffield and the pyrolysis instrument used at Southampton could both be evolved to understand the glass/waste systems discussed in this thesis. Firstly, a filter system could be installed on the furnace exhaust close to the heating elements to capture any condensates and deposits from species that we could not detect in this study. Analysing the solids captured on the filter could give a clearer picture on the speciation of caesium and chlorine gaseous species from glass melt environments. Another adaptation could be a higher temperature heated line (<180 °C) connected to solution capture vessels or an MS system so that caesium and chlorine containing gases could travel through rather than deposit in the line.

Scaling up the experiments could be very useful for the nuclear industry, most long term treatment facilities have a volume of around ~700 L (with around 30 kg/h throughput)[222] and sample masses in this study have been from around 25 mg to 20 g. There are clear benefits to understanding larger scale melt environments and therefore some future experiments could include a crucible with a larger volume in an off-gas capture system or similar. Full scale experiments could be completed on any of the vitrification test rigs worldwide (UK, USA, France, Switzerland etc.)[75,91,222] available to understand the full process better.

9 Appendix

Appendix A

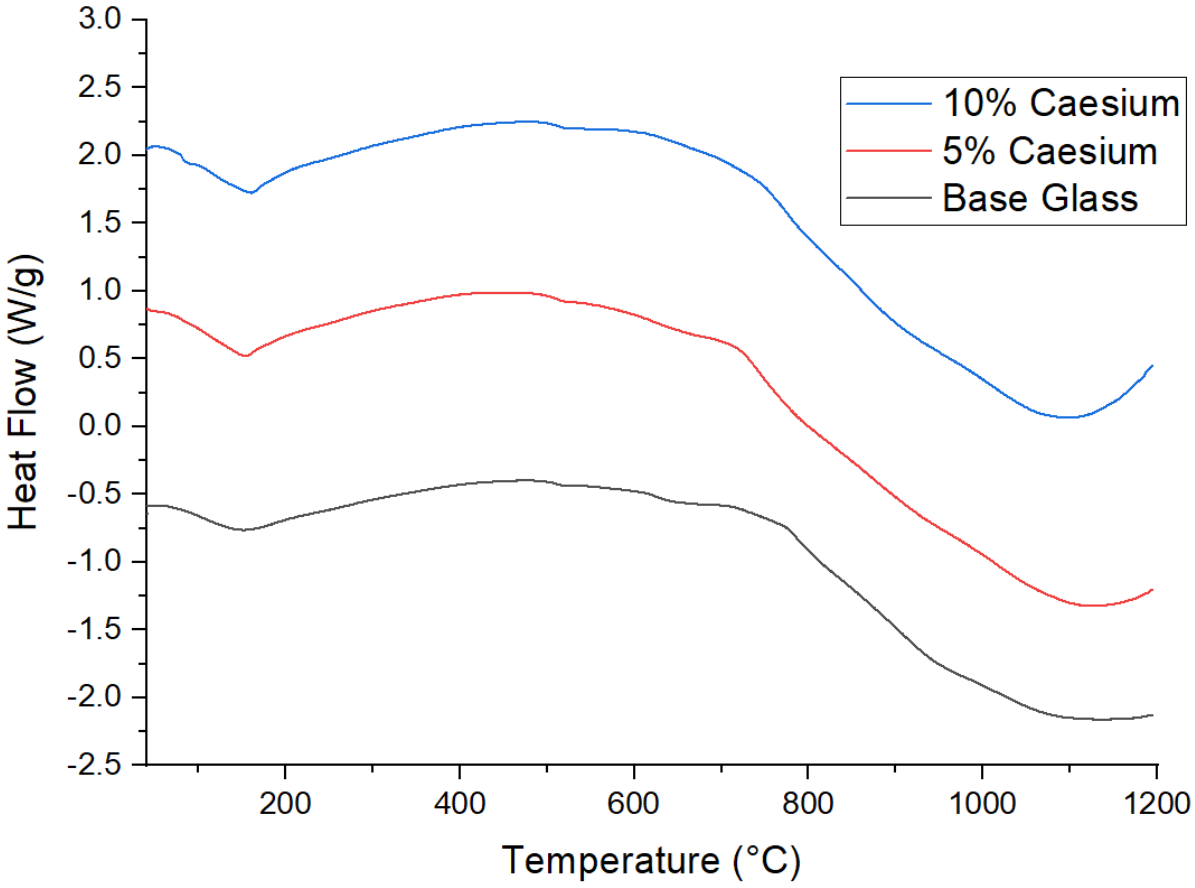

Figure A. DTA traces of heat flow between 0 – 1200 °C in MW glass with the addition of 5 and 10 wt% caesium

Appendix B

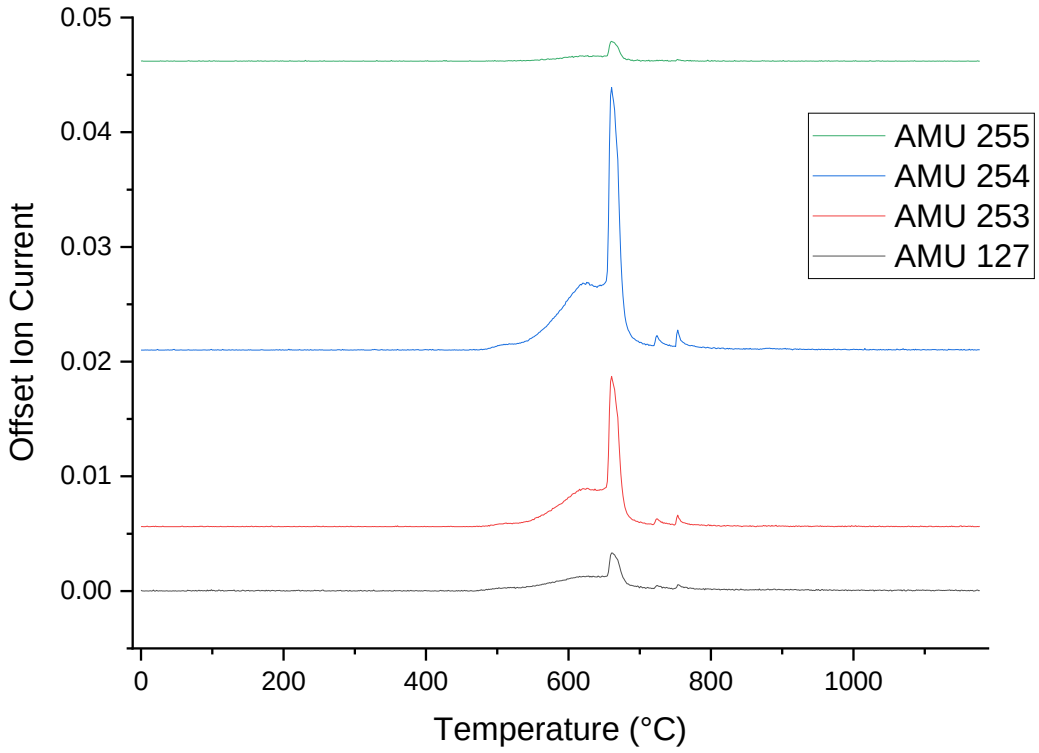

Figure B. MS intensity for mass units 127, 253, 254 and 255 demonstrating the isotopic distribution and fragments of I_2. AMU 127 is an I^- fragment of the most abundant isotope ^{127}I, AMU 253 is a combination of ^{126}I and ^{127}I isotope in a molecule of I_2, AMU 254 is the most abundant form of I_2 made up of two ^{127}I units and 255 is the combination of ^{127}I and ^{128}I.

Appendix C

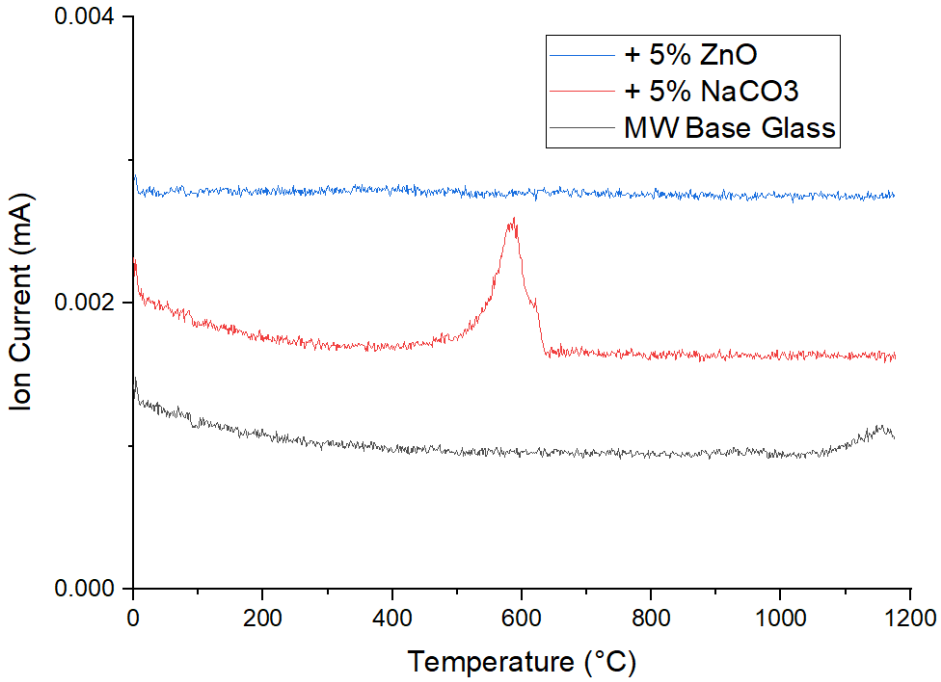

Figure C. Graph of MS data from AMU 44 (CO_2) for samples MW base glass, MW + 5% Na_2CO_3, MW and MW + 5% ZnO all with the addition of 5% iodine added as sodium iodide between 0 – 1200 °C

Appendix D

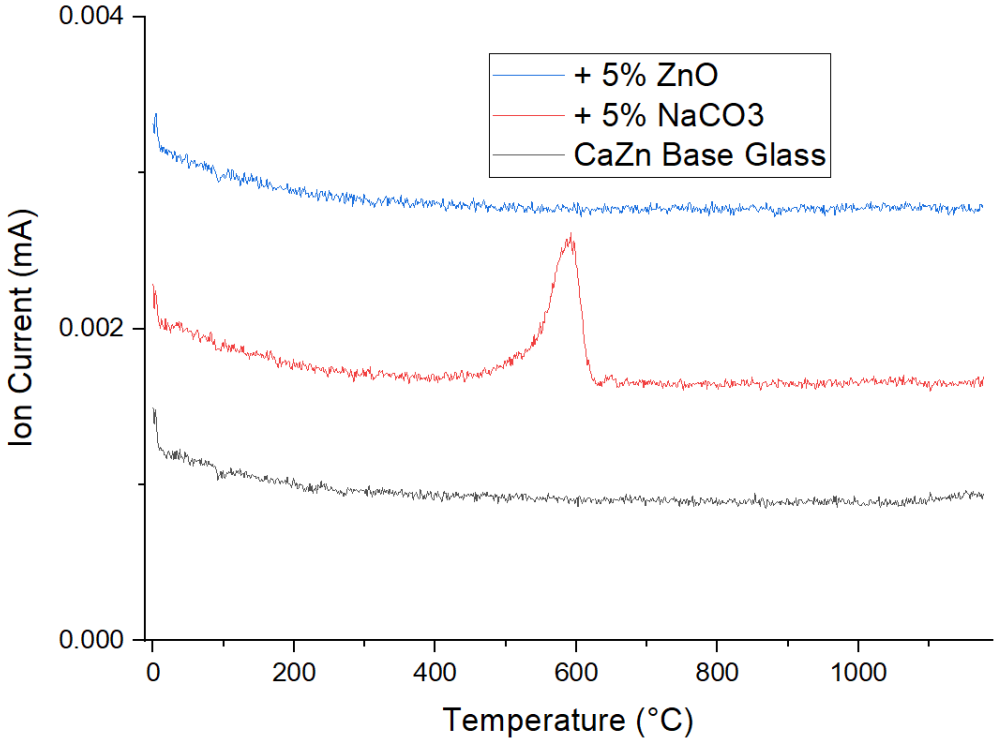

Figure D. Graph of MS data from AMU 44 (CO_2) for samples CaZn base glass, CaZn + 5% Na_2CO_3, CaZn and CaZn + 5% ZnO all with the addition of 5% iodine added as sodium iodide between 0 – 1200 °C

References

1. Nuclear Decommissioning Authority, Department for Business Energy and Industrial Strategy. 2019 UK Radioactive Waste Detailed Data. Published online 2019:172.

2. The Parliamentary Office of Science and Technology. Managing the UK Plutonium Stockpile. 2016;(531):1-5. researchbriefings.files.parliament.uk/documents/POST-PN-0531/POST-PN-0531.pdf%0A

3. Hyatt NC. Plutonium management policy in the United Kingdom: The need for a dual track strategy. *Energy Policy*. 2017;101:303-309. doi:https://doi.org/10.1016/j.enpol.2016.08.033

4. Nuclear Decommissioning Authority. Stakeholder Response Report March 2021. 2021;(March).

5. Metcalfe BL, Donald IW. Management of radioactive waste (RAW) from nuclear weapons programmes. *Radioact Waste Manag Contam Site Clean-Up Process Technol Int Exp*. Published online 2013:775-800. doi:10.1533/9780857097446.3.775

6. Sellafield Ltd. NDA, Waste Stream 2D03 Plutonium Contaminated Materials; Drums. Published online 2019.

7. Dyer A, Hriljac J, Evans N, et al. The use of columns of the zeolite clinoptilolite in the remediation of aqueous nuclear waste streams. *J Radioanal Nucl Chem*. 2018;318(3):2473-2491. doi:10.1007/s10967-018-6329-8

8. Tan S, Kirk N, Marshall M, McGann O, Hand RJ. Vitrification of an intermediate level Magnox sludge waste. *J Nucl Mater*. 2019;515:392-400. doi:https://doi.org/10.1016/j.jnucmat.2019.01.007

9. Nuclear Decommissioning Authority. *NDA Annual Report and Accounts*.; 2019. https://www.rtda.gov.rw/fileadmin/templates/publications/RWANDA_Annual_Report_2018-2019_SHARING.pdf,

10. NDA. UK Radioactive Waste Inventory. Published online 2019. https://ukinventory.nda.gov.uk/?action=export_pdf&tid=90299adf9b76a9c0d448a1bbc39b1b6f&display_format=100&summary=Showing all unfiltered results.

11. Gin S, Jollivet P, Tribet M, Peuget S, Schuller S. Radionuclides containment in nuclear glasses: An overview. *Radiochim Acta*. 2017;105(11):927-959. doi:10.1515/ract-2016-2658

12. Jansson P, Karlberg L. A model of accumulation of radionuclides in biosphere originating from groundwater contamination. *Swedish Nucl Fuel Waste Manag*. Published online 2006.

13. Caurant D. *Glasses, Glass-Ceramics and Ceramics for Immobilization of Highly Radioactive Nuclear Wastes*. Nova Science Publishers, Inc.; 2009.

14. Beauvy M, Berthoud G, Defranceschi M, et al. *CEA DEN Monograph: Treatment and Recycling Actinide Partitioning – Application to Waste Management*.; 2008.

15. Kim D, Kruger AA. Volatile species of technetium and rhenium during waste vitrification. *J Non Cryst Solids*. 2018;481(October 2017):41-50. doi:10.1016/j.jnoncrysol.2017.10.013

16. Lelek V, Mikisek M, Marek T. FISSION PRODUCTS IN THE SPENT NUCLEAR FUEL FROM CZECH NUCLEAR POWER PLANTS. *Nucl Res Inst Rez plc*. Published online 1999:753-754.

17. Delmore JE, Snyder DC, Tranter T, Mann NR. Cesium isotope ratios as indicators of nuclear

power plant operations. *J Environ Radioact*. 2011;102(11):1008-1011. doi:https://doi.org/10.1016/j.jenvrad.2011.06.013

18. Price L. Cs-135 Content of Cesium Capsules and Strontium/Cesium Heat Sources. *WM2018 Conf*. Published online 2018:1-5.

19. Parkinson BG, Holland D, Smith ME, Howes AP, Scales CR. Effect of minor additions on structure and volatilization loss in simulated nuclear borosilicate glasses. *J Non Cryst Solids*. 2007;353(44-46):4076-4083. doi:10.1016/j.jnoncrysol.2007.06.016

20. Hrma PR. *Retention of Halogens in Waste Glass*.; 2010. doi:10.2172/981571

21. Rodríguez M, Piña G, Lara E. Radiochemical analysis of chlorine-36. *Czechoslov J Phys*. 2006;56(1):D211-D217. doi:10.1007/s10582-006-1019-0

22. NDA. The 2019 Inventory. NDA Department for Business, Energy and Industrial Strategy. Published 2020. Accessed September 1, 2020. https://ukinventory.nda.gov.uk/the-2019-inventory/2019-uk-data/

23. EDF. Nuclear decommissioning. Published 2023. Accessed March 9, 2023. https://www.edfenergy.com/about/nuclear/decommissioning#:~:text=In 2022%2C Hunterston B became,– defueling – in August 2022.

24. Heep Wuerenlingen WZISF. The Zwilag interim storage plasma plant technology to handle operational waste from nuclear plants. In: American Society of Mechanical Engineers - ASME, New York (United States); 2007. https://www.osti.gov/biblio/21156400

25. Harrison MT. Vitrification of High Level Waste in the UK. *Procedia Mater Sci*. 2014;7:10-15. doi:10.1016/j.mspro.2014.10.003

26. Veolia. Our GeoMelt® Vitrification Technologies to Stabilize Waste. Published 2020. Accessed September 2, 2020. https://www.nuclearsolutions.veolia.com/en/our-expertise/technologies/our-geomelt-vitrification-technologies-stabilize-waste

27. Hyatt NC, Schwarz RR, Bingham PA, et al. Thermal treatment of simulant plutonium contaminated materials from the Sellafield site by vitrification in a blast-furnace slag. *J Nucl Mater*. 2014;444(1-3):186-199. doi:10.1016/j.jnucmat.2013.08.019

28. Schofield JM, Swanton SW, Farahani B, et al. Experimental studies of the chemical durability of UK HLW and ILW glasses. *AMEC/103498/03 Issue 1*. 2016;(01):1-241. https://rwm.nda.gov.uk/publication/experimental-studies-of-the-chemical-durability-of-uk-hlw-and-ilw-glasses-interim-progress-report-amec103498ipr02-revision-3/

29. Crossland I. *Nuclear Power: Origins and Outlook*. Woodhead Publishing Limited; 2012. doi:10.1533/9780857096388.1.3

30. Soelberg N. Advanced off-gas control system design for radioactive and mixed waste treatment. *Proc - 10th Int Conf Environ Remediat Radioact Waste Manag ICEM'05*. 2005;2005:2216-2224.

31. Westinghouse Nuclear. Nuclear fuel manufacture at Springfields. *Westinghouse Nucl*. Published online 2020:2.

32. THE NUCLEAR FUEL CYCLE. European Parlimentary Reaserch Service Blog. Published 2016. Accessed August 21, 2020. https://epthinktank.eu/2016/01/20/the-nuclear-agreement-with-iran/eprs-briefing-572820-iran-nuclear-agreement_final3_2/

33. NDA. FACTSHEET : Operating a nuclear power reactor Overview Types of nuclear power

reactors Nuclear fission in a power reactor. *UK Radioact Waste Invent*. Published online 2013.

34. Jubin RT, Soelberg NR, Strachan DM, Ilas G. Fuel Age Impacts on Gaseous Fission Product Capture during Separations. Published online 2012.

35. Lin Y, Couture RM, Klein H, et al. Modelling Environmental Impacts of Cesium-137 Under a Hypothetical Release of Radioactive Waste. *Bull Environ Contam Toxicol*. 2019;103(1):69-74. doi:10.1007/s00128-019-02601-5

36. Rauwel P, Rauwel E. Towards the Extraction of Radioactive Cesium-137 from Water via Graphene/CNT and Nanostructured Prussian Blue Hybrid Nanocomposites: A Review. *Nanomater (Basel, Switzerland)*. 2019;9(5). doi:10.3390/nano9050682

37. Spalding BP. Volatilization of Cesium-137 from Soil with Chloride Amendments during Heating and Vitrification. *Environ Sci Technol*. 1994;28(6):1116-1123. doi:10.1021/es00055a022

38. Kamizono H, Kikkawa S, Togashi Y, Tashiro S. Volatilization of 137Cs and 106Ru from Borosilicate Glass Containing Actual High-Level Waste. *J Am Ceram Soc*. 1989;72(8):1438-1441. doi:10.1111/j.1151-2916.1989.tb07669.x

39. L.L. Burger, R.D. Scheele KDW. Selection of a Form for Fixation of Iodine-129. *Pnl-4045*. Published online 1981:4045.

40. Sakurai T, Takahashi A, Ishikawa N, Komaki Y. The behavior of iodine in a simulated spent-fuel solution. *Nucl Technol*. 1989;85(2 MAY):206-212. doi:10.13182/nt89-a34241

41. Pacey N, Beadle I, Heaton A, et al. *Chemical Discharges from Nuclear Power Stations : Historical Releases and Implications for Best Available Techniques*.; 2011.

42. "Clough RL, “Gillen Albuquerque, NM (USA)]” KT [Sandia NL. Radiation-thermal degradation of PE and PVC: mechanism of synergism and dose rate effects. [Gamma radiation]. In: Vol 18:3-4. ; 1981. doi:https://doi.org/

43. Starks JB. The purex process. *US Energy Res Dev Adm*. Published online 1977:1-41.

44. World Nuclear News. First radioactive waste removed from Magnox storage pond. *World Nuclear News*. https://www.world-nuclear-news.org/WR-First-radioactive-waste-removed-from-Magnox-storage-pond-24031501.html. Published 2015.

45. Heath PG, Stewart MWA, Moricca S, Hyatt NC. Hot-isostatically pressed wasteforms for Magnox sludge immobilisation. *J Nucl Mater*. 2018;499:233-241. doi:https://doi.org/10.1016/j.jnucmat.2017.11.034

46. Vis M, O’Kane D, Shenton M. SWM Sludge and Clinoptilolite Properties for Thermal IPT. Published online 2017:8.

47. Sylvester P. Strontium From Nuclear Wastes: Ion Exchange. *Encycl Sep Sci*. Published online 2000:4261-4267. doi:10.1016/b0-12-226770-2/05441-7

48. mindat. Mud Hills Mine, Rainbow Basin, Mud Hills (Strontium Hills), Barstow District, San Bernardino Co., California, USA. mindat. Published 2005. Accessed March 16, 2023. https://www.mindat.org/loc-89104.html

49. Mastinu A, Kumar A, Maccarinelli G, et al. Zeolite Clinoptilolite: Therapeutic Virtues of an Ancient Mineral. *Molecules*. 2019;24(8). doi:10.3390/molecules24081517

50. mindat. Clinoptilolite. mindat. Published 2013. Accessed March 16, 2023. https://www.mindat.org/min-1082.html

51. Snellings RA, Gualtieri AF, Elsen J. The rietveld structure refinement of an exceptionally pure sample of clinoptilolite from Ecuador and its Na-, K-, and Caexchanged forms. *Zeitschrift fur Krist Suppl*. 2009;(30):395-400. doi:10.1524/zksu.2009.0058

52. EDF. What does graphite do in Advanced Gas-cooled Reactors? Published 2023. Accessed March 17, 2023. https://www.edfenergy.com/about/nuclear/graphite-core#:~:text=What does graphite do in,nuclear reaction to be sustained.

53. Office for Nuclear Regulation. Graphite core of AGRs. ONR. Published 2022. Accessed March 17, 2023. https://www.onr.org.uk/civil-nuclear-reactors/graphite-core-of-agrs.htm

54. IAEA. Processing of Irradiated Graphite to Meet Acceptance Criteria for Waste Disposal. *Tech Reports Ser*. 2016;1790:1-150.

55. Ghorai S, Sarkar A, Panda AB, Pal S. Evaluation of the Flocculation Characteristics of Polyacrylamide Grafted Xanthan Gum/Silica Hybrid Nanocomposite. *Ind Eng Chem Res*. 2013;52(29):9731-9740. doi:10.1021/ie400550m

56. KANG KS, PETTITT DJ. CHAPTER 13 - XANTHAN, GELLAN, WELAN, AND RHAMSAN. In: WHISTLER ROYL, BEMILLER JNBT-IG (Third E, eds. Academic Press; 1993:341-397. doi:https://doi.org/10.1016/B978-0-08-092654-4.50017-6

57. Tempio JS, Zatz JL. Flocculation effect of xanthan gum in pharmaceutical suspensions. *J Pharm Sci*. 1980;69(10):1209-1214. doi:10.1002/jps.2600691024

58. International Atomic Energy Agency. Low and Intermediate Level Waste From Nuclear Applications. Published online 1996.

59. Sellafield Ltd. *The Magnox Swarf Storage Silo at Sellafield - The Start of Retrievals*.; 2022. https://www.youtube.com/watch?v=XLUzRgVqpcE

60. Ojovan MI, Lee WE. Glassy Wasteforms for Nuclear Waste Immobilization. *Metall Mater Trans A*. 2011;42(4):837-851. doi:10.1007/s11661-010-0525-7

61. Ericson JE, Makishima A, Mackenzie JD, Berger R. Chemical and physical properties of obsidian: a naturally occuring glass. *J Non Cryst Solids*. 1975;17(1):129-142. doi:https://doi.org/10.1016/0022-3093(75)90120-9

62. Short R. Phase Separation and Crystallisation in UK HLW Vitrified Products. *Procedia Mater Sci*. 2014;7:93-100. doi:10.1016/j.mspro.2014.10.013

63. Mühlbauer A. Innovative Induction Melting Technologies : A Historical Review. *Model Mater Process*. Published online 2006:13-20.

64. National Nuclear Laboratory. Position Paper: Thermal Processes for Immobilising Intermediate Level Wastes. Published online 2019. http://www.nnl.co.uk/science-technology/position-papers/

65. Grayson K. Cold Crucible Induction Melting. Published 2021. Accessed March 9, 2023. https://mo-sci.com/cold-crucible-induction-melting/

66. Jantzen CM, Ojovan MI. On Selection of Matrix (Wasteform) Material for Higher Activity Nuclear Waste Immobilization (Review). *Russ J Inorg Chem*. 2019;64(13):1611-1624. doi:10.1134/S0036023619130047

67. ZWILAG. Plasma plant. Published 2020. Accessed December 21, 2020. https://www.zwilag.ch/en/plasma-plant-_content---1--1047.html

68. Vance ER, Zhang Y, Gregg DJ. Ceramic Waste Forms. In: *Comprehensive Nuclear Materials*. Elsevier; 2020:445-466. doi:10.1016/b978-0-12-803581-8.11795-3

69. ANSTO. Synroc: Australian innovation increases technology readiness for waste treatment plant. Published 2016. https://www.ansto.gov.au/news/synroc-australian-innovation-increases-technology-readiness-for-waste-treatment-plant

70. Marsh AI, Williams LG, Lawrence JA. The important role and performance of engineered barriers in a UK geological disposal facility for higher activity radioactive waste. *Prog Nucl Energy*. 2021;137(April):103736. doi:10.1016/j.pnucene.2021.103736

71. Marsh AI, Williams LG, Lawrence JA. The important role and performance of engineered barriers in a UK geological disposal facility for higher activity radioactive waste. *Prog Nucl Energy*. 2021;137(April):103736. doi:10.1016/j.pnucene.2021.103736

72. INTERNATIONAL ATOMIC ENERGY AGENCY. *Sealing of Underground Repositories for Radioactive Wastes*. INTERNATIONAL ATOMIC ENERGY AGENCY; 1990. https://www.iaea.org/publications/1423/sealing-of-underground-repositories-for-radioactive-wastes

73. Sellin P, Leupin OX. The use of clay as an engineered barrier in radioactive-waste management - A review. *Clays Clay Miner*. 2014;61(6):477-498. doi:10.1346/CCMN.2013.0610601

74. Hench LL, Clark DE, Campbell J. High level waste immobilization forms. *Nucl Chem Waste Manag*. 1984;5(2):149-173. doi:10.1016/0191-815X(84)90045-7

75. Jantzen CM. Systems approach to nuclear waste glass development. *J Non Cryst Solids*. 1986;84(1-3):215-225. doi:10.1016/0022-3093(86)90780-5

76. Park S-J, Seo M-K. Chapter 6 - Element and Processing. In: Park S-J, Seo M-KBT-IS and T, eds. *Interface Science and Composites*. Vol 18. Elsevier; 2011:431-499. doi:https://doi.org/10.1016/B978-0-12-375049-5.00006-2

77. Ojovan MI, Lee WE, Kalmykov SN. Chapter 19 - Immobilisation of Radioactive Wastes in Glass. In: Ojovan MI, Lee WE, Kalmykov SN, eds. *An Introduction to Nuclear Waste Immobilisation (Third Edition)*. Elsevier; 2019:319-368. doi:https://doi.org/10.1016/B978-0-08-102702-8.00019-4

78. Schaeffer HA. Diffusion-controlled processes in glass forming melts. *J Non Cryst Solids*. 1984;67(1):19-33. doi:https://doi.org/10.1016/0022-3093(84)90138-8

79. Thorpe CL, Neeway JJ, Pearce CI, et al. Forty years of durability assessment of nuclear waste glass by standard methods. *npj Mater Degrad*. 2021;5(1):61. doi:10.1038/s41529-021-00210-4

80. Thorpe CL, Neeway JJ, Pearce CI, et al. Forty years of durability assessment of nuclear waste glass by standard methods. *npj Mater Degrad*. 2021;5(1). doi:10.1038/s41529-021-00210-4

81. Aréna H, Godon N, Rébiscoul D, et al. Impact of iron and magnesium on glass alteration: Characterization of the secondary phases and determination of their solubility constants. *Appl Geochemistry*. 2017;82:119-133. doi:10.1016/j.apgeochem.2017.04.010

82. Bouakkaz R, Abdelouas A, Grambow B. Kinetic study and structural evolution of SON68 nuclear waste glass altered from 35 to 125 °C under unsaturated H2O and D2O18 vapour conditions. *Corros Sci*. 2018;134:1-16. doi:https://doi.org/10.1016/j.corsci.2017.12.035

83. Pierce E, Windisch C, Burton S, et al. Integrated Disposal Facility FY2010 Glass Testing Summary Report. 2010;(September).

84. Hall A., Dalton JT, Hudson B, Marples JAC. In management of waste from the nuclear fuel cycle. In: *IAEA Vienna*. Vol 2. ; 1976:3.

85. Dalton TJ, Boult KA, Chamberlain HE, Marples JAC. *Proceedings of the International Seminar on Chemistry and Process Engineering for High-Level Liquid Waste Solidification*. Zentralbibl. der Kernforschungsanlage; 1981. https://books.google.co.uk/books?id=Gax7xQEACAAJ

86. Marples JAC. The preparation, properties, and disposal of vitrified high level waste from nuclear fuel reprocessing. *Glas Technol*. 1988;29(6):230-247.

87. Miekina M. Crystal formation during the vitrification of HLW in Ca/Zn base glass. Published online 2018. https://core.ac.uk/download/pdf/210998699.pdf

88. Nicoleau E, Schuller S, Angeli F, et al. Phase separation and crystallization effects on the structure and durability of molybdenum borosilicate glass. *J Non Cryst Solids*. 2015;427:120-133. doi:https://doi.org/10.1016/j.jnoncrysol.2015.07.001

89. Nicoleau E, Schuller S, Angeli F, et al. Phase separation and crystallization effects on the structure and durability of molybdenum borosilicate glass. *J Non Cryst Solids*. 2015;427:120-133. doi:https://doi.org/10.1016/j.jnoncrysol.2015.07.001

90. Saiki K, Sakida S, Benino Y, Nanba T. Phase Separation of Borosilicate Glass Containing Sulfur. *J Ceram Soc Japan*. 2010;118:603-607. doi:10.2109/jcersj2.118.603

91. Gin S, Abdelouas A, Criscenti LJ, et al. An international initiative on long-term behavior of high-level nuclear waste glass. *Mater Today*. 2013;16(6):243-248. doi:https://doi.org/10.1016/j.mattod.2013.06.008

92. Shelby JE. *Introduction to Glass Science and Technology* . 2nd ed. Royal Society of Chemistry; 2005.

93. Polyakova I. The Main Silica Phases and Some of Their Properties. In: ; 2014:197-268. doi:10.1515/9783110298581.197

94. Zachariasen WH. THE ATOMIC ARRANGEMENT IN GLASS. *J Am Chem Soc*. 1932;54(10):3841-3851. doi:10.1021/ja01349a006

95. Van Limpt H, Beerkens R, Verheijen O. Models and experiments for sodium evaporation from sodium containing silicate melts. *J Am Ceram Soc*. 2006;89(11):3446-3455. doi:10.1111/j.1551-2916.2006.01233.x

96. Yuan X, Cormack AN. Si–O–Si bond angle and torsion angle distribution in vitreous silica and sodium silicate glasses. *J Non Cryst Solids*. 2003;319(1):31-43. doi:https://doi.org/10.1016/S0022-3093(02)01960-9

97. Max-Planck-Gesellschaft. From thin silicate films to the atomic structure of glass.

98. Minakova NA, Zaichuk A V, Belyi YI. The structure of borate glass. *Glas Ceram*. 2008;65(3):70-73. doi:10.1007/s10717-008-9017-2

99. Januchta K, Bauchy M, Youngman RE, Rzoska SJ, Bockowski M, Smedskjaer MM. Modifier field strength effects on densification behavior and mechanical properties of alkali aluminoborate glasses. *Phys Rev Mater*. 2017;1(6):63603. doi:10.1103/PhysRevMaterials.1.063603

100. Veléz MH, Tuller HL, Uhlmann DR. Chemical durability of lithium borate glasses. *J Non Cryst Solids*. 1982;49(1):351-362. doi:https://doi.org/10.1016/0022-3093(82)90131-4

101. Parkinson BG. Influence of Composition on Structure and Caesium Volatilisation from Glasses

for HLW Confinement. Published online 2007.

102. Zhong J, Bray PJ. Change in boron coordination in alkali borate glasses, and mixed alkali effects, as elucidated by NMR. *J Non Cryst Solids*. 1989;111(1):67-76. doi:https://doi.org/10.1016/0022-3093(89)90425-0

103. Ehrt D, Flügel S. Properties of Zinc Silicate Glasses and Melts. *J Mater Sci Eng A1*. 2011;1:312-320.

104. Besmann TM, Spear KE. Thermochemical Modeling of Oxide Glasses. *J Am Ceram Soc*. 2004;85(12):2887-2894. doi:10.1111/j.1151-2916.2002.tb00552.x

105. Saloumi N, Daki I, El Bouchti M, et al. Development and Characterization of Phosphate Glass Fibers and Their Application in the Reinforcement of Polyester Matrix Composites. *Materials (Basel)*. 2022;15(21). doi:10.3390/ma15217601

106. Strizhalo VA, Voitenko AF. Elastic characteristics of iron-glass materials at low temperatures. *Strength Mater*. 1998;30(1):31-35. doi:10.1007/BF02764416

107. Hashimoto H, Onodera Y, Tahara S, et al. Structure of alumina glass. *Sci Rep*. 2022;12(1):516. doi:10.1038/s41598-021-04455-6

108. Bisbrouck N, Micoulaut M, Delaye JM, Gin S, Angeli F. Structure--property relationship and chemical durability of magnesium-containing borosilicate glasses with insight from topological constraints. *npj Mater Degrad*. 2022;6(1):58. doi:10.1038/s41529-022-00268-8

109. Karakuzu-Ikizler B, Terzioğlu P, Basaran-Elalmis Y, Tekerek BS, Yücel S. Role of magnesium and aluminum substitution on the structural properties and bioactivity of bioglasses synthesized from biogenic silica. *Bioact Mater*. 2020;5(1):66-73. doi:https://doi.org/10.1016/j.bioactmat.2019.12.007

110. van Limpt H, Beerkens R, van Kersbergen M. Effect of Small Glass Composition Changes on Flue Gas Emissions of Glass Furnaces. *Adv Mater Res*. 2008;39-40:653-658. doi:10.4028/www.scientific.net/AMR.39-40.653

111. Beerkens RGC. Sulfate Decomposition and Sodium Oxide Activity in Soda-Lime-Silica Glass Melts. *J Am Ceram Soc*. 2003;86(11):1893-1899. doi:10.1111/j.1151-2916.2003.tb03578.x

112. Parkinson BG, Holland D, Smith ME, Howes AP, Scales CR. The effect of Cs2O additions on HLW wasteform glasses. *J Non Cryst Solids*. 2005;351(30-32):2425-2432. doi:10.1016/j.jnoncrysol.2005.06.035

113. Dehelean A, Rada S, Zhang J. Determination of the lead environment in samarium – Lead oxide-borate glasses and vitroceramics using XANES and EXAFS studies. *Radiat Phys Chem*. 2020;174(February):108927. doi:10.1016/j.radphyschem.2020.108927

114. Sheffield Assay Office. What is Lead Crystal Glass. Published online 2023:2. https://www.assayoffice.co.uk/assets/uploads/Crystal Glass Factsheet.pdf

115. Gerlach TM. Volcanic sources of tropospheric ozone-depleting trace gases. *Geochemistry, Geophys Geosystems*. 2004;5(9). doi:https://doi.org/10.1029/2004GC000747

116. Rahimi R, Ahmadi A, Kakooei S, Sadrnezhaad SK. Corrosion behavior of ZrO2–SiO2–Al2O3 refractories in lead silicate glass melts. *J Eur Ceram Soc*. 2013;31:715-721. doi:10.1016/j.jeurceramsoc.2010.11.022

117. Murray JL, McAlister AJ. The Al-Si (Aluminum-Silicon) system. *Bull Alloy Phase Diagrams*. 1984;5(1):74-84. doi:10.1007/BF02868729

118. Stebbins JF, Xu Z. NMR evidence for excess non-bridging oxygen in an aluminosilicate glass. *Nature*. 1997;390(6655):60-62. doi:10.1038/36312

119. Yamane M, Okuyama M. Coordination number of aluminum ions in alkali-free alumino-silicate glasses. *J Non Cryst Solids*. 1982;52(1):217-226. doi:https://doi.org/10.1016/0022-3093(82)90297-6

120. Mascaraque N, Januchta K, Frederiksen KF, Youngman RE, Bauchy M, Smedskjaer MM. Structural dependence of chemical durability in modified aluminoborate glasses. *J Am Ceram Soc*. 2019;102(3):1157-1168. doi:10.1111/jace.15969

121. Witwer K, Dysland E, Ave J. Thermal Treatment of UK Intermediate and Low Level Radioactive Waste : A Demonstration of the GeoMelt Process Towards Treatment of Sellafield Waste. *Proc Waste Manag Symp*. Published online 2010:1-9.

122. Sinclair RN, Haworth R, Wright AC, et al. Neutron spectroscopic studies of caesium borate crystals and glasses. *Phys Chem Glas Eur J Glas Sci Technol Part B*. 2006;47(4):405-411.

123. O'Shaughnessy C, Henderson GS, Nesbitt HW, Bancroft GM, Neuville DR. Structure-property relations of caesium silicate glasses from room temperature to 1400 K: Implications from density and Raman spectroscopy. *Chem Geol*. 2017;461:82-95. doi:10.1016/j.chemgeo.2016.11.028

124. Stoch P. Structure and Properties of 137Cs Containing Waste Glass. *Adv Mater Res*. 2008;39-40:671-674. doi:10.4028/www.scientific.net/AMR.39-40.671

125. Januchta K, Stepniewska M, Jensen LR, et al. Breaking the Limit of Micro-Ductility in Oxide Glasses. *Adv Sci*. 2019;6(18):1901281. doi:https://doi.org/10.1002/advs.201901281

126. CABLE M, FERNANDES MH V. The volatilisation of molten sodium metaborate. *Glas Technol*. 1987;28(3):135-140.

127. Stoch P. Cs containing borosilicate waste glasses. *Opt Appl*. 2008;38(1):237-243.

128. Banerjee D, Sudarsan VK, Joseph A, et al. Role of TiO2 on the physicochemical properties of cesium borosilicate glasses. *J Am Ceram Soc*. 2010;93(10):3252-3258. doi:10.1111/j.1551-2916.2010.03909.x

129. N. S, D. B-A, J. C, M. F. Cesium Incorporation Into Phosphate Silicate Apatites. *Phosphorus Res Bull*. 1999;10(0):353-358. doi:10.3363/prb1992.10.0_353

130. Click CA, Brow RK, Alam TM. Properties and structure of cesium phosphate glasses. *J Non Cryst Solids*. 2002;311(3):294-303. doi:10.1016/S0022-3093(02)01417-5

131. Aubin-Chevaldonnet V, Caurant D, Dannoux A, et al. Preparation and characterization of (Ba,Cs)(M,Ti)8O16 (M = Al3+, Fe3+, Ga3+, Cr3+, Sc3+, Mg2+) hollandite ceramics developed for radioactive cesium immobilization. *J Nucl Mater*. 366(1-2):137-160. doi:DOI:101016/jjnucmat200612051

132. Aubin V, Caurant D, Gourier D, et al. Synthesis, Characterization and Study of the Radiation Effects on Hollandite Ceramics Developed for Cesium Immobilization. *MRS Proc*. 2003;807:315. doi:DOI: 10.1557/PROC-807-315

133. Bell AMT, Henderson CMB. High-temperature synchrotron X-ray powder diffraction study of Cs2XSi5O12 (X = Cd, Cu, Zn) leucites. *Mineral Mag*. 2012;76(5):1257-1280. doi:10.1180/minmag.2012.076.5.12

134. Cicconi MR, Pili E, Grousset L, et al. Iodine solubility and speciation in glasses. *Sci Rep*.

2019;9(1):1-13. doi:10.1038/s41598-019-44274-4

135. Stern KH. High Temperature Properties and Decomposition of Inorganic Salts Part 3, Nitrates and Nitrites. *J Phys Chem Ref Data*. 1972;1(3):747-772. doi:10.1063/1.3253104

136. Riley BJ, Schweiger MJ, Kim DS, et al. Iodine solubility in a low-activity waste borosilicate glass at 1000 °c. *J Nucl Mater*. 2014;452(1-3):178-188. doi:10.1016/j.jnucmat.2014.04.027

137. Riley BJ, Vienna JD, Strachan DM, McCloy JS, Jerden JL. Materials and processes for the effective capture and immobilization of radioiodine: A review. *J Nucl Mater*. 2016;470:307-326. doi:10.1016/j.jnucmat.2015.11.038

138. Wren JC, Ball JM, Glowa GA. The Chemistry of Iodine in Containment. *Nucl Technol*. 2000;129(3):297-325. doi:10.13182/NT129-297

139. Jolivet V, Morizet Y, Hamon J, Paris M, Suzuki-Muresan T. The influence of iodide on glass transition temperature of high-pressure nuclear waste glasses. *J Am Ceram Soc*. 2021;104(3):1360-1369. doi:10.1111/jace.17571

140. Oppenheim AL. *Glass and Glassmaking in Ancient Mesopotamia : An Edition of the Cuneiform Texts Which Contain Instructions for Glassmakers : With a Catalogue of Surviving Objects / A. Leo Oppenheim ... [et Al.].* Corning : Corning Museum of Glass Press : London : Associated University Presses, 1988 printing, c1970.; 1988.

141. Hood HP. Method of fining borosilicate glasses. Published online 1936:3.

142. Obranovic, Barham D, Hancock R. On the behaviour of chlorine in glass. In: ; 2006:229-231.

143. McKeown DA, Gan H, Pegg IL, Stolte WC, Demchenko IN. X-ray absorption studies of chlorine valence and local environments in borosilicate waste glasses. *J Nucl Mater*. 2011;408(3):236-245. doi:https://doi.org/10.1016/j.jnucmat.2010.11.035

144. Jin T, Rivers EL, Kim D, et al. Effect of chlorine and chromium on sulfur solubility in low-activity waste glass. *Int J Appl Glas Sci*. 2022;13(1):82-93.

145. Thomas RW, Wood BJ. The chemical behaviour of chlorine in silicate melts. *Geochim Cosmochim Acta*. 2021;294:28-42. doi:https://doi.org/10.1016/j.gca.2020.11.018

146. Beermann O, Botcharnikov RE, Nowak M. Partitioning of sulfur and chlorine between aqueous fluid and basaltic melt at 1050°C, 100 and 200MPa. *Chem Geol*. 2015;418:132-157. doi:https://doi.org/10.1016/j.chemgeo.2015.08.008

147. Bureau H, Keppler H, Métrich N. Volcanic degassing of bromine and iodine: experimental fluid/melt partitioning data and applications to stratospheric chemistry. *Earth Planet Sci Lett*. 2000;183(1-2):51-60.

148. Thomas RW, Wood BJ. The chemical behaviour of chlorine in silicate melts. *Geochim Cosmochim Acta*. 2021;294:28-42. doi:https://doi.org/10.1016/j.gca.2020.11.018

149. Dobiszewska M, Beycioglu A. Physical Properties and Microstructure of Concrete with Waste Basalt Powder Addition. *Materials (Basel)*. 2020;13:3503. doi:10.3390/ma13163503

150. Hrma P. Retention of Halogens in Waste. 2010;(May).

151. Vaishnav S. Structural characterization of sulphate and chloride doped glasses for radioactive waste immobilisation. Published online 2018.

152. Bell AMT, Backhouse DJ, Deng W, et al. X-ray Fluorescence Analysis of Feldspars and Silicate Glass: Effects of Melting Time on Fused Bead Consistency and Volatilisation. *Miner* . 2020;10(5).

doi:10.3390/min10050442

153. Westwater JW, Drickamer HG. The Mathematics of Diffusion. *J Am Chem Soc*. 1957;79(5):1267-1268. doi:10.1021/ja01562a072

154. CABLE M, MA C. Volatilisation From Soda-Lime-Silica Melts At One Atmosphere And Reduced Preessures. Published online 1975.

155. Iguchi M, Ilegbusi OJ. Diffusion and Mass Transfer BT - Basic Transport Phenomena in Materials Engineering. In: Iguchi M, Ilegbusi OJ, eds. Springer Japan; 2014:135-147. doi:10.1007/978-4-431-54020-5_8

156. Cooper A. *Mass Transport Phenomena in Ceramics*. Vol 9. Springer Science & Business Media; 2012.

157. Bingham PA, Hyatt NC, Hand RJ, Forder SD. Vitrification of UK intermediate level radioactive wastes arising from site decommissioning. Initial laboratory trials. *Glas Technol Eur J Glas Sci Technol Part A*. 2013;54(1):1-19.

158. Bonnell DW, Plante ER, Hastie JW. Vaporization of simulated nuclear waste glass. *J Non Cryst Solids*. 1986;84(1):268-275. doi:https://doi.org/10.1016/0022-3093(86)90785-4

159. Banerjee D, Joseph A, Sudarsan VK, Wattal PK, Das D. Effect of composition and temperature on volatilization of Cs from borosilicate glasses. *J Am Ceram Soc*. 2012;95(4):1284-1289. doi:10.1111/j.1551-2916.2012.05077.x

160. ASANO M, YASUE Y. Vapor Species over Na2O-B2O3-SiO2-Cs2O Glass. *J Nucl Sci Technol*. 1985;22(12):1029-1032. doi:10.1080/18811248.1985.9735760

161. Asano M, Kou T, Yasue Y. Mass spectrometric study of vaporization of cesium-containing borosilicate glasses. *J Non Cryst Solids*. 1987;92(2):245-260. doi:https://doi.org/10.1016/S0022-3093(87)80042-X

162. Nakajima K, Takai T, Furukawa T, Osaka M. Thermodynamic study of gaseous CsBO2 by Knudsen effusion mass spectrometry. *J Nucl Mater*. Published online 2017. doi:10.1016/j.jnucmat.2017.05.001

163. Vance ER, Hayward PJ, Hamon RF. Volatile Losses from Sphene Glass-Ceramic and Borosilicate Glass Melts. *J Am Ceram Soc*. 1988;71(7):C-318-C-320. doi:10.1111/j.1151-2916.1988.tb05927.x

164. Xu K, Pierce DA, Hrma P, Schweiger MJ, Kruger AA. Rhenium volatilization in waste glasses. *J Nucl Mater*. 2015;464:382-388. doi:10.1016/j.jnucmat.2015.05.005

165. Hrma PR. *Retention of Halogens in Waste Glass*.; 2010. doi:10.2172/981571

166. Xian Q, Xiao X, Yu J, et al. High Retention Immobilization of Iodine in B–Bi–Zn Oxide Glass Using Bi2O3 as a Stabilizer under a N2 Atmosphere. *Inorg Chem*. 2022;61(48):19633-19641. doi:10.1021/acs.inorgchem.2c03601

167. Marra JC. Vitrification in the presence of salts. *Am Ceram Soc - 96th Annu Meet*. Published online 1994.

168. Sekiguchi Y, Uozumi K, Koyama T, Terai T. Fundamental study on the vaporization of cesium and iodine dissolved in LiF-NaF-KF molten salt. *J Nucl Mater*. 2019;522:136-143. doi:10.1016/j.jnucmat.2019.05.014

169. Wren JC, Ball JM, Glowa GA. The Chemistry of Iodine in Containment. *Nucl Technol*.

2000;129(3):297-325. doi:10.13182/NT129-297

170. Vasile C, Butnaru E. Radiation chemistry of organic solids. *Appl Ioniz Radiat Mater Process*. 2017;1:117-141.

171. Lin C-C. Volatility of iodine in dilute aqueous solutions. *J Inorg Nucl Chem*. 1981;43(12):3229-3238. doi:https://doi.org/10.1016/0022-1902(81)80094-2

172. Shade JW, Whyatt W., Steegen G. *Volatility and Entrainment of Feed Components and Product Glass Characteristics during Pilot-Scale Vitrification of Simulated Hanford Site Low-Level Waste*. Westinghouse Hanford Co.; 1996.

173. Matlack KS, Gong W, Pegg IL. *Compositional Variation Tests on DuraMelter 100 with LAW Sub-Envelope A3 Feed in Support of the LAW Pilot Melter, VSL-01R62N0-1, Rev. 2*. Hanford Site (HNF), Richland, WA (United States); 2003.

174. Haskins JD, Jaeglé L, Shah V, et al. Wintertime Gas-Particle Partitioning and Speciation of Inorganic Chlorine in the Lower Troposphere Over the Northeast United States and Coastal Ocean. *J Geophys Res Atmos*. 2018;123(22):12,812-897,916. doi:https://doi.org/10.1029/2018JD028786

175. Metrich N, Rutherford MJ. Experimental study of chlorine behavior in hydrous silicic melts. *Geochim Cosmochim Acta*. 1992;56(2):607-616. doi:https://doi.org/10.1016/0016-7037(92)90085-W

176. Wikström E, Ryan S, Touati A, Telfer M, Tabor D, Gullett BK. Importance of Chlorine Speciation on de Novo Formation of Polychlorinated Dibenzo-p-dioxins and Polychlorinated Dibenzofurans. *Environ Sci Technol*. 2003;37(6):1108-1113. doi:10.1021/es026262d

177. Stromberg RR, Straus S, Achhammer BG. Thermal decomposition of poly (vinyl chloride). *J Polym Sci*. 1959;35(129):355-368.

178. Nisar J, Khan MS, Iqbal M, et al. Thermal decomposition study of polyvinyl chloride in the presence of commercially available oxides catalysts. *Adv Polym Technol*. 2018;37(6):2336-2343. doi:https://doi.org/10.1002/adv.21909

179. Cheng J, Wang P, Su X. Recent Progress on the Detection of Dioxins Based on Surface-enhanced Raman Spectroscopy. *Acta Chim Sin*. 2019;77(10):977-983. doi:10.6023/A19040139

180. Schlüter S, Popovska-Leipertz N, Seeger T, Leipertz A. Gas Sensor for Volatile Anesthetic Agents Based on Raman Scattering. In: *Physics Procedia*. ; 2012. doi:10.1016/j.phpro.2012.10.108

181. Heland J, Schäfer K. Determination of major combustion products in aircraft exhausts by FTIR emission spectroscopy. *Atmos Environ*. 1998;32(18):3067-3072. doi:10.1016/S1352-2310(97)00395-6

182. Environmental Agency. M2 Monitoring of stack emissions to air. *Environ Agency*. 2017;(August). https://assets.publishing.service.gov.uk/government/uploads/system/uploads/attachment_data/file/635235/LIT_6405.pdf

183. Civiš S, Matulková I, Cihelka J, Kubelík P, Kawaguchi K, Chernov VE. Time-resolved FTIR emission spectroscopy of Cu in the 1800-3800 cm -1 region: Transitions involving f and g states and oscillator strengths. *J Phys B At Mol Opt Phys*. 2011;44(2). doi:10.1088/0953-4075/44/2/025002

184. Mettler Toledo. Measuring Density with Laboratory Balance. Published 2023. Accessed February 5, 2023.

https://www.mt.com/gb/en/home/applications/Laboratory_weighing/density-measurement.html

185. Andreev GA, Hartmanoá M. Flotation method of precise density measurements. *Phys status solidi*. 1989;116(2):457-468. doi:https://doi.org/10.1002/pssa.2211160203

186. Klomfar J, Součková M, Pátek J. Buoyancy density measurements for 1-alkyl-3-methylimidazolium based ionic liquids with tetrafluoroborate anion. *Fluid Phase Equilib*. 2009;282(1):31-37. doi:https://doi.org/10.1016/j.fluid.2009.04.021

187. Thomas R. *Practical Guide to ICP-MS : A Tutorial for Beginners, Third Edition*. Taylor & Francis Group; 2013. http://ebookcentral.proquest.com/lib/shu/detail.action?docID=1186512

188. Wilschefski SC, Baxter MR. Inductively Coupled Plasma Mass Spectrometry: Introduction to Analytical Aspects. *Clin Biochem Rev*. 2019;40(3):115-133. doi:10.33176/AACB-19-00024

189. Pitts K, Trejos T, Watling J, Almirall J. A Guide for the quantitative elemental analysis of glass using LA-ICP-MS. *At Spectrosc*. 2006;27:68-75.

190. Sun W, Yang K, Xia L. Application of ICP-MS Method in Environmental Field. *IOP Conf Ser Earth Environ Sci*. 2021;769(2):22028. doi:10.1088/1755-1315/769/2/022028

191. de Loos-Vollebregt G. INDUCTIVELY COUPLED PLASMA (ICP) - MS. Ghent University. Published 2023. Accessed February 3, 2023. https://www.chromedia.org/chromedia?waxtrapp=aennduEsHiemBpdmBlIEcCFH&subNav=rggpgpDsHiemBpdmBlIEcCFHtB

192. Jauncey GE. The Scattering of X-Rays and Bragg's Law. *Proc Natl Acad Sci U S A*. 1924;10(2):57-60. doi:10.1073/pnas.10.2.57

193. RAMAN C V, SOGANI CM. X-ray Diffraction in Liquids. *Nature*. 1927;119(2999):601. doi:10.1038/119601a0

194. Sakurai K, Tsuji K, Cesareo R, et al. Special Configurations. In: *X-Ray Spectrometry: Recent Technological Advances*. ; 2004:277-433. doi:https://doi.org/10.1002/0470020431.ch5

195. Weltje GJ, Tjallingii R. Calibration of XRF core scanners for quantitative geochemical logging of sediment cores: Theory and application. *Earth Planet Sci Lett*. 2008;274(3):423-438. doi:https://doi.org/10.1016/j.epsl.2008.07.054

196. Madhu. What is the Difference Between X-ray Diffraction and X-ray Fluorescence. Difference Between. Published 2022. Accessed March 23, 2023. https://www.differencebetween.com/what-is-the-difference-between-x-ray-diffraction-and-x-ray-fluorescence/

197. Rautiyal P, Gupta G, Edge R, et al. Gamma irradiation-induced defects in borosilicate glasses for high-level radioactive waste immobilisation. *J Nucl Mater*. 2021;544:152702. doi:https://doi.org/10.1016/j.jnucmat.2020.152702

198. Prime RB, Bair HE, Vyazovkin S, Gallagher PK, Riga A. Thermogravimetric analysis (TGA). *Therm Anal Polym Fundam Appl*. Published online 2009:241-317.

199. Harbour JR. Volatility of Simulated High-Level Nuclear Waste Glass by Thermogravimetric Analysis. *J Am Ceram Soc*. 1992;75(3):507-513. doi:10.1111/j.1151-2916.1992.tb07834.x

200. Heide K. Thermogravimetric and mass spectrometric investigations of the decomposition and volatilization of raw materials by heating of a glass batch. *J Therm Anal*. 1989;35(2):305-318. doi:10.1007/BF01904433

201. Shi L, Qu T, Liu D, Deng Y, Yang B, Dai Y. Process of Thermal Decomposition of Lithium Carbonate BT - Materials Processing Fundamentals 2020. In: Lee J, Wagstaff S, Lambotte G, Allanore A, Tesfaye F, eds. Springer International Publishing; 2020:107-116.

202. Coats AW, Redfern JP. Thermogravimetric analysis. A review. *Analyst*. 1963;88(1053):906-924.

203. Reguigui N. *Gamma Ray Spectrometry*.; 2014.

204. Semiconductor Detectors for Gamma-Ray Spectrometry. In: *Practical Gamma-Ray Spectrometry*. ; 2008:39-60. doi:https://doi.org/10.1002/9780470861981.ch3

205. Horrocks D. *Applications of Liquid Scintillation Counting*. Elsevier; 2012.

206. Kuwata H, Tazoe H, Kranrod C, et al. PERFORMANCE EVALUATION OF COMMERCIAL SCINTILLATION COCKTAILS FOR LOW-LEVEL TRITIUM COUNTING BY HIGH-CAPACITY LIQUID SCINTILLATION COUNTER. *Radiat Prot Dosimetry*. 2022;198(13-15):1014-1018. doi:10.1093/rpd/ncac040

207. Sevim F, Demir F, Bilen M, Okur H. Kinetic analysis of thermal decomposition of boric acid from thermogravimetric data. 2006;23(5):736-740.

208. Nakano M, Wada T, Koga N. Exothermic Behavior of Thermal Decomposition of Sodium Percarbonate: Kinetic Deconvolution of Successive Endothermic and Exothermic Processes. *J Phys Chem A*. 2015;119(38):9761-9769. doi:10.1021/acs.jpca.5b07044

209. Gitzhofer K. Reduction of Gaseous Boron Compounds in the Waste Gas of Glass Melting Furnaces. *Adv Mater Res*. 2008;39-40:641-646. doi:10.4028/www.scientific.net/AMR.39-40.641

210. Hudson LK, Misra C, Perrotta AJ, Wefers K, Williams FS. Aluminum Oxide. In: *Ullmann's Encyclopedia of Industrial Chemistry*. ; 2000. doi:https://doi.org/10.1002/14356007.a01_557

211. FEIL V, FELLER S. THE DENSITY OF SODIUM BOROSILICATE GLASSES RELATED TO ATOMIC ARRANGEMENTS. *J Non Cryst Solids*. 1990;119(90):103-111.

212. Farnan I. The Effect of Compositional Differences on UK Radioactive Glass Durability High-level waste glass in UK. 2020;(September).

213. Guéneau C, Flèche J. CALPHAD : Computer Coupling of Phase Diagrams and Thermochemistry Thermodynamic assessment of the cesium – oxygen system by coupling density functional theory and CALPHAD approaches. *Calphad*. 2015;49:67-78. doi:10.1016/j.calphad.2015.02.002

214. National Center for Biotechnology Information. PubChem Compound Summary for CID 5238, Sodium Iodide. Pubmed.

215. Broström M, Enestam S, Backman R, Mäkelä K. Condensation in the KCl–NaCl system. *Fuel Process Technol*. 2011;105:142–148. doi:10.1016/j.fuproc.2011.08.006

216. Zhang T, Zou Q. Tuning the thermal properties of borosilicate glass ceramic seals for solid oxide fuel cells. *J Eur Ceram Soc*. 2012;32(16):4009-4013. doi:https://doi.org/10.1016/j.jeurceramsoc.2012.07.036

217. Sill CW. Volatility of cesium and strontium from a synthetic basalt. *Nucl Chem Waste Manag*. 1988;8(2):97-105. doi:https://doi.org/10.1016/0191-815X(88)90068-X

218. Haynes W. *CRC Handbook of Chemistry and Physics*.; 2014.

219. SATO T, IKOMA S, OZAWA F, NAKAMURA T. Thermal Decomposition of Magnesium Hydroxide. *Gypsum Lime*. 1982;1982(181):283-289. doi:10.11451/mukimate1953.1982.283

220. MatouŠek J. Chemistry of evaporation from silicate melts. In: *In: 6th ESG Conference*. ; 2002.

221. Guo R. Investigating the effects of magnesium on the structure and durability of radioactive waste glasses by solid-state NMR. Published online 2019.

222. Baehr W. Design And Operation Of High Level Waste Vitrification And Storage Facilities. *Tech Rep Ser No 339*. Published online 1992.